Does the Protein Aggregation State Affect the Digestibility and Safety of Foods?

A thesis submitted in partial fulfilment of the requirements for the

Degree of Doctor of Philosophy in Biochemistry

2013

Moritz Lassé

University of Canterbury

Acknowledgments

Foremost, I would like to thank you, Juliet, for your consistent support, encouragement, cheerfulness, and dedication to your supervising role throughout my PhD. Your generosity in the form of conference trips, shouted beers and the occasional German bread or salami on my desk were appreciated a lot. I would also like to thank the other members of my supervisor team, Jolon, Grant, and Nigel for their support and expert advice.

Special thanks must also go to the Riddet Institute (Palmerston North, New Zealand), for funding my research. Additionally, I would like to thank AgResearch for being a specifically generous collaborator. Jolon and Santanu (AgResearch, Lincoln, New Zealand), you have been always fun to work with. I value my collaboration with you and I thank you both for introducing me to the world of mass spectrometry. Dulantha (AgResearch, Grasslands, New Zealand) thank you very much for helping me carry out cell culture experiments and for fun times in Palmerston North. Thank you, Kenny (University of Otago, New Zealand) and Antonia (Callaghan Innovation, Christchurch, New Zealand) for your advice and help with cell culturing in our lab.

Duncan (University of Auckland, New Zealand), I am forever grateful to you for helping me understand the principles of small angle X-ray scattering and for your help and advice on small angle X-ray scattering analysis. Thanks to Grant (University of Canterbury, New Zealand) and the Australian Synchrotron scientist team (Australian Synchrotron, Melbourne, Australia) for your amazing dedication.

Jackie (University of Canterbury), thank you for all your help with transmission electron microscopy, and Neil (University of Canterbury) for introducing me to scanning electron microscopy. Thanks to the Gerrard, Dobson, and Pearce labs as well as to Callaghan Innovation (Andy and Susie thanks for all your help!). I had a fun time with all of you in and out of the lab. Jeremy, Kat, Amy P., Amy Y., Rachel, and Madhu I am glad to stay on for my postdoc (Thank you so much for my new job, Ren!). Jared, thank you for being such a good friend and lab buddy over the last few years.

My dear family, Mama, Papa, Florian, Marie, and Juna; despite the long distance between New Zealand and Germany, I was always sure of your support and encouragement and I am happy to have you. Thanks to my grandparents and to my friends both here in New Zealand and in Germany for your support. Mark, Bronwyn, and Lewis, thanks for being my family here in New Zealand.

Anne, you are the best friend that I have. Thank you for all your love and the support you offered me over the last few years. You were a tremendous help and always made my life happy and exciting.

Table of Contents

Abbreviations

%	percent
ΔG_{unf}	change of free energy required for protein unfolding
ΔH	change in enthalpy
$\Delta\rho$	scattering length density contrast
°C	degree Celcius
1D	one-dimensional
2D	two-dimensional
3D	three-dimensional
Å	Ångstrom
aa_{eq}	α-NH_2 equivalents
aa_{mod}	number of specific amino acid residue with a specific modification
aa_{tot}	total number of specific amino acid residues observed
Abs	absorbance
ACE	angiotensin-converting enzyme
AD	Alzheimer's disease
AFM	atomic force microscopy
AGE	advanced glycation endproduct
ANS	8-anilinonaphthalene-1-sulfonic acid
APP	amyloid precursor protein
AU	arbitrary unit
Aβ	amyloid β-peptides
bis-tris	2-[bis(2-hydroxyethyl)amino]-2-(hydroxymethyl)propane-1,3-diol
bkg	residual incoherent background
BSA	bovine serum albumin
Caco-2	caucasian colon adenocarcinoma-2
CD	circular dichroism
c_g	protein gelation concentration
CR	congo red
D	diffusion constant
d	diameter

d	distance
d	dilution factor
Da	Daltons
DEAE	2-(diethylamino)ethyl
d_H	hydrodynamic diameter
DH	degree of hydrolysis
DHA	dehydroalanine
DLS	dynamic light scattering
d_{max}	maximum distance
DMSO	dimethyl sulfoxide
DOPA	3,4-dihydroxyphenylalanine
DSC	differential scanning calorimetry
DSF	differential scanning fluorometry
DTT	(2S,3S)-1,4-bis(sulfanyl)butane-2,3-diol
E. coli	*Escherichia coli*
EC	enzyme commission number
EDTA	ethylenediaminetetraacetic acid
EM	electron microscopy
EMBOSS	european molecular biology open software suite
EW	egg white
ExPASy	expert protein analysis system
f(z)	scattering amplitude
FBS	foetal bovine serum
FITC	fluorescein isothiocyanate
f_{mod}	modification factor
FTIR	fourier transform infrared
g	gram
h	hour(s)
h	hydrolysis equivalents
HAS	human serum albumin
Hec-1a	human endometrial cancer - 1a
HI	hydroimidazolone

HMF	hydroxymethylfurfural
HMP	high-methoxyl pectin
HPLC	high performance liquid chromatography
h_{tot}	hydrolysis equivalents of complete protein hydrolysis
I	scattering intensity
I(Q)	Q dependent intensity
IEP	isoelectric point
incoh. bkg	residual incoherent background
INS	insulin
k	scattered wave vector
k_0	incident wave vector
k_b	Boltzmann constant
kDa	kilo Dalton
keV	kilo electron volt
kg	kilogram
KPI	kidney bean protein isolate
kV	kilo volt
L	litre
LAL	lysinoalanine
LC	liquid chromatography
LDS	lithium salt of dodecyl sulfate
ln	natural logarithm
m	mass
m	metre
M	molar
M cell	microfold cell
m/z	mass to charge ratio
mA	milliampere
mDeg	millidegree
mg	milligram
min	minute(s)
mL	millilitre

mm	millimetre
mM	millimolar
mmol	millimole
MOPS	3-morpholinopropane-1-sulfonic acid
MPa	megapascal
mPMS	1-methoxy-5-methyl-phenazinium methyl sulfate
MS	mass spectrometry
MS/MS	tandem mass spectrometry
MWCO	molecular weight cut off
n	integer
n	the number of particles in the scattering volume
NAD+	nicotamide adenine dinucleotide
NADH	nicotamide adenine dinucleotide, reduced form
NCBInr	National Center for Biotechnology Information (non redundant)
NCNR SANS	NIST Centre for Neutron Research (small angle neutron scattering)
nm	nanometer
non-ox	non oxidative
OPA	*o*-phthalaldehyde
OVA	ovalbumin
ox	oxidative
$P(Q)$	form factor
$P(Q)_{Cyl}$	elliptical cross-section form factor
$P(Q)_{ell}$	elliptical form factor
$P(r)$	pair distance distribution function
PAGE	polyacrylamide gel electrophoresis
PBS	phosphate buffered saline
PDB	protein data bank
PDDF	pair distance distribution function
PepT1	peptide transporter 1
pH	negative decadic logarithm of the hydrogen ion concentration
PIC	protease inhibitor cocktail
PK	Proteinase K

pK_a	negative decadic logarithm of the acid dissociation constant
PP buffer	pancreatin and Proteinase K buffer
Q	scattering vector
Q_p	Porod invariant
r	geometrical radius
r_e	classical electron radius
R_g	radius of gyration
RI	refractive index
ROS	reactive oxygen species
rpm	revolutions per minute
s	second
$S(Q)$	structure factor
$S(Q)_{SC}$	Coulomb structure factor
SAXS	small angle X-ray scattering
SDS	sodium dodecyl sulfate
SDS PAGE	sodium dodecyl sulfate polyacrylamide gel electrophoresis
SEM	scanning electron microscopy
SLD	scattering length density
SOA	soluble ovalbumin aggregates
SPI	soy protein isolate
s_w	weighted amino acid modification score
T	temperature (°C)
$T_{\Delta G=Max}$	maximum unfolding temperature
T_a	absolute temperature (K)
TCA	tricarboxylic acid cycle
TCEP	tris(2-carboxyethyl)phosphine
TEM	transmission electron microscope
TGAse	transglutaminase
ThT	thioflavin T
T_m	melting temperature
Tris	2-Amino-2-hydroxymethyl-propane-1,3-diol
U	unit

UniProt	universal protein resource
UV A_{280}	ultra violet absorbance at 280 nm
V	particle volume
V	volt
v/v	volume per volume
w/w	weight per weight
WPI	whey protein isolate
WST	water soluble tetrazolium
X-ray	electromagnetic radiation
β_2m	β2-microglobulin
β-lg	β-lactoglobulin
ΔH	change in enthalpy
η	viscosity
ϑ	Bragg angle
λ	wavelength
µL	microlitre
µm	micrometre
ξ	instrument constant for SAXS
ρ_e	electron density
ρ_{ell}	protein scattering length density
ρ_{solv}	solvent scattering length density

Abstract

This thesis explores the complex relationship between food protein structure and digestibility. Food proteins are important nutrients that play a central role in controlling the textural properties of many foods. Processing of food proteins may alter the protein aggregate structure and digestibility. The degree of protein aggregation during food processing depends on the denaturing conditions and the presence of other food components. Sugars and lipids may contribute to protein glycation and protein cross-linking via the Maillard reaction. Furthermore, amino acid residues of food proteins may be chemically modified during processing, thereby influencing both the structure and the nutritional value of proteins.

An *in vitro* digestibility assay was used to investigate the relationship between protein aggregate structure and protein digestibility. Raw and boiled egg whites were exposed to a wide range of conditions: pH 2 - 12, in the presence and absence of 200 mM NaCl. It was found that pH and NaCl treatment prior to *in vitro* digestion resulted in significantly different protein ultrastructures, but did not markedly influence protein digestibility under the tested conditions. Raw egg white was less digestible than boiled egg white under all test conditions. The inclusion of Maillard reaction partners caused protein cross-linking concurrent with a decrease in digestibility. The digestibility decreased with the reactivity of the Maillard reaction partner and with increasing heating time.

Proteomic analysis, using tandem mass spectrometry, of raw and heated egg white showed an increase in hydrothermally induced amino acid modifications. In the presence of glucose and methylglyoxal, a Maillard reaction specific increase in arginine modification to hydroimidazolone was observed with increasing heating times. The observed modifications are likely to contribute to a change in the nutritional quality of egg white.

Aggregation kinetics of the major egg white protein, ovalbumin, were studied by dynamic light scattering, small angle X-ray scattering, and transmission electron microscopy. Shape determination was only possible for ordered aggregates, but not for disordered aggregates. Prior to heating, ovalbumin molecules in the presence of water and glucose repelled each other in concentrated solution. The presence of NaCl shielded electrostatic repulsion, leading to early onset dimerisation and disordered aggregation upon heating. Methylglyoxal treated ovalbumin formed more ordered aggregates. The scattering of these structures was able to be fitted to cylindrical shape models showing an increase of cylinder length with time while the cylinder diameter remained near constant over 24 hours of heating.

In addition, food protein derived amyloid fibril aggregates were characterised. Amyloid fibrils are a common ordered protein fold that has been linked to neurodegenerative diseases. In the recent literature, amyloid fibrils have been proposed as new functional macromolecules in proteinaceous foods because of their desirable textural properties. Food fibrils formed from whey, egg white, soy bean and kidney bean protein were tested to establish whether they are protease resistant or display toxicity to human Caco-2 cells (a model intestinal cell line). The food fibrils were compared to insulin amyloid fibrils, a well characterised amyloid system. It was shown that the food fibrils displayed some resistance towards *in vitro* hydrolysis and were not found to be toxic.

This work contributes to the understanding of food protein aggregation and digestibility under relevant conditions. It highlights the relationship of aggregate structure and digestibility and the particular role of the Maillard reaction. Moreover, evidence is provided that food protein derived amyloid fibrils may be safe ingredients in consumables. These findings may contribute to optimising industrial food processes and creating safe new food products.

Chapter One

1 Introduction

The aim of this thesis is to investigate the influence of processing on food proteins from a structural and nutritional view point. More often than not, food proteins are altered chemically and structurally during domestic or industrial processing. This has complex implications for the quality of proteins and for their usability in food stuffs.

Structural changes of proteins may occur during denaturation processes. The conformational changes may in turn result in alteration of their textural and nutritional properties. However, an accurate prediction of a protein's aggregation behaviour is difficult. An in depth knowledge of the molecular mechanisms that underlie the changes in structure is therefore desirable in order to get away from observational studies towards the development of models that accurately predict the impact of certain processes on protein structure and nutrition.

Protein aggregates of specific interest in recent years include amyloid-like fibrils. Amyloid-like fibrils have been proposed as new food ingredients with desirable structural properties. However, the link to neurodegenerative diseases has afforded amyloid fibrils a bad reputation because of their potential cytotoxicity. This work investigates amyloid-like fibrillar aggregates formed from food proteins with regard to their resistance to physiologically relevant proteases in order to explore the relationship between aggregate structure and nutritional availability. Their impact on human cell culture *in vitro* is also examined to examine potential cytotoxic behaviour.

This introductory chapter gives a brief overview of protein aggregation and the nutritional value of proteins to set a context for the thesis. Each chapter will contain a dedicated introduction describing the material discussed in the respective chapter.

1.1 Overview of Processing Implications for Food Proteins

The native protein structure is frequently altered during food processing. Often, aggregation occurs during food processing and storage (Gerrard et al. 2012; Pearce et al. 2007). Depending on the chosen conditions the pathway of aggregation and the final aggregate structure may vary (Lucey 2002; Foegeding et al. 2006). Different structures in turn may impact the functional properties of the resultant protein network. In addition to mere aggregation, proteins may be modified chemically during processing (e.g. oxidation) or as a result of reactions with other food ingredients (e.g. Maillard reaction) (Liu et al. 2012). The combination of structural and chemical modifications may influence the nutritional value of the proteins (Wang & Ismail 2012). Figure 1.1 shows the intricate relationship between protein structure, chemical modifications, and nutritional value.

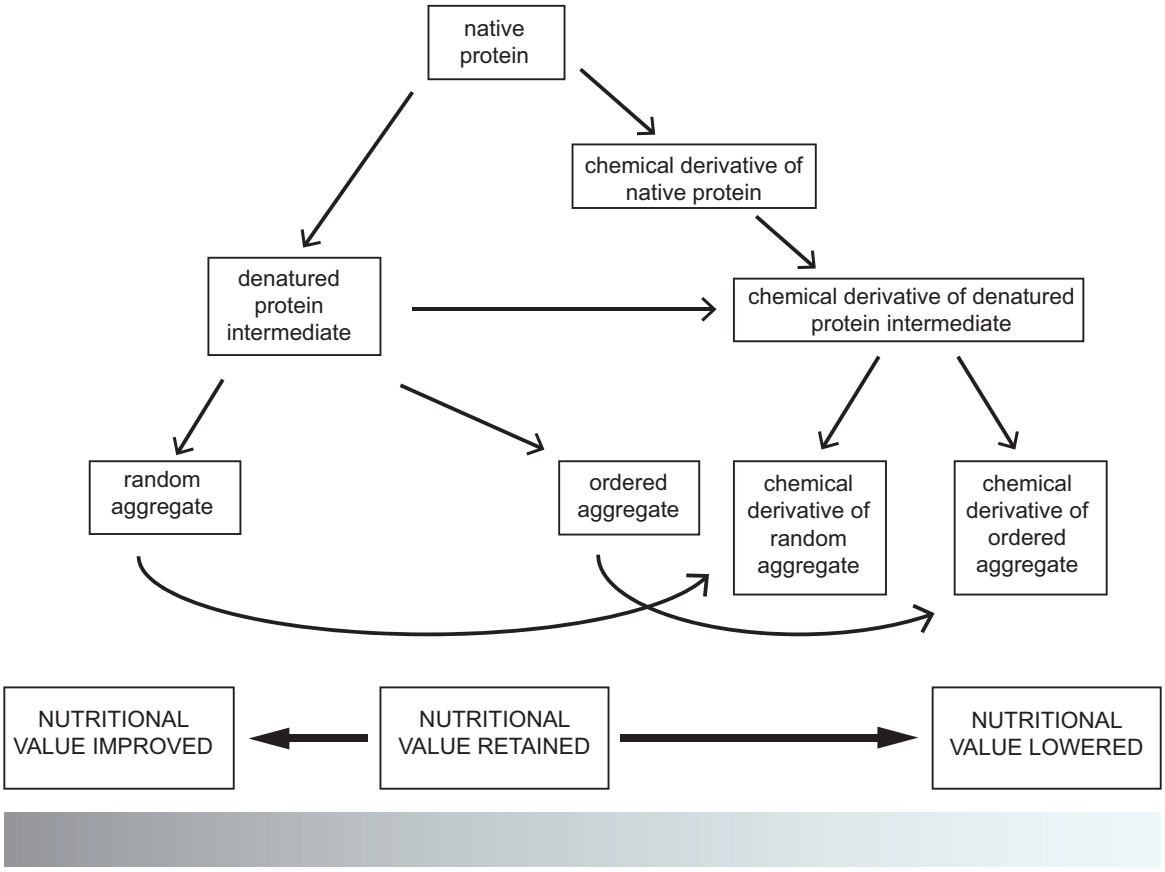

Figure 1.1: *Example interaction map of native protein undergoing aggregation. Fields and arrows at the bottom suggest the changes of nutritional value of protein upon aggregation and chemical derivatisation. Diagram adapted from (Gerrard et al. 2012).*

1.2 Protein Aggregation

Protein folding and unfolding are thermodynamically driven processes. Therefore, aggregation depends on parameters that change the thermodynamics of a given system. These parameters include temperature, pressure, pH, salt concentration, protein concentration, etc., which are all known to influence protein stability. Proteins can assume a wide variety of conformations ranging from unfolded peptide chains to partially folded intermediates and completely folded native forms (Dobson 2001; Frauenfelder et al. 1991; Hartl & Hayer-Hartl 2009). Each conformation has an inherent Gibbs energy. Gibbs energy can be regarded as the thermodynamic potential analogous to the potential energy found in mechanics. Just as in all other closed systems, the state of lowest energy will be assumed by a given protein system over time. In the highly complex protein energy landscape, many conformations (including native, partially unfolded, and aggregated protein) have a low Gibbs energy (Hartl & Hayer-Hartl 2009). The low energy corresponds to highly stable conformations and can be thought of as a local minimum in the overall energy landscape. Therefore, specific conformations are stabilised in local minima "traps" (Figure 1.2).

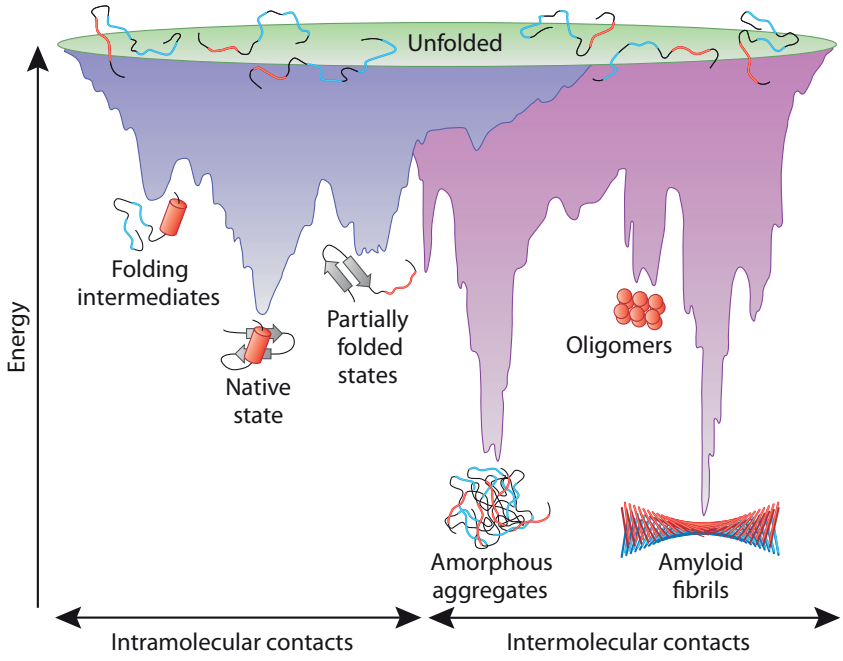

Figure 1.2 *Energy funnel of protein folding. Amyloid fibrils reside in a low energy minimum. The purple area (intramolecular contacts) represents the energy landscape leading to natively folded protein. The pink area (intermolecular contacts) indicates the pathway that leads to aggregation and polymerisation. Diagram taken from (Hartl & Hayer-Hartl 2009).*

There are numerous local minima in the energy landscape of proteins which can be populated. Under physiological conditions the native fold is favoured because it has a very low associated Gibbs energy and therefore resides in a deep minimum (Dobson 2001; Frauenfelder et al. 1991; Hartl & Hayer-Hartl 2009; Onuchic et al. 1997). If the delicate balance of the protein surroundings (buffer composition, protein concentration, pH, ionic concentration, temperature, pressure, etc.) is disturbed, the thermodynamic energy landscape is necessarily influenced. This enables proteins to transition to new minima and in many cases may lead to aggregation. Depending on the conditions, the aggregation process can result in random aggregates or in highly ordered structures such as the amyloid fibril (Dobson 2001). The highly ordered amyloid fibrils populate a low energy minimum and are therefore stable protein folds (Hartl & Hayer-Hartl 2009) as indicated in Figure 1.2. The diagram in Figure 1.3 illustrates the many pathways of protein unfolding and aggregation of a protein. Interestingly, this scheme can be transposed onto a food protein aggregation system. Starting from the intact native state (N), the protein may unfold (U) into an intermediate state (I), from which it can aggregate. There may be more than one intermediate state for any given protein.

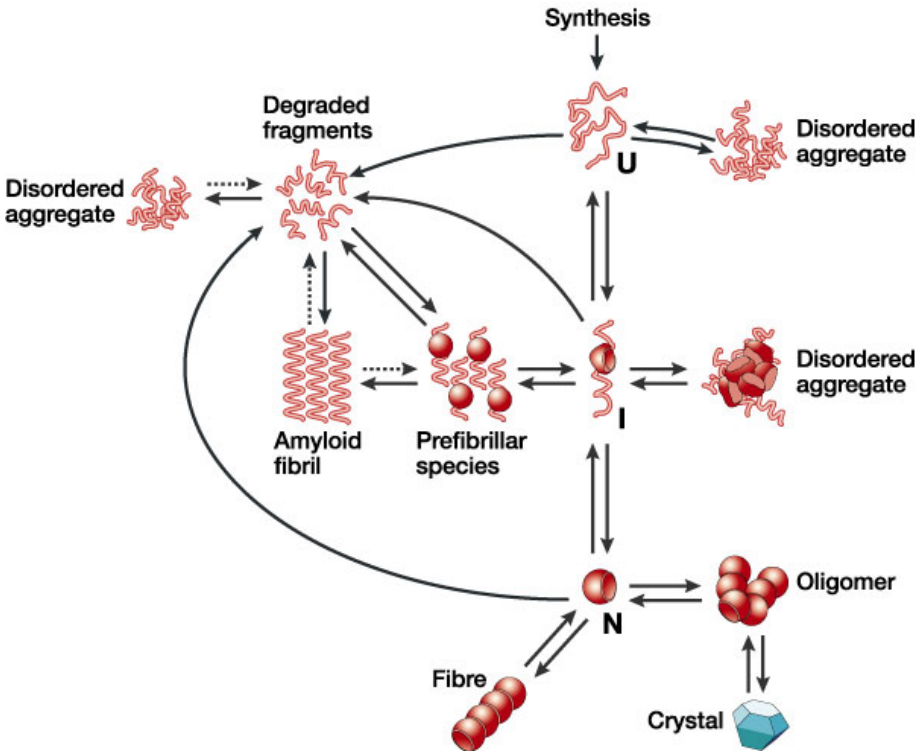

Figure 1.3 *Protein aggregation scheme from (Dobson 2003).*

The wealth of protein folding and aggregation literature that considers molecular details generally relies on pure protein model systems (Whittingham et al. 2002; Hamada et al. 2009; Arnaudov & de Vries 2005). However, in proteinaceous food systems (e.g. dairy products, baked goods, meats) it is rare to encounter highly purified protein systems. Instead, heterogeneous protein mixtures (often in combination with a non-protein component such as fats and sugars) are used which adds more complexity for deciphering underlying molecular mechanisms. Therefore food research is often limited to description of macroscopic and microscopic changes and prediction of structure is difficult (Ubbink 2012).

Enzymatic or pH hydrolysis during food processing can cause protein fragmentation. The peptide fragments have been linked to the formation of ordered amyloid-like structures. The described mechanism of food protein unfolding and aggregation compares very well with the protein aggregation diagram from Dobson et al., who analysed the manifold pathways involved in protein aggregation *in vivo* (Figure 1.3).

It is noteworthy that proteins do not need to be completely unfolded in order to aggregate. Partially unfolded intermediates can induce aggregation (Dong et al. 1995; Khurana et al. 2001). Depending on the degree of denaturation the intermediates may retain certain structural properties of the native fold. The degree of unfolding may then determine the final structure of the aggregate by promoting or inhibiting specific interactions between intermediates (Fink 1998; Roberts 2007; Weiss et al. 2007). Therefore, any given denaturation method may generate one or more predominant intermediate species based on the thermodynamics during the denaturation process. Aggregation can involve all molecular interactions including van der Waals, ionic, and covalent bonds. The proportion depends on the primary sequence of amino acids as well as on the denaturing conditions.

1.2.1 Nucleation

The initial step of aggregation is protein unfolding. Unfolding, however, is reversible and does not necessarily result in aggregation. The process from unfolding to aggregation requires that at least two proteins associate to form a stable initial aggregate. This initial aggregate is often described as a nucleation seed, implying that once a seed has been

formed, aggregation can progress rapidly. The formation of seeds may take a considerable amount of time in the absence of external factors. This is largely due to the unfolded protein being thermodynamically less favoured than the native protein. Therefore, a long initial lag phase without obvious aggregation precedes the aggregation of proteins in solution (Wang et al. 2010). However, if a stress factor changes the protein environment (e.g., through processing or storage conditions in food), the intermediates are formed more easily and aggregation seeds form rapidly.

Support for the nucleation theory comes from *in vitro* analysis of protein solutions that were stored over time. If a pre-formed aggregates were added (as nucleation seeds) the aggregate formation occurred more rapidly in the protein solution compared to the control without the added aggregate (Hamada et al. 2009; Pedersen 2010; Krebs et al. 2000; Otzen et al. 2007). The nuclei thus reduce the time of the lag phase considerably, reducing incubation times, sometimes from days to hours. Nuclei formation may also be facilitated by interfaces such as air-liquid, solid-liquid, and liquid-liquid, as interfaces play a key role in protein stabilisation/destabilisation (Linse et al. 2007).

1.2.2 Ordered and Disordered Aggregate Structure

It is possible to choose the denaturation parameters and thereby control aggregate structure. However, random aggregation is often favoured whereas ordered aggregation requires careful tuning of the aggregation conditions.

Disordered/ random/ amorphous aggregates are the predominant form of aggregate under most physiological conditions as well as during food processing. This is because, in general, the sum of prevalent forces will influence the native protein to take on a disordered rather than an ordered form. However, as assessed by infrared and circular dichroism studies, the random aggregates are not totally disordered but may still contain high levels of secondary structure (Fink 1998). Moreover, it appears that the β-sheet fold is favoured over the α-helix conformation. It was shown that β-sheet formation of previously unstructured protein domains is common (Fink 1998). The exposure of specific hydrophobic polypeptide regions leads to the formation of non-native dimers, trimers, etc. followed by a "random" assembly of many more proteins (Fink 1998).

Ordered aggregates include protein fibrils or amyloid fibrils. Amyloid fibrils form in a narrow window of specific denaturation parameters (Dobson 2001). As opposed to random aggregates, thermodynamics drive the proteins to align in an ordered network. It is hypothesised that the amyloid feature is a generic fold amongst proteins (Stefani & Dobson 2003). Typical characteristics of amyloid fibrils include a high degree of antiparallel beta sheets that run perpendicular to the fibril axis. Often, single strands of these fibrils will twist ropelike around other strands to form larger and stronger mature fibrils. For a detailed description of the amyloid fold refer to Section 5.1.

1.3 Protein Aggregation in Food

Proteins in food play an important role as nutrients and as structural elements. High protein diets have been described to have a more satiating effect compared to control meals of the same calorie content but a lower content of protein (Westerterp-Plantenga et al. 2012). Moreover, regular and sufficient protein consumption is important for normal growth, especially important for children, pregnant women, the elderly, but also for high intensity athletes.

In addition to nutritional improvement of proteinaceous foods it may be desirable to improve structural features. For these two reasons, controlling protein aggregation of food grade proteins is of growing interest to the food industry (Purwanti et al. 2010).

1.3.1 Protein Processing and Texture

The process of aggregation is often a desired outcome of food manufacturing processes. However, protein aggregation can also be undesirable, for example in high protein foods where gelation may be unwanted (Purwanti et al. 2010). The concept of deliberately inducing and harnessing protein aggregation stands in stark contrast to the pharmaceutical industry, which aims to eliminate the aggregation of peptide and protein drugs (Wang et al. 2010). Food proteins are used as foaming and thickening agents as well as emulsion stabilisers (Purwanti et al. 2010). Food aggregates include yoghurts and cheeses where acidification through bacterial fermentation and rennet application results in curdled

protein (Lucey 2002; Sodini et al. 2004). Additionally, egg white aggregation is desired in foams, baked goods, and desserts (Foegeding et al. 2006; Licciardello et al. 2012; Pernell et al. 2002; Yang et al. 2009). Soy protein derived tofu is a further example of a widely consumed and processed protein rich food where aggregation is desired (Renkema et al. 2002).

Traditionally, industrial and domestic food processes that influence protein aggregation include heating, pH modifications, salt concentration, and pressure treatments. Further industrial processes include spray drying (Kim et al. 2002; Nesterenko et al. 2013), extrusion for porous, low moisture products (Alonso et al. 1998; Gibbs et al. 1999; Matalanis et al. 2011), and spinning for fibril formation (Purwanti et al. 2010; Rampon et al. 1999). Substantial effort has been put into evaluating the impact of these parameters and processes on protein aggregation and gelation (Croguennec et al. 2002; Koike et al. 1996; Needs et al. 2000; Nicolai et al. 2011).

Despite this versatility in domestic and industrial processes, there is some need for innovative food processes that allow further fine tuning of protein matrices (Manski et al. 2007). This is especially true as the demand of greater quality high protein products is increasing. New means of protein denaturation for food manufacturing purposes include shear flow, high intensity ultrasound (Arzeni et al. 2012; Ashokkumar et al. 2008), ultraviolet processing (Bhat & Karim 2009; Bintsis et al. 2000; Manzocco et al. 2012), and high pressure treatment (Galazka et al. 2000; Molina et al. 2001; Needs et al. 2000). The nature of most of these studies is empirical, providing only vague theoretical models of food networks (Ubbink 2012). This indicates that the underlying molecular mechanisms that govern protein aggregation are not fully understood. Moreover, there is a plethora of protein functionality that is yet to be harnessed by food manufacturers (Purwanti et al. 2010).

1.3.2 Protein Aggregation in New Foods

From a structural perspective, there are two common goals of current food protein research. Firstly, to improve food texture and secondly, to develop new functional food systems including protein enriched foods, and delivery vehicles for pharmaceuticals and nutraceuticals (Aguilera 2005; Chen et al. 2006; Lesmes & McClements 2009; Livney

2010; Matalanis et al. 2011). There are numerous approaches to create new functional protein rich foods (Manski et al. 2007; Purwanti et al. 2010; van der Goot et al. 2008).

Shear flow has been used to fine tune protein gelation and to create desirable anisotropic protein structures in protein rich gels (Manski et al. 2007). Proteins are bio-polymers and have been shown to react to shear flow in a manner reminiscent of artificial polymers. However, in contrast to synthetic polymers protein heating often induces irreversible aggregation (Manski et al. 2007).

Intake of probiotic bacterial cultures such as *Bifidobacterium bifidum* has been shown to increase intestinal health. However, the shelf life for which probiotics remain alive and active is limited to a few days. Moreover, probiotic bacterial survival is challenged during passage of food through the stomach. Both issues may be circumvented by encapsulation of probiotics in a protein matrix (Nicolai et al. 2011). Furthermore, encapsulation of hydrophobic bioactives (such as antioxidants, vitamin D, retinol, and α-tocopherol) has been shown to protect the chemical compounds and to facilitate absorption of the active compound by the body (Livney 2010; Relkin & Shukat 2012). Proteins with the potential to be used as an encapsulation matrix for sensitive compounds include milk proteins such as the casein micelle and β-lactoglobulin (β-lg), vegetable proteins, and egg white proteins (Chen et al. 2006; Livney 2010; Nesterenko et al. 2013).

It has been shown that the appearance of food affects the subjective taste perception and consumption behaviour markedly (Cassens et al. 1996; Spence et al. 2010). The opacity of protein solutions usually increases with protein aggregation and gel formation. However, to satisfy consumer perception, a transparent or clear protein matrix may be desirable to prevent discolouration of protein rich foods or to use in clear beverages (Livney 2010). Recent studies showed that food grade proteins, including whey protein isolate (WPI) and egg white powder are able to form transparent gels (Weijers et al. 2006). Other transparent egg white gels have been known for generations. Alkaline pickled century eggs are a delicacy in China (Eiser et al. 2009) that also form transparent gels. However, the adjustment and maintenance of pH 12.5, which is used during formation of century eggs, is not common in everyday food manufacturing.

Another process that restructures typical food proteins involves partial hydrolysis of proteins (either enzymatically or chemically). The partial hydrolysis into peptides has an impact on the gelling properties of proteins (Ipsen et al. 2001). Under appropriate

conditions, the hydrolysis of proteins leads to a weakened gel structure compared to a non-hydrolysed protein, thereby allowing more protein inclusion into a food system. This in turn would allow higher concentrations of hydrolysed protein to achieve a similar texture. The creation of protein rich foods with similar textural properties is therefore possible through partial hydrolysis. A more recent discovery was that food protein hydrolysates are able to form amyloid like fibrils, especially at acidic pH (Loveday et al. 2010; Tang et al. 2010; Veerman et al. 2003b; Wang et al. 2011). Fibril forming food proteins include egg white, whey protein, soy protein, kidney bean protein, and hydrophobins. These fibrils display a completely different structure and therefore textural properties compared to the native protein (Gosal et al. 2004; Loveday et al. 2009; Rao et al. 2012; Veerman et al. 2003a). Due to the fibrillar morphology food derived amyloid-like fibrils have been proposed as stabilising agents and as a low calorie alternative to carbohydrate stabilisers. The inclusion of amyloid fibrils in food systems is covered in more detail in Section 5.1.3 addressing the concern that food fibrils may be detrimental to human health (Section 5.1.4). This is due to the bad reputation of amyloid fibrils as they are commonly associated with many neurodegenerative diseases (Stefani & Dobson 2003).

In conclusion, structural studies on protein aggregation in food merits further investigation because it opens up a new field of opportunities for food engineering by the food industry. In order to harness the full range of possibilities in engineering new food products it is therefore necessary to understand the basic mechanisms that underlie structural changes during food processing.

1.4 Nutritional Impact of Protein Processing

Certain food processing methods may influence the nutritional value of protein. It is therefore necessary to evaluate the digestibility and bioavailability of proteinaceous foods. The term digestibility in this work is defined as the degree of hydrolysis, or how well a given protein can be hydrolysed by enzymatic action (Nielsen et al. 2001). Bioavailability on the other hand is a measure of protein absorption and utilisation in anabolism by the body (Rutherfurd & Moughan 2008; Levesque et al. 2010; Rutherfurd & Moughan 2012).

Proteins are usually made up of 20 different proteinogenic amino acids. Amino acids are classified as essential, conditionally essential, or non-essential (Table 1.1) (Fürst & Stehle 2004; Friedman 1996). Essential amino acids have to be taken up by an organism through the diet, as pathways for synthesis of the respective amino acids are absent. Non-essential amino acids can be synthesised by the organism (Friedman 1996).

Table 1.1: *List of essential and nonessential amino acids. The asterisk (*) indicates conditionally essential amino acids in infants or in recovery from injury.*

Essential	Non-essential
Arginine*	Alanine
Histidine*	Asparagine
Isoleucine	Aspartate
Leucine	Glutamate
Lysine	Glutamine
Methionine/ Cysteine	Glycine
Phenylalanine/ Tyrosine	Proline
Threonine	Serine
Tryptophan	
Valine	

Food proteins and the constituent amino acids can undergo several chemical modifications during food storage and processing. These modifications include oxidation, nitration, dehydration, carboxymethylation, and many more (Section 3.2). Some of these modifications have been linked to a lower bioavailability and even toxicity (Robbins et al. 1980; Šebeková & Somoza 2007; Gross et al. 2011; Friedman 1999). The Maillard reaction between sugars or lipids and proteins is one of the most prominent and studied modifications.

Nutritional value of food is determined by nutrient absorption and subsequent utilisation by the body (Friedman 1996). Therefore, it is arguably the most important quality of food. The nutritional value of protein is a combination of the amino acid composition of the protein source and the processing methods, including the interactions with other dietary compounds (Friedman 1996; Meade et al. 2005). For high quality protein sources that are rich in essential amino acids, such as egg white, milk, meat, fish, legumes (e.g. soy), structural changes and chemical modifications during processing contribute most to

changes in the protein nutritional value. Experimental conditions often do not allow a clear cut distinction between entirely structural or chemical modifications because these two properties usually go hand in hand. However, there are some predominantly structural aspects when it comes to the nutritional value of a given protein.

There are at least two structural features that directly affect the digestibility of food proteins. Firstly, the intrinsic structure of the protein may influence the nutritional value. The denaturation of some (but not all) native proteins, such as ovalbumin (OVA) and β-lg, increases the susceptibility to proteolysis during *in vitro* digestion (Barbé et al. 2013; Takagi et al. 2003; Yoshino et al. 2004). This suggests better enzyme accessibility to proteolytic sites in denatured protein (Takagi et al. 2003). Secondly, the macro structure of the food matrix itself, i.e., the type of gel formation and cross-linking of proteins, may change the rate of hydrolysis and of amino acid absorption. *In vivo* studies on minipigs showed that gelation of milk by rennet or heat caused a decrease of amino acid bioavailability compared to untreated milk samples (Barbé et al. 2013; Feunteun et al. 2013).

The denaturation method may also influence the degree by which the nutritional value of a protein is altered. For example, heating and pressure treatment of egg white (EW) both increase the protein digestibility (Hoppe et al. 2013; van der Plancken et al. 2004). Pressure treatment at 800 MPa at 9 °C increased the susceptibility of egg white protein to pepsin hydrolysis even further than a heat treatment at 95 °C. Structural differences between the two types of aggregates, mainly a higher degree of β-sheet formation in heat aggregated egg white, are likely to have caused differences in nutritional value of the two aggregates. However, the impact of structure on digestibility is not yet fully understood.

1.5 Protein Digestion

Protein digestion begins in the stomach where pepsin begins the enzymatic hydrolysis of proteins. The low pH of 1.5-2 of the stomach supports protein hydrolysis by denaturing the protein. Protein digestion continues in the small intestine where the pH is raised to about 7.5-8. A pancreatic enzyme mixture of trypsin, chymotrypsin and carboxypeptidases hydrolyse proteins further into smaller peptides. In the small intestine single amino acids

as well as di- and tri-peptides are absorbed by enterocytes (Newey & Smyth 1960; Webb 1990; Gilbert et al. 2008). The transport of single amino acids across the cell membrane occurs via active Na^+ symporters. Di- and tri-peptides are transported via a proton peptide symporter, peptide transporter 1 (*pepT1*) (Craft et al. 1968; Steinhardt & Adibi 1986; Adibi & Morse 1971; Rubio-Aliaga & Daniel 2002; Daniel 2004; Webb et al. 1992). *PepT1* is regulated by leptin, a naturally occurring protein hormone that regulates energy intake (Hindlet et al. 2009). An *in vivo* study on mice was conducted over 4 weeks in which mice were overfed. The study showed a relationship between energy intake and *pepT1* activity. There was a 46 % decrease of dipeptide transport when mice were overfed (Hindlet et al. 2009). The transport of peptides via the *pepT1* system is controlled at the transcriptional mRNA level, as found in studies of feeding and fasting chicken broilers (Gilbert et al. 2010).

After peptide absorption into the cytosol of the enterocyte, cytoplasmic peptidases further hydrolyse the peptides into single amino acids. These amino acids are then excreted into the blood stream. Alternatively, peptides can be digested by the enterocyte brush border associated enzymes such as aminopeptidase-A, -N, -P, and -W, angiotensin-converting enzyme (ACE) 1 and 2, carboxypeptidase P, dipeptidyl peptidase IV, endopeptidase-2 and -24.11 (Kowalczuk et al. 2008). From the blood stream the amino acids are delivered to tissues across the body.

Many intact proteins (including ovalbumin) as well as protein aggregates (prions), have also been shown to cross the intestinal barrier (Cobb & Surewicz 2009; Gardner 1988). However, the degree of absorption and the mechanism of whole protein uptake are not fully understood. The uptake of prion protein for example has been suggested to occur via microfold cells (M cells) or via dentritic cells (Cobb & Surewicz 2009). Addtional studies found a ferritin-prion co-transport in Caco-2 cells *in vitro* (Mishra et al. 2004).

1.6 *In Vivo* and *In Vitro* Digestion Models

Although different ways to holistically monitor the loss of amino acids from food are well established (Deglaire et al. 2009; Elango et al. 2009), there is a need for replicable and fast methods to evaluate protein quality at the molecular level in a wide range of food materials after processing. Additionally, a greater understanding is required of how specific protein

modification profiles change through commercial and domestic processes. This in turn needs to be correlated to the subsequent effects on digestion (Meade et al. 2005). Herein we suggest a proteomic-based approach of coupling *in vitro* digestibility studies to detailed mass spectrometric analysis to achieve comprehensive amino acid damage profiling. There are several different approaches to *in vitro* digestion studies, some using a single enzyme, others employing enzyme combinations. The *in vitro* digestion setup is currently not standardised (Hur et al. 2011), and can range from the use of very sophisticated assay conditions to simple microtitre plate systems.

1.7 Choice of Model System

Egg white (EW) was chosen as a model system as it is often considered the gold standard of protein sources because of high levels of essential amino acids and a high digestibility value (Huopalahti et al. 2007). Egg white is readily available and widely used in food formulations. Moreover, large quantities of purified ovalbumin can be obtained fairly easily. There have been a multitude of both *in vivo* and *in vitro* assays that show consistent results when comparing raw *vs.* boiled egg white digestibility, enabling ready comparison to existing literature methods. *In vivo* studies in humans showed that 91% of boiled egg white was absorbed whereas only 51% of raw egg white was absorbed (Evenepoel et al. 1998). Van der Plancken et al. (2003) found that heating egg white at 75 °C increased the *in vitro* digestibility 4.8 fold after 10 minutes of proteolysis compared to raw egg white (van der Plancken et al. 2003).

1.8 Thesis Objectives

There is a variety of underlying mechanisms that govern food protein aggregation and nutritional value which are not fully understood. This prompted a study to investigate the underlying mechanisms of both protein aggregation and nutritional value changes from a variety of angles.

In the first instance this thesis therefore aims at screening the influence of salt, temperature, and Maillard reaction partners on ovalbumin aggregation structure and

in vitro digestibility. In addition to *in vitro* digestibility further insight into chemical changes during protein processing are of high importance. Therefore, a holistic amino acid modification profile of native *versus* heat denatured egg white, generated through mass spectrometric analysis, is discussed in detail.

The physical aspect of protein aggregate formation is studied at a molecular level using dynamic light scattering (DLS), small angle X-ray scattering (SAXS), and electron microscopy (EM). SAXS is traditionally used for analysis of monodisperse systems. However, here SAXS is evaluated as a technique to assist the analysis of polydisperse, aggregating protein systems using egg white ovalbumin as a model protein.

Finally, a newly proposed food ingredient, i.e. amyloid-like fibrils made from different food protein sources, is studied with regard to protease resistance and toxicity towards human cell lines *in vitro*.

1.9 References

Adibi, S.A. & Morse, E.L., 1971. Intestinal transport of dipeptides in man: relative importance of hydrolysis and intact absorption. *Journal of Clinical Investigation*, 50(11), pp.2266–2275.

Aguilera, J.M., 2005. Why food microstructure? *Journal of Food Engineering*, 67(1-2), pp.3–11.

Alonso, R., Orúe, E. & Marzo, F., 1998. Effects of extrusion and conventional processing methods on protein and antinutritional factor contents in pea seeds. *Food Chemistry*, 63(4), pp.505–512.

Arnaudov, L.N. & de Vries, R., 2005. Thermally induced fibrillar aggregation of hen egg white lysozyme. *Biophysical Journal*, 88(1), pp.515–526.

Arzeni, C., Pérez, O.E. & Pilosof, A.M.R., 2012. Functionality of egg white proteins as affected by high intensity ultrasound. *Food Hydrocolloids*, 29(2), pp.308–316.

Ashokkumar, M., Sunartio, D., Kentish, S., Mawson, R., Simons, L., Vilkhu, K. & Versteeg, C. (Kees), 2008. Modification of food ingredients by ultrasound to improve functionality: a preliminary study on a model system. *Innovative Food Science and Emerging Technologies*, 9(2), pp.155–160.

Barbé, F. et al., 2013. The heat treatment and the gelation are strong determinants of the kinetics of milk proteins digestion and of the peripheral availability of amino acids. *Food Chemistry*, 136(3–4), pp.1203–1212.

Bhat, R. & Karim, A.A., 2009. Ultraviolet irradiation improves gel strength of fish gelatin. *Food Chemistry*, 113(4), pp.1160–1164.

Bintsis, T., Litopoulou-Tzanetaki, E. & Robinson, R.K., 2000. Existing and potential applications of ultraviolet light in the food industry - a critical review. *Journal of the Science of Food and Agriculture*, 80(6), pp.637–645.

Cassens, D., Johnson, E. & Keelan, S., 1996. Enhancing taste, texture, appearance, and presentation of pureed food improved resident quality of life and weight status. *Nutrition Reviews*, 54(1), p.S51.

Chen, L., Remondetto, G.E. & Subirade, M., 2006. Food protein-based materials as nutraceutical delivery systems. *Trends in Food Science and Technology*, 17(5), pp.272–283.

Cobb, N.J. & Surewicz, W.K., 2009. Prion diseases and their biochemical mechanisms. *Biochemistry*, 48(12), pp.2574–2585.

Craft, I.L., Geddes, D., Hyde, C.W., Wise, I.J. & Matthews, D.M., 1968. Absorption and malabsorption of glycine and glycine peptides in man. *Gut*, 9(4), p.425.

Croguennec, T., Nau, F. & Brule, G., 2002. Influence of pH and salts on egg white gelation. *Journal of Food Science*, 67(2), pp.608–614.

Daniel, H., 2004. Molecular and integrative physiology of intestinal peptide transport. *Annual Review of Physiology*, 66(1), pp.361–384.

Deglaire, A., Bos, C., Tomé, D. & Moughan, P.J., 2009. Ileal digestibility of dietary protein in the growing pig and adult human. *British Journal of Nutrition*, 102(12), pp.1752–1759.

Dobson, C.M., 2003. Protein folding and disease: a view from the first horizon symposium. *Nature Reviews. Drug Discovery*, 2(2), pp.154–60.

Dobson, C.M., 2001. The structural basis of protein folding and its links with human disease. *Philosophical Transactions of the Royal Society of London. Series B: Biological Sciences*, 356(1406), pp.133–145.

Dong, A., Prestrelski, S.J., Allison, S.D. & Carpenter, J.F., 1995. Infrared spectroscopic studies of lyophilization- and temperature-induced protein aggregation. *Journal of Pharmaceutical Sciences*, 84(4), pp.415–424.

Eiser, E., Miles, C.S., Geerts, N., Verschuren, P. & MacPhee, C.E., 2009. Molecular cooking: physical transformations in Chinese 'century' eggs. *Soft Matter*, 5(14), pp.2725–2730.

Elango, R., Ball, R.O. & Pencharz, P.B., 2009. Amino acid requirements in humans: with a special emphasis on the metabolic availability of amino acids. *Amino Acids*, 37(1), pp.19–27.

Evenepoel, P., Geypens, B., Luypaerts, A., Hiele, M., Ghoos, Y. & Rutgeerts, P., 1998. Digestibility of cooked and raw egg protein in humans as assessed by stable isotope techniques. *Journal of Nutrition*, 128(10), pp.1716–1722.

Feunteun, S., Barbé, F., Rémond, D., Ménard, O., Gouar, Y., Dupont, D. & Laroche, B., 2013. Impact of the dairy matrix structure on milk protein digestion kinetics: mechanistic modelling based on mini-pig *in vivo* data. *Food and Bioprocess Technology*, In Press.

Fink, A.L., 1998. Protein aggregation: folding aggregates, inclusion bodies and amyloid. *Folding and Design*, 3(1), pp.R9–R23.

Foegeding, E.A., Luck, P.J. & Davis, J.P., 2006. Factors determining the physical properties of protein foams. *Food Hydrocolloids*, 20(2–3), pp.284–292.

Frauenfelder, H., Sligar, S.G. & Wolynes, P.G., 1991. The energy landscapes and motions of proteins. *Science*, 254(5038), pp.1598–1603.

Friedman, M., 1999. Chemistry, biochemistry, nutrition, and microbiology of lysinoalanine, lanthionine, and histidinoalanine in food and other proteins. *Journal of Agricultural and Food Chemistry*, 47(4), pp.1295–1319.

Friedman, M., 1996. Nutritional value of proteins from different food sources. A review. *Journal of Agricultural and Food Chemistry*, 44(1), pp.6–29.

Fürst, P. & Stehle, P., 2004. What are the essential elements needed for the determination of amino acid requirements in humans? *Journal of Nutrition*, 134(6), p.1558S–1565S.

Galazka, V.B., Dickinson, E. & Ledward, D.A., 2000. Effect of high pressure on ovalbumin-polysaccharide interactions. *High Pressure Research: An International Journal*, 19(1), pp.125–130.

Gardner, M.L.G., 1988. Gastrointestinal absorption of intact proteins. *Annual Review of Nutrition*, 8(1), pp.329–350.

Gerrard, J.A. et al., 2012. Aspects of physical and chemical alterations to proteins during food processing - some implications for nutrition. *The British Journal of Nutrition*, 108(S2), pp.S288–297.

Gibbs, B.F., Kermasha, S., Alli, I. & Mulligan, C.N., 1999. Encapsulation in the food industry: a review. *International Journal of Food Sciences and Nutrition*, 50(3), pp.213–224.

Gilbert, E.R., Li, H., Emmerson, D.A., Webb, K.E. & Wong, E.A., 2010. Dietary protein composition influences abundance of peptide and amino acid transporter messenger ribonucleic acid in the small intestine of 2 lines of broiler chicks. *Poultry Science*, 89(8), pp.1663–1676.

Gilbert, E.R., Wong, E.A. & Webb Jr., K.E., 2008. Board-invited review: peptide absorption and utilization: implications for animal nutrition and health. *Journal of Animal Science*, 86(9), pp.2135–2155.

Van der Goot, A.J., Peighambardoust, S.H., Akkermans, C. & van Oosten-Manski, J.M., 2008. Creating novel structures in food materials: the role of well-defined shear flow. *Food Biophysics*, 3(2), pp.120–125.

Gosal, W.S., Clark, A.H. & Ross-Murphy, S.B., 2004. Fibrillar β-lactoglobulin gels: part 1. Fibril formation and structure. *Biomacromolecules*, 5(6), pp.2408–2419.

Gross, M.-L., Piecha, G., Bierhaus, A., Hanke, W., Henle, T., Schirmacher, P. & Ritz, E., 2011. Glycated and carbamylated albumin are more 'nephrotoxic' than unmodified albumin in the amphibian kidney. *American Journal of Physiology - Renal Physiology*, 301(3), pp.F476–F485.

Hamada, D. et al., 2009. Competition between folding, native-state dimerisation and amyloid aggregation in β-lactoglobulin. *Journal of Molecular Biology*, 386(3), pp.878–890.

Hartl, F.U. & Hayer-Hartl, M., 2009. Converging concepts of protein folding *in vitro* and *in vivo*. *Nature Structural and Molecular Biology*, 16(6), pp.574–581.

Hindlet, P. et al., 2009. Reduced intestinal absorption of dipeptides via PepT1 in mice with diet-induced obesity is associated with leptin receptor down-regulation. *Journal of Biological Chemistry*, 284(11), pp.6801 –6808.

Hoppe, A., Jung, S., Patnaik, A. & Zeece, M.G., 2013. Effect of high pressure treatment on egg white protein digestibility and peptide products. *Innovative Food Science and Emerging Technologies*, 17(1), pp.54–62.

Huopalahti, R., López-Fandiño, R., Anton, M. & Schade, R., 2007. *Bioactive egg compounds*, Berlin: Springer.

Hur, S.J., Lim, B.O., Decker, E.A. & McClements, D.J., 2011. *In vitro* human digestion models for food applications. *Food Chemistry*, 125(1), pp.1–12.

Ipsen, R., Otte, J. & Qvist, K.B., 2001. Molecular self-assembly of partially hydrolysed α-lactalbumin resulting in strong gels with a novel microstructure. *Journal of Dairy Research*, 68(2), pp.277–286.

Khurana, R., Gillespie, J.R., Talapatra, A., Minert, L.J., Ionescu-Zanetti, C., Millett, I. & Fink, A.L., 2001. Partially folded intermediates as critical precursors of light chain amyloid fibrils and amorphous aggregates. *Biochemistry*, 40(12), pp.3525–3535.

Kim, E.H.-J., Chen, X.D. & Pearce, D., 2002. Surface characterization of four industrial spray-dried dairy powders in relation to chemical composition, structure and wetting property. *Colloids and Surfaces B: Biointerfaces*, 26(3), pp.197–212.

Koike, A., Nemoto, N. & Doi, E., 1996. Structure and dynamics of ovalbumin gels: 1. Gel induced by high-temperature heat treatment. *Polymer*, 37(4), pp.587–593.

Kowalczuk, S., Bröer, A., Tietze, N., Vanslambrouck, J.M., Rasko, J.E.J. & Bröer, S., 2008. A protein complex in the brush-border membrane explains a Hartnup disorder allele. *FASEB Journal*, 22(8), pp.2880 –2887.

Krebs, M.R.. et al., 2000. Formation and seeding of amyloid fibrils from wild-type hen lysozyme and a peptide fragment from the β-domain. *Journal of Molecular Biology*, 300(3), pp.541–549.

Lesmes, U. & McClements, D.J., 2009. Structure-function relationships to guide rational design and fabrication of particulate food delivery systems. *Trends in Food Science and Technology*, 20(10), pp.448–457.

Levesque, C.L., Moehn, S., Pencharz, P.B. & Ball, R.O., 2010. Review of advances in metabolic bioavailability of amino acids. *Livestock Science*, 133(1-3), pp.4–9.

Licciardello, F., Frisullo, P., Laverse, J., Muratore, G. & Del Nobile, M.A., 2012. Effect of sugar, citric acid and egg white type on the microstructural and mechanical properties of meringues. *Journal of Food Engineering*, 108(3), pp.453–462.

Linse, S. et al., 2007. Nucleation of protein fibrillation by nanoparticles. *Proceedings of the National Academy of Sciences of the United States of America*, 104(21), pp.8691–8696.

Liu, J., Ru, Q. & Ding, Y., 2012. Glycation a promising method for food protein modification: physicochemical properties and structure, a review. *Food Research International*, 49(1), pp.170–183.

Livney, Y.D., 2010. Milk proteins as vehicles for bioactives. *Current Opinion in Colloid and Interface Science*, 15(1–2), pp.73–83.

Loveday, S.M., Rao, M.A., Creamer, L.K. & Singh, H., 2009. Factors affecting rheological characteristics of fibril gels: the case of β-lactoglobulin and α-lactalbumin. *Journal of Food Science*, 74(3), pp.47–55.

Loveday, S.M., Wang, X.L., Rao, M.A., Anema, S.G., Creamer, L.K. & Singh, H., 2010. Tuning the properties of β-lactoglobulin nanofibrils with pH, NaCl and $CaCl_2$. *International Dairy Journal*, 20(9), pp.571–579.

Lucey, J.A., 2002. Formation and physical properties of milk protein gels. *Journal of Dairy Science*, 85(2), pp.281–294.

Manski, J.M., van der Goot, A.J. & Boom, R.M., 2007. Advances in structure formation of anisotropic protein-rich foods through novel processing concepts. *Trends in Food Science and Technology*, 18(11), pp.546–557.

Manzocco, L., Panozzo, A. & Nicoli, M.C., 2012. Effect of ultraviolet processing on selected properties of egg white. *Food Chemistry*, 135(2), pp.522–527.

Matalanis, A., Jones, O.G. & McClements, D.J., 2011. Structured biopolymer-based delivery systems for encapsulation, protection, and release of lipophilic compounds. *Food Hydrocolloids*, 25(8), pp.1865–1880.

Meade, S.J., Reid, E.A. & Gerrard, J.A., 2005. The impact of processing on the nutritional quality of food proteins. *Journal of AOAC International*, 88(3), pp.904–922.

Mishra, R.S. et al., 2004. Protease-resistant human prion protein and ferritin are cotransported across Caco-2 epithelial cells: implications for species barrier in prion uptake from the intestine. *Journal of Neuroscience*, 24(50), pp.11280–11290.

Molina, E., Papadopoulou, A. & Ledward, D.A., 2001. Emulsifying properties of high pressure treated soy protein isolate and 7S and 11S globulins. *Food Hydrocolloids*, 15(3), pp.263–269.

Needs, E.C., Stenning, R.A., Gill, A.L., Ferragut, V. & Rich, G.T., 2000. High-pressure treatment of milk: effects on casein micelle structure and on enzymic coagulation. *Journal of Dairy Research*, 67(01), pp.31–42.

Nesterenko, A., Alric, I., Silvestre, F. & Durrieu, V., 2013. Vegetable proteins in microencapsulation: a review of recent interventions and their effectiveness. *Industrial Crops and Products*, 42, pp.469–479.

Newey, H. & Smyth, D.H., 1960. Intracellular hydrolysis of dipeptides during intestinal absorption. *Journal of Physiology*, 152(2), pp.367–380.

Nicolai, T., Britten, M. & Schmitt, C., 2011. β-lactoglobulin and WPI aggregates: formation, structure and applications. *Food Hydrocolloids*, 25(8), pp.1945–1962.

Nielsen, P.M., Petersen, D. & Dambmann, C., 2001. Improved method for determining food protein degree of hydrolysis. *Journal of Food Science*, 66(5), pp.642–646.

Onuchic, J.N., Luthey-Schulten, Z. & Wolynes, P.G., 1997. Theory of protein folding: the energy landscape perspective. *Annual Review of Physical Chemistry*, 48(1), pp.545–600.

Otzen, D.E. et al., 2007. Aggregation and fibrillation of bovine serum albumin. *Biochimica et Biophysica Acta - Proteins & Proteomics*, 1774(9), pp.1128–1138.

Pearce, F.G., Mackintosh, S.H. & Gerrard, J.A., 2007. Formation of amyloid-like fibrils by ovalbumin and related proteins under conditions relevant to food processing. *Journal of Agricultural and Food Chemistry*, 55(2), pp.318–322.

Pedersen, J.S., 2010. The nature of amyloid-like glucagon fibrils. *Journal of Diabetes Science and Technology*, 4(6), pp.1357–1367.

Pernell, C.W., Foegeding, E.A., Luck, P.J. & Davis, J.P., 2002. Properties of whey and egg white protein foams. *Colloids and Surfaces A: Physicochemical and Engineering Aspects*, 204(1–3), pp.9–21.

Van der Plancken, I., Delattre, M., Indrawati, Van Loey, A. & Hendrickx, M.E.G., 2004. Kinetic study on the changes in the susceptibility of egg white proteins to enzymatic hydrolysis induced by heat and high hydrostatic pressure pretreatment. *Journal of Agricultural and Food Chemistry*, 52(18), pp.5621–5626.

Van der Plancken, I., Van Remoortere, M., Indrawati, Van Loey, A. & Hendrickx, M.E., 2003. Heat-induced changes in the susceptibility of egg white proteins to enzymatic hydrolysis: a kinetic study. *Journal of Agricultural and Food Chemistry*, 51(13), pp.3819–3823.

Purwanti, N., van der Goot, A.J., Boom, R. & Vereijken, J., 2010. New directions towards structure formation and stability of protein-rich foods from globular proteins. *Trends in Food Science and Technology*, 21(2), pp.85–94.

Rampon, V., Robert, P., Nicolas, N. & Dufour, E., 1999. Protein structure and network orientation in edible films prepared by spinning process. *Journal of Food Science*, 64(2), pp.313–316.

Rao, S.P., Meade, S.J., Healy, J.P., Sutton, K.H., Larsen, N.G., Staiger, M.P. & Gerrard, J.A., 2012. Amyloid fibrils as functionalizable components of nanocomposite materials. *Biotechnology Progress*, 28(1), pp.248–256.

Relkin, P. & Shukat, R., 2012. Food protein aggregates as vitamin-matrix carriers: impact of processing conditions. *Food Chemistry*, 134(4), pp.2141–2148.

Renkema, J.M.S., Gruppen, H. & van Vliet, T., 2002. Influence of pH and ionic strength on heat-induced formation and rheological properties of soy protein gels in relation

to denaturation and their protein compositions. *Journal of Agricultural and Food Chemistry*, 50(21), pp.6064–6071.

Robbins, K.R., Baker, D.H. & Finley, J.W., 1980. Studies on the utilization of lysinoalanine and lanthionine. *Journal of Nutrition*, 110(5), pp.907–915.

Roberts, C.J., 2007. Non-native protein aggregation kinetics. *Biotechnology and Bioengineering*, 98(5), pp.927–938.

Rubio-Aliaga, I. & Daniel, H., 2002. Mammalian peptide transporters as targets for drug delivery. *Trends in Pharmacological Sciences*, 23(9), pp.434–440.

Rutherfurd, S.M. & Moughan, P.J., 2012. Available versus digestible dietary amino acids. *British Journal of Nutrition*, 108(S2), pp.S298–S305.

Rutherfurd, S.M. & Moughan, P.J., 2008. Determination of sulfur amino acids in foods as related to bioavailability. *Journal of AOAC International*, 91(4), pp.907–913.

Šebeková, K. & Somoza, V., 2007. Dietary advanced glycation endproducts (AGEs) and their health effects – PRO. *Molecular Nutrition and Food Research*, 51(9), pp.1079–1084.

Sodini, I., Remuef, F., Haddad, S. & Corriue, G., 2004. The relative effect of milk base, starter, and process on yogurt texture: a review. , 44(2), pp.113 – 137.

Spence, C., Levitan, C.A., Shankar, M.U. & Zampini, M., 2010. Does food color influence taste and flavor perception in humans? *Chemosensory Perception*, 3(1), pp.68–84.

Stefani, M. & Dobson, C.M., 2003. Protein aggregation and aggregate toxicity: new insights into protein folding, misfolding diseases and biological evolution. *Journal of Molecular Medicine*, 81(11), pp.678–699.

Steinhardt, H.J. & Adibi, S.A., 1986. Kinetics and characteristics of absorption from an equimolar mixture of 12 glycyl-dipeptides in human jejunum. *Gastroenterology*, 90(3), p.577.

Takagi, K., Teshima, R., Okunuki, H. & Sawada, J.-I., 2003. Comparative study of *in vitro* digestibility of food proteins and effect of preheating on the digestion. *Biological and Pharmaceutical Bulletin*, 26(7), pp.969–973.

Tang, C.-H., Zhang, Y.-H., Wen, Q.-B. & Huang, Q., 2010. Formation of amyloid fibrils from kidney bean 7S globulin (phaseolin) at pH 2.0. *Journal of Agricultural and Food Chemistry*, 58(13), pp.8061–8068.

Ubbink, J., 2012. Soft matter approaches to structured foods: from 'cook-and-look' to rational food design? *Faraday Discussions*, 158, pp.9–35.

Veerman, C., Sagis, L.M.C., Heck, J. & Van Der Linden, E., 2003a. Mesostructure of fibrillar bovine serum albumin gels. *International Journal of Biological Macromolecules*, 31(4-5), pp.139–146.

Veerman, C., de Schiffart, G., Sagis, L.M.C. & van der Linden, E., 2003b. Irreversible self-assembly of ovalbumin into fibrils and the resulting network rheology. *International Journal of Biological Macromolecules*, 33(1-3), pp.121–127.

Wang, J.-M., Yang, X.-Q., Yin, S.-W., Yuan, D.-B., Xia, N. & Qi, J.-R., 2011. Growth kinetics of amyloid-like fibrils derived from individual subunits of soy β-conglycinin. *Journal of Agricultural and Food Chemistry*, 59(20), pp.11270–11277.

Wang, Q. & Ismail, B., 2012. Effect of Maillard-induced glycosylation on the nutritional quality, solubility, thermal stability and molecular configuration of whey protein. *International Dairy Journal*, 25(2), pp.112–122.

Wang, W., Nema, S. & Teagarden, D., 2010. Protein aggregation-pathways and influencing factors. *International Journal of Pharmaceutics*, 390(2), pp.89–99.

Webb, K.E., 1990. Intestinal absorption of protein hydrolysis products: a review. *Journal of Animal Science*, 68(9), pp.3011–3022.

Webb, K.E., Matthews, J.C. & DiRienzo, D.B., 1992. Peptide absorption: a review of current concepts and future perspectives. *Journal of Animal Science*, 70(10), pp.3248–3257.

Weijers, M., van de Velde, F., Stijnman, A., van de Pijpekamp, A. & Visschers, R., 2006. Structure and rheological properties of acid-induced egg white protein gels. *Food Hydrocolloids*, 20(2-3), pp.146–159.

Weiss, W.F., Hodgdon, T.K., Kaler, E.W., Lenhoff, A.M. & Roberts, C.J., 2007. Nonnative protein polymers: structure, morphology, and relation to nucleation and growth. *Biophysical Journal*, 93(12), pp.4392–4403.

Westerterp-Plantenga, M.S., Lemmens, S.G. & Westerterp, K.R., 2012. Dietary protein – its role in satiety, energetics, weight loss and health. *British Journal of Nutrition*, 108(S2), pp.S105–S112.

Whittingham, J.L., Scott, D.J., Chance, K., Wilson, A., Finch, J., Brange, J. & Guy Dodson, G., 2002. Insulin at pH 2: structural analysis of the conditions promoting insulin fibre formation. *Journal of Molecular Biology*, 318(2), pp.479–490.

Yang, X., Berry, T.K. & Foegeding, E.A., 2009. Foams prepared from whey protein isolate and egg white protein: 1. Physical, microstructural, and interfacial properties. *Journal of Food Science*, 74(5), pp.E259–E268.

Yoshino, K., Sakai, K., Mizuha, Y., Shimizuike, A. & Yamamoto, S., 2004. Peptic digestibility of raw and heat-coagulated hen's egg white proteins at acidic pH range. *International Journal of Food Sciences and Nutrition*, 55(8), pp.635–640.

Chapter Two

2 Structure and Digestibility of Egg White Aggregates

2.1 Introduction

The structure-function relationship of protein in food has been studied extensively. The focus of these studies often lies on the formation and stability of protein gels because they are widely used in food formulations (Giosafatto et al. 2012; Loveday et al. 2009; Lucey 2002; Nicolai et al. 2011; Renkema et al. 2002). In general, the gel structure can be controlled by controlling the molecular protein structure. This is usually achieved by protein denaturing methods (e.g., heat, pressure, ultrasound, etc.), additives (e.g., salt, carbohydrates, lipid), pH adjustment, and (non-) enzymatic protein hydrolysis and cross-linking (Unterhaslberger et al. 2006). Depending on the chosen parameters, the resulting protein aggregates often differ markedly in their physicochemical properties and form different gel structures. The incentives for optimising the protein gel structure are diverse. They include improvement of texture as well as the controlling of flavour and nutrient release.

The relationship between protein structure and protein digestibility is currently not completely understood. This chapter introduces the effects of some of the most commonly studied protein denaturing parameters on protein structure. This will be followed by an analysis of egg white (EW) protein to probe the relationship between structure and digestibility. Figure 1.1 shows the intricate relationship between the protein structure, the chemical modifications, and nutritional value.

2.1.1 Protein Structure – Salt

Salt affects water structure and in turn affects solubilised protein in aqueous solutions. The water that interacts with proteins can be categorised into internal water, hydration shell, and bulk water (Russo 2008). The internal water is often a functional part of the protein. The hydration shell is a 2-3 water molecule thick water layer that is strongly associated with the protein due to electrostatic interactions. Bulk water is the water surrounding this hydration shell (Figure 2.1) (Russo 2008).

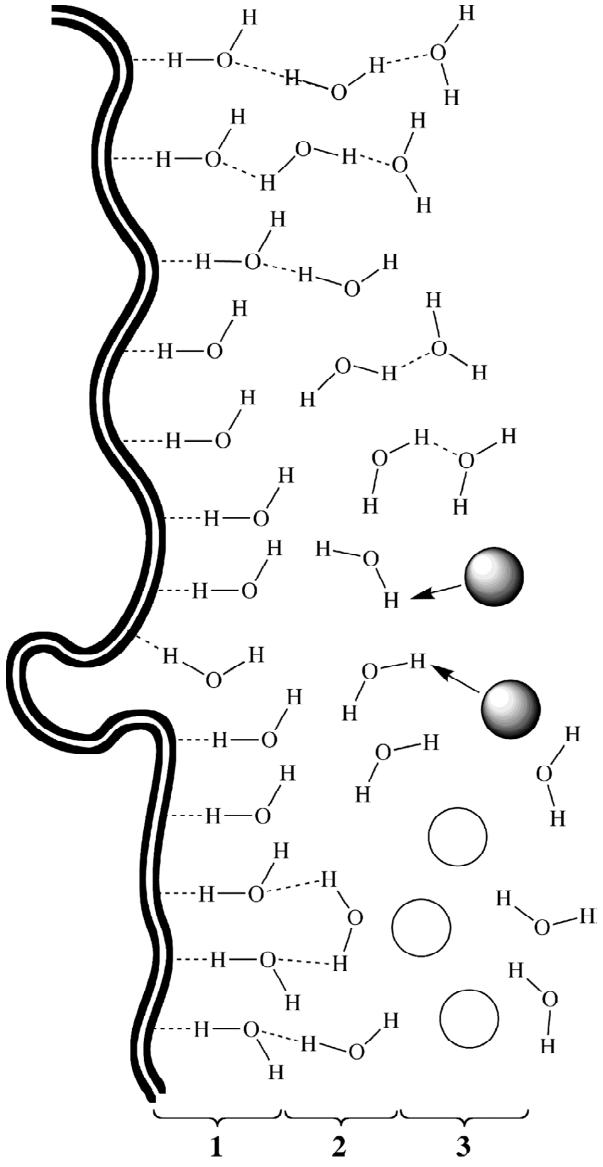

Figure 2.1 *The three layers of the water hydration shell around a protein. 1) solvation layer, 2) transition layer, 3) bulk layer. Ions (kosmotrope = dark spheres and chaotrope = white spheres). Schematic taken from (Lo Nostro & Ninham 2012)*

Salts may influence the structure and dynamics of the hydration shell and thereby influence protein stability and eventually the aggregation of proteins (Russo 2008). Kosmotropic (order making) salts have a stabilising effect on proteins whilst chaotropic (disorder making) salts may act to destabilise proteins in solution. Kosmotropes increase, and chaotropes decrease the viscosity of water compared to pure water (Lo Nostro & Ninham 2012). Kosmotropes build strong hydrogen bond networks and thus increase surface tension compared to pure water. The increased polarity of the water results in stronger hydrophobic interactions within proteins (Zhang & Cremer 2006). Protein stabilisation using kosmotropes such as sulfate (SO_4^{2-}) and ammonium (NH_4^+) ions even persists at high kosmotrope concentrations (e.g., for salting out a protein). During salting out the proteins retain their native structure. Chaotropes on the other hand weaken the polarity of water and thus favour a more flexible protein due to a decreased hydrophobic effect. As a result, chaotropes tend to denature proteins (Zhang & Cremer 2006).

The Hofmeister series (Figure 2.2) ranks common salts based on their ability to precipitate (salt out) proteins from solution whilst keeping them intact (i.e., non-denatured) (Curtis et al. 2002; Lo Nostro & Ninham 2012; Zhang & Cremer 2006). It is worth noting that for some proteins (e.g. lysozyme) the Hofmeister series is true above the isoelectric point (IEP) of a protein but follows the reverse order below the isoelectric point of a protein (Lo Nostro & Ninham 2012).

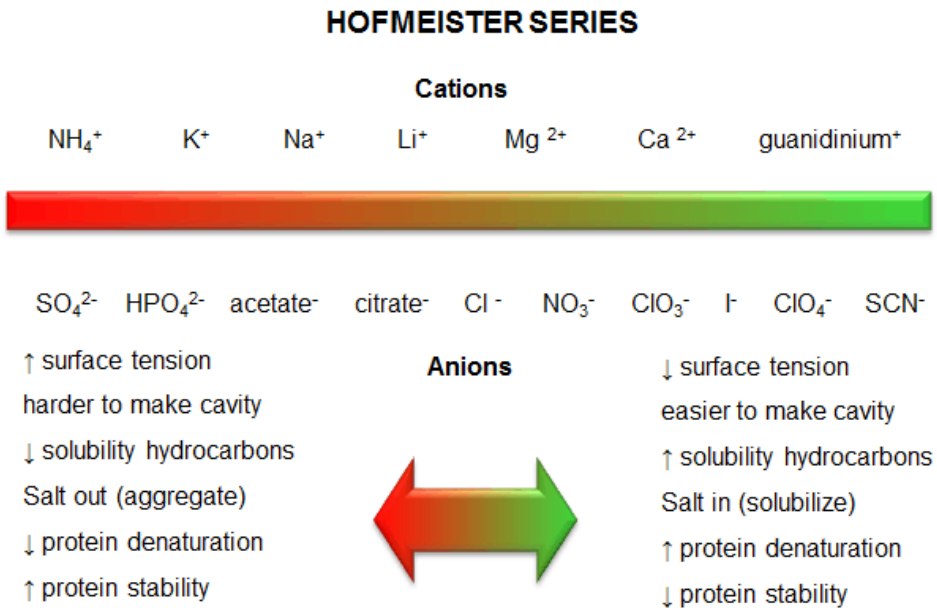

Figure 2.2 *Hofmeister series of cations and anions with regard to up- or down regulation of surface tension, solubility of hydrocarbons, protein denaturation and protein stability. Diagram taken from (Zhang & Cremer 2006).*

When studying protein aggregation in the context of food systems, it is therefore important to be aware of possible salt effects. Slight disruption of finely balanced salt composition of biological systems, including proteins, may cause stress (Lo Nostro & Ninham 2012).

Measuring the effect of salt on the aggregation of specific proteins is challenging. β-Lg is a well characterised food protein with an isoelectric point of 5.1 (Nicolai et al. 2011). At pH 7 the addition of salt to native β-lg was reported to induce aggregation. $CaCl_2$ was reported to have induced a much stronger protein aggregation compared to NaCl. This is in good agreement with the Hofmeister series as Ca^{2+} promotes protein denaturation more than Na^+ (Figure 2.2). At a pH close to the IEP the addition of NaCl decreased β-lg aggregation. At pH 2 the addition of NaCl increased aggregation (Nicolai et al. 2011; Unterhaslberger et al. 2006).

The inter-particle distance of ovalbumin has been reported to decrease due to addition of 100 mM salt (Ianeselli et al. 2010; Sugiyama et al. 2001), thereby facilitating aggregation in the presence of salt. In the cited papers the electrostatic shielding of NaCl was deemed responsible for the decrease of inter-protein distances. Heat denatured ovalbumin has been

shown to increase in size at different rates depending on the type of anion present (Shirai et al. 1997). Interestingly, there was an observed Hofmeister relationship between aggregate size and the type of anion present, where sulfate ions strongly promoted aggregate size increase. This work includes 100 mM NaCl as a salt control. NaCl is widely used in food and a comparatively neutral salt (middle of the Hofmeister series). The concentration has previously been shown to decrease inter-protein distance by electrostatic shielding (Ianeselli et al. 2010; Sugiyama et al. 2001).

2.1.2 Protein Structure – pH

The pH of protein solutions is also important for protein stability. Changes in pH cause changes in the protein net charge. The net charge changes because the amino acids of the protein become protonated (below the IEP) or deprotonated (above the IEP), as shown in Figure 2.3.

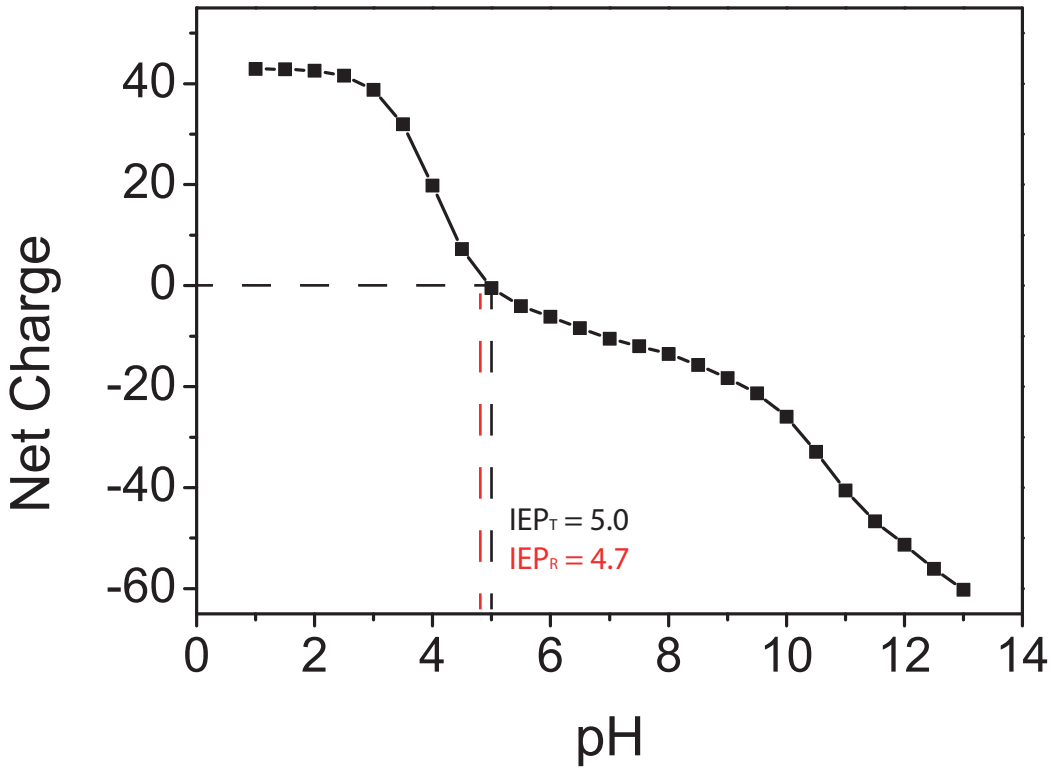

Figure 2.3 *The theoretical isoelectric point of ovalbumin is 5.0 (real IEP is 4.7) at which the protein is uncharged. All theoretical values were determined based on* pK_a *values of amino acid residues using* the *EMBOSS software suite* ***(Rice et al. 2000).***

The calculated theoretical IEP (IEP = 5.0) is slightly higher than the experimentally determined IEP of 4.7 (Grinberg et al. 1988). The discrepancy between theoretical and experimental IEP may be due to residue modifications, such as phosphorylation of serine residues. A higher degree of phosphorolyation results in the decrease of the IEP. Previous studies have reported three ovalbumin species with either two, one, or no phosphorylated serine residues (Kinoshita-Kikuta et al. 2012; Grinberg et al. 1988).

The protein net-charge determines the resulting Coulomb repulsion of proteins in solution. At the isoelectric point the Coulomb repulsion between proteins is smallest. This can lead to aggregation of proteins. The required protein gelation concentration (c_g) is often directly proportional to the net charge (i.e., the electrostatic repulsion) of the proteins in solution (Nicolai et al. 2011). At pH values far away from the IEP the net charge increases and results in protein-protein repulsion. It has been reported that ovalbumin at pH 2 and in the presence of K_2SO_4 retains native-like secondary elements whilst undergoing a conformational change of the tertiary structure as assessed by 8-anilinonaphthalene-1-sulfonic acid (ANS) fluorescence (Naeem et al. 2010). In an early study on the viscoelastic properties of ovalbumin it was reported that gel elasticity was weak at pHs close to the IEP (4.7) and increased far away from this pH (pH 2.5 - 4 and pH 5.5 - 10) for gels formed at 80 °C (Grinberg et al. 1988). For samples near the IEP the heating temperatures had to be increased to 105 °C in order to achieve similar gel elasticity. A similar effect of pH dependence on gelling was observed in a mixture of ovalbumin and ovotransferrin. The study showed that the formed gels were stable between pH 2.0 and 4.0 and pH 7.0 - 11.0 (Hu et al. 2007). Since gels were stable at acidic and basic pH, the gels were proposed as drug delivery matrices with amphoteric character (Hu et al. 2007). It was observed in a study at low pH and low ionic strengths that transparent gels were formed after heating to 80 °C at pH 2 - 3 and low ionic strength (0 mM - 15 mM), whereas turbid gels formed at high pH values. The authors proposed that the difference in transparency is caused by the underlying structural differences (Weijers et al. 2002).

2.1.3 Protein Structure – Temperature

High average kinetic energies of molecules at elevated temperatures may cause protein unfolding. At high temperatures, increased molecular dynamics and a higher diffusion rate may contribute to unfolding and aggregation of proteins (Wang et al. 2010). There is usually one specific temperature at which a given protein is most stable in its native state (if ionic strength and pH are held constant). This temperature is sometimes referred to as the maximum unfolding temperature ($T_{\Delta G=Max}$) based on the free energy change between native and unfolded state (Rees & Robertson 2001). At any other temperature, denaturation is more likely to occur. Denaturation is commonly associated with elevated temperatures which often entail irreversible protein denaturation followed by aggregation. Interestingly, temperatures below ($T_{\Delta G=Max}$) may destabilise proteins too (Rees & Robertson 2001; Wang et al. 2010).

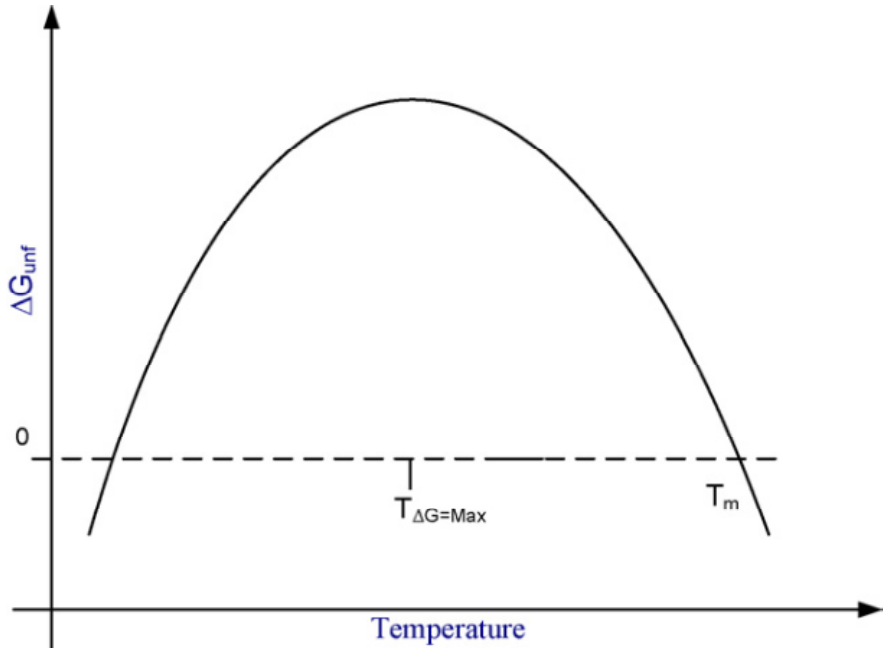

Figure 2.4 *Change of free energy required for unfolding of a protein (ΔG_{unf}) plotted against temperature. T_m is the melting temperature of the protein. Diagram taken from (Wang et al. 2010).*

Temperature increase is probably the most common cause for protein aggregation. It is used ubiquitously during domestic and industrial food processing. Temperature and duration of heat application both influence gel formation and stability (Grinberg et al. 1988).

2.1.4 Protein Structure – Maillard Reaction

The Maillard reaction is the reaction between the aldehyde of a sugar or lipid predominantly with the ε-NH_2 group of lysine residues and N-termini of proteins to form an imine bond (Figure 2.5). The formation of the imine bond is reversible. However, in an isomerisation reaction the more stable Amadori rearrangement takes place. Compared to lysine, histidine and arginine residues are weaker nucleophiles and therefore the glycation reaction is slower.

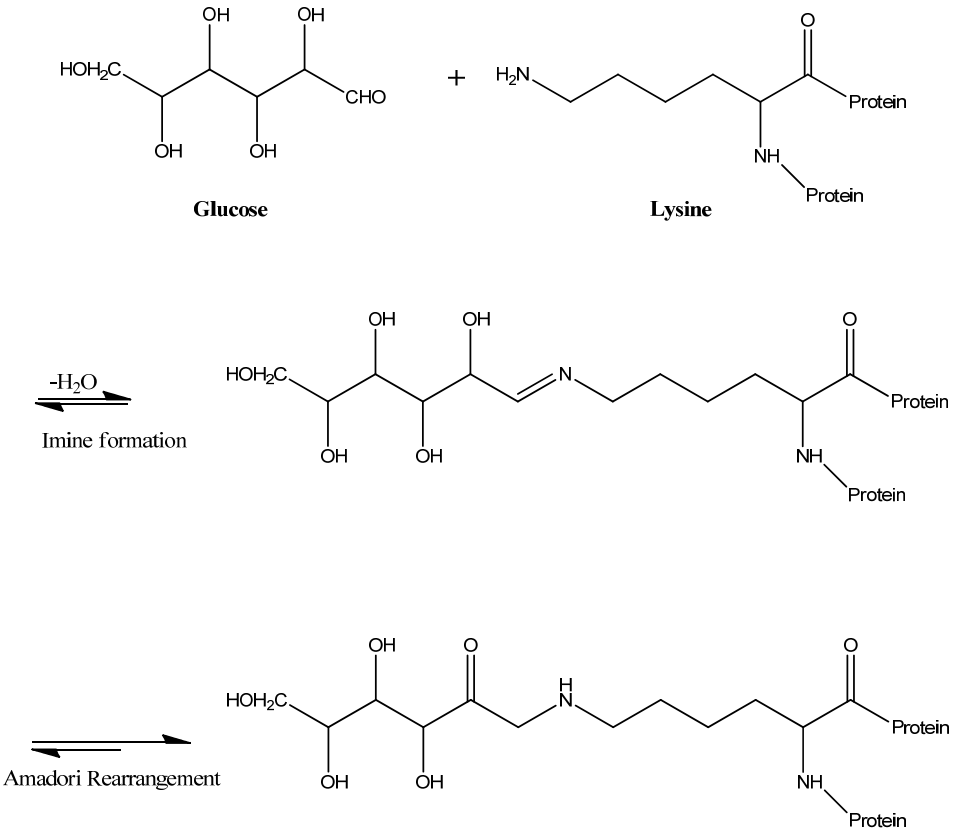

Figure 2.5 *Glycation reaction of the aldehyde group of glucose with the ε-amino group of lysine as an example for Maillard reaction. The mechanism for the studied reaction partners (glucose, fructose, lactose, methylglyoxal, and glutaraldehyde) follows this pattern.*

Following the Amadori rearrangement there are several chemical reactions that may lead to the formation of advanced glycation end products (AGEs) which are associated with food browning and aroma development (Fay & Brevard 2005). These reactions have been summarised in Hodge's reaction scheme for the Maillard reaction (Hodge 1953) (Figure 2.6).

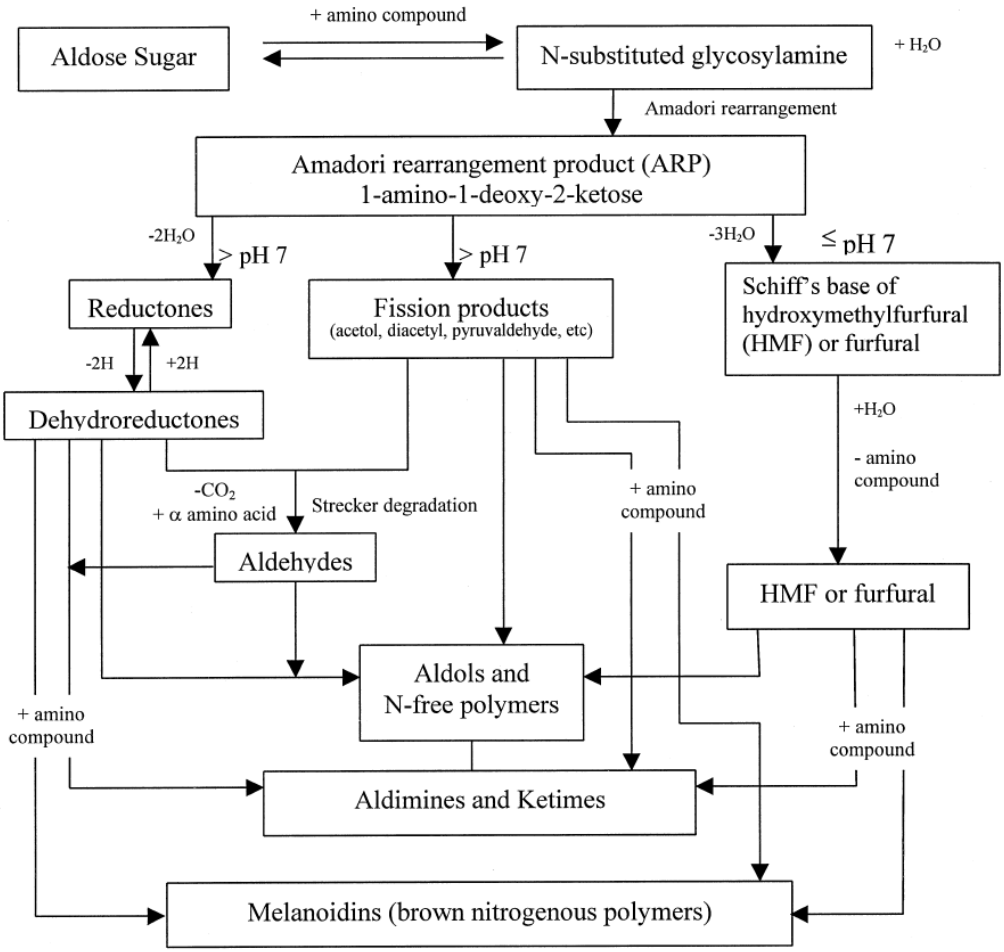

Figure 2.6 *Maillard reaction progression after Hodge. Diagram from (Martins et al. 2000).*

In recent years it has been acknowledged that the Maillard reaction has the potential to be harnessed as a means to adjust and improve food protein structure (Gerrard et al. 2002; Liu et al. 2012a; Oliver et al. 2006). Protein glycation has been reported to improve protein solubility, emulsifying, foaming, and textural properties (Liu et al. 2012a). The increase of protein solubility has been reported for insoluble fish and shellfish muscle proteins (Saeki & Inoue 1997). It has been suggested that steric bulk and the loss of filament formation ability may have been the cause of an increased solubility (Katayama et al. 2002). Glycated whey protein isolate (WPI) was also reported to have a higher solubility, even around the IEP, compared to non-glycated WPI (Wang & Ismail 2012). A higher degree of emulsifying activity (and increased solubility) can be obtained by glycating milk, egg white, or rice protein with glucose, lactose, maltodextrin, dextran, or pectin (Al-Hakkak & Al-Hakkak 2010; Al-Hakkak & Kavale 2002; Li et al. 2009; Li et al. 2013). Moreover, the

foaming properties can be improved by conjugating protein (egg white, milk, and peanut protein) with different saccharides (Corzo-Martínez et al. 2012a; Corzo-Martínez et al. 2012b; Haar et al. 2011; Liu et al. 2012b).

This work focused on a range of Maillard reaction partners and their effect on protein digestibility and structure. The Maillard reaction partners were glucose, fructose, lactose, methylglyoxal, and glutaraldehyde (Figure 2.7). All of these compounds have been shown to react with lysine residues in Maillard reactions (Yeboah et al. 1999; Meltretter et al. 2007; Jumnongpon et al. 2012; Meade et al. 2003). Glucose, fructose, and lactose are widely used in food formulations.

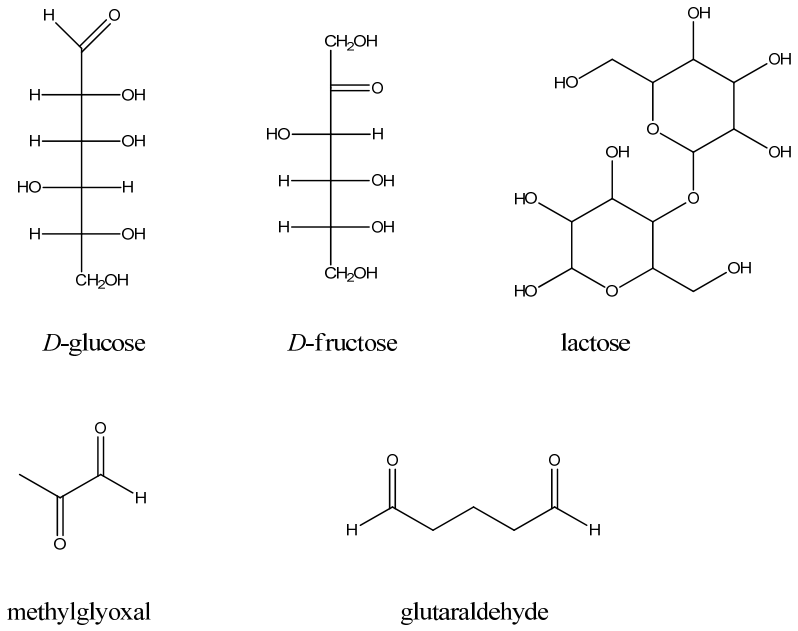

Figure 2.7 *Chemical structure of studied Maillard reaction partners.*

Methylglyoxal and glutaraldehyde are two model Maillard reaction partners which have been reported previously to quickly react with protein and to contribute to protein cross-linking via the Maillard reaction (Meade et al. 2003). Methylglyoxal (reaction mechanism shown in Figure 2.8) is a degradation product of glucose and has also been reported to be present in honey (Mavric et al. 2008; Lima et al. 2009). Glutaraldehyde is not currently approved as a food ingredient (Augustin & Hemar 2009) but is commonly used as a model protein cross-linker (Payne 1973; Gerrard et al. 2003; Fadouloglou et al. 2008; Tong et al. 2008; Jumnongpon et al. 2012).

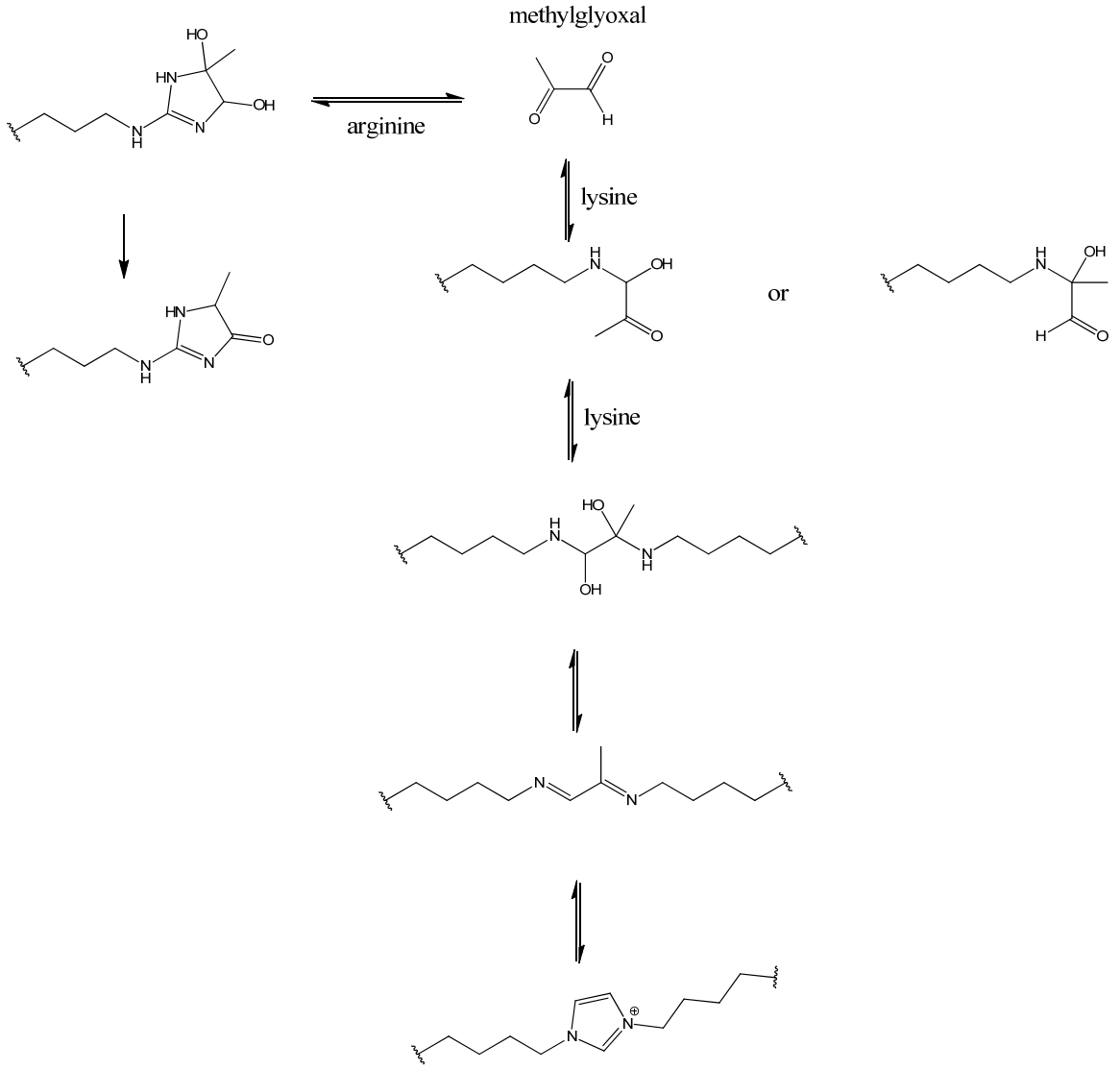

Figure 2.8 *Schematic of reaction mechanism of methylglyoxal with lysine and arginine residues that can lead to protein cross-linking. Diagram adapted from (Bechara et al. 2007; Lima et al. 2009).*

2.2 Effect of Protein Structure on Protein Digestibility

Protein aggregate structure may affect protein digestibility (Sections 1.5). Unravelling the relationship between aggregate structure and nutritional value is of interest because it may affect decisions about food preparation and food intake. This section investigates the relationship between protein structure and protein digestibly using an *in vitro* model. Because salt, pH, temperature, and the Maillard reaction all markedly impact on protein structure, these four factors were included when assessing the structure/digestibility relationship. Chicken egg white (EW) was used as a model system. The differently treated EW gels were then tested for resistance to degradation by pepsin and pancreatin *in vitro*.

In a first step, fresh EW was adjusted to five different pH levels (2, 5, 7, 9, 12) in the presence and absence of 200 mM salt (10 samples total). The experimental conditions were chosen to represent a wide range of food products likely to be encountered in a regular diet. In general, natural and processed foods are acidic. Examples include fruit and vegetables (pH 3-5), but also yoghurt, milk, and butter (pH 3-6) (Gabriel 2008). Egg white is slightly alkaline (pH 8). Century eggs (pH 12), a traditional Chinese delicacy, are an example of a strong alkaline food (Eiser et al. 2009). The recommended daily salt intake for healthy adult humans is 1.5 g of sodium per day with an upper limit of 2.3 g of sodium per day (National Research Council 2005). This equates to about 125 mL to 200 mL of a 200 mM NaCl solution. It has been reported that up to 77 % of salt intake derives from processed rather than from natural foods (Mattes & Donnelly 1991).

Figure 2.9 shows the ten EW samples before and after heat treatment. The heated samples display a heterogeneous series with gels of varying consistency and colour indicating different underlying protein network structure.

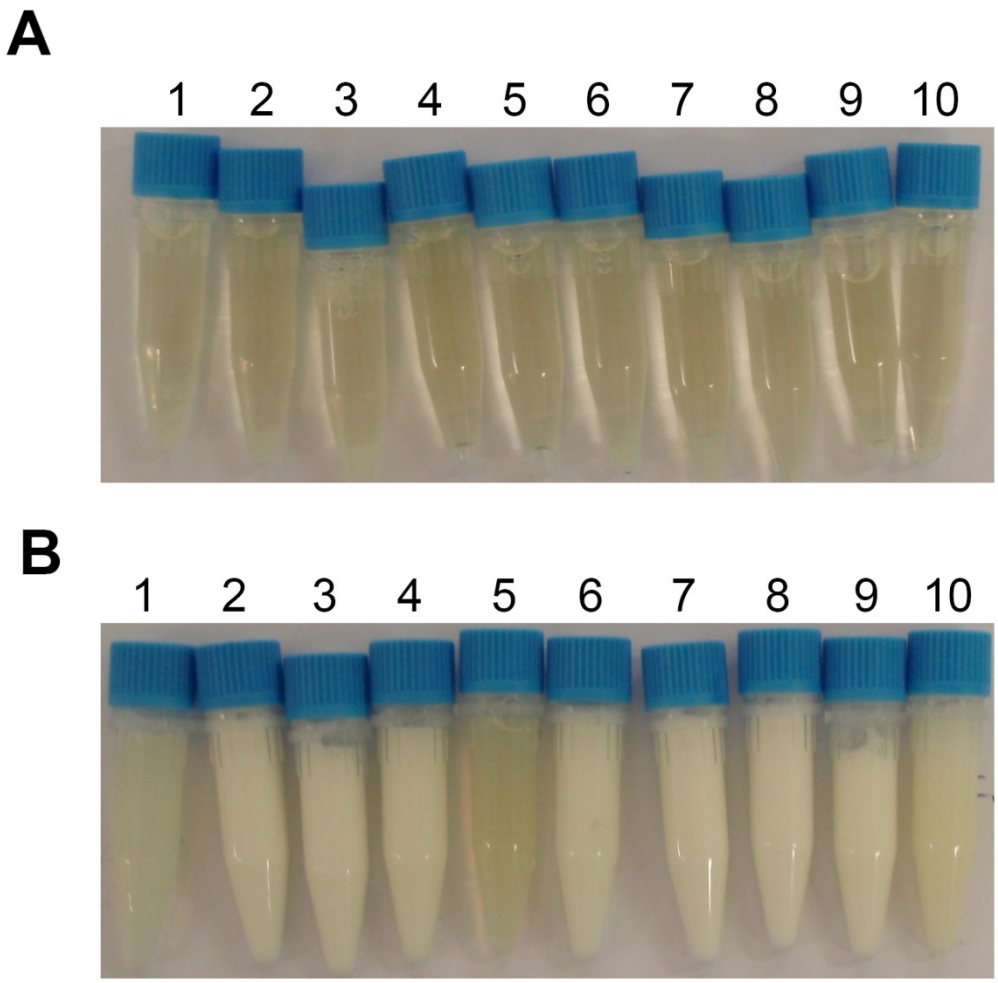

Figure 2.9 *A) raw EW; B) boiled EW. 1) pH 2; 2) pH 2, 200 mM NaCl; 3) pH 5; 4) pH 5, 200 mM NaCl; 5) pH 7; 6) pH 7, 200 mM NaCl; 7) pH 9; 8) pH 9, 200 mM NaCl; 9) pH 12; 10) pH 12, 200 mM NaCl.*

The unheated samples were analysed by scanning electron microscopy (SEM) before digestion (Figure 2.10). The micrographs are the result of snap freezing liquid egg white samples and subsequent freeze drying. Due to possible freezing artefacts the shown structures may therefore not represent the exact *in situ* structure of the different egg white solutions. However, the distinct differences in the observed protein structure indicate that there is a pH and salt dependent structural effect. There are marked structural differences between samples. At low pH the EW protein structure is coarse with fine pores. The pore size changes with increasing pH to a smooth and wider pored structure. The inclusion of 200 mM salt also promotes smoother structures.

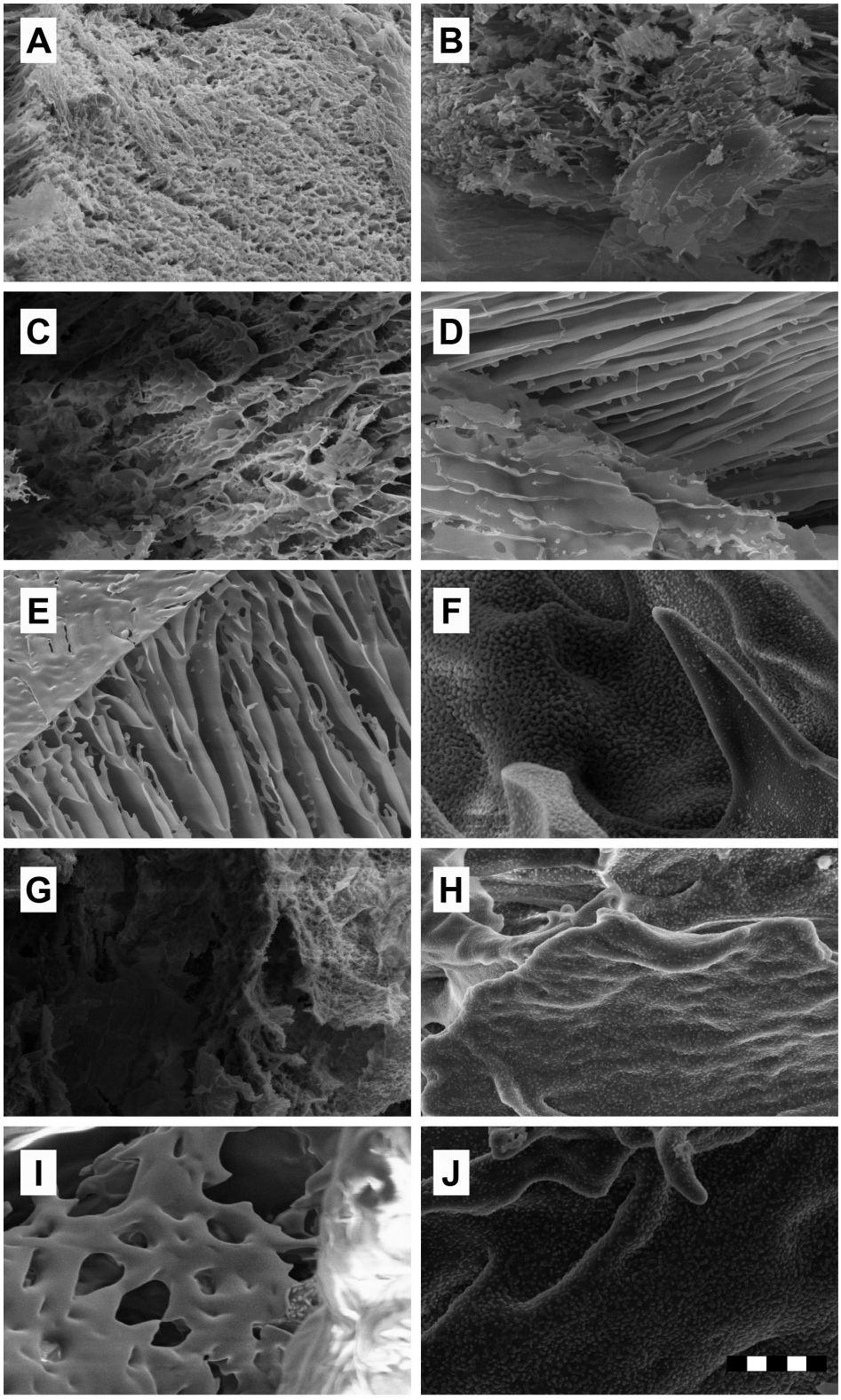

Figure 2.10 *SEM micrographs of egg white after freeze-drying. A) pH 2; B) pH 2, 200 mM NaCl; C) pH 5; D) pH 5, 200 mM NaCl; E) pH 7; F) pH 7, 200 mM NaCl; G) pH 9; H) pH 9, 200 mM NaCl; I) pH 12; J) pH 12, 200 mM NaCl. Images are representative of 2-3 replications. The scale bar represents 25 μm and all micrographs are of the same scale.*

The ten different EW samples were subjected to an *in vitro* digestibility assay in order to investigate the structure/digestibility relationship. The digestion assay (Section 7.7) was based on previous models developed by others (Fu et al. 2002; Kim et al. 2008; United States Pharmacopeia 2009) with slight modifications. In brief, a peptic digest at pH 1.5 was followed by pH neutralisation and subsequent pancreatic digestion *in vitro*. In brief, a peptic digest at pH 1.5 was followed by pH neutralisation and subsequent pancreatic digestion *in vitro*. The substrate (protein) to enzyme ratio was 0.4 (w/w) for pepsin and 0.5 (w/w) for pancreatin. The appropriate ratio of substrate to enzyme ratio for food hydrolysis experiment is currently not established (Moreno 2007; Wickham et al. 2009). As a result, enzyme to substrate ratios employed for *in vitro* digestion experiments vary by orders of magnitude. However, this variation is consistent with inter individual variation of digestive enzyme concentrations in gastric juice, which may differ by up to four orders of magnitude (Moreno 2007). Furthermore, enzyme activity between different commercially available products may vary which further complicates standardisation of the *in vitro* assay. In this chapter the enzyme concentration were adjusted to the concentrations recommended by the US Pharmacopeia. These concentrations are standard but higher than physiologically relevant (Moreno 2007; Wickham et al. 2009; Schnell & Herman 2009). The model was chosen because it allowed a rapid and reliable evaluation of protein digestion patterns via SDS PAGE.

Sample aliquots were taken at various time points and analysed by SDS PAGE. Figure 2.11 shows the SDS PAGE profile of the enzymes (pepsin and pancreatin) and of raw EW before and after *in vitro* digestion. The majority of the high molecular weight proteins were hydrolysed into smaller peptide fragments ranging from about 20 kDa to below 3.5 kDa with the highest peptide density present between 15 kDa and 3.5 kDa. The primary sequence of ovalbumin was analysed for the presence of potential restriction sites for pepsin, trypsin, and chymotrypsin (using ExPASy PeptideCutter tool (http://web.expasy.org)) (Gasteiger et al. 2005). Selecting pepsin, trypsin, and chymotrypsin in the PeptideCutter tool yielded an average mass of 300 Da which corresponds to di- or tripeptide (if estimating the average amino acid mass in the protein to be 110 Da). The theoretical peptide size is therefore in good agreement with the observed peptide fragment size measured during the *in vitro* digestion assay of boiled egg white (Figure 2.12) which displayed a degree of hydrolysis (DH) corresponding to tripeptides

(DH = 34 %) after 3 hours and a DH of 44 % corresponding to a mixture of di- and tripeptides after 8 hours of incubation. A DH of 100 % corresponds to the complete hydrolysis of the protein into single amino acids (a DH of 50 % results in dipeptides).

The visible protein bands in Figure 2.11, lane A shows the presence of pepsin (36 kDa). Lane B shows pancreatin which contains trypsin (23 kDa) and chymotrypsin (25 kDa), amongst other proteins such as amylase (55 kDa). Lane C shows raw undigested EW with distinct protein bands visible for lysozyme, ovalbumin, ovotransferrin, and ovomucin (molecular weight label on the right). Lane D shows raw EW after pancreatic digestion. It is evident that many pancreatic enzymes withstood the pancreatic digestion, while EW and pepsin were hydrolysed into small peptide fragments (fragment size is from below 3.5 kDa to 20 kDa).

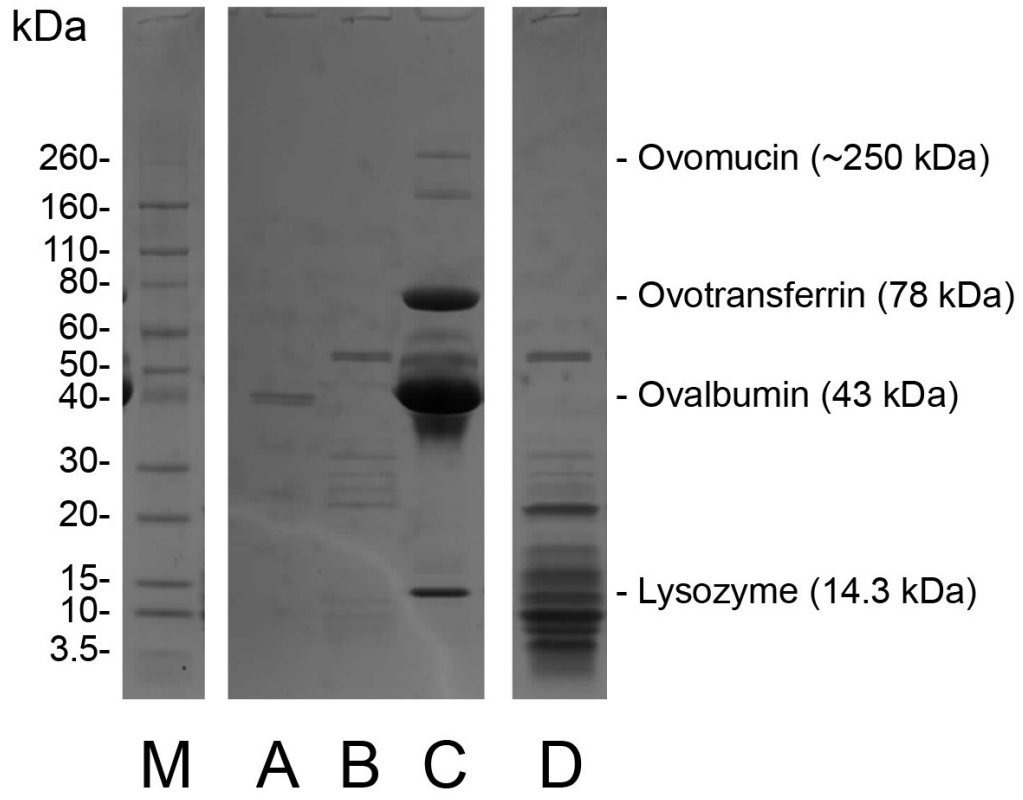

Figure 2.11 *Denaturing and reducing SDS PAGE of EW before and after in vitro digestion. M) Marker; A) pepsin; B) pancreatin; C) raw EW before digestion; D) raw EW after pepsin and pancreatin digestion.*

The degree of digestibility observed via SDS PAGE was further quantified by measuring the degree of hydrolysis (DH) between raw and boiled EW. In order to quantify the enzymatic breakdown of raw and boiled EW the *o*-phthalaldehyde (OPA) assay was used (Section 7.8). The spectrophotometric assay measures the amount of free reactive amino residues. The concentration of free amino groups in a sample can be determined using a serine standard curve (Section 7.8). Because increasing hydrolysis results in increasing amounts of free peptide N-termini this method can be used to assess the DH (Nielsen et al. 2001). The results of the OPA assay for raw and boiled egg white were consistent with the initial SDS PAGE analysis. There was an observed 2 - 3 fold higher DH of boiled EW compared to raw EW as assessed by *in vitro* digestion (Figure 2.12). Peptic and pancreatic hydrolysis were both well defined and an increased DH of boiled egg white was visible for peptic as well as pancreatic hydrolysis, as indicated by the steepness of the slope of both curves

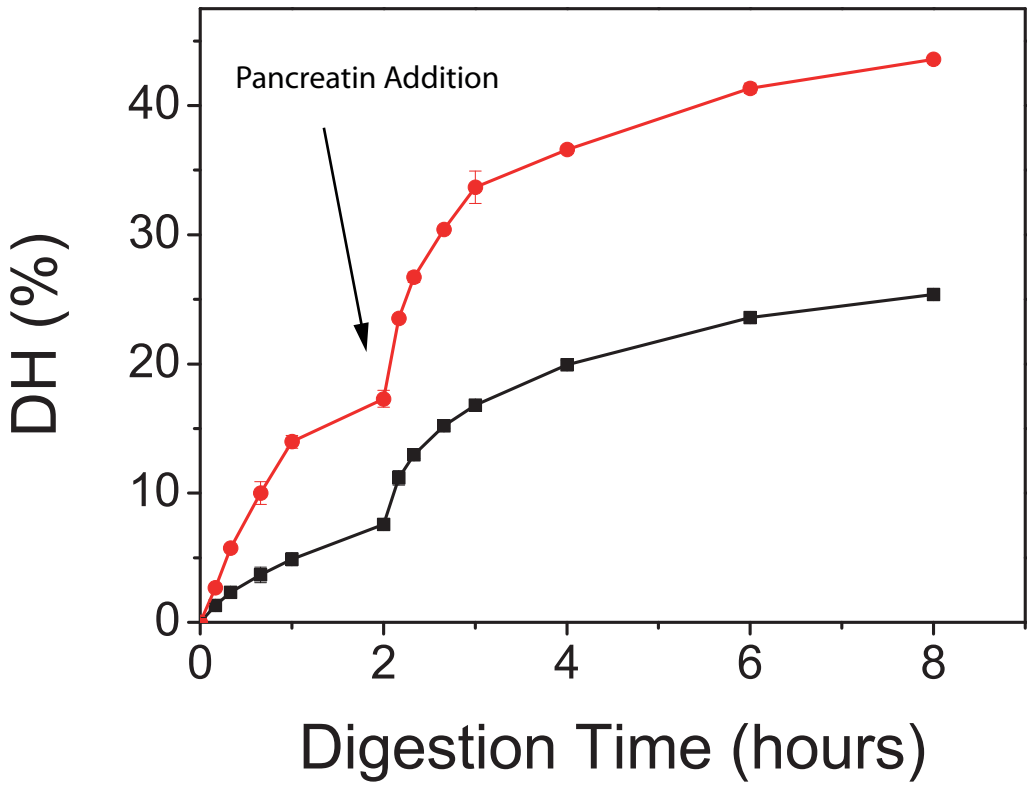

Figure 2.12 *DH of raw EW (black) and boiled EW (red). 0 - 2 hours pepsin digestion, 2 - 8 hours pancreatin digestion. Error bars show one standard deviation of the mean from triplicate experiments.*

Figure 2.13 shows the *in vitro* digestion pattern of ten raw EW samples (pHs 2, 5, 7, 9, and 12; each pH in the presence and absence of 200 mM NaCl). It is evident that there is no marked difference in the digestion pattern in any of the ten EW samples. There is no indication that different protein structures (Figure 2.10) show a change in protein susceptibility to digestion *in vitro*. Furthermore, there is no visible change between treated (Figure 2.13, lanes 1-10) and completely untreated EW (Figure 2.13, lane D).

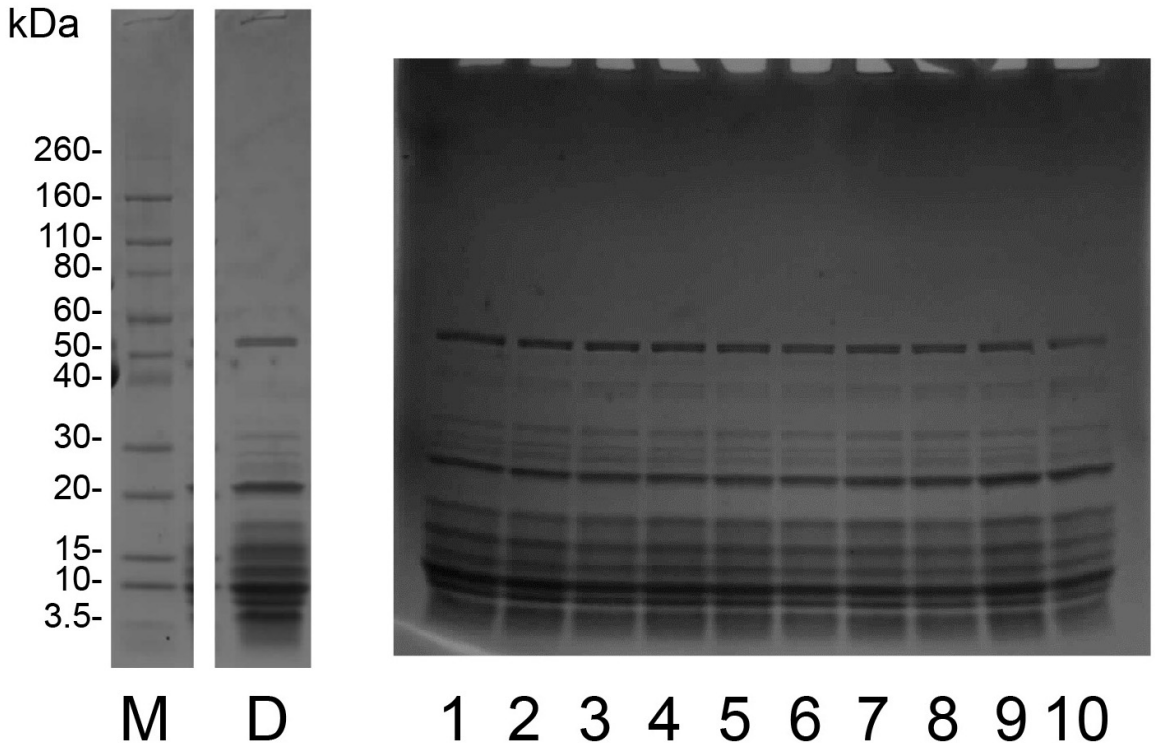

Figure 2.13 *Denaturing and reducing SDS PAGE of treated raw EW after in vitro digestion. M) Marker; D) raw EW after pepsin and pancreatin digestion; 1) EW pH 2; 2) EW pH 2, 200 mM NaCl; 3) EW pH 5; 4) EW pH 5, 200 mM NaCl; 5) EW pH 7; 6) EW pH 7, 200 mM NaCl; 7) EW pH 9; 8) EW pH 9, 200 mM NaCl; 9) EW pH 12; 10) EW pH 12, 200 mM NaCl.*

Figure 2.14 shows the same experimental conditions as Figure 2.13 with the only difference being that the EW samples were boiled for 10 minutes after pH adjustment and salt addition. The direct comparison shows evidence that heat treatment is able to increase the *in vitro* digestibility of EW. Figure 2.14 shows that EW is digested nearly completely when boiled at all pHs and both salt concentrations as indicated by the disappearance of

the protein and peptide bands. Only the enzymes of the pancreatic mixture are present after digestion. Previous studies have reported this increase in digestibility of EW after heatin (Valle-Riestra & Barnes 1970; Hoppe et al. 2013; Yoshino et al. 2004). The slight differences of low molecular weight peptides observed for lanes 5-8 are an artefact of unequal loading of the gel. When replicate experiments were conducted (data not shown) these patterns were observed in different lanes. The most probable explanation is an unequal total protein concentration per lane. Loading inaccuracies may have arisen due to differences in EW aggregate homogenisation and homogenate pipetting for the *in vitro* digestion assays. A relatively high pipetting variability of differently sized homogenised particles necessarily would lead to a high variability of the generated peptides. To circumvent this problem for future experiments, it is advisable to freeze-dry and powderise the egg white aggregates in order to facilitate a more accurate weighing of sample.

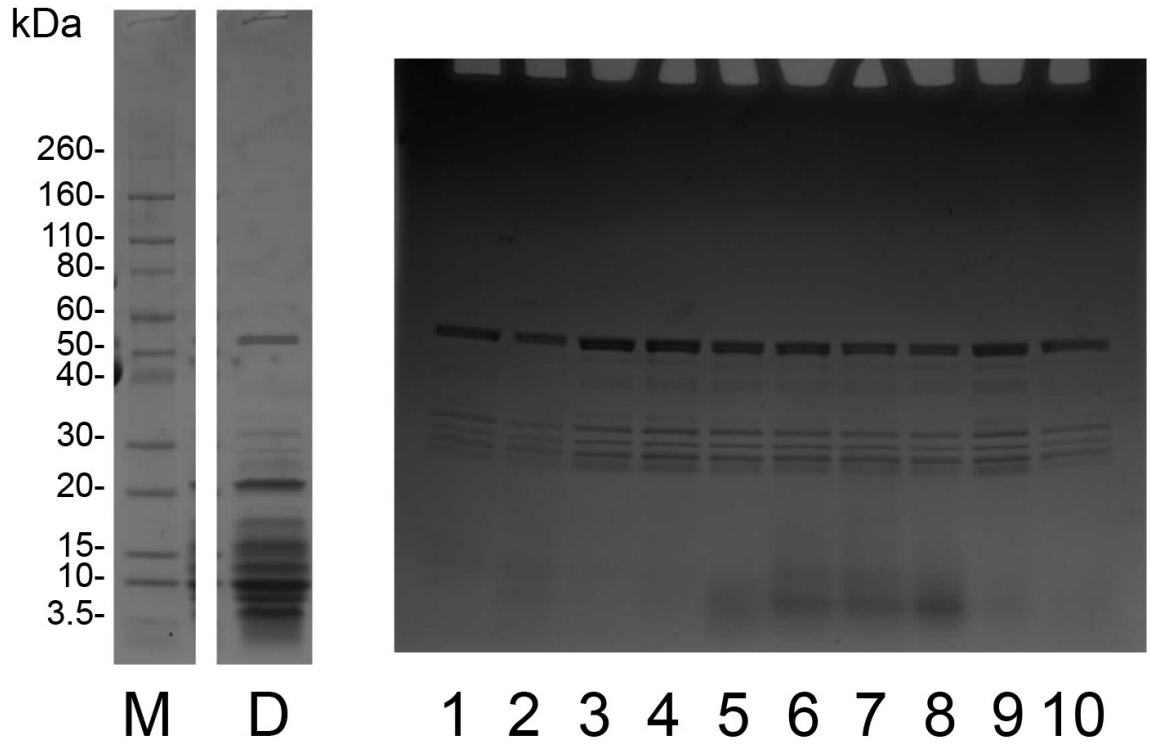

Figure 2.14 *Denaturing and reducing SDS PAGE of treated boiled EW (10 minutes) after in vitro digestion. M) Marker; D) raw EW after pepsin and pancreatin digestion; 1) EW pH 2; 2) EW pH 2, 200 mM NaCl; 3) EW pH 5; 4) EW pH 5, 200 mM NaCl; 5) EW pH 7; 6) EW pH 7, 200 mM NaCl; 7) EW pH 9; 8) EW pH 9, 200 mM NaCl; 9) EW pH 12; 10) EW pH 12, 200 mM NaCl.*

2.3 Egg White Gel Structure in the Presence of Maillard Reaction Partners

The gel structure of EW aggregates that formed in the presence of Maillard reaction partners was assessed by SEM. Already after 10 minutes of heating at 80 °C there are only subtle differences in the network structure of the EW gels Figure 2.15. Most of the treated EW has very homogenous pore size connecting strands of different diameter (Panels A - F). The most notable structural difference is seen for the glutaraldehyde treated EW sample (Panel G). The biggest difference is the lack of the open pore structure compared to the remaining six sample conditions. The effect of glutaraldehyde on gel structure of soy proteins has previously been described. Gel pore size and network structure depended on the glutaraldehyde concentration and time of addition (before or after heat denaturation) (Yasir et al. 2007). The reactivity of glutaraldehyde may cause protein cross-linking reactions via Schiff base (imine) formation with free amino groups. However, other mechanisms for protein cross-linking reaction with glutaraldehyde have been proposed, including Michael addition and pyridinium cross-links (Migneault et al. 2004; Gerrard et al. 2002).

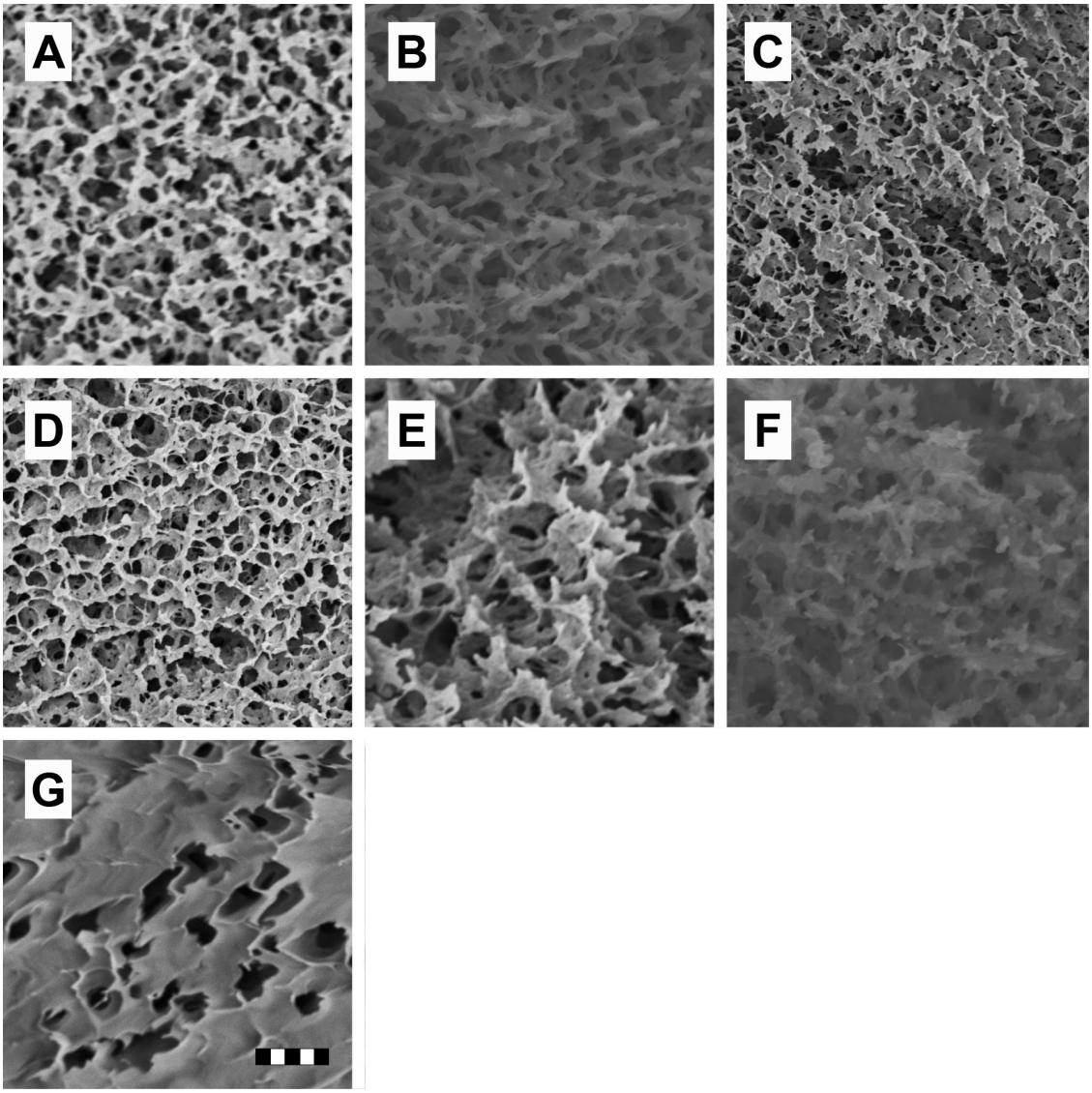

Figure 2.15 *SEM micrographs of EW after 10 minutes heating at 80 °C. The scale is the same for all images and the scale bar is 5 µm. The protein concentration was 80 mg/mL, the cosolute concentration was 100 mM. A) EW + water; B) EW + NaCl; C) EW + glucose D) EW + fructose; E) EW + lactose; F) EW + methylglyoxal; G) EW + glutaraldehyde. The images are representative of three replicate experiments.*

2.4 Ovalbumin Secondary Structure

Circular dichroism (CD) measurements were carried out in order to determine if there is a relationship between the microscopic structure and the secondary protein structure. To obtain information about the ratio of secondary structural elements such as α-helices, β-strands, random coil, and loops it is necessary to work with purified proteins rather than with a protein mixture, such as EW. Therefore, ovalbumin, the major EW protein, was purified from EW and used for analysis of the secondary structure changes in the presence

and absence of Maillard reaction partners before and after heating for 10 minutes at 80 °C. The ratio of helix, strand, turn, and coil were estimated with the widely used CDNN software (http://gerald-boehm.de) (Böhm et al. 1992; Greenfield 2006). The results are listed in Table 2.1. It is evident that the observed CD spectra overlay very accurately indicating that the secondary structure of all unheated EW samples was identical.

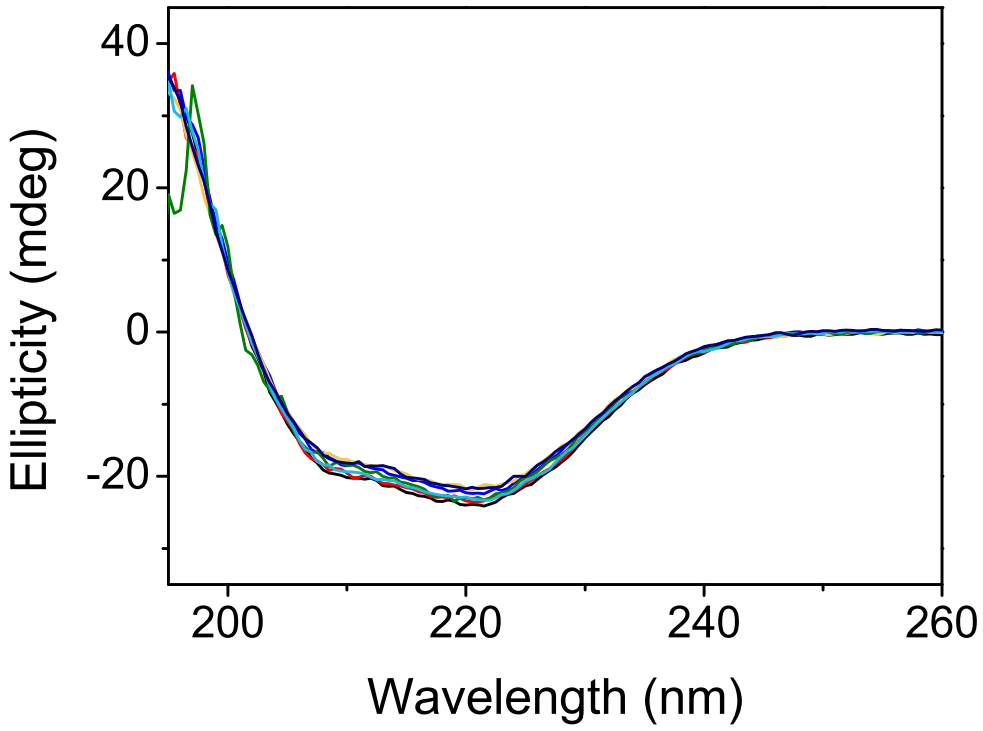

Figure 2.16 *CD spectra of ovalbumin (0.1 mg/mL) before heating in the presence of water (dark blue) and cosolutes at 50 mM, NaCl (light blue) glucose (black), fructose (red), lactose (blue), glutaraldehyde (yellow), and methylglyoxal (green). Three replicates were measured and automatically averaged for each protein.*

Table 2.1 *Estimation of secondary structure elements before heating, using CDNN software. In grey are the values derived from the PDB entry 1OVA (Stein et al. 1991).*

	water	NaCl	Glucose	Fructose	Lactose	Glutar-aldehyde	Methyl-glyoxal	PDB 1OVA
Helix	34%	37%	38%	37%	35%	34%	36%	32%
Strand	33%	32%	31%	32%	33%	33%	32%	32%
Coil	33%	31%	31%	31%	32%	33%	32%	36%
Total	100%	100%	100%	100%	100%	100%	100%	100%

The estimated ratios of secondary structure elements (Table 2.1) are in good agreement with the 3D structure of the PDB entry 1OVA (Stein et al. 1991). The structure shows approximately equal parts of helix, strand, and coil (Figure 2.17 monomeric 1OVA).

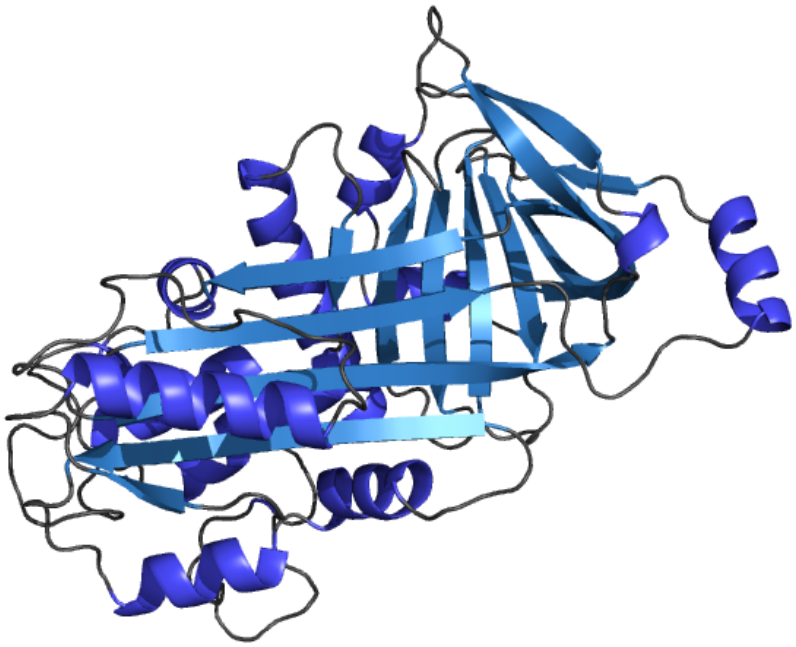

Figure 2.17 *Crystal structure of momomeric ovalbumin, PDB entry 1OVA* ***(Stein et al. 1991)****. Cartoon representation with helices in dark blue, strands in light blue, and coil in grey colour.*

After heating at 80 °C for 10 minutes the secondary structure was monitored again to observe conformational changes (Figure 2.18). It is evident that there is still a significant amount of intact secondary structure present in most samples. Compared to the spectra of non-heated ovalbumin solutions, there are marked changes in the CD spectra of heated protein sample. Most importantly there is a decrease of intensity at about 208 and 222 nm. The decrease of absorbance at 208 and 222 nm is commonly used to assess the decrease of α-helical secondary structure and the unfolding of the protein (Greenfield 2006; Hirst & Brooks 1994; Kelly et al. 2005). The CD spectrum of ovalbumin in the presence of glutaraldehyde differs strongly from the other samples. There is a significant loss of secondary structure (indicated by the low signal compared to the other samples). This big influence of glutaraldehyde is consistent with the major structural differences observed in the EW gel structure (Figure 2.15). The absorption spectrum in the presence of NaCl (light blue graph) also differs from the remaining samples at 208 nm indicative of remaining

helical structures. The secondary structure estimation by CDNN software is consistent with these observations (

Table 2.2). The relatively high concentrations of glutaraldehyde and methylglyoxal (50 mM) compared to a low concentration of protein (0.1 mg/mL) caused a decrease of pH from pH 7 to pH 4. This pH change may have contributed to the drastic change of ovalbumin secondary structure in the presence of glutaraldehyde. The low pH of the glutaraldehyde and methylglyoxal solution is likely to be due to oxidation of the aldehyde groups to their corresponding carboxylic acid forms. However, this change was not observed in methylglyoxal treated ovalbumin.

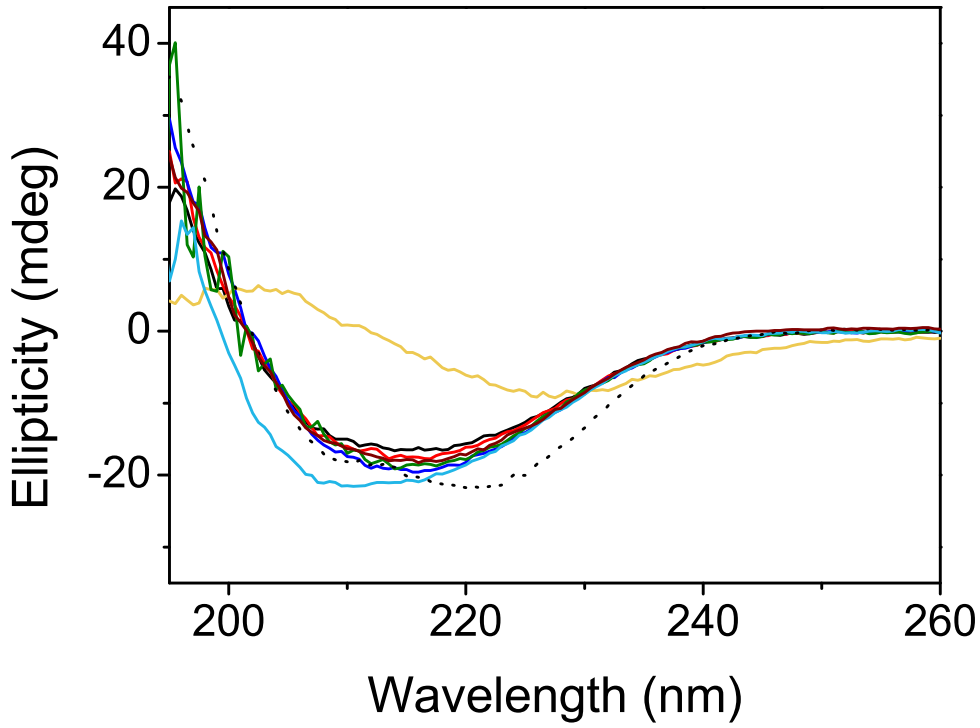

Figure 2.18 *CD spectra of ovalbumin (0.1 mg/mL) after 10 minutes heating at 80 °C in the presence of water (dark blue) and cosolutes at 50 mM, NaCl (light blue) glucose (black), fructose (red), lactose (blue), glutaraldehyde (yellow), and methylglyoxal (green). Three replicates were measured and automatically averaged for each protein. Dashed line represents unheated ovalbumin in water before heating.*

Table 2.2 *Estimation of secondary structure elements after heating, using CDNN software. In grey are the values of PDB entry 1OVA (Stein et al. 1991).*

	water	NaCl	Glucose	Fructose	Lactose	Glutar-aldehyde	Methyl-glyoxal	PDB 1OVA
Helix	29%	33%	26%	27%	31%	11%	29%	32%
Strand	37%	36%	38%	37%	35%	46%	36%	32%
Coil	35%	31%	36%	35%	34%	44%	35%	36%
Total	100%	100%	100%	100%	100%	100%	100%	100%

2.5 Egg White Denaturation Temperature

Differential scanning fluorometry (DSF) (Section 7.10) was used in order to establish whether the Maillard reaction partners influence the heat stability of EW protein. Untreated native EW was mixed with Maillard reaction partners and subsequently heated at 1 °C/minute from 20 °C to 90 °C. Figure 2.19 shows that the melting temperature of egg white is approximately 66 °C in the absence of any Maillard reaction partner. Previous studies reported egg white protein melting temperature of 65 °C (Perez & Pilosof 2004; Donovan et al. 1975) which was attributed to the denaturation of conalbumin. Ovotransferrin has a melting temperature (T_m) of 60 °C and ovalbumin 80 °C (Rao et al. 2012; Wang et al. 2009). Glucose, fructose, lactose, and NaCl do not largely influence the melting temperature while there is a concentration dependent decrease of T_m with increasing methylglyoxal and glutaraldehyde concentration. The T_m decreased to 55 °C and 44 °C at 210 mM methylglyoxal and glutaraldehyde concentration respectively. The concentration dependent pH changes caused by methylglyoxal and glutaraldehyde are likely to have contributed to the decreased heat stability.

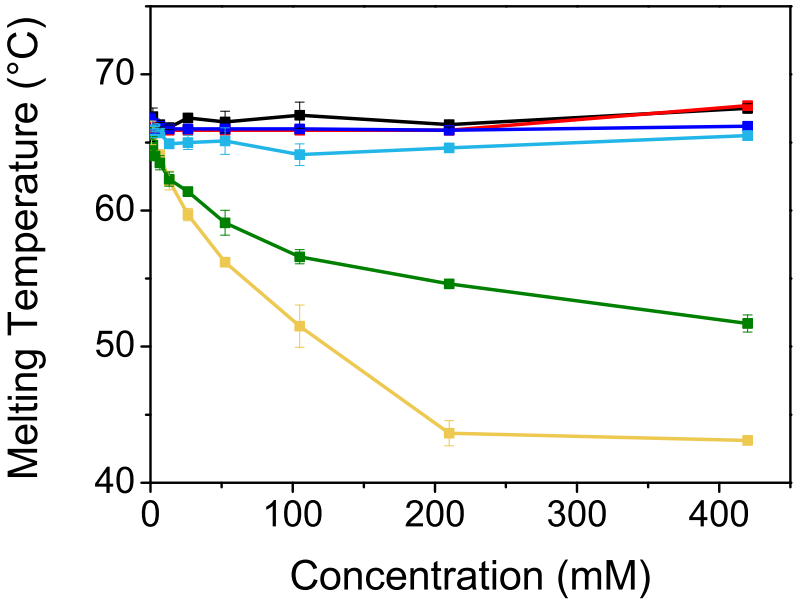

Figure 2.19 *Protein melting temperature in relation to Maillard reaction partner concentration. Ovalbumin (1 mg/mL) in the presence of NaCl (light blue) glucose (black), fructose (red), lactose (blue), methylglyoxal (green), glutaraldehyde (yellow). Error bars show one standard deviation of the mean from triplicate experiments.*

2.6 Effect of Maillard Reaction on Protein Digestibility

The Maillard reaction has previously been reported to reduce protein digestibility (de Jongh et al. 2011). The effect of different Maillard reaction partners on aggregate structure (Section 2.3 to Section 2.5) and aggregate digestibility was investigated. In the first instance the highly reactive Maillard reaction partner glutaraldehyde (Figure 2.7, 40 mM final concentration), was reacted with raw EW (no heating). As a model Maillard reaction partner, glutaraldehyde is highly reactive and causes protein cross-linking as well as the formation of brown colour (Caillard et al. 2009; Jumnongpon et al. 2012; Meade et al. 2003; Yasir et al. 2007). An initial SDS PAGE analysis (Figure 2.20) showed that the cross-linking of EW proteins was successful, as indicated by the high intensity band (Lane 2) which shows the protein fraction that did not migrate into the gel matrix. At 50 mM glutaraldehyde no secondary structure changes were observed (Figure 2.16). Cross-linking may not have perturbed the secondary structure or, more likely, the low protein

concentration of 0.1 mg/mL used in the CD measurements was sufficiently low to prevent measurable cross-linking via CD measurements. The protein band at 43 kDa (Lane 2) may be attributed to non-cross-linked ovalbumin or to cross-linked low molecular weight species (such as lysozyme).

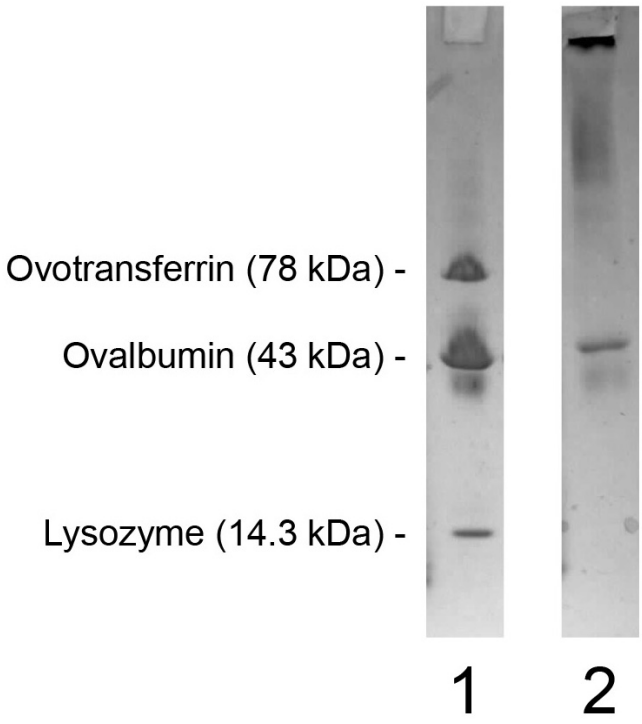

Figure 2.20 *Denaturing and reducing SDS PAGE of 1) raw EW; 2) glutaraldehyde treated raw EW.*

Figure 2.21 shows the digestion pattern of raw EW incubated with glutaraldehyde. Most lanes (2 - 10) show remaining undigested cross-linked protein (indicated by the protein "smear" above ~50 kDa). Lane 4 shows the highest level of resistance to enzymatic breakdown. It was deemed an artefact due to an unequal loading of the gel because replicate experiments showed different patterns. The most probable explanation is an unequal total protein concentration per lane. Loading inaccuracies may have arisen due to differences in EW aggregate homogenisation and homogenate pipetting for the *in vitro* digestion assays. A relatively high pipetting variability of differently sized homogenised particles necessarily would lead to a high variability of the generated peptides. To circumvent this problem for future experiments, it is advisable to freeze-dry and powderise the egg white aggregates in order to facilitate a more accurate weighing of sample.

Apart from the observed smear, the peptide pattern of digested glutaraldehyde treated EW shows less band intensity of small peptides (peptides ≤ 15 kDa) compared to untreated EW. This decrease in low molecular weight species can be explained by the presence of the protein smear caused by less digestible protein.

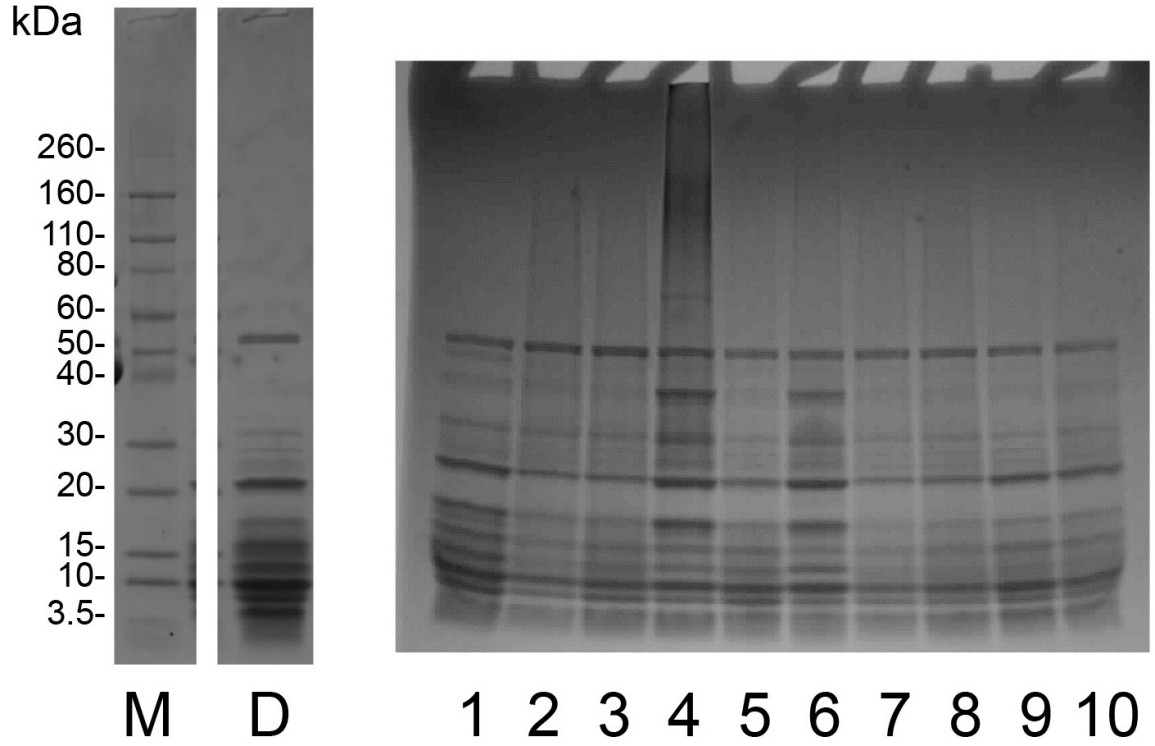

Figure 2.21 *Denaturing and reducing SDS PAGE of glutaraldehyde treated raw EW (10 minutes) after in vitro digestion. M) Marker; D) raw EW after pepsin and pancreatin digestion; 1) EW pH 2; 2) EW pH 2, 200 mM NaCl; 3) EW pH 5; 4) EW pH 5, 200 mM NaCl; 5) EW pH 7; 6) EW pH 7, 200 mM NaCl; 7) EW pH 9; 8) EW pH 9, 200 mM NaCl; 9) EW pH 12; 10) EW pH 12, 200 mM NaCl.*

The decrease of the digestibly of raw EW by glutaraldehyde showed that the Maillard reaction can change protein hydrolysis. This confirmed that the Maillard reaction reduces protein digestibility as reported by others (Wang & Ismail 2012; de Jongh et al. 2011; Corzo-Martínez et al. 2010; Valle-Riestra & Barnes 1970; van Soest & Mason 1991). In further *in vitro* digestion experiments a series of food relevant Maillard reaction partners was included (Figure 2.7). The studied food relevant reaction partners included glucose, fructose, lactose, and methylglyoxal. Raw EW and heated EW (10 minutes, 5 hours, and 24 hours) in the presence of Maillard reaction partners were compared.

The resistance against proteolysis was assessed. As can be seen in Figure 2.22A, the pancreatic *in vitro* digestion is incomplete for glutaraldehyde even before heating while the other Maillard reaction partners do not influence digestibility of EW markedly compared to EW without reaction partner. After 10 minutes heating of EW at 80 °C (Figure 2.22B) the digestion is more complete (as observed earlier). Glutaraldehyde cross-linked EW (Lane 4) is the least digestible as indicated by the smeared protein band. Methylglyoxal treated EW (Lane 5) is also gaining resistance to pancreatic hydrolysis at 10 minutes and this resistance is further pronounced at 5 hours heating (Figure 2.22C). After 24 hours heating, the Maillard reaction renders glucose, fructose, and lactose reacted EW less digestible (Figure 2.22D), similar to the methylglyoxal treated EW.

The resistance of Maillard products to proteolytic enzymes *in vitro* is likely to reduce the nutritional value of proteins *in vivo*. There is a relatively late onset of marked digestibility resistance in the presence of EW and glucose, fructose, and lactose. This indicates that short cooking times at 100 °C are likely to only cause minor losses of protein nutritional value *in vivo*. On the other hand, there is a significant decrease of protein digestibility is at long heating times. Higher temperatures (which were not included in the presented experiments) may contribute further to an earlier onset of Maillard reaction and thereby to a loss of protein nutritional value. Therefore, there is a plethora of proteinaceous foods that may undergo Maillard causing degradation of protein nutritional value. These foods include baked goods such as cakes, breads, and biscuits, but also roasted or fried meats and vegetables, as well as chocolates, and toffees.

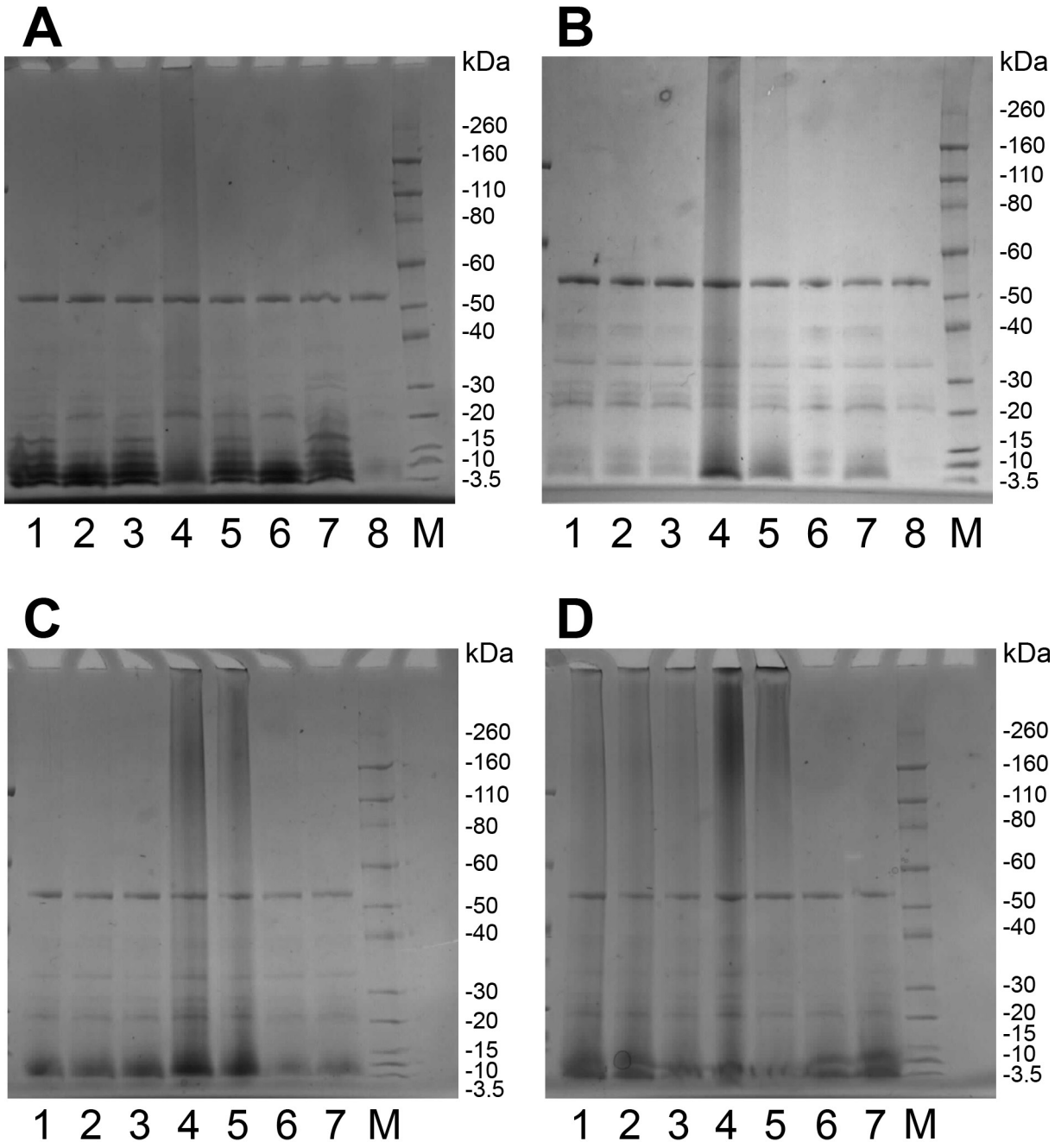

Figure 2.22 *Denaturing and reducing SDS PAGE Maillard treated at different heating times at 80 °C, after sequential in vitro digestion by pepsin and pancreatin (30 minutes each). A) raw; B) 10 minutes heating; C) 5 hours heating; D) 24 hours heating. M) Marker; 1) EW + glucose; 2) EW + fructose; 3) EW + lactose 4) EW + glutaraldehyde; 5) EW + methylglyoxal; 6) EW + NaCl; 7) EW + water; 8) Digestive enzymes only. Gels are representative of three replicates.*

2.7 Summary and Discussion

Effects of pH and Salt on Digestibility

From a nutritional perspective it is desirable to maintain or enhance the degree of protein digestibility (Friedman 2003; Friedman 1996; Meade et al. 2005). An increase of digestibility improves protein absorption and thereby the nutritional value (Erickson & Kim 1990). High quality protein is a limiting nutrient, especially in the developing world (Müller 2005; Smil 2002). Additionally, high protein intake is required for infants, children, pregnant or lactating women, the elderly, and athletes (Fukagawa 2013; Sullivan 1999; Godfrey et al. 1996). Protein quality may therefore be measured as a function of digestibility. Understanding the mechanisms that govern protein digestibility is important to improve food processes and dietary recommendations.

It was shown that adjusting the salt content and the pH of EW solutions influenced the structure of EW as judged by visual differences, and SEM analysis. As can be seen in Figure 2.9A, there is no obvious macroscopic difference in pH and salt adjusted unheated EW. SEM analysis of the same samples Figure 2.10 showed differences in structure (see Section 2.2). Most heated EW samples turned white due to protein denaturation. EW was more opaque at pH 2 and pH 5 without added salt and at pH 12 with added salt (Figure 2.9B). Interestingly these are the conditions far away (pH 2 and pH 12) and close to the isoelectric point (pH 5) of ovalbumin, the main protein fraction of egg white.

While the presence of 200 mM NaCl and pH adjustment of raw EW may change the protein network structure, the presented work indicates that these adjustments prior to *in vitro* digestion did not result in any marked differences to the *in vitro* digestibility of the EW proteins as judged by SDS PAGE analysis. In the studied system, structural changes did not cause marked changes in digestibility. This behaviour may be similar in other protein rich solutions and gels.

However, pH may contribute in other ways to changes of protein digestibility. The gastrointestinal tract is highly pH regulated (Kararli 1995; Hur et al. 2011; Evans et al. 1988). Both, during *in vivo* digestion and in the here employed *in vitro* digestion assay the first step of gastric digestion is the adjustment of food to pH 1.5 - 2. The pH of the ingested food affects the amount of acid or base required to regulate the pH value of the

food. For example, more alkaline food requires larger amounts of hydrochloric acid production in the stomach than acidic food (Walsh et al. 1975). The time to produce the required amount of acid for pepsin proteolysis to be effective may thereby influence the rate of food digestion (Walsh et al. 1975). However, it seems that once the pH has reached optimum for enzymatic hydrolysis (e.g., pH 1.5 - 2 for pepsin) the pre-treatment does not influence digestibility. The results indicate that the initial pH of a protein solution does not improve or decrease the *in vitro* digestibility as long as the pH during digestion is constant.

Heating of EW at 80 °C caused protein denaturation which resulted in an increased protein digestibility. The increased digestibility of heat denatured proteins has been observed previously (Takagi et al. 2003; Hoppe et al. 2013; Yoshino et al. 2004). Similar to raw EW digestibility there was no observed difference of digestibility between heated EW at different pH values or in the presence of salt. The employed pH range (pH 2 - 12) and salt concentration (0 mM and 200 mM) covered a large proportion of existing foods likely to be encountered in everyday life. It is therefore probable that pH and salt treatment of protein during food processing does not markedly affect the protein digestibility directly by pH or salt induced structural changes of proteins. However, pH sensitive chemical reactions that affect protein digestibility (e.g., Maillard reaction) may occur faster or slower during food processing at different pH values.

Effects of Maillard Reaction on Digestibility

The Maillard reaction can lead to protein cross-linking which carries implications for potential food application because it affects gel structure and thereby food consistency (Yasir et al. 2007). By adjusting the degree of Maillard reaction it is therefore possible to vary rheological properties. Understanding the time and temperature dependence on the formation rate of Maillard reaction products is therefore likely to be important in terms of design of new food products. The cross-linking often involves lysine and arginine residues which are especially reactive (Jumnongpon et al. 2012). This also carries implications with regard to the nutritional value of Maillard reaction products because lysine is often a limiting amino acid in many foods and may be less bioavailable after modification (Section 3.2). Incidentally lysine and arginine also mark important recognition sites for proteolytic enzymes such as trypsin (Keil 1992). Since modified amino acid residues may not function as recognition sites, the protein may become more resistant to proteolysis as a

result (Seiquer et al. 2006; Wang et al. 2005; Brock et al. 2007). However, chymotrypsin and pepsin cleavage occurs preferentially at tryptophan, tyrosine and phenylalanine residues. Pepsin cleavage also occurs at leucine residues (Keil 1992). Steric hindrance could prevent access towards these residues if lysine or arginine residues are in close proximity. Maillard reaction products are generally detrimental to protein digestibility (Wang & Ismail 2012; Friedman 2003; Meade et al. 2005). The work presented here is consistent with this finding. EW that was linked with either methylglyoxal or glutaraldehyde was more resistant to *in vitro* proteolysis by pepsin and pancreatin even after short incubation times (10 minutes at 80 °C).

Fructose, glucose, and lactose treated proteins show a similar resistance to proteolysis, but only after long incubation times (5 hours to 24 hours at 80 °C). Analyses of the structural features reveal that glutaraldehyde and methylglyoxal cause the most pronounced differences. While glutaraldehyde has an impact on the gel structure, secondary structure, and on the heat stability of EW protein, it was shown that methylglyoxal leaves the gel structure and secondary structure largely intact. It was observed that methylglyoxal, too, decreased the melting temperature of EW.

For further studies it was decided to employ methylglyoxal as a model Maillard reaction partner because it was a good mimic of the food grade Maillard reaction partners (glucose, fructose, and lactose) while glutaraldehyde was deemed too reactive. Additionally, the reaction of glutaraldehyde with proteins may yield a wide variety of reactions and cross-linked products which could complicate further analysis (Section 2.3). On the other hand, the reaction of methylglyoxal with protein is well characterised (Figure 2.8). Furthermore, methylglyoxal is more relevant to food processes as it is a degradation product of glucose (Lima et al. 2009) (Figure 3.2) and has also been found in detectable concentrations in natural sources, such as honey (Mavric et al. 2008).

2.8 References

Augustin, M.A. & Hemar, Y., 2009. Nano- and micro-structured assemblies for encapsulation of food ingredients. *Chemical Society Reviews*, 38(4), pp.902–912.

Bechara, E.J.H., Dutra, F., Cardoso, V.E.S. & Sartori, A., 2007. The dual face of endogenous α-aminoketones: pro-oxidizing metabolic weapons. *Comparative Biochemistry and Physiology, Part C*, 146(1), pp.88–110.

Böhm, G., Muhr, R. & Jaenicke, R., 1992. Quantitative analysis of protein far UV circular dichroism spectra by neural networks. *Protein Engineering*, 5(3), pp.191–195.

Brock, J.W.C., Cotham, W.E., Thorpe, S.R., Baynes, J.W. & Ames, J.M., 2007. Detection and identification of arginine modifications on methylglyoxal-modified ribonuclease by mass spectrometric analysis. *Journal of Mass Spectrometry*, 42(1), pp.89–100.

Caillard, R., Remondetto, G.E. & Subirade, M., 2009. Physicochemical properties and microstructure of soy protein hydrogels co-induced by Maillard type cross-linking and salts. *Food Research International*, 42(1), pp.98–106.

Corzo-Martínez, M., Carrera Sánchez, C., Moreno, F.J. & Rodríguez Patino, J.M., 2012a. Interfacial and foaming properties of bovine β-lactoglobulin: galactose Maillard conjugates. *Food Hydrocolloids*, 27(2), pp.438–447.

Corzo-Martínez, M., Carrera-Sánchez, C., Villamiel, M. & Rodríguez-Patino, J.M., 2012b. Assessment of interfacial and foaming properties of bovine sodium caseinate glycated with galactose. *Journal of Food Engineering*, 113(3), pp.461–470.

Corzo-Martínez, M., Soria, A.C., Belloque, J., Villamiel, M. & Moreno, F.J., 2010. Effect of glycation on the gastrointestinal digestibility and immunoreactivity of bovine β-lactoglobulin. *International Dairy Journal*, 20(11), pp.742–752.

Curtis, R.A., Ulrich, J., Montaser, A., Prausnitz, J.M. & Blanch, H.W., 2002. Protein–protein interactions in concentrated electrolyte solutions. *Biotechnology and Bioengineering*, 79(4), pp.367–380.

Donovan, J.W., Mapes, C.J., Davis, J.G. & Garibaldi, J.A., 1975. A differential scanning calorimetric study of the stability of egg white to heat denaturation. *Journal of the Science of Food and Agriculture*, 26(1), pp.73–83.

Eiser, E., Miles, C.S., Geerts, N., Verschuren, P. & MacPhee, C.E., 2009. Molecular cooking: physical transformations in Chinese 'century' eggs. *Soft Matter*, 5(14), pp.2725–2730.

Erickson, R.H. & Kim, Y.S., 1990. Digestion and absorption of dietary protein. *Annual Review of Medicine*, 41(1), pp.133–139.

Evans, D.F., Pye, G., Bramley, R., Clark, A.G., Dyson, T.J. & Hardcastle, J.D., 1988. Measurement of gastrointestinal pH profiles in normal ambulant human subjects. *Gut*, 29(8), pp.1035–1041.

Fadouloglou, V.E., Kokkinidis, M. & Glykos, N.M., 2008. Determination of protein oligomerization state: Two approaches based on glutaraldehyde crosslinking. *Analytical Biochemistry*, 373(2), pp.404–406.

Fay, L.B. & Brevard, H., 2005. Contribution of mass spectrometry to the study of the Maillard reaction in food. *Mass Spectrometry Reviews*, 24(4), pp.487–507.

Friedman, M., 2003. Nutritional consequences of food processing. *Forum of Nutrition*, 56(1), pp.350–352.

Friedman, M., 1996. Nutritional value of proteins from different food sources. A review. *Journal of Agricultural and Food Chemistry*, 44(1), pp.6–29.

Fu, T.J., Abbott, U.R. & Hatzos, C., 2002. Digestibility of food allergens and nonallergenic proteins in simulated gastric fluid and simulated intestinal fluid - a comparative study. *Journal of Agricultural and Food Chemistry*, 50(24), pp.7154–7160.

Fukagawa, N.K., 2013. Protein and amino acid supplementation in older humans. *Amino Acids*, In Press.

Gabriel, A.A., 2008. Estimation of water activity from pH and °Brix values of some food products. *Food Chemistry*, 108(3), pp.1106–1113.

Gasteiger, E., Hoogland, C., Gattiker, A., Duvaud, S., Wilkins, M.R., Appel, R.D. & Bairoch, A., 2005. Protein identification and analysis tools on the ExPASy server. In J. M. Walker, ed. *The Proteomics Protocols Handbook*. Portland: Humana Press, pp. 571–607.

Gerrard, J.A., Brown, P. & Fayle, S., 2002. Maillard crosslinking of food proteins I: the reaction of glutaraldehyde, formaldehyde and glyceraldehyde with ribonuclease. *Food Chemistry*, 79(3), pp.343–349.

Gerrard, J.A., Brown, P. & Fayle, S., 2003. Maillard crosslinking of food proteins II: the reactions of glutaraldehyde, formaldehyde and glyceraldehyde with wheat proteins *in vitro* and *in situ*. *Food Chemistry*, 80(1), pp.35–43.

Giosafatto, C.V.L., Rigby, N.M., Wellner, N., Ridout, M., Husband, F. & Mackie, A.R., 2012. Microbial transglutaminase-mediated modification of ovalbumin. *Food Hydrocolloids*, 26(1), pp.261–267.

Godfrey, K., Robinson, S., Barker, D., Osmond, C. & Cox, V., 1996. Maternal nutrition in early and late pregnancy in relation to placental and fetal growth. *British Medical Journal*, 312(7028), pp.410–410.

Greenfield, N.J., 2006. Using circular dichroism spectra to estimate protein secondary structure. *Nature Protocols*, 1(6), pp.2876–2890.

Grinberg, N.V., Bibkov, T.M., Grinberg, V.Y. & Tolstoguzov, V.B., 1988. Thermotropic gelation of ovalbumin 1. Viscoelastic properties of gels as a function of heating conditions and protein concentration at various pH values. *Colloid and Polymer Science*, 266(1), pp.52–59.

Haar, R., Westphal, Y., Wierenga, P.A. & Schols, H.A., 2011. Cross-linking behavior and foaming properties of bovine α-lactalbumin after glycation with various saccharides. *Journal of Agricultural and Food Chemistry*, 59(23).

Al-Hakkak, J. & Al-Hakkak, F., 2010. Functional egg white–pectin conjugates prepared by controlled Maillard reaction. *Journal of Food Engineering*, 100(1), pp.152–159.

Al-Hakkak, J. & Kavale, S., 2002. Improvement of emulsification properties of sodium caseinate by conjugating to pectin through the Maillard reaction. *International Congress Series*, 1245, pp.491–499.

Hirst, J.D. & Brooks, C.L., 3rd, 1994. Helicity, circular dichroism and molecular dynamics of proteins. *Journal of Molecular Biology*, 243(2), pp.173–178.

Hodge, J.E., 1953. Dehydrated foods, chemistry of browning reactions in model systems. *Journal of Agricultural and Food Chemistry*, 1(15), pp.928–943.

Hoppe, A., Jung, S., Patnaik, A. & Zeece, M.G., 2013. Effect of high pressure treatment on egg white protein digestibility and peptide products. *Innovative Food Science and Emerging Technologies*, 17(1), pp.54–62.

Hu, J., Yu, S. & Yao, P., 2007. Stable amphoteric nanogels made of ovalbumin and ovotransferrin via self-assembly. *Langmuir*, 23(11), pp.6358–6364.

Hur, S.J., Lim, B.O., Decker, E.A. & McClements, D.J., 2011. *In vitro* human digestion models for food applications. *Food Chemistry*, 125(1), pp.1–12.

Ianeselli, L. et al., 2010. Protein-protein interactions in ovalbumin solutions studied by small-angle scattering: effect of ionic strength and the chemical nature of cations. *The Journal of Physical Chemistry B*, 114(11), pp.3776–3783.

De Jongh, H.H.J., Taylor, S.L. & Koppelman, S.J., 2011. Controlling the aggregation propensity and thereby digestibility of allergens by Maillardation as illustrated for cod fish parvalbumin. *Journal of Bioscience and Bioengineering*, 111(2), pp.204–211.

Jumnongpon, R., Chaiseri, S., Hongsprabhas, P., Healy, J.P., Meade, S.J. & Gerrard, J.A., 2012. Cocoa protein crosslinking using Maillard chemistry. *Food Chemistry*, 134(1), pp.375–380.

Kararli, T.T., 1995. Comparison of the gastrointestinal anatomy, physiology, and biochemistry of humans and commonly used laboratory animals. *Biopharmaceutics and Drug Disposition*, 16(5), pp.351–380.

Katayama, S., Shima, J. & Saeki, H., 2002. Solubility improvement of shellfish muscle proteins by reaction with glucose and its soluble state in low-ionic-strength medium. *Journal of Agricultural and Food Chemistry*, 50(15), pp.4327–4332.

Keil, B., 1992. *Specificity of proteolysis*, Berlin Heidelberg: Springer.

Kelly, S.M., Jess, T.J. & Price, N.C., 2005. How to study proteins by circular dichroism. *Biochimica et Biophysica Acta - Proteins and Proteomics*, 1751(2), pp.119–139.

Kim, E., Petrie, J., Motoi, L., Morgenstern, M., Sutton, K., Mishra, S. & Simmons, L., 2008. Effect of structural and physicochemical characteristics of the protein matrix in pasta on *in vitro* starch digestibility. *Food Biophysics*, 3(2), pp.229–234.

Kinoshita-Kikuta, E., Kinoshita, E. & Koike, T., 2012. Separation and identification of four distinct serine-phosphorylation states of ovalbumin by Phos-tag affinity electrophoresis. *Electrophoresis*, 33(5), pp.849–855.

Li, Y., Lu, F., Luo, C., Chen, Z., Mao, J., Shoemaker, C. & Zhong, F., 2009. Functional properties of the Maillard reaction products of rice protein with sugar. *Food Chemistry*, 117(1), pp.69–74.

Li, Y., Zhong, F., Ji, W., Yokoyama, W., Shoemaker, C.F., Zhu, S. & Xia, W., 2013. Functional properties of Maillard reaction products of rice protein hydrolysates with mono-, oligo- and polysaccharides. *Food Hydrocolloids*, 30(1), pp.53–60.

Lima, M., Moloney, C. & Ames, J.M., 2009. Ultra performance liquid chromatography-mass spectrometric determination of the site specificity of modification of β-casein by glucose and methylglyoxal. *Amino Acids*, 36(3), pp.475–481.

Liu, J., Ru, Q. & Ding, Y., 2012a. Glycation a promising method for food protein modification: physicochemical properties and structure, a review. *Food Research International*, 49(1), pp.170–183.

Liu, Y., Zhao, G., Zhao, M. & Ren, J., 2012b. Improvement of functional properties of peanut protein isolate by conjugation with dextran through Maillard reaction. *Food Chemistry*, 131(3), p.901.

Loveday, S.M., Rao, M.A., Creamer, L.K. & Singh, H., 2009. Factors affecting rheological characteristics of fibril gels: the case of β-lactoglobulin and α-lactalbumin. *Journal of Food Science*, 74(3), pp.47–55.

Lucey, J.A., 2002. Formation and physical properties of milk protein gels. *Journal of Dairy Science*, 85(2), pp.281–294.

Martins, S.I.F.S., Jongen, W.M.F. & van Boekel, M.A.J.S., 2000. A review of Maillard reaction in food and implications to kinetic modelling. *Trends in Food Science and Technology*, 11(9–10), pp.364–373.

Mattes, R.D. & Donnelly, D., 1991. Relative contributions of dietary sodium sources. *Journal of the American College of Nutrition*, 10(4), pp.383–393.

Mavric, E., Wittmann, S., Barth, G. & Henle, T., 2008. Identification and quantification of methylglyoxal as the dominant antibacterial constituent of Manuka (Leptospermum scoparium) honeys from New Zealand. *Molecular Nutrition and Food Research*, 52(4), pp.483–489.

Meade, S.J., Miller, A.G. & Gerrard, J.A., 2003. The role of dicarbonyl compounds in non-enzymatic crosslinking: a structure–activity study. *Bioorganic and Medicinal Chemistry*, 11(6), pp.853–862.

Meade, S.J., Reid, E.A. & Gerrard, J.A., 2005. The impact of processing on the nutritional quality of food proteins. *Journal of AOAC International*, 88(3), pp.904–922.

Meltretter, J., Seeber, S., Humeny, A., Becker, C.-M. & Pischetsrieder, M., 2007. Site-specific formation of Maillard, oxidation, and condensation products from whey proteins during reaction with lactose. *Journal of Agricultural and Food Chemistry*, 55(15), pp.6096–6103.

Migneault, I., Dartiguenave, C., Bertrand, M.J. & Waldron, K.C., 2004. Glutaraldehyde: behavior in aqueous solution, reaction with proteins, and application to enzyme crosslinking. *Biotechniques*, 37(5), p.790.

Moreno, F.J., 2007. Gastrointestinal digestion of food allergens: Effect on their allergenicity. *Biomedicine & Pharmacotherapy*, 61(1), pp.50–60.

Müller, O., 2005. Malnutrition and health in developing countries. *Canadian Medical Association Journal*, 173(3), pp.279–286.

Naeem, A., Khan, T.A., Muzaffar, M., Ahmad, S. & Saleemuddin, M., 2010. A partially folded state of ovalbumin at low pH tends to aggregate. *Cell Biochemistry and Biophysics*, 59(1), pp.29–38.

National Research Council, 2005. *Dietary reference intakes for water, potassium, sodium, chloride, and sulfate*, Washington, D.C.: The National Academies Press.

Nicolai, T., Britten, M. & Schmitt, C., 2011. β-lactoglobulin and WPI aggregates: formation, structure and applications. *Food Hydrocolloids*, 25(8), pp.1945–1962.

Nielsen, P.M., Petersen, D. & Dambmann, C., 2001. Improved method for determining food protein degree of hydrolysis. *Journal of Food Science*, 66(5), pp.642–646.

Lo Nostro, P. & Ninham, B.W., 2012. Hofmeister phenomena: an update on ion specificity in biology. *Chemical Reviews*, 112(4), pp.2286–2322.

Oliver, C.M., Melton, L.D. & Stanley, R.A., 2006. Creating proteins with novel functionality via the Maillard reaction: a review. *Critical Reviews in Food Science and Nutrition*, 46(4), pp.337–350.

Payne, J.W., 1973. Polymerization of proteins with glutaraldehyde. Soluble molecular-weight markers. *Biochemical Journal*, 135(4), p.867.

Perez, O.E. & Pilosof, A.M.R., 2004. Pulsed electric fields effects on the molecular structure and gelation of β-lactoglobulin concentrate and egg white. *Food Research International*, 37(1), pp.102–110.

Rao, S.P., Meade, S.J., Healy, J.P., Sutton, K.H., Larsen, N.G., Staiger, M.P. & Gerrard, J.A., 2012. Amyloid fibrils as functionalizable components of nanocomposite materials. *Biotechnology Progress*, 28(1), pp.248–256.

Rees, D.C. & Robertson, A.D., 2001. Some thermodynamic implications for the thermostability of proteins. *Protein Science*, 10(6), pp.1187–1194.

Renkema, J.M.S., Gruppen, H. & van Vliet, T., 2002. Influence of pH and ionic strength on heat-induced formation and rheological properties of soy protein gels in relation to denaturation and their protein compositions. *Journal of Agricultural and Food Chemistry*, 50(21), pp.6064–6071.

Rice, P., Longden, I. & Bleasby, A., 2000. EMBOSS: The European Molecular Biology Open Software Suite. *Trends in Genetics*, 16(6), pp.276–277.

Russo, D., 2008. The impact of kosmotropes and chaotropes on bulk and hydration shell water dynamics in a model peptide solution. *Chemical Physics*, 345(2-3), pp.200–211.

Saeki, H. & Inoue, K., 1997. Improved solubility of carp myofibrillar proteins in low ionic strength medium by glycosylation. *Journal of Agricultural and Food Chemistry*, 45(9), pp.3419–3422.

Schnell, S. & Herman, R.A., 2009. Should digestion assays be used to estimate persistence of potential allergens in tests for safety of novel food proteins? *Clinical and Molecular Allergy*, 7(1), p.1.

Seiquer, I., Díaz-Alguacil, J., Delgado-Andrade, C., López-Frías, M., Hoyos, A.M., Galdó, G. & Navarro, M.P., 2006. Diets rich in Maillard reaction products affect protein digestibility in adolescent males aged 11–14 y. *American Journal of Clinical Nutrition*, 83(5), pp.1082–1088.

Shirai, N., Tani, F., Higasa, T. & Yasumoto, K., 1997. Linear polymerization caused by the defective folding of a non-inhibitory serpin ovalbumin. *Journal of Biochemistry*, 121(4), pp.787–797.

Smil, V., 2002. Nitrogen and food production: proteins for human diets. *Ambio*, 31(2), pp.126–131.

Van Soest, P.J. & Mason, V.C., 1991. The influence of the Maillard reaction upon the nutritive value of fibrous feeds. *Animal Feed Science and Technology*, 32(1-3), pp.45–53.

Stein, P.E., Leslie, A.G., Finch, J.T. & Carrell, R.W., 1991. Crystal structure of uncleaved ovalbumin at 1.95 A resolution. *Journal of Molecular Biology*, 221(3), pp.941–959.

Sugiyama, M., Nakamura, A., Hiramatsu, N., Annaka, M., Kuwajima, S. & Hara, K., 2001. Effect of salt and heating on a mesoscopic structure composed of ovalbumin globules in aqueous solution. *Biomacromolecules*, 2(4), pp.1071–1073.

Sullivan, D.H., 1999. Protein-energy undernutrition among elderly hospitalized patients: a prospective study. *Journal of the American Medical Association*, 281(21), pp.2013–2019.

Takagi, K., Teshima, R., Okunuki, H. & Sawada, J.-I., 2003. Comparative study of *in vitro* digestibility of food proteins and effect of preheating on the digestion. *Biological and Pharmaceutical Bulletin*, 26(7), pp.969–973.

Tong, W., Gao, C. & Möhwald, H., 2008. pH-responsive protein microcapsules fabricated via glutaraldehyde mediated covalent layer-by-layer assembly. *Colloid and Polymer Science*, 286(10), pp.1103–1109.

United States Pharmacopeia, 2009. *The United States Pharmacopeia and National Formulary (NSF 32-NF27)* 32nd ed., Rockville: United States Pharmacopeial Convention.

Unterhaslberger, G., Schmitt, C., Sanchez, C., Appolonia-Nouzille, C. & Raemy, A., 2006. Heat denaturation and aggregation of β-lactoglobulin enriched WPI in the presence of arginine HCl, NaCl and guanidinium HCl at pH 4.0 and 7.0. *Food Hydrocolloids*, 20(7), pp.1006–1019.

Valle-Riestra, J. & Barnes, R.H., 1970. Digestion of heat-damaged egg albumen by the rat. *Journal of Nutrition*, 100(8), pp.873–882.

Walsh, J.H., Richardson, C.T. & Fordtran, J.S., 1975. pH dependence of acid secretion and gastrin release in normal and ulcer subjects. *Journal of Clinical Investigation*, 55(3), p.462.

Wang, J., Tang, J., Wang, Y. & Swanson, B., 2009. Dielectric properties of egg whites and whole eggs as influenced by thermal treatments. *LWT - Food Science and Technology*, 42(7), pp.1204–1212.

Wang, L., Amphlett, G., Blättler, W.A., Lambert, J.M. & Zhang, W., 2005. Structural characterization of the maytansinoid–monoclonal antibody immunoconjugate, huN901–DM1, by mass spectrometry. *Protein Science*, 14(9), pp.2436–2446.

Wang, Q. & Ismail, B., 2012. Effect of Maillard-induced glycosylation on the nutritional quality, solubility, thermal stability and molecular configuration of whey protein. *International Dairy Journal*, 25(2), pp.112–122.

Wang, W., Nema, S. & Teagarden, D., 2010. Protein aggregation-pathways and influencing factors. *International Journal of Pharmaceutics*, 390(2), pp.89–99.

Weijers, M., Sagis, L.M.C., Veerman, C., Sperber, B. & Van Der Linden, E., 2002. Rheology and structure of ovalbumin gels at low pH and low ionic strength. *Food Hydrocolloids*, 16(3), pp.269–276.

Wickham, M., Faulks, R. & Mills, C., 2009. *In vitro* digestion methods for assessing the effect of food structure on allergen breakdown. *Molecular Nutrition & Food Research*, 53(8), pp.952–958.

Yasir, S.B.M., Sutton, K.H., Newberry, M.P., Andrews, N.R. & Gerrard, J.A., 2007. The impact of Maillard cross-linking on soy proteins and tofu texture. *Food Chemistry*, 104(4), pp.1502–1508.

Yeboah, F.K., Alli, I. & Yaylayan, V.A., 1999. Reactivities of D-glucose and D-fructose during glycation of bovine serum albumin. *Journal of Agricultural and Food Chemistry*, 47(8), pp.3164–3172.

Yoshino, K., Sakai, K., Mizuha, Y., Shimizuike, A. & Yamamoto, S., 2004. Peptic digestibility of raw and heat-coagulated hen's egg white proteins at acidic pH range. *International Journal of Food Sciences and Nutrition*, 55(8), pp.635–640.

Zhang, Y. & Cremer, P.S., 2006. Interactions between macromolecules and ions: the Hofmeister series. *Current Opinion in Chemical Biology*, 10(6), pp.658–663.

Chapter Three

3 Proteomic Analysis of Heat Induced Amino Acid Modifications

3.1 Introduction

The uptake of sufficient protein by the body is essential to ensure good physical and mental health. Proteins are required to be hydrolysed into single amino acids, di- and tripeptides in order to be absorbed by enterocytes (Newey & Smyth 1960; Webb 1990; Gilbert et al. 2008) (Section 1.5). If amino acids and peptides are chemically modified they can have a lower bioavailability compared to their unmodified counterparts (Elango et al. 2009; Gilani et al. 2005). Any food processing resulting in an increase of modified amino acids is therefore likely to lower the nutritional value of the protein. This is especially important for essential amino acids. If an organism is deprived of an essential amino acid, protein synthesis is halted and the remaining amino acids are oxidised after absorption (Elango et al. 2009). Additionally, a range of modified amino acids possibly pose health risks if consumed (Friedman 2010).

This section focuses on the discussion of food relevant amino acid modifications and a holistic approach for the identification of such amino acid modifications in processed protein via mass spectrometry using EW as a model system. There is a need for replicable and fast methods to accurately evaluate protein quality of food materials after processing (Rutherfurd & Moughan 2012). Additionally, it is desirable to understand how and when protein modifications occur during commercial and domestic processes (Friedman 2003). *In vitro* digestibility studies coupled with a comprehensive amino acid damage profiling may grant an in depth insight of the nutritional quality of a given food.

Analysis of proteinaceous food products via mass spectrometry is a powerful tool to simultaneously profile a wide range of chemical changes, giving this technique an advantage over other methods including spectrophotometric methods. Pioneering work by Yates et al. (1995) established a method to include chemical modification parameters when conducting a database search (Yates et al. 1995). Recently, the approach has been adapted

and used to evaluate environmental and process-induced modification of proteinaceous materials including skin, textiles, and food (Grosvenor et al. 2011). Examples of common food relevant amino acid modifications are listed in Table 3.1. The chemical structures of example modifications are displayed in Figure 3.1.

Table 3.1 *List of food-relevant amino acid modifications included for the assessment of the protein damage score.*

Modification	**Amino Acid(s)**	**Chemical Modification**
Oxidation	CMFHWY	O(1)
Dioxidation	CFWY	O(2)
Trioxidation	C	O(3)
Dehydrated	CST	H(-2) O(-1)
Quinone	Y	H(-2) O(1)
Kynurenine	W	C(-1) O(1)
Nitration	FHWY	H(-1) N(1) O(2)
Carbamylation	N-term	H(1) C(1) N(1) O(1)
Deamidation	NQ, N-term	H(-1) N(-1) O(1)
Carboxymethylated	K	C(2) H(2) O(2)

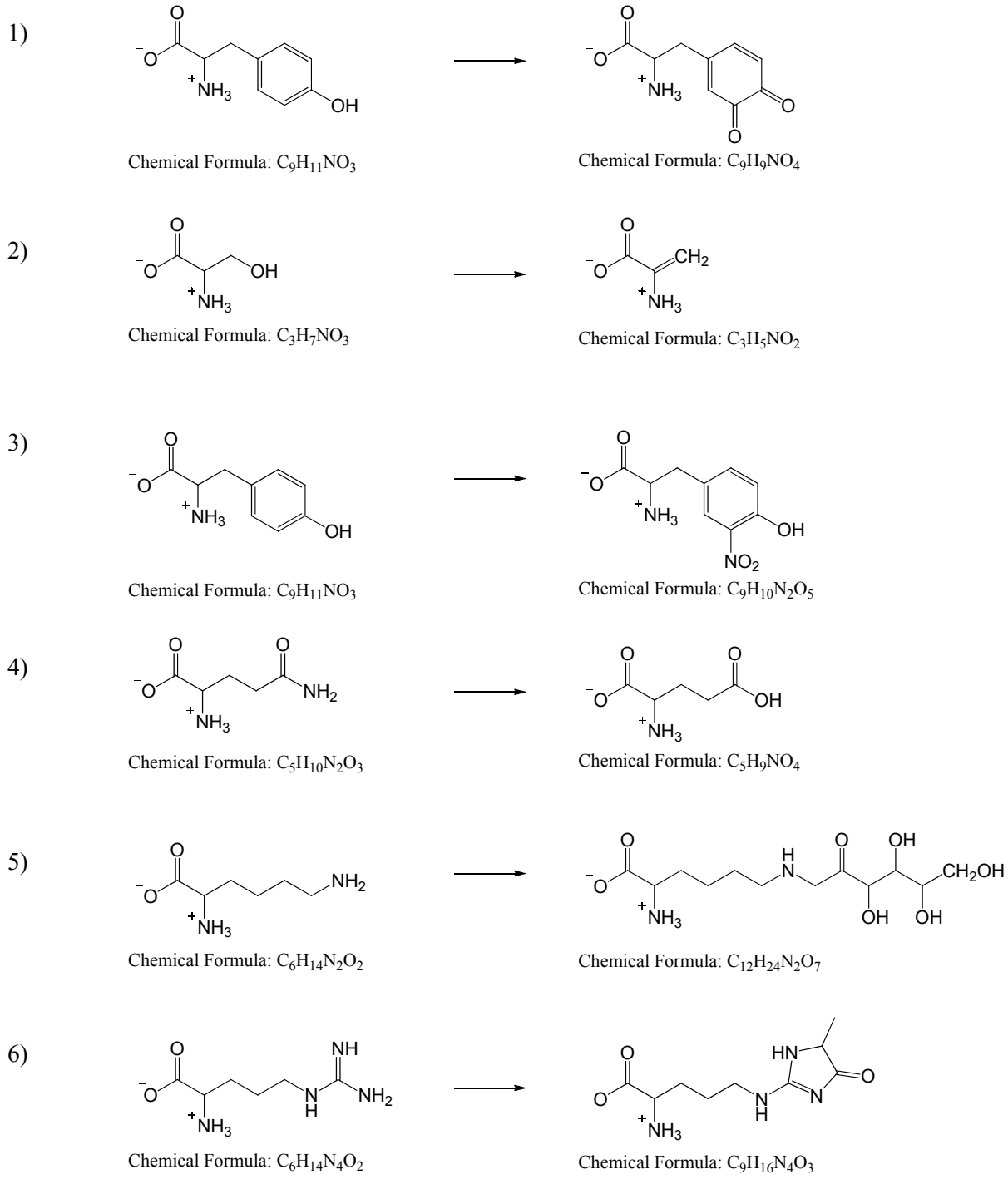

Figure 3.1 *Examples of chemical modifications that may occur during food processing. 1) oxidation of tyrosine; 2) dehydration of serine; 3) nitration of tyrosine; 4) deamidation of glutamine; 5) glycation of lysine; 6) hydroimidazolone formation from arginine (Giulivi et al. 2003; Finot 2005; Abello et al. 2009; Zhang et al. 1993; Lima et al. 2009; Brock et al. 2007).*

3.2 Amino Acid Modifications

Proteinaceous foods that are stored or processed are likely to develop some amino acid residue damage over time. These chemical modifications of amino acids include oxidation, deamidation, nitration, dehydration, and carboxymethylation, amongst many others. Modifications may lead to a lower bioavailability and have been shown to be toxic in some cases (Robbins et al. 1980; Šebeková & Somoza 2007; Gross et al. 2011; Friedman 1999).

3.2.1 Oxidation Products

Food processing may lead to oxidative damage of amino acids, including both single and multiple oxidation events leading to a range of products. Oxidative damage of amino acids can be inferred by oxidising metal ions, photo oxidation, and oxidation by enzymes or lipids (Meade et al. 2005; Stadtman & Levine 2003). During food processing, particularly where heating is involved, formation of reactive oxygen species (ROS) such as $^{\bullet}OH$ and $O_2^{\bullet-}$ may occur. These species may react with amino acids, peptides and proteins resulting in peptide bond cleavage, peptide cross-linking, and oxidative amino acid modification (Stadtman & Levine 2003) which in turn may affect the nutritional value of a given protein.

The single oxidation of cysteine and methionine is enzymatically reversible. The bioavailability of cysteine and cystine was found to be similar in the *L*-configuration but not in the *D*-configuration (Baker 2006). However, previous studies found that the reduction of disulfide bonds in soy flour increases the digestibility of the protein fraction (Faris et al. 2008). The dioxidation of methionine and the trioxidation of cysteine have been reported to render the respective amino acids unavailable (Rutherfurd & Moughan 2008).

The oxidation of aromatic amino acids such as tyrosine (Figure 3.1) may lead to the formation of 3,4-dihydroxyphenylalanine (DOPA), quinones or bityrosine (Giulivi et al. 2003). Histidine can be converted to 2-oxohistidine. These changes of amino acid profiles during processing are likely to alter the nutritional properties of food.

3.2.2 Nitration Products

The presence of reactive oxygen species may facilitate the formation of reactive nitrating agents (Abello et al. 2009). In the presence of nitrating agents, such as peroxynitrite ($ONOO^-$) and nitrogen dioxide (NO_2), aromatic amino acids (tyrosine, phenylalanine, and tryptophan) as well as the non-aromatic amino acids histidine, cysteine, and methionine may be nitrated (Figure 3.1) (Abello et al. 2009). The nitration of proteins and peptides has been observed *in vivo* (Ischiropoulos 1998; Abello et al. 2009). It has been reported that peptide cleavage by chymotrypsin was attenuated in the presence of nitrated tyrosine compared to the unmodified tyrosine control (Souza et al. 2000). A higher degree of nitration is therefore likely to influence protein digestibility.

3.2.3 Dehydration Products

Amino acids can undergo dehydration reactions under processing conditions such as heat treatment or alkaline treatment. Serine (Figure 3.1), and threonine are commonly modified in this way. Heat treatment of food proteins can cause the formation of dehydroalanine (DHA) from cysteine, cystine, and serine phosphate at neutral and alkaline pH, for example during alkaline treatment of protein extracts such as soy and caseinate (Finot 2005). DHA can subsequently react with lysine to form lysinoalanine (LAL), which is commonly found in considerable concentration in processed foods. Up to 653 mg of LAL per kg of crude protein (653 mg/kg crude protein) was observed in ultra-heat treated milk (Faist et al. 2000) and up to 514 mg/kg protein was found in infant formulas (D'Agostina et al. 2003). High levels of LAL were also found in pickled century eggs (Chang et al. 1999). LAL enriched diets have been linked to a decreased digestibility of protein and toxic effect towards rat kidneys (Robbins et al. 1980).

3.2.4 Deamidation Products

The functional groups of glutamine and asparagine, as well as the N-terminal amino group of proteins and peptides may undergo deamidation reactions (Figure 3.1) during food processing (Riha et al. 1996). During deamidation, the free amino group is replaced by a

hydroxyl group ,i.e., glutamine is transformed to glutamate while asparagine is transformed to aspartate (Zhang et al. 1993). During the deamidation reaction, ammonia is released which may react in Maillard type reactions influencing the nutritional value of proteins (see Section 3.2.5) (Zhang et al. 1993).

3.2.5 Maillard Reaction Products

Lysine and arginine residues readily react in the Maillard reaction with reducing sugars and lipids. Maillard modified amino acids are commonly produced during the heating of food. The Maillard reaction is influenced by pH, the presence or absence of water, and temperature (Ajandouz et al. 2008). The reaction products have been reported to cause a loss in the bioavailability of the modified amino acids and proteins as soon as the reaction has progressed past the Amadori compound state, e.g. premelanoidins such as carboxymethyllysine, and melanoidins (Finot 2005; Wang & Ismail 2012) (Section 2.6). Subsequent complex reactions cause the formation of advanced glycation endproducts (AGEs) and may also lead to the cross-linking between two peptides or proteins. Positive effects of AGEs are attributed mostly to antioxidant activity (Ames 2007; Lindenmeier et al. 2002), whereas negative effects potentially include the promotion of atherosclerosis, inflammation, oxidative stress, and nephrotoxicity (Šebeková & Somoza 2007).

N^{ε}-(fructosyl)lysine and hydroimidazolone (HI) (Figure 3.1) can both be generated during the Maillard reaction when glucose is present (Figure 3.2). These two modifications modify lysine and arginine residues respectively (Lima et al. 2009; Brock et al. 2007), thereby influencing the recognition by trypsin (Keil 1992). Modification of trypsin cleavage sites may lead to a decreased protein digestibility as well as lower absorption of the modified amino acids (Rérat et al. 2002).

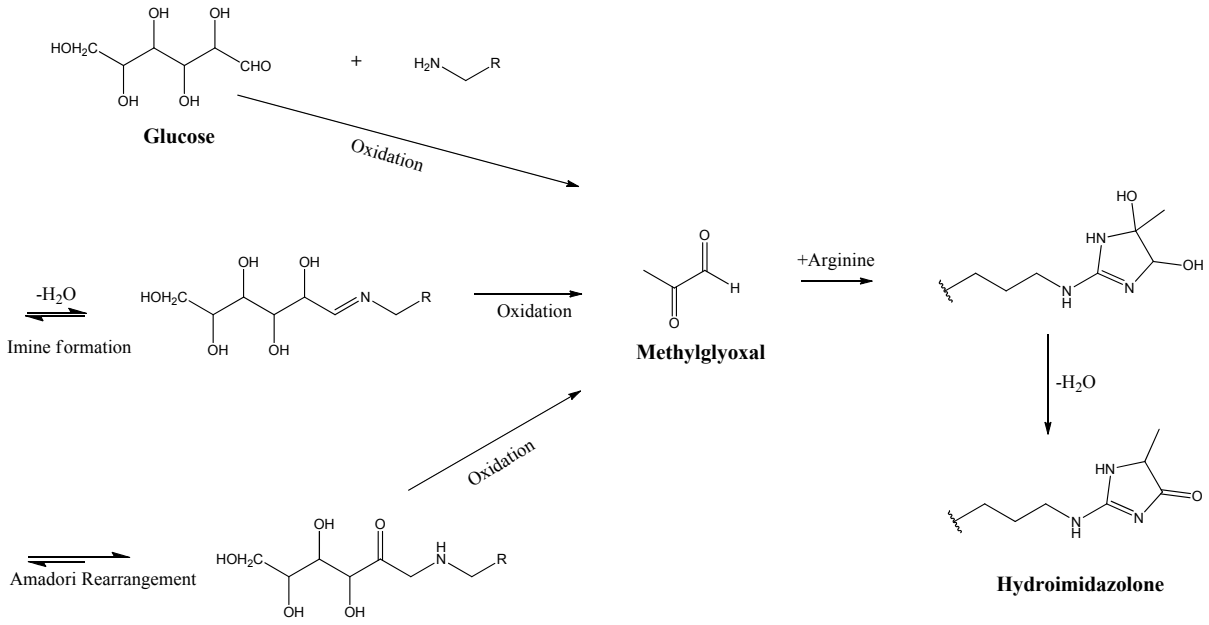

Figure 3.2 *Proposed mechanism for hydroimidazolone (HI) formation from glucose or methylglyoxal and arginine as precursors. Adapted from (Lima et al. 2009).*

3.2.6 Carbamylation Products

Carbamylation of proteins occurs during the reaction of cyanate (a decomposition product of urea) with an N-terminal amine. It has been reported that carbamylated albumin is more toxic to kidneys compared to unmodified albumin (Gross et al. 2011).

3.2.7 Formation of *D*-Amino Acids

It is well known that the racemisation of naturally prevalent *L*-amino acids into their *D*-isomers can occur under acidic, alkaline and heat treatment (Friedman 1999; Friedman 2010). Alkaline treatment is commonly applied in food processes such as protein extraction from flours and meats (Omana et al. 2010).

Depending on the amino acid, the ingestion of free *D*-amino acids by mammals can have one of three effects: 1) The *D*-isomer is utilised to a certain percentage via enzymatic conversion into the *L*-isomer for example *D*-phenylalanine, *D*-tryptophan, 2) The *D*-

isomer is not utilised because conversion cannot be carried out for example for *D*-methionine, *D*-lysine or 3) the D-isomer has a toxic effect for example *D*-cysteine, *D*-serine, *D*-proline (Friedman 1999). Toxicology mechanisms are not well characterised but assimilation of certain *D*-amino acids including *D*-serine and *D*-lysinoalanine in kidney tissues has been related to acute necrosis of tubili (Kaltenbach et al. 1979; Carone et al. 1985; Friedman 1999). The antagonistic or toxic effects of *D*-cysteine result in a slower weight gain in growing mice (Friedman & Gumbmann 1984) and abnormal behaviour in chicks (Yamane et al. 2009). The effect of protein bound *D*-amino acids is not yet fully understood and merits further studies.

3.2.8 Enzymatic Modification Products

Enzymatic protein cross-linking via microbial transglutaminase (TGAse) (EC 2.3.2.13) is often used as structure enhancer and is extensively used as meat glue. TGAse covalently creates a ε-(γ-glutamine)-lysine bond (Zhu et al. 1995; Gerrard & Sutton 2005) involving a ε-amino group of lysine and the γ-amide group of glutamine residues. It has been observed that TGAse cross-linked proteins such as whey proteins exhibit high resistance to proteolytic degradation (Cortez et al. 2004; Motoki & Seguro 1998) by common enzymes. However, ε-(γ-glutamine)-lysine bonds may be cleaved by the enzyme γ-glutamyltransferase (EC 2.3.2.2) (Okada et al. 2006; Seguro et al. 1995; Seguro et al. 1996). γ-glutamyltransferase is found in different tissues including at the brush-border membrane inside the small intestine, inside the kidney, and in the blood. Thus, if ε-(γ-glutamine)-lysine bonds are present due to transglutaminase activity, γ-glutamyltransferase may help in hydrolysing these and make the respective single amino acids bioavailable. In fact, it was reported that rats showed no significant difference in growth when being fed TGAse cross-linked casein compared to free casein (Seguro et al. 1996). The study showed that 99% of the ^{14}C labelled lysine was taken up and assimilated by the rat.

The assessment of the whole impact of food processing on the nutritional value of foodstuffs is complicated. Food processing may influence the bioavailability of amino acids dramatically. The described amino acid modifications indicate only a limited number of the many different pathways that can impact on nutritional availability of certain proteins and peptides.

3.3 Proteomic Profiling

In order to determine the character of amino acid modifications, proteomic profiling via tandem mass spectrometry (MS/MS) was undertaken. In brief, raw and boiled EW was subjected to a tryptic digest, the peptides were cleaned and analysed via high performance liquid chromatography (HPLC) separation followed by MS/MS acquisition. The generated mass to charge (m/z) mass spectrum was compared to expected theoretical fragments (against the NCBInr database using Mascot v2.2.) (Section 7.9). Modifications of peptides were detected by including variable modification that corresponded to the expected mass change of the modification during database search. Proteomic profiling of EW samples by MS/MS characterisation of amino acid modifications showed that a certain baseline level of modifications was detectable even in freshly laid eggs. However, a marked increase of amino acid damage was induced by boiling the egg white (Table 3.2). The scoring system used to assess the amino acid damage (Section 7.9) was based around modification hierarchies and takes into account the ratio of observed modified to non-modified amino acid residues in combination with a weighting of the severity of the damage (Dyer et al. 2010). The scores for raw EW (0.70) and boiled EW (1.27) are the sum of all weighted scores of the respective sample. The individual damaged amino acids are listed and generally show a higher ratio of damaged to undamaged amino acids in the heat treated samples.

Table 3.2 *Protein modifications of raw EW and boiled EW. s_w = weighted modification score, aa_{mod} = number of a specific amino acid residue carrying a specific modification, aa_{tot}= total number of a specific amino acid residue observed, f_{mod}= modification factor (e.g. f_{mod} = 0 for non-oxidative modification, f_{mod} = 1 for single oxidation, f_{mod} = 2 for double oxidation, f_{mod} = 3 for triple oxidation), qualifying peptides = the number of unique peptide identifications meeting the MS/MS score threshold of 45.*

			Raw Egg White Score: 0.70				**Boiled Egg White Score: 1.27**			
Modification	**Amino Acid**	**f_{mod}**	**aa_{mod}**	**aa_{mod}/aa_{tot}**	**$s_{w(Ox)}$**	**$s_{w(Non-Ox)}$**	**aa_{mod}**	**aa_{mod}/aa_{tot}**	**$s_{w(Ox)}$**	**$s_{w(Non-Ox)}$**
Oxidation	CMFHWY	1	15	C(1/60), F(4/86), M(3/30), W(1/27), Y(6/69)	0.29	-	9	F(4/57), M(1/23), W(3/28), Y(1/35)	0.25	-
Dioxidation	CFWY	2	1	F(1/86)	0.02	-	2	W(2/28)	0.14	-
Trioxidation	C	3	-	-	-	-	-	-	-	-
Nitration	FHWY	3	3	F(2/86), Y(1/69)	0.11	-	4	F(3/57), H(1/13)	0.39	-
Kynurenine	W	3	-	-	-	-	-	-	-	-
Quinone	Y	3	-	-	-	-	-	-	-	-
Carbamylated	KR, N-term	1	-	-	-	-	-	-	-	-
Deamidated	NQ, N-term	1	21	N(14/114), Q(7/81)	-	0.21	25	N(19/95), Q(6/66)	-	0.29
Dehydrated	ST	1	6	S(5/131), T(1/112)	-	0.05	2	S(2/93)	-	0.20
Carboxy-methylated	K	1	1	K(1/100)	-	0.01	-	-	-	-
			$s_{w(raw)}$		**0.43**	**0.27**	**$s_{w(boiled)}$**		**0.78**	**0.49**

The comparison of raw and boiled EW (Table 3.2) shows that commonly occurring oxidative modifications include single oxidations, dioxidation, and nitration which can affect the nutritional properties of proteins in various ways (Section 3.2.1 and Section 3.2.2). No marked difference was observed between raw and boiled EW for single oxidations. However, nitration and, to a lesser degree, dioxidation of amino acids increased in the heated sample. Deamidation (Section 3.2.4) and dehydration (Section 3.2.3) modifications were common non-oxidative modifications. There was a marked increase of dehydration of serine and threonine residues as well as deamidation of asparagine and glutamine residues in the boiled sample (Table 3.2). Hydrothermal degradation of proteins has previously been reported (Friedman 1999), resulting initially in DHA formation, as observed here, and subsequently in protein-protein cross-linking influencing protein digestibility.

3.3.1 Amino Acid Damage in the Presence of Maillard Reaction Partners at Prolonged Heating Times

The observed difference in the amino acid damage profile between raw and boiled EW prompted further investigations of the relationship between heating time and amino acid damage. Furthermore, the effects of the Maillard reaction partners, glucose and methylglyoxal, were studied. This allowed a correlation of the observed digestibility changes in the presence of Maillard reaction partners (Section 2.6) with observed amino acid modifications. A total of nine samples (Table 3.3) were analysed for amino acid modifications.

Table 3.3 *Sample list for the determination of time dependence and effect of Maillard partner on amino acid modifications.*

	Heating Time [minutes]		
	0	**10**	**60**
EW in Milli-Q water	S1	S2	S3
EW in 100 mM glucose	S4	S5	S6
EW in 100 mM methylglyoxal	S7	S8	S9

Pure EW in the absence of additional Maillard reaction partners was analysed in order to measure the background amino acid modification of a non-oxidative nature (deamidation, dehydration, and dehydrogenation). As observed in the preliminary experiment, an increase in temperature to 100 °C resulted in the rise of amino acid modifications after 10 minutes. The replicate experiments showed an increase of the non-oxidative damage score from 0.15 to 0.17 (Figure 3.3) which is below the previously observed 0.27 to 0.49 change (Table 3.2). The discrepancy in baseline could potentially be accounted for by slight variations of experimental conditions. The degree of protein aggregation, the efficiency of the tryptic digests, as well as differences in egg whites (two suppliers of day fresh hen eggs were used) could have contributed to the observed differences. The observed higher total differences before and after heating for the first sample (0.22) compared to the second sample (0.02) is likely based on the pre-heating modifications. These pre-existing modifications (0.27 and 0.15) are likely to contribute to further modifications of the peptide due to their altered chemistry. Furthermore, peptide material present in the control samples (unheated) may already be modified. There are likely to be additional modified peptides present that are below the quality threshold which prevents these peptides to be included in the final score. However, only a small amount of further modification is necessary to produce sufficient quantities of modified peptides for robust characterization after heating. These small changes may therefore cause previously disregarded peptides to be included in the final scoring. Thereby, small changes may contribute to the seemingly large difference between the samples. This is a further reason why the unheated control sample with already high levels of baseline modification showed a larger difference on heating than the unheated control sample with low levels of baseline modifications.

Since deamidation and dehydration modifications were commonly observed in the treated samples they were chosen as marker modifications to assess the heat damage of protein EW. There is a marked increase from 0.17 to 0.26 (Figure 3.3) of non-oxidative damage (pooled deamidation and dehydration modifications) between 10 minutes and 60 minutes of heating. This indicates that prolonged heat exposure results in the increase of amino acid modifications. The dehydration of serine and threonine can influence the nutritional value of proteins by contributing to cross-linking reactions (Section 3.2.3). The deamidation induced amino acid profile change (Section 3.2.4) may not contribute directly to a marked loss of nutritional quality. However, it has been reported that the deamidation

of proteins alter the structural characteristics of proteins dramatically. Rice and soy protein solubility was increased markedly by non-enzymatic and enzymatic deamidation respectively (Paraman et al. 2007; Suppavorasatit et al. 2013). Increased deamidation causes exposure of acidic glutamate and aspartate which in turn may alter the protein aggregate structure and therefore protein digestibility (Carbonaro et al. 1997). However, the increased digestibility is unlikely to be an amino acid specific effect because pepsin, trypsin, and chymotrypsin do not usually cleave the peptide backbone near glutamine or asparagine (or glutamate, aspartate) residues (Keil 1992).

In addition to dehydration and deamidation, the effects of glucose and methylglyoxal on amino acid modifications were monitored. Potential modifications of EW amino acids induced by the presence of glucose could be monitored by formation of N^{ϵ}-(fructosyl)lysine (Figure 3.1). However, MS/MS analysis of the samples did not reveal detectable N^{ϵ}-(fructosyl)lysine modifications when searching for modifications with the mass of +162, which would correspond to the condensation of a hexose, such as glucose, to lysine. The absence of N^{ϵ}-(fructosyl)lysine may indicate that the compound had not formed at detectable concentrations, or alternatively, had progressed to more advanced glycation products. N^{ϵ}-(carboxymethyl)lysine (Lima et al. 2009) and N^{ϵ}-(carboxyethyl)lysine (Ahmed et al. 1997), two further glycation products involving lysine were only sporadically detected via MS/MS of the nine samples. However, arginine residues were readily modified by methylglyoxal to form hydroimidazolone (Figure 3.2) which was detectable by MS/MS analysis. Therefore, hydroimidazolone was used to monitor the progression of Maillard modification by methylglyoxal. The stacked column diagram in Figure 3.3 depicts 1) the non-oxidative damage observed for pure EW (black), and 2) the hydroimidazolone modification observed for EW in the presence of 100 mM methylglyoxal (red).

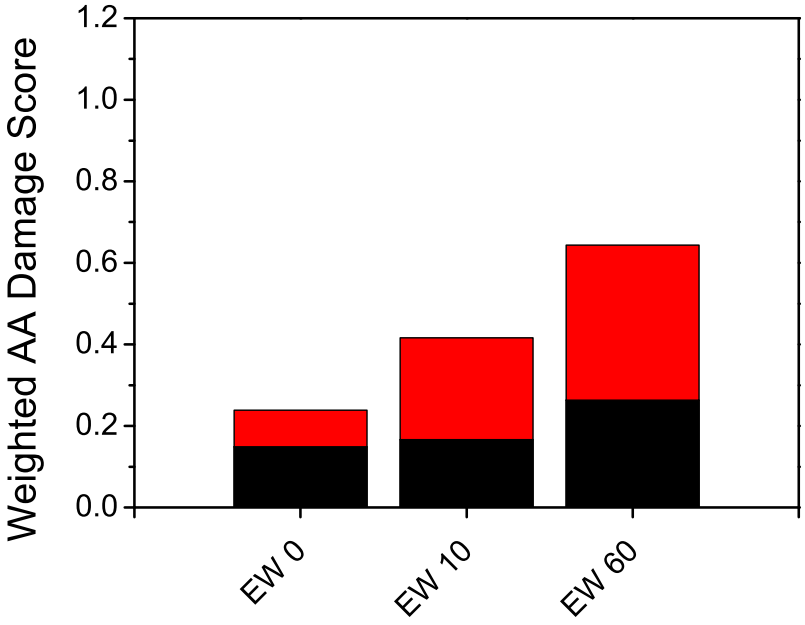

Figure 3.3 *Weighted amino acid modification score. Black) combined deamidation (glutamine and asparagine residues) and dehydration (serine and threonine residues) damage of EW in Milli-Q water. Red) hydroimidazolone (arginine residues) damage of EW arginine in 100 mM methylglyoxal.*

Methylglyoxal reacted instantaneously with arginine residues as judged by the formation of hydroimidazolone even before heating (t = 0). The increase of hydroimidazolone formation over time reached a total of 0.38 after 60 minutes of heating at 100 °C which corresponds to 38 % of observed arginine residues modified to hydroimidazolone. The progress of hydroimidazolone formation was monitored for all nine samples. As expected, no hydroimidazolone was detected in the pure EW sample (Figure 3.4). However, in the presence of glucose, hydroimidazolone was also detected after 60 minutes of heating. This indicates that the Maillard modification of glucose treated EW protein has progressed into the advanced Maillard reaction products which could possibly explain the lack of detectable N^{ε}-(fructosyl)lysine, N^{ε}-(carboxymethyl)lysine, and N^{ε}-(carboxyethyl)lysine. The presence of hydroimidazolone may decrease protein quality, because the presence of advanced Maillard reaction products generally decrease the nutritional value by described mechanisms (Section 3.2.5). The presence of hydroimidazolone in a glucose treated sample further supports that methylglyoxal is a useful model to assess the Maillard reaction in food systems.

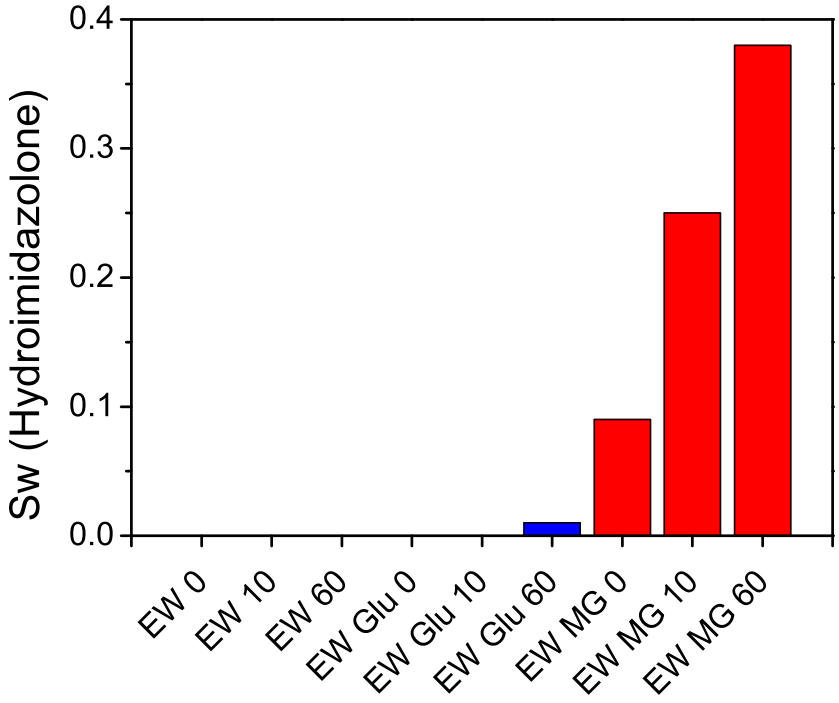

Figure 3.4 *Weighted hydroimidazolone score (arginine residues) of EW.*

3.3.2 Ovalbumin as Marker Protein

Often it is desirable to monitor the chemical modifications that occur in a mixture of proteins. However, if the modifications are drastic, some proteins may become undetectable during the modification process due to a mass spectrum that is too convoluted. In order to monitor sample quality it can therefore be desirable to have an internal marker that is affected by the measured modifications. The abundance of the marker may in turn be used to quantify modification induced changes of the sample during sample treatment.

Ovalbumin (PDB entry: 1OVA (Stein et al. 1991)) was evaluated as an internal standard because it was the protein most commonly identified during MS/MS analysis of derived peptides. Ovalbumin is the most abundant protein in chicken egg white and therefore likely to remain present in samples for a long time compared to lower abundance proteins such as lysozyme. Table 3.4 lists the identified peptides of all nine samples (S1-S9) from MS/MS analysis that were matched to ovalbumin. The observed modifications are also

listed. Carbamidomethylation of cysteine is an artefact of the sample preparation using iodoacetamide to alkylate cysteine residues (Section 7.9). The untreated EW sample (S1) did not show the presence of ovalbumin derived peptides. This is likely due to protease inhibiting proteins present in raw EW. The two remaining unheated samples (S4 and S7) also show low abundance of ovalbumin derived peptides. Increasing the temperature to 100 °C generally resulted in a higher abundance of ovalbumin derived peptides (S2, S5, and S8) indicating that trypsin digestion is generating more peptides compared to unheated EW. This is in good agreement with the results obtained during the *in vitro* digestibility assays that showed increased digestibility of heated EW (Section 2.2). After a prolonged heating time of 60 minutes (S3, S6, S9) there were even more peptides generated in sample S6 while S3 remained on a similar level as S2. However, for the methylglyoxal treated sample (S9) the number of detected ovalbumin peptides decreased markedly compared to sample S8. This behaviour may reflect either the increased resistance to tryptic digestion (caused by modified arginine residues (Keil 1992)) or the fact that some abundant modifications may mask the signal.

Reassuringly, ovalbumin could be detected in almost all samples and corresponded to the overall observation of increased amino acid modifications with increasing harshness of the EW treatments. Therefore, ovalbumin seemed a good marker of the total observed modifications. It is likely that in other systems (e.g., whey protein or milk) the study of a marker protein such as β-lactoglobulin (β-lg) may be of equal value.

Table 3.4 *Identified peptides including modification and modification position.*

Sample	Sequence	Modifications
S1	-	-
S2	R.ADHPFLFCIK.H	Carbamidomethyl: 8
	R.LYAEERYPILPEYLQCVK.E	Carbamidomethyl: 16
	R.YPILPEYLQCVK.E	Carbamidomethyl: 10
	R.YPILPEYLQCVKELYR.G	Carbamidomethyl: 10
S3	R.DILNQITKPNDVYSFSLASR.L	Carboxymethyl: 8
	R.ADHPFLFCIK.H	Carbamidomethyl: 8
	R.YPILPEYLQCVK.E	Carbamidomethyl: 10

S4	R.ADHPFLFCIK.H	Carbamidomethyl: 8
	R.LYAEERYPILPEYLQCVK.E	Carbamidomethyl: 16
	R.YPILPEYLQCVK.E	Carbamidomethyl: 10
S5	R.ELINSWVESQTNGIIR.N	Oxidation: 6
	K.ISQAVHAAHAEINEAGR.E	Oxidation: 6
	Y.PILPEYLQCVK.E	Carbamidomethyl: 9
	R.ADHPFLFCIK.H	Carbamidomethyl: 8
	R.LYAEERYPILPEYLQCVK.E	Carbamidomethyl: 16
S6	R.GGLEPINFQTAADQAR.E	Deamidated: 9
	N.SWVESQTNGIIR.N	Deamidated: 8
	R.GGLEPINFQTAADQAR.E	Deamidated: 7
	N.SWVESQTNGIIR.N	Deamidated: 6
	R.DILNQITKPNDVYSFSLASR.L	Deamidated: 4, 5
	R.ELINSWVESQTNGIIR.N	Deamidated: 4, 2
	R.DILNQITKPNDVYSFSLASR.L	Deamidated: 4, 10
	K.ISQAVHAAHAEINEAGR.E	Deamidated: 3
	R.GGLEPINFQTAADQAR.E	Deamidated: 14
	K.ISQAVHAAHAEINEAGR.E	Deamidated: 13
	Y.PILPEYLQCVK.E	Carbamidomethyl: 9
	R.ADHPFLFCIK.H	Carbamidomethyl: 8
	R.LYAEERYPILPEYLQCVK.E	Carbamidomethyl: 16
	R.YPILPEYLQCVK.E	Carbamidomethyl: 10
S7	R.YPILPEYLQCVK.E	Carbamidomethyl: 10
S8	K.IKVYLPRMK.M	hydroimidazolone: 7
	R.LYAEERYPILPEYLQCVK.E	hydroimidazolone: 6
	K.VYLPRMK.M	hydroimidazolone: 5
	K.ELYRGGLEPINFQTAADQAR.E	hydroimidazolone: 4
	K.LTEWTSSNVMEERK.I	hydroimidazolone: 13
	Y.PILPEYLQCVK.E	Carbamidomethyl: 9
	R.ADHPFLFCIK.H	Carbamidomethyl: 8
	P.ILPEYLQCVK.E	Carbamidomethyl: 8
	R.LYAEERYPILPEYLQCVK.E	Carbamidomethyl: 16
	R.YPILPEYLQCVK.E	Carbamidomethyl: 10
S9	K.DSTRTQINK.V	hydroimidazolone: 4
	R.YPILPEYLQCVK.E	Carbamidomethyl: 10

3.4 Summary and Discussion

The use of mass spectrometry for determining amino acid modifications in processed EW was demonstrated. Oxidative damage, deamidation and dehydration were observed to increase over time as EW was heated at 100 °C. Furthermore, the reaction with methylglyoxal was detectable and showed a similar trend of increasing modification with heating time. Together these results indicate that significant damage occurs to the amino acid profile of EW proteins during processing. The achieved degree of sensitivity implies that even relatively mild processing can induce detectable amino acid modification. Ovalbumin proved to be a reasonably good internal standard with sufficient abundance in the generated mass spectra even after harsh sample treatment (60 minutes, 100 °C, 100 mM methylglyoxal).

The information gained may contribute to the understanding of food protein damage on a molecular level. The holistic approach of assessing a series of protein samples can yield information on a large proportion of amino acid modifications. To this end, the samples should be representative of actual food systems (as was the case here). If the exact mass change, resulting from chemical modification, is known, the use of MS/MS analysis is reliable and replicable. It should be remembered that some modifications may mask the signal of other modifications (as was the case for methylglyoxal modified EW). Furthermore, it was demonstrated that a complex sample mixture of proteins can be used which is relevant for most food systems as they generally contain protein mixtures.

3.5 References

Abello, N., Kerstjens, H.A.M., Postma, D.S. & Bischoff, R., 2009. Protein tyrosine nitration: selectivity, physicochemical and biological consequences, denitration, and proteomics methods for the identification of tyrosine-nitrated proteins. *Journal of Proteome Research*, 8(7), p.3222.

Ahmed, M.U., Brinkmann Frye, E., Degenhardt, T.P., Thorpe, S.R. & Baynes, J.W., 1997. N-epsilon-(carboxyethyl)lysine, a product of the chemical modification of proteins by methylglyoxal, increases with age in human lens proteins. *Biochemical Journal*, 324(Pt 2), pp.565–570.

Ajandouz, E.H., Desseaux, V., Tazi, S. & Puigserver, A., 2008. Effects of temperature and pH on the kinetics of caramelisation, protein cross-linking and Maillard reactions in aqueous model systems. *Food Chemistry*, 107(3), pp.1244–1252.

Ames, J.M., 2007. Evidence against dietary advanced glycation endproducts being a risk to human health. *Molecular Nutrition and Food Research*, 51(9), pp.1085–1090.

Baker, D.H., 2006. Comparative species utilization and toxicity of sulfur amino acids. *Journal of Nutrition*, 136(6), p.1670S.

Brock, J.W.C., Cotham, W.E., Thorpe, S.R., Baynes, J.W. & Ames, J.M., 2007. Detection and identification of arginine modifications on methylglyoxal-modified ribonuclease by mass spectrometric analysis. *Journal of Mass Spectrometry*, 42(1), pp.89–100.

Carbonaro, M., Cappelloni, M., Nicoli, S., Lucarini, M. & Carnovale, E., 1997. Solubility−digestibility relationship of legume proteins. *Journal of Agricultural and Food Chemistry*, 45(9), pp.3387–3394.

Carone, F.A., Nakamura, S. & Goldman, B., 1985. Urinary loss of glucose, phosphate, and protein by diffusion into proximal straight tubules injured by D-serine and maleic acid. *Laboratory Investigation; a Journal of Technical Methods and Pathology*, 52(6), pp.605–610.

Chang, H.M., Tsai, C.F. & Li, C.F., 1999. Changes of amino acid composition and lysinoalanine formation in alkali-pickled duck eggs. *Journal of Agricultural and Food Chemistry*, 47(4), pp.1495–1500.

Cortez, J., Bonner, P.L.R. & Griffin, M., 2004. Application of transglutaminases in the modification of wool textiles. *Enzyme and Microbial Technology*, 34(1), pp.64–72.

D'Agostina, A., Boschin, G., Rinaldi, A. & Arnoldi, A., 2003. Updating on the lysinoalanine content of commercial infant formulae and beicost products. *Food Chemistry*, 80(4), pp.483–488.

Dyer, J.M., Plowman, J.E., Krsinic, G.L., Deb-Choudhury, S., Koehn, H., Millington, K.R. & Clerens, S., 2010. Proteomic evaluation and location of UVB-induced photo-

oxidation in wool. *Journal of Photochemistry and Photobiology B: Biology*, 98(2), pp.118–127.

Elango, R., Ball, R.O. & Pencharz, P.B., 2009. Amino acid requirements in humans: with a special emphasis on the metabolic availability of amino acids. *Amino Acids*, 37(1), pp.19–27.

Faist, V., Drusch, S., Kiesner, C., Elmadfa, I. & Erbersdobler, H.F., 2000. Determination of lysinoalanine in foods containing milk protein by high-performance chromatography after derivatisation with dansyl chloride. *International Dairy Journal*, 10(5–6), pp.339–346.

Faris, R.J., Wang, H. & Wang, T., 2008. Improving digestibility of soy flour by reducing disulfide bonds with thioredoxin. *Journal of Agricultural and Food Chemistry*, 56(16), pp.7146–7150.

Finot, P.A., 2005. The absorption and metabolism of modified amino acids in processed foods. *Journal of AOAC International*, 88(3), pp.894–903.

Friedman, M., 1999. Chemistry, biochemistry, nutrition, and microbiology of lysinoalanine, lanthionine, and histidinoalanine in food and other proteins. *Journal of Agricultural and Food Chemistry*, 47(4), pp.1295–1319.

Friedman, M., 2003. Nutritional consequences of food processing. *Forum of Nutrition*, 56(1), pp.350–352.

Friedman, M., 2010. Origin, microbiology, nutrition, and pharmacology of D-amino acids. *Chemistry and Biodiversity*, 7(6), pp.1491–1530.

Friedman, M. & Gumbmann, M.R., 1984. The utilization and safety of isomeric sulfur-containing amino acids in mice. *Journal of Nutrition*, 114(12), p.2301.

Gerrard, J.A. & Sutton, K.H., 2005. Addition of transglutaminase to cereal products may generate the epitope responsible for coeliac disease. *Trends in Food Science and Technology*, 16(11), pp.510–512.

Gilani, G.S., Cockell, K.A. & Sepehr, E., 2005. Effects of antinutritional factors on protein digestibility and amino acid availability in foods. *Journal of AOAC International*, 88(3), pp.967–987.

Gilbert, E.R., Wong, E.A. & Webb Jr., K.E., 2008. Board-invited review: peptide absorption and utilization: implications for animal nutrition and health. *Journal of Animal Science*, 86(9), pp.2135–2155.

Giulivi, C., Traaseth, N.J. & Davies, K.J.A., 2003. Tyrosine oxidation products: analysis and biological relevance. *Amino Acids*, 25(3-4), pp.227–232.

Gross, M.-L., Piecha, G., Bierhaus, A., Hanke, W., Henle, T., Schirmacher, P. & Ritz, E., 2011. Glycated and carbamylated albumin are more 'nephrotoxic' than unmodified albumin in the amphibian kidney. *American Journal of Physiology - Renal Physiology*, 301(3), pp.F476–F485.

Grosvenor, A.J., Morton, J.D. & Dyer, J.M., 2011. Proteomic characterisation of hydrothermal redox damage. *Journal of the Science of Food and Agriculture*, 91(15), pp.2806–2813.

Ischiropoulos, H., 1998. Biological tyrosine nitration: a pathophysiological function of nitric oxide and reactive oxygen species. *Archives of Biochemistry and Biophysics*, 356(1), pp.1–11.

Kaltenbach, J.P., Ganote, C.E. & Carone, F.A., 1979. Renal tubular necrosis induced by compounds structurally related to D-serine. *Experimental and Molecular Pathology*, 30(2), pp.209–214.

Keil, B., 1992. *Specificity of proteolysis*, Berlin Heidelberg: Springer.

Lima, M., Moloney, C. & Ames, J.M., 2009. Ultra performance liquid chromatography-mass spectrometric determination of the site specificity of modification of β-casein by glucose and methylglyoxal. *Amino Acids*, 36(3), pp.475–481.

Lindenmeier, M., Faist, V. & Hofmann, T., 2002. Structural and functional characterization of pronyl-lysine, a novel protein modification in bread crust melanoidins showing *in vitro* antioxidative and phase I/II enzyme modulating activity. *Journal of Agricultural and Food Chemistry*, 50(24), pp.6997–7006.

Meade, S.J., Reid, E.A. & Gerrard, J.A., 2005. The impact of processing on the nutritional quality of food proteins. *Journal of AOAC International*, 88(3), pp.904–922.

Motoki, M. & Seguro, K., 1998. Transglutaminase and its use for food processing. *Trends in Food Science and Technology*, 9(5), pp.204–210.

Newey, H. & Smyth, D.H., 1960. Intracellular hydrolysis of dipeptides during intestinal absorption. *Journal of Physiology*, 152(2), pp.367–380.

Okada, T., Suzuki, H., Wada, K., Kumagai, H. & Fukuyama, K., 2006. Crystal structures of γ-glutamyltranspeptidase from *Escherichia coli*, a key enzyme in glutathione metabolism, and its reaction intermediate. *Proceedings of the National Academy of Sciences of the United States of America*, 103(17), pp.6471 –6476.

Omana, D.A., Moayedi, V., Xu, Y. & Betti, M., 2010. Alkali-aided protein extraction from chicken dark meat: Textural properties and color characteristics of recovered proteins. *Poultry Science*, 89(5), pp.1056–1064.

Paraman, I., Hettiarachchy, N.S. & Schaefer, C., 2007. Glycosylation and deamidation of rice endosperm protein for improved solubility and emulsifying properties. *Cereal Chemistry*, 84(6), pp.593–599.

Rérat, A., Calmes, R., Vaissade, P. & Finot, P.-A., 2002. Nutritional and metabolic consequences of the early Maillard reaction of heat treated milk in the pig. *European Journal of Nutrition*, 41(1), pp.1–11.

Riha, W.E., 3rd, Izzo, H.V., Zhang, J. & Ho, C.T., 1996. Nonenzymatic deamidation of food proteins. *Critical Reviews in Food Science and Nutrition*, 36(3), pp.225–255.

Robbins, K.R., Baker, D.H. & Finley, J.W., 1980. Studies on the utilization of lysinoalanine and lanthionine. *Journal of Nutrition*, 110(5), pp.907–915.

Rutherfurd, S.M. & Moughan, P.J., 2012. Available versus digestible dietary amino acids. *British Journal of Nutrition*, 108(S2), pp.S298–S305.

Rutherfurd, S.M. & Moughan, P.J., 2008. Determination of sulfur amino acids in foods as related to bioavailability. *Journal of AOAC International*, 91(4), pp.907–913.

Šebeková, K. & Somoza, V., 2007. Dietary advanced glycation endproducts (AGEs) and their health effects – PRO. *Molecular Nutrition and Food Research*, 51(9), pp.1079–1084.

Seguro, K., Kumazawa, Y., Kuraishi, C., Sakamoto, H. & Motoki, M., 1996. The ε-(γ-glutamyl)lysine moiety in crosslinked casein is an available source of lysine for rats. *Journal of Nutrition*, 126(10), p.2557.

Seguro, K., Kumazawa, Y., Ohtsuka, T., Ide, H., Nio, N., Motoki, M. & Kubota, K., 1995. ε-(γ-glutamyl)lysine: Hydrolysis by γ-glutamyltransferase of different origins, when free or protein bound. *Journal of Agricultural and Food Chemistry*, 43(8), pp.1977–1981.

Souza, J.M. et al., 2000. Proteolytic degradation of tyrosine nitrated proteins. *Archives of Biochemistry and Biophysics*, 380(2), pp.360–366.

Stadtman, E.R. & Levine, R.L., 2003. Free radical-mediated oxidation of free amino acids and amino acid residues in proteins. *Amino Acids*, 25(3-4), pp.207–218.

Stein, P.E., Leslie, A.G., Finch, J.T. & Carrell, R.W., 1991. Crystal structure of uncleaved ovalbumin at 1.95 A resolution. *Journal of Molecular Biology*, 221(3), pp.941–959.

Suppavorasatit, I., Lee, S.-Y. & Cadwallader, K.R., 2013. Effect of enzymatic protein deamidation on protein solubility and flavor binding properties of soymilk. *Journal of Food Science*, 78(1), pp.C1–C7.

Wang, Q. & Ismail, B., 2012. Effect of Maillard-induced glycosylation on the nutritional quality, solubility, thermal stability and molecular configuration of whey protein. *International Dairy Journal*, 25(2), pp.112–122.

Webb, K.E., 1990. Intestinal absorption of protein hydrolysis products: a review. *Journal of Animal Science*, 68(9), pp.3011–3022.

Yamane, H., Asechi, M., Tsuneyoshi, Y., Denbow, D.M. & Furuse, M., 2009. Central L-cysteine induces sleep, and D-cysteine induces sleep and abnormal behavior during acute stress in neonatal chicks. *Animal Science Journal*, 80(4), pp.428–432.

Yates, J.R., Eng, J.K., McCormack, A.L. & Schieltz, D., 1995. Method to correlate tandem mass spectra of modified peptides to amino acid sequences in the protein database. *Analytical Chemistry*, 67(8), pp.1426–1436.

Zhang, J., Lee, T.C. & Ho, C.T., 1993. Comparative study on kinetics of nonenzymatic deamidation of soy protein and egg white lysozyme. *Journal of Agricultural and Food Chemistry*, 41(12), pp.2286–2290.

Zhu, Y., Rinzema, A., Tramper, J. & Bol, J., 1995. Microbial transglutaminase-a review of its production and application in food processing. *Applied Microbiology and Biotechnology*, 44(3-4), pp.277–282.

Chapter Four

4 Dynamic Light and Small Angle X-ray Scattering of Protein Aggregates

4.1 Introduction

In recent years, much effort has been put into investigating the molecular mechanisms of protein aggregation. Proteins and peptides for pharmaceutical use with short shelf-life (Manning et al. 2010; Wang 1999), aggregation prone proteins in disease (Chiti & Dobson 2006), highly stable enzymes for commercial use (Eijsink et al. 2005), etc., are targets of these studies. In addition, food research focuses on exploiting the versatility of protein aggregation because of the structure-function relationship: differently aggregated forms of food proteins are likely to offer different functionalities in foods (Gerrard et al. 2012). Therefore it is desirable to understand mechanisms of aggregate formation in food proteins and the factors that drive aggregation along a certain pathway.

The common conclusion of many aggregation studies (and reviews) is that it is a particularly difficult task to unravel the underlying molecular details, because protein aggregation usually occurs rapidly and is often irreversible (Mahler et al. 2009; Wang et al. 2010). Ionic strength, pH, and protein concentration affect the protein aggregation pathway. More often than not, random aggregates are present rather than ordered aggregates. Figure 4.1 illustrates the correlation between different aggregate morphologies as a function of pH and ionic strength for a generic protein. The branching of aggregates is low at pHs far away from the isoelectric point (IEP) and at low ionic strengths (van der Linden & Venema 2007).

Protein can react covalently with other food molecules, for example, with sugars and lipids to form Maillard reaction products (Al-Hakkak & Al-Hakkak 2010). The glycation and the formation of advanced glycation products of food proteins by different sugars via the Maillard reaction both changes the IEP and affects the structural properties markedly (Gan et al. 2008) (Sections 2.3 - 2.5).

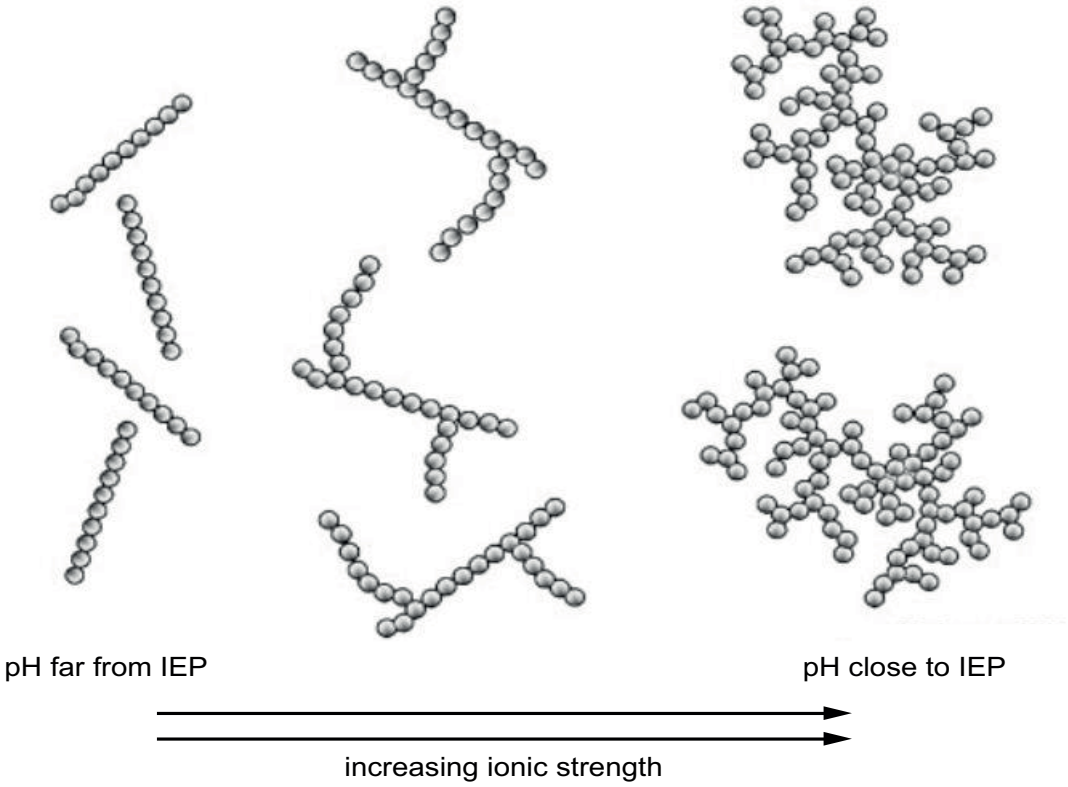

Figure 4.1 *Proposed mechanism of aggregation patterns caused by pH and ionic strength. Schematic taken from (van der Linden & Venema 2007).*

There is a suite of techniques available to answer some of the questions of protein unfolding. However, many of these techniques are limited in their capabilities to measure molecular interactions during aggregation. In general, two or more complementary techniques such as electron microscopy (EM), atomic force microscopy (AFM), dynamic light scattering (DLS), circular dichroism (CD) spectroscopy, or Fourier transform infrared (FTIR) spectroscopy are used to study protein aggregation (Gregoire et al. 2012). Additionally, the binding of fluorescent probes, such as fluorescein isothiocyanate (FITC), 8-anilinonaphthalene-1-sulfonic acid (ANS), Thioflavin T (ThT), Congo red, SYPRO Orange, can yield more information on protein conformation and thereby on aggregate formation (Jorbágy & Király 1966; Cattoni et al. 2009; Groenning et al. 2007; Howie et al. 2007; Vedadi et al. 2006). Turbidity measurements are often used as a fairly crude

measurement of aggregate formation at a given wavelength, e.g. 500 nm (Weijers et al. 2008), 540 nm (Xu et al. 1998), 590 nm (Kaewmanee et al. 2011), 660 nm (Tang et al. 2006). These techniques allow the characterisation of overall structure (microscopy) and secondary structure (CD, FTIR and fluorescent probes) of aggregates to a certain degree. However, there is a need for a more precise tool to monitor dynamic molecular changes along the entire aggregation pathway (from native protein to intermediates to final aggregate structure). So far, it has only been possible in very well characterised and fairly monodisperse systems, such as amyloid fibril systems, to generate a complete aggregation scheme where detailed information is available on intermediate states (Juárez et al. 2009; Khurana et al. 2001; Moraitakis & Goodfellow 2003; Oliveira et al. 2009; Svane et al. 2008). For the majority of proteins however, the aggregate formation is not uniform and therefore challenging to characterise. Small angle X-ray scattering (SAXS) bridges the gap between high and low resolution techniques. Whilst crystallographers would describe SAXS as a low resolution technique, SAXS offers much higher resolution than conventional light scattering and electron microscopy. With SAXS the exploration of nanometre length scales is possible. This enables the characterisation of both individual proteins as well as protein-protein interactions (Jacques & Trewhella 2010; Koch et al. 2003; Mertens & Svergun 2010; Putnam et al. 2007; Tashiro et al. 2008). However, as with other scattering techniques, aggregate formation during SAXS experiments is traditionally avoided at all costs because the analysis of polydisperse solutions can be challenging (Jacques & Trewhella 2010). In this work, SAXS studies of a polydisperse ovalbumin aggregation system were carried out to derive data about the aggregation pathway and kinetics of ovalbumin in solution.

In this chapter, the scattering techniques DLS and SAXS will be discussed with regard to their ability to give details about protein aggregation in complex model food systems. Studies were carried out on a food-relevant system, using the major EW protein, ovalbumin, and two glycation partners (glucose and methylglyoxal (Sections 2.1.4 and 3.2.5). Ovalbumin in Milli-*Q* water and ovalbumin in NaCl solution were used as references. A series of typical samples that were analysed is shown in Figure 4.2, displaying ovalbumin at 0.6 mg/mL under four different test conditions. The findings of the DLS and SAXS studies were then compared to transmission electron microscopy (TEM) micrographs.

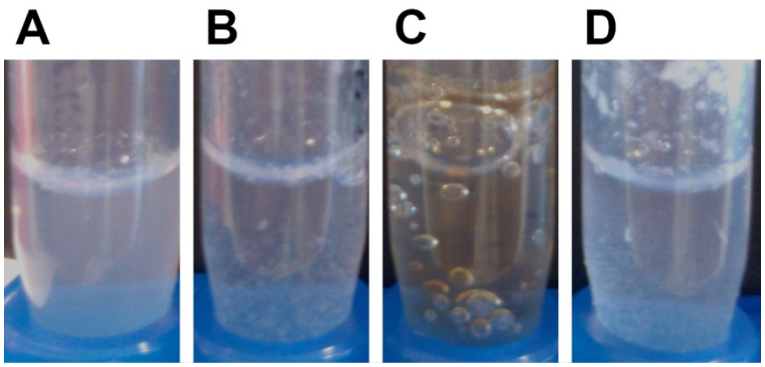

Figure 4.2 *Ovalbumin samples after 24 hour heating at 80 °C. Ovalbumin in A) Milli-Q water, B) 100 mM glucose, C) 100 mM methylglyoxal, D) 100 mM NaCl.*

4.2 Scattering of Electromagnetic Waves

The propagation of waves in matter is often categorised into macroscopic phenomena such as reflection, diffraction, absorption, and transmission. However, all of these macroscopic categories are examples of scattering of waves on matter. The wave interaction with matter occurs between the electrons of the medium and the electromagnetic wave and are described by Maxwell's equations (Als-Nielsen & McMorrow 2011). Maxwell's equations describe the generation and interaction of electric and magnetic fields at the atomic scale. Therefore, microscopic and macroscopic phenomena can be explained fully by the Maxwell equations. For the scattering of electromagnetic waves on particles there are several approximations to the Maxwell equations such as the Rayleigh solution and the Mie solution (Als-Nielsen & McMorrow 2011). The Rayleigh approximation describes the scattering of electromagnetic waves on spherical particles that are much smaller than the wavelength of the light (the diameter of the molecule is less than 1/10-th of the wavelength). For example, the laser of the DLS instrument (Malvern Zetasizer) used in the experiments operates at 633 nm (red light) which is large compared to most proteins (e.g. the longest axis of ovalbumin is about 7-8 nm long). The Mie approximation is a more accurate solution of Maxwell's equations than the Rayleigh approximation. It explains the scattering of electromagnetic waves on spherical or cylindrical particles of any particle size. Therefore there is no limitation to the particle/wavelength ratio (Als-Nielsen &

McMorrow 2011). This is why the Mie approximation is used in analysis of large structures, such as protein aggregates, in solution.

Scattering of electromagnetic waves occurs every time there is a change of refractive index (RI) between two different media. This means that at the interface/surface between different media (such as water and protein) the change in RI causes scattering of the waves (Als-Nielsen & McMorrow 2011).

X-ray scattering (including SAXS) depends on the interface/surface scattering, too. However, the refractive index for X-rays is close to 1 for most materials and is therefore not used to describe material/ media differences. Instead of the refractive index, the scattering length density (SLD) of a material is used in X-ray scattering. For X-ray scattering the SLD is directly proportional to the classical electron radius (r_e = 2.82 x 10^{-15} m) and the electron density (ρ_e) of a material (Equation 4.1) (Als-Nielsen & McMorrow 2011).

Equation 4.1

$$SLD = r_e \rho_e$$

In general, one can distinguish between elastic and inelastic scattering. Elastic scattering occurs if the incident wave (or primary wave) and the scattered wave (or secondary wave) have the same frequency and energy. In an inelastic scattering process some energy is transferred between the primary wave and the scattering particle so that the secondary wave is of a different energy and wavelength. Both elastic and inelastic scattering can occur simultaneously. For example electrons can scatter visible light or X-rays elastically and inelastically. Shape information about the scattering particle can only be obtained from elastic scattering because of the coherence of the secondary waves. Inelastic scattering is incoherent and contains no shape information but is always present as background scattering (Glatter & Kratky 1982).

4.2.1 *Dynamic Light Scattering (DLS)*

Dynamic light scattering is a well established technique to study protein size in solution (Aymard et al. 1999; Nemoto et al. 1993; Weijers et al. 2002). The technique measures the scattering of molecules in solution. The signal scattering arises from variations in the RI of the material, in this case between the protein aggregates and the surrounding buffer solution. The RI at optical wavelengths is related to the electron density of a material. For a freely diffusing and unaligned system of low viscosity the molecules in solution scatter light in all directions. The multitude of scattering molecules in solution causes destructive and constructive interference of the scattered light. This interference pattern can be detected by a photo-detector. The resulting speckle pattern (Figure 4.3) is not stationary because molecules move around due to Brownian motion (Malvern Instruments 2011).

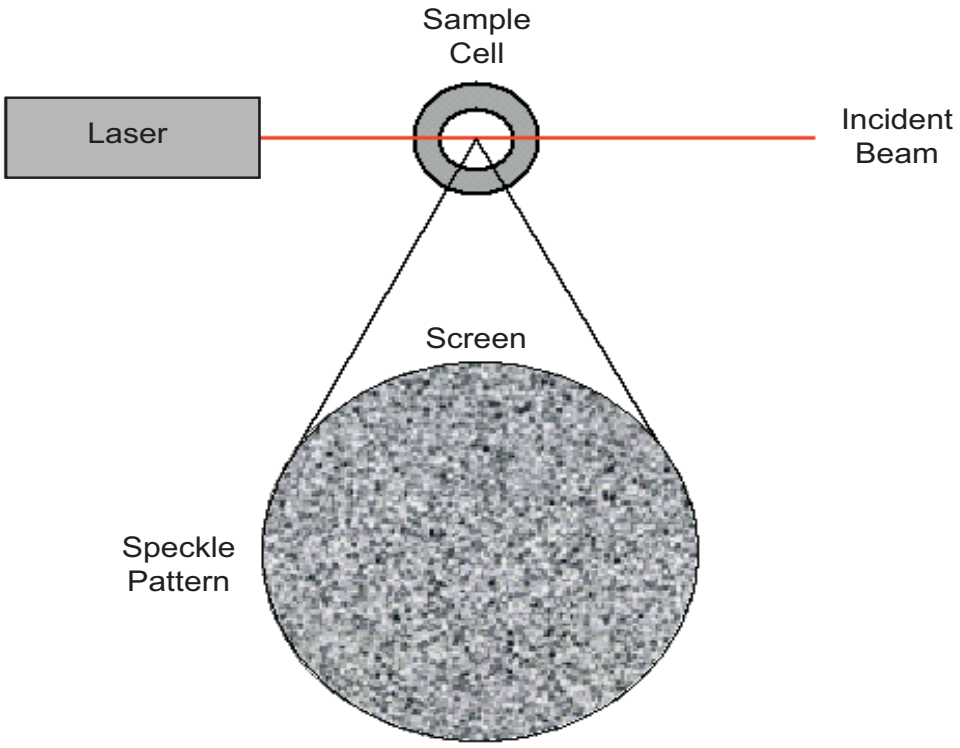

Figure 4.3 *Speckle pattern caused by interference of scattered light. Figure adapted from (Malvern Instruments 2011).*

The speckle pattern fluctuations can be correlated to the size of the particles because large particles cause long period fluctuations compared to the short fluctuations caused by small particles. More specifically, the size of particles can be estimated by determining the diffusion coefficient of the particles. The diffusion coefficient is then used to determine the hydrodynamic diameter (d_H) via the Stokes-Einstein equation (Equation 4.2) (Berne & Pecora 1976). This in turn means that the d_H is not a just measurement of the core of the particle but includes surface structures such as carbohydrates. Moreover, in protein aggregation, an increased d_H may indicate a partially unfolded protein.

Equation 4.2 *Stokes-Einstein equation to determine the d_H of particles in solution.*

$$d_H = \frac{k_b T_a}{3\pi\eta \mathrm{D}}$$

Where d_H is the hydrodynamic diameter, k_b is the Boltzmann constant, T_a is the absolute temperature, η is the viscosity, and D is the diffusion constant. One limitation of the technique is that the Stokes-Einstein equation assumes a spherical object that diffuses through the solution. This spherical model does not accurately represent other geometrical shapes such as cylinders or disks. Therefore the calculated d_H of the particles in the test sample is only that of a theoretical sphere with the same d_H (Berne & Pecora 1976).

4.2.2 *Small Angle X-ray Scattering (SAXS)*

SAXS scattering relies on similar principles to X-ray diffraction in terms of wave interactions with matter. The simplest case, scattering of X-rays from parallel planes is illustrated in Figure 4.4.

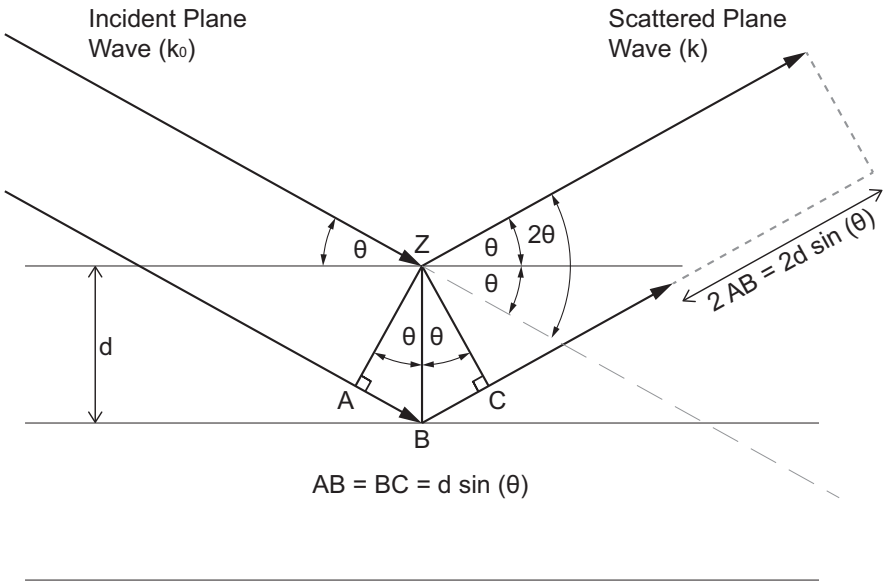

Figure 4.4 *Bragg's law of X-ray scattering. Diagram modified from (Als-Nielsen & McMorrow 2011).*

For elastic X-ray scattering the angle (ϑ) is the same for both the incident wave and scattered wave with regard to the scattering plane, where the scattering plane arises from fluctuations in the electron density of the system. The distance (d) between different scattering planes can be inferred from the interference between the scattered X-rays from each point. The distance can be calculated from the trigonometry of the triangle A, Z, B (Equation 4.3) (Als-Nielsen & McMorrow 2011).

Equation 4.3 *Distance between scattering particles or planes.*

$$d = \frac{AB}{\sin(\theta)}$$

The distance AB cannot be measured directly. However, when measuring X-ray scattering or diffraction, a detector can measure the interference patterns of scattered X-rays. From the interference pattern, calculations about distances between scattering centres can be

made (Jacques & Trewhella 2010; Mertens & Svergun 2010). An inherent problem of X-ray scattering is that only the intensity of the scattered wave is known and not the phase. Therefore, there may be more than one arrangement of scattering centres that will give the same scattering pattern. This uncertainty is commonly referred to as the "phase problem" (Glatter & Kratky 1982).

X-rays that interfere constructively (are in phase) are detected as bright circular constructive interference patterns (and rings) on the detector. From the diagram (Figure 4.4) it is obvious that for constructive interference to occur, the second wave (bottom wave) has to travel the extra distance AB + BC compared to the top wave. Therefore, the distance AB + BC added together must be an integer (n) multiple of the wavelength λ to fulfil constructive interference. The distances AB and BC are equal. Taking Equation 4.3 into account yields the equation for Bragg's law (Equation 4.4) for constructive interference (Als-Nielsen & McMorrow 2011).

Equation 4.4 *Bragg's law for constructive interference: AB + BC must be an integer multiple of λ.*

$$n\lambda = AB + BC = 2AB = 2d\sin(\theta)$$

Where n is an integer (1, 2, 3, etc.), λ the X-ray wavelength, d the distance between scattering centres (or planes in a crystal). The angle ϑ is the angle between the incident ray and the scattering plane. The diagram of X-ray scattering (Figure 4.4) also shows that the angle between incident beam and scattered beam is 2ϑ. This information is valuable when carrying out SAXS measurements.

In a typical SAXS measurement, the detector measures the interference patterns of scattering particles (Figure 4.5). If the scattering centres are randomly oriented relative to the incident beam, as is the case for non-oriented protein molecules diffusing freely in solution, the interference patterns are isotropic (uniform in all directions) and appear as circular patterns on the detector. The incident X-ray wave k_0 and the scattered wave k are at an angle of 2ϑ to each other. The interference pattern on the detector can be analysed to determine the distance between the incident wave and the scattered wave, which can in turn be used to calculate the scattering vector Q. For data analysis, the magnitude of the calculated Q is then plotted versus the scattering intensity.

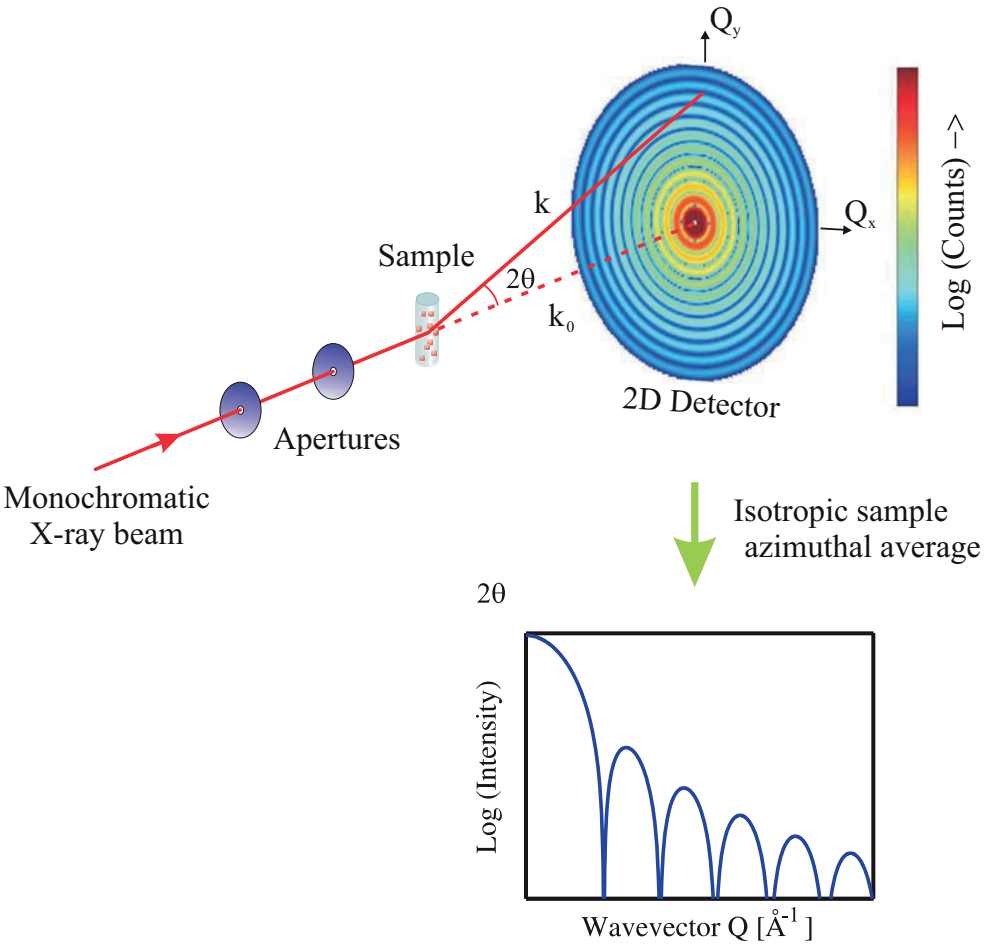

Figure 4.5 *Typical small angle X-ray scattering setup. Diagram taken from (Als-Nielsen & McMorrow 2011) with slight modifications.*

The scattering vector Q is known as the "momentum transfer" and is calculated from the change in the X-ray wave vector, i.e., k - k_0 where k and k_0 are the scattered X-ray wave vector and incident wave vector respectively. In the case of elastic scattering, $k = k_0$ (Als-Nielsen & McMorrow 2011).

Equation 4.5 *Definition of the magnitude of the wave vectors k and k_0.*

$$k_0 = k = \frac{2\pi}{\lambda}$$

From Equation 4.5 it is clear that the magnitude of the wavevector has the dimension of an inverse length (typically $Å^{-1}$ is used for SAXS). The diagram in Figure 4.6 shows the vector addition (k - k_0 = Q), and shows that Q is a function of k_0 and k and the scattering angle ϑ.

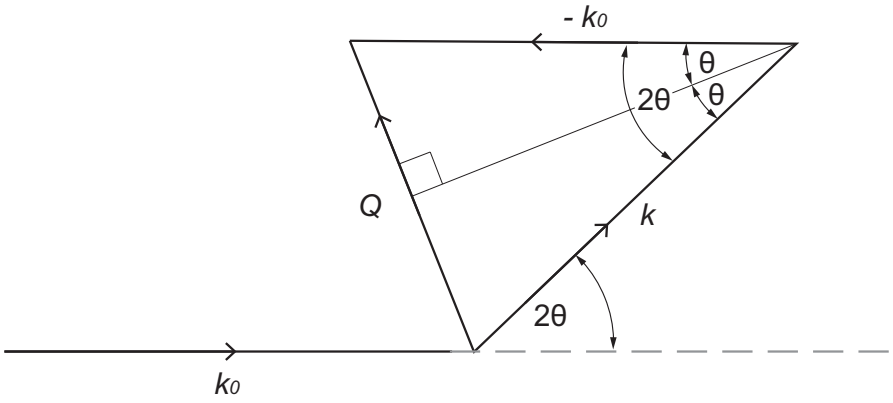

Figure 4.6 *The scattering vector Q, modified from (Als-Nielsen & McMorrow 2011).*

Trigonometry of the triangle described in Figure 4.6 can be used to solve for Q.

Equation 4.6

$$Q = 2\,k \sin(\theta)$$

Combining Equation 4.5 and Equation 4.6 yields the following angle and wavelength dependent definition of Q (Equation 4.7).

Equation 4.7 *Angle and wavelength dependent definition of Q (Als-Nielsen & McMorrow 2011).*

$$Q = 2\,\frac{2\pi}{\lambda}\sin(\vartheta) = \frac{4\pi}{\lambda}\sin(\vartheta)$$

The scattering vector Q is therefore related to both the scattering angle ϑ and the wavelength and is the preferred unit for reporting the X-ray scattering as it is independent of the specific instrumental conditions used. Q can also be shown to be inversely proportional to the molecular distances d in the sample solution by combining the definition of Q (Equation 4.7) with Bragg's equation (Equation 4.4) to give Equation 4.8.

Equation 4.8 *Relationship between real space distances and scattering vector Q.*

$$d = \frac{2\pi}{Q}$$

4.2.3 SAXS for Protein Structure Studies in Solution

The use of small angle X-ray scattering as a technique to study proteins in solution is becoming well established (Jacques & Trewhella 2010; Koch et al. 2003; Putnam et al. 2007). Due to the small wavelength of X-rays (< 1 nm) finer structural detail can be resolved by SAXS compared to DLS. Additionally, SAXS measurements do not rely on Brownian motion but are a direct representation of the average scattering of the proteins in solution (in the X-ray pathway). The information gained during SAXS experiments is often used to establish whether the solution structure of a soluble protein is consistent with that of the crystal structure (Svergun et al. 1995). Additionally, the quaternary structure and even domain movements of proteins in solution may be monitored (Petoukhov & Svergun 2013). This is often used to verify the applicability of crystallographic data to physiologically relevant environments. If the crystal structure is unknown, SAXS can be used to create a 3D bead model of the protein structure consistent with the measured scattering data. However, the relatively low information density of SAXS means that for reliable modelling it is crucial to have a well characterised protein system in order to constrain parameters during modelling (Glatter & Kratky 1982; Putnam et al. 2007).

Since SAXS measures the total scattering from all particles in the X-ray beam, the aggregation pathway of proteins is difficult to analyse. This is due to the mixed contributions from different protein species. An inherent difficulty of SAXS data analysis is extracting valuable data from polydisperse systems (just as with DLS) (Jacques &

Trewhella 2010). In a typical SAXS experiment the scattering intensity *I(Q)* is measured as a function of the scattering vector *Q* (Figure 4.5). The value of *I(Q)* depends on several parameters (Equation 4.9).

Equation 4.9 *Contributing factors to scattering intensity I(Q) (Glatter & Kratky 1982; Kline 2006).*

$$I(Q) = \xi\, n\Delta\rho^2 V^2 P(Q) S(Q) + bkgd$$

Where ξ is the instrument constant accounting for features such as detector efficiency and beam intensity, n is the number of particles in the scattering volume, $\Delta\rho$ is the SLD contrast ($\Delta\rho = \rho_{particle} - \rho_{solvent}$), V is the particle volume, $P(Q)$ is the form factor, and $S(Q)$ is the structure factor. The form factor describes the size, shape, and surface of the scattering particle as shown in Figure 4.7. Obtaining $P(Q)$ directly from the scattering pattern by inversion is impossible (Als-Nielsen & McMorrow 2011). However, several approaches can be taken to interpret the scattering data. These include model independent approaches such as Guinier and Porod analysis and model dependent approaches including pair-distribution fitting, form factor fitting of analytical models, and dummy atom modelling (Kline 2006; Konarev et al. 2003; Mertens & Svergun 2010).

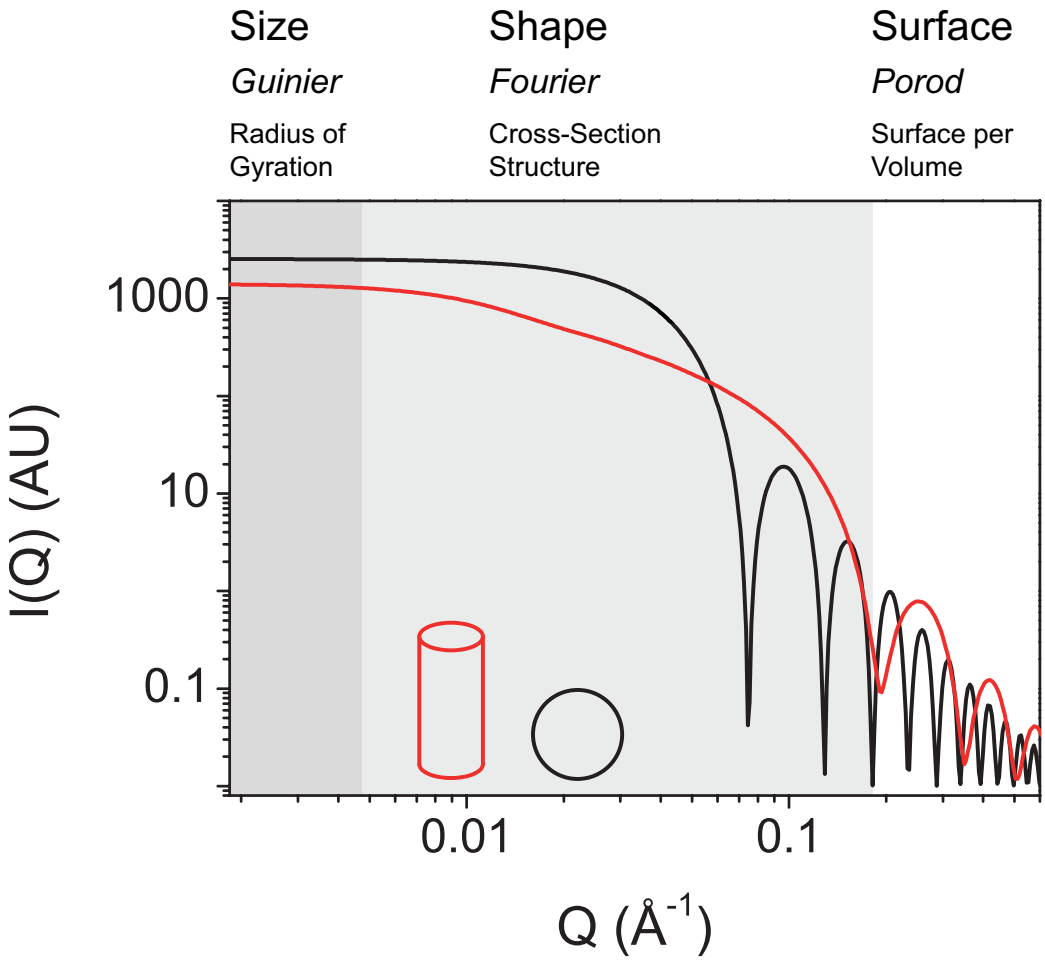

Figure 4.7 *Information content of P(Q) from a typical scattering experiment of different geometric shapes such as spheres (black) and cylinders (red). The P(Q) profile can be split into three regions which contain different information about the particle. The Guinier Region ($Q \leq 1/R_g$) is used to determine the particle size. The intermediate region contains shape information about the particle (e.g. cylinder or sphere), while the surface properties of the particle can be deduced rom the Porod region (Glatter & Kratky 1982; Kline 2006).*

P(Q) is measured in dilute solutions where interparticle interactions are absent, and the structure factor, which contains information about interparticle structure/distances, is therefore negligible (*S(Q)* = 1). At higher particle (protein) concentrations information about interparticle distances can be gathered because the separation of the molecules is not completely random. The higher order in the separation distances of concentrated proteins is usually an effect of electrostatic repulsion or steric hindrance.

4.2.3.1 Guinier Analysis

To gain an overview of the scattering pattern, the raw scattering data are usually plotted as intensity vs. scattering vector (*I(Q)* vs. *Q*). The Guinier plot (*ln*(*I(Q)*) vs. Q^2) of SAXS data allows the determination of the approximate molecular mass and the radius of gyration (R_g) of the scattering particle (Guinier 1955; Petoukhov & Svergun 2013). The radius of gyration is defined as the mean square distance from the centre of gravity (Glatter & Kratky 1982). Equation 4.10 is used to approximate the R_g of any scattering particle under the assumption that the form factor of any given particle can be described by a Gaussian curve (Guinier 1955).

Equation 4.10 *R_g approximation (Glatter & Kratky 1982).*

$$I(Q) = I(0)e^{-\frac{(QR_g)^2}{3}}$$

I(Q)) is the scattering intensity, *I(0)* is the extrapolated intensity at $Q = 0$ (sometimes described as forward scattering intensity). This equation can be rewritten into Equation 4.11

Equation 4.11 *Logarithmically expanded Equation 4.10.*

$$ln(I(Q)) = ln\big(I(0)\big) - \frac{{R_g}^2}{3}Q^2$$

The equation can be regarded as a simple linear y = b + mx equation, where y = *ln*(*I*(*Q*), $b = ln(I(0)$, $m = -\frac{{R_g}^2}{3}$, and x = *Q*. Plotting the scattering intensity data in this fashion will yield the Guinier plot in which the slope of the graph will yield R_g. If the particle shape (sphere, rod, ellipse, etc.) is known the determined R_g value can be used to describe the dimensions of the scattering particle. The geometrical radius (r) of a sphere for example can be calculated from the determined R_g value using Equation 4.12 (Glatter & Kratky 1982)

Equation 4.12 *Radius of gyration of a sphere.*

$$R_g{}^2 = \frac{3}{5}r^2$$

The $I(0)$ determined from the Guinier plot can be used to determine the molecular weight, M [g/mol], of a scattering particle if the particle concentration is known. The molecular weight will be known to the same accuracy as the protein concentration (Putnam et al. 2007). The Guinier plot also allows qualitative assessment of the polydispersity of the sample. A monodisperse scattering system will yield a straight plot line therefore calculation of R_g from the slope of the line is possible. However, a polydisperse system (such as aggregating protein) will yield a non-linear Guinier plot where the determination of R_g is not possible (Glatter & Kratky 1982). Moreover, the Guinier approximation is only appropriate when $R_gQ < 1.3$. Software such as *AutoRg* can automatically calculate the R_g from the scattering data (Petoukhov et al. 2012; Petoukhov et al. 2007).

4.2.3.2 Porod Analysis

Porod analysis allows the determination of particle volume and surface roughness from scattering data. This is achieved by slope analysis of the high Q region where $I(Q) \propto Q^{-4}$ (for a smooth surface) and by determination of $I(0)$ of a scattering particle (Putnam et al. 2007).

Equation 4.13 *Particle volume determination (Putnam et al. 2007).*

$$V = 2\pi \frac{I(0)}{Q_P}$$

Where V is the total particle volume and Q_P is the Porod invariant.

Equation 4.14 *Particle volume determination (Putnam et al. 2007).*

$$Q_P = \int_0^\infty Q^2 I(Q) dQ$$

The determination of the particle volume via Porod approximation relies on good quality data as it relies on the entire measured Q range (Putnam et al. 2007).

4.2.3.3 Pair-Distance Distribution Function

The pair distance distribution function (PDDF or *P(r)*) is a different representation of the scattering data. The *P(r)* function is a Fourier transform of the *I*(*Q*) function (Equation 4.15). The *P(r)* shows the relative distance of scattering centres from one another (in X-ray scattering the scattering centres are electrons). Therefore the *P(r)* plots are utilised to determine the shape of an object as well as monitoring conformational changes of a given macromolecule such as a protein (Glatter & Kratky 1982).

Equation 4.15 *Indirect Fourier transform function for pair distance distribution function from the intensity function (Putnam et al. 2007).*

$$P(r) = \frac{r}{2\pi^2}\int_0^\infty I(Q)Q\sin(Qr)\,dQ$$

An overview of different shapes, their corresponding theoretical scattering function as well as the *P(r)* function are shown in Figure 4.8.

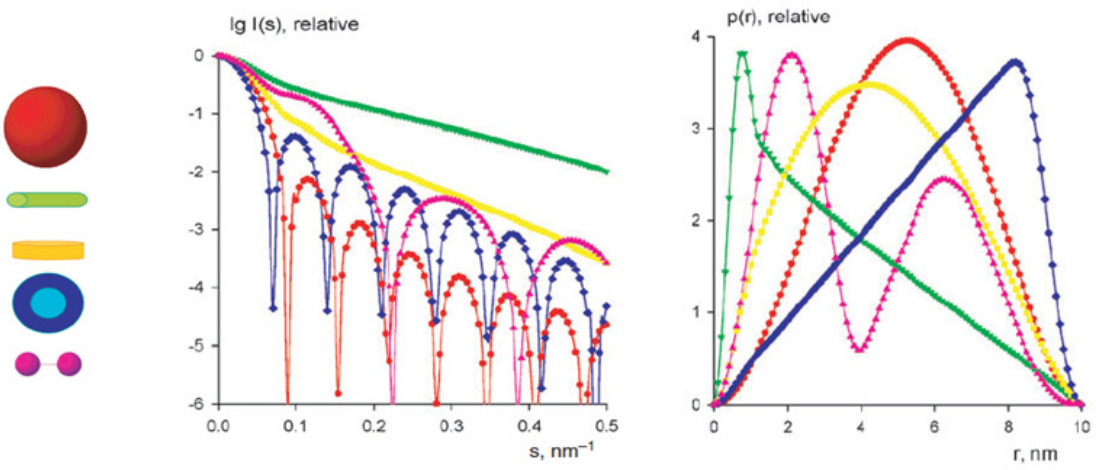

Figure 4.8: *P(r) plot of ideally shaped solid sphere (red), rod (green), disc (yellow), hollow sphere (blue), dumbbell (pink). Diagram from (Svergun & Koch 2003).*

Because *P(r)* plots are one dimensional they cannot be used to definitely determine the three dimensional shape of the scattering particle. However, a good indication of particle shape can be obtained because the *P(r)* plot describes the probability of the distance between one electron and another in a scattering particle (e.g., a protein molecule). For

example, a globular object will display a bell shaped *P(r)* function (Figure 4.8, red line) and a rod shaped object will result in a function with a peak at short distances and an elongated tail at larger distances (green line), whereas disks show a broad peak (yellow line), multi-domain objects show two or more peaks (pink line), and hollow spheres display a high proportion of long distances between electrons (blue line).

4.2.3.4 Fitting of Form Factor Functions

The shape of the scattering intensity function ($I(Q)$) by dilute monodisperse particles such as proteins in solution can be compared to the theoretical scattering of geometrical shapes including spheres, rods, ellipsoids, etc. Geometrical shapes can be described by mathematical functions. Computer software is usually used to perform the fitting of the experimental data to the theoretical form factor. For fitting purposes, *IgorPro 6.2.1.0* software and the *NCNR SANS* package were employed (Kline 2006). The shape of a uniform ellipsoid was used as a model to represent native ovalbumin. The description of the uniform ellipsoid $P(Q)_{ell}$ function is given in Equation 4.16.

Equation 4.16 *$P(Q)_{ell}$ form factor function (Kline 2006).*

$$P(Q)_{ell} = \frac{scale}{V_{ell}}(\rho_{ell} - \rho_{solv})^2 \int_0^1 f^2[Qr_b(1 + x^2(v^2 - 1))^{1/2}]\, dx + bkg$$

Further terms are explained in Equation 4.17, Equation 4.18, and Equation 4.19.

Equation 4.17

$$f(z) = 3V_{ell}\frac{(\sin z - \cos z)}{z^3}$$

Equation 4.18

$$V_{ell} = \frac{4\pi}{3} r_a r_b^2$$

Equation 4.19

$$\nu = \frac{r_a}{r_b}$$

The function $f(z)$ is the scattering amplitude where $z = Qr_b(1 + x^2(\nu^2 - 1))^{1/2}$. The radius r_a is the radius of the short axis of the ellipsoid, r_b the radius of the long axis. The volume V_{ell} is the volume of the ellipsoid and $x = R_g^2 Q^2$ (Norman et al. 2005). The terms ρ_{ell} and ρ_{solv} refer to the protein and solvent SLD respectively. During fitting, the software changes variable parameters and returns fitted intensity values that are scaled (*scale*) to the absolute intensity scale to match the experimental data. The *scale* parameter can be used to determine the protein volume fraction of the sample. The fitted line is also adjusted to account for residual incoherent background (*bkg*). In addition to the $P(Q)_{ell}$ function, some aggregate structures were fitted to a cylinder with elliptical cross-section form factor ($P(Q)_{Cyl}$) function (Kline 2006; Svergun & Feigin 1987).

4.2.3.5 Fitting to Crystallographic Data

While it is not possible to derive a definite particle structure directly from SAXS, the deriving of a theoretical scattering form factor from a known structure is possible. The $P(Q)$ of a protein in solution can be approximated by that of a simple geometrical shape, as described in Section 4.2.3.4. However, it is also possible to employ the crystal structure of a given protein as a geometrical template to generate the respective form factor. The generation of a form factor of crystallographic data can be used to compare the crystal structure to the solution structure of a protein. The comparison of experimental SAXS of a protein solution with the theoretical scattering of the respective crystal structure can help establish if the crystal structure is the biologically relevant structure (Putnam et al. 2007). Software such as *CRYSOL* can generate form factors of any crystal structure which in turn can be compared to the experimental data (Svergun et al. 1995). A good fit of experimental and theoretical scattering indicates that the solution structure is consistent with the crystal structure.

4.2.3.6 *Ab-initio* Shape Determination by Fitting of Bead Models

There are several approaches to approximate the 3D shape of a scattering particle. Without prior knowledge of particle size and shape the *ab-initio* determination of the 3D structure

from the 1D scattering data is often employed (Franke & Svergun 2009; Putnam et al. 2007). There are several approaches of modelling the 3D structure. The algorithms of the different computer software employ dummy particles (such as atoms, residues, or beads) that start out at a random distribution. From this distribution the theoretical scattering profile is generated and compared with the experimental scattering profile. Computer software such as *DAMMIF* and *GASBOR* cycle through iterations of dummy particle distributions until a converging fit with the experimental data is achieved (Franke & Svergun 2009; Putnam et al. 2007).

4.2.3.7 Fitting of Structure Factor Functions

The previous sections described how scattering data can be used to analyse the size and shape of the scattering particle. However, these types of analysis are only possible in dilute concentration in the absence of a structure factor (*S(Q)*). In more concentrated solutions the particles (e.g., proteins) will often assume a more ordered distribution because of particle-particle interactions often due to Coulombic interaction (Ianeselli et al. 2010). If Coulombic interactions are the dominant factor in the *S(Q)* they can be modelled analytically considering the ionic strength and permittivity of the solution, the net charge on the particles and the concentration of the particles. *IgorPro 6.2.1.0* software and the *NCNR SANS* package were employed to fit a Coulombic structure factor to concentrated protein solutions (Kline 2006).

4.3 Dynamic Light Scattering of Soluble Ovalbumin Aggregates

The biggest caveat for the interpretation of DLS data is that more light is scattered by large particles than by small particles. The scattering intensity (I) of scattered light is proportional to the 6th power of the diameter ($I \propto d^6$) (Malvern Instruments 2011). Therefore, large particles are over-represented in the raw intensity data if mixtures of different particle sizes are measured. However, in DLS, particle size distribution can be approximated not only by particle scattering intensity but also by particle volume via Mie approximation. An example of intensity vs. volume distribution is shown in Figure 4.9. The volume distribution shows a monodisperse solution (monodispersity 99.7 %) of native ovalbumin molecules. On the other hand, the intensity distribution shows the presence of large structures with diameters up to 200 nm in the sample solution. In this example the 0.3 % of large aggregates (by volume) contributes to about 88 % of the total scattering while the native ovalbumin molecules contribute to only 12 % of the total scattering. Because of the large aggregate sizes during ovalbumin aggregation DLS experiments could only be conducted for the soluble fraction of protein. The insoluble fraction was removed by centrifugation. For size analysis of the soluble aggregates particle size distribution by volume rather than by intensity was chosen.

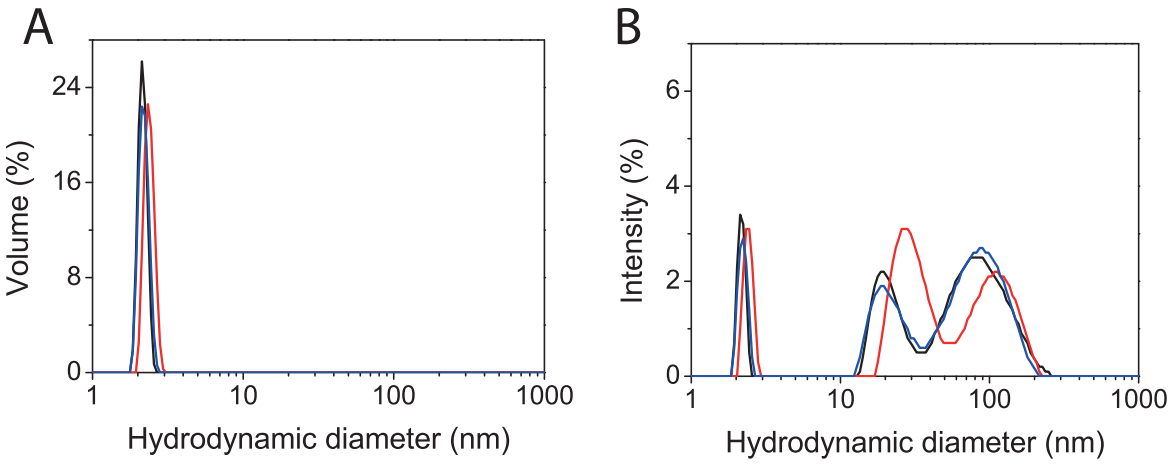

Figure 4.9 *DLS particle size distribution of ovalbumin in water before heat treatment by volume (A), and by intensity (B). Data were measured in triplicate (red, blue, and black lines).*

The ovalbumin solutions for DLS were prepared at the same protein concentration (0.6 mg/mL) as used in subsequent SAXS measurements (Section 4.4). The starting pH of all

solutions was measured to be between 6.5 and 7 for ovalbumin in water, glucose, and NaCl. The pH of methylglyoxal treated ovalbumin was between pH 4 (at 0.6 mg/mL protein concentration) and pH 5 (at high protein concentrations (45.5 mg/mL)). The concentrations of NaCl, glucose, and methylglyoxal were 100 mM.

Samples were heated to 80 °C which is just above the protein melting point (78 °C) of ovalbumin (Kosters et al. 2003). Following heat incubation the samples were kept on ice until further analysis. Before analysis, samples were centrifuged to pellet insoluble aggregate because only smaller aggregates were accessible by the scattering technique. The insoluble fraction was not characterised because the focus of this thesis was to characterise the soluble fraction which likely represent early aggregation.

In general, the samples incubated in the presence of NaCl displayed the highest proportion of aggregated protein. After 5 hours incubation, there was a high proportion of insoluble aggregate in all samples. However, the methylglyoxal treated solution remained clear even after 24 hours heating (Figure 4.2). The high propensity of ovalbumin to aggregate in the presence of NaCl is likely due to closer inter-particle distances of ovalbumin molecules in solution. The closer packing is made possible by electrostatic shielding of the charged ovalbumin molecules and thereby reduced repulsive forces between similarly charged ovalbumin molecules (Ianeselli et al. 2010).

The size distribution graphs (Figure 4.10 to Figure 4.13) show the hydrodynamic diameter of the soluble aggregates formed by ovalbumin in the presence of Milli-*Q* water (Figure 4.10), 100 mM glucose (Figure 4.11), 100 mM methylglyoxal (Figure 4.12), and 100 mM NaCl (Figure 4.13). The chosen buffer conditions supplied an excess of possible reaction partners (glucose and methylglyoxal) with respect to available lysine residues and were compared to the salt (NaCl) and no salt conditions (water). For data analysis the volume weighted representation was chosen to give a better understanding of the overall distribution of the protein in solution.

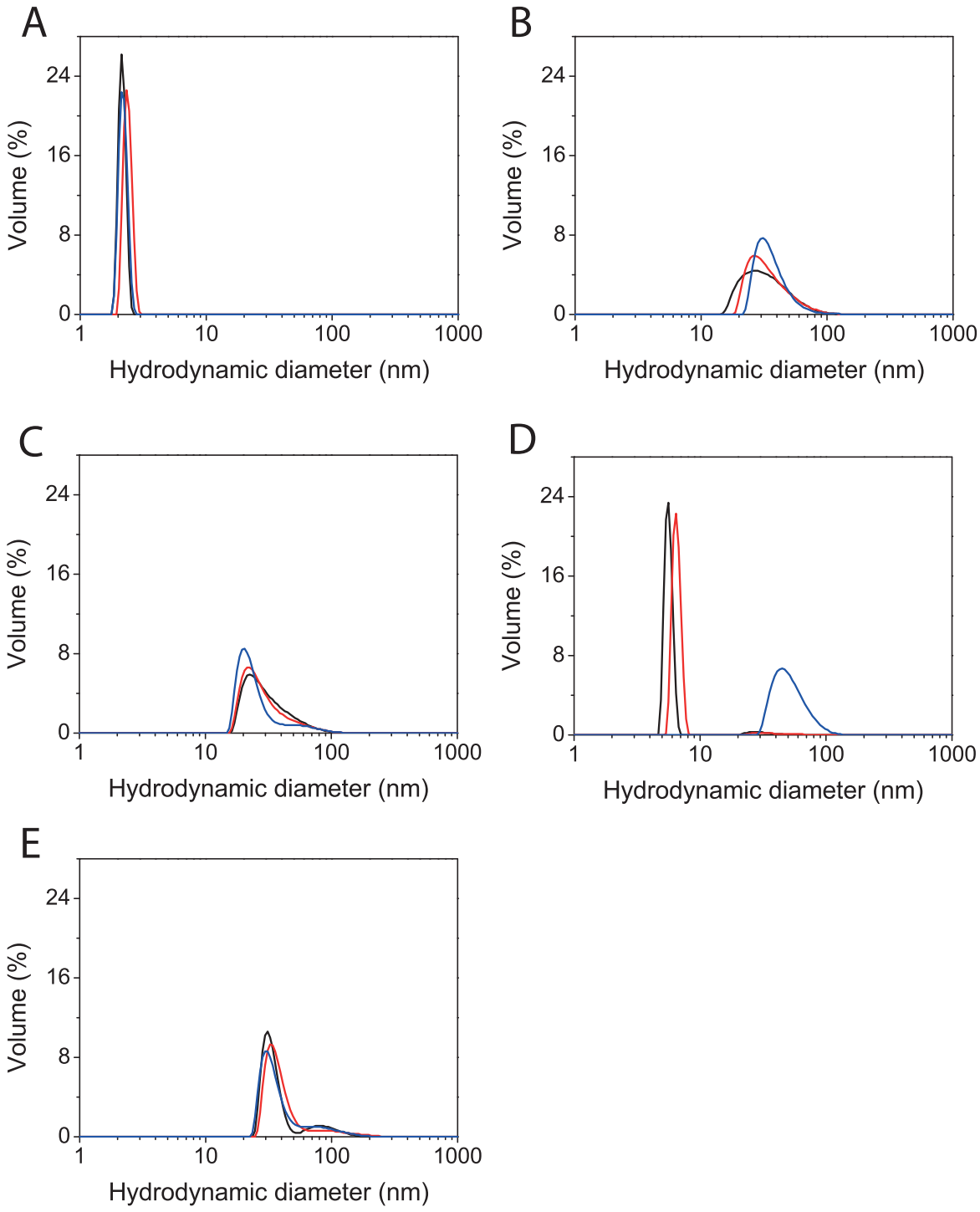

Figure 4.10: *Size distribution of soluble ovalbumin aggregate in Milli-Q water over a heating period of 24 hours at 80 °C. A) 0 minutes heating, B) 30 minutes heating, C) 1 hour heating, D) 5 hours heating, E) 24 hours heating. Triplicate measurements represented by black, blue, and red lines.*

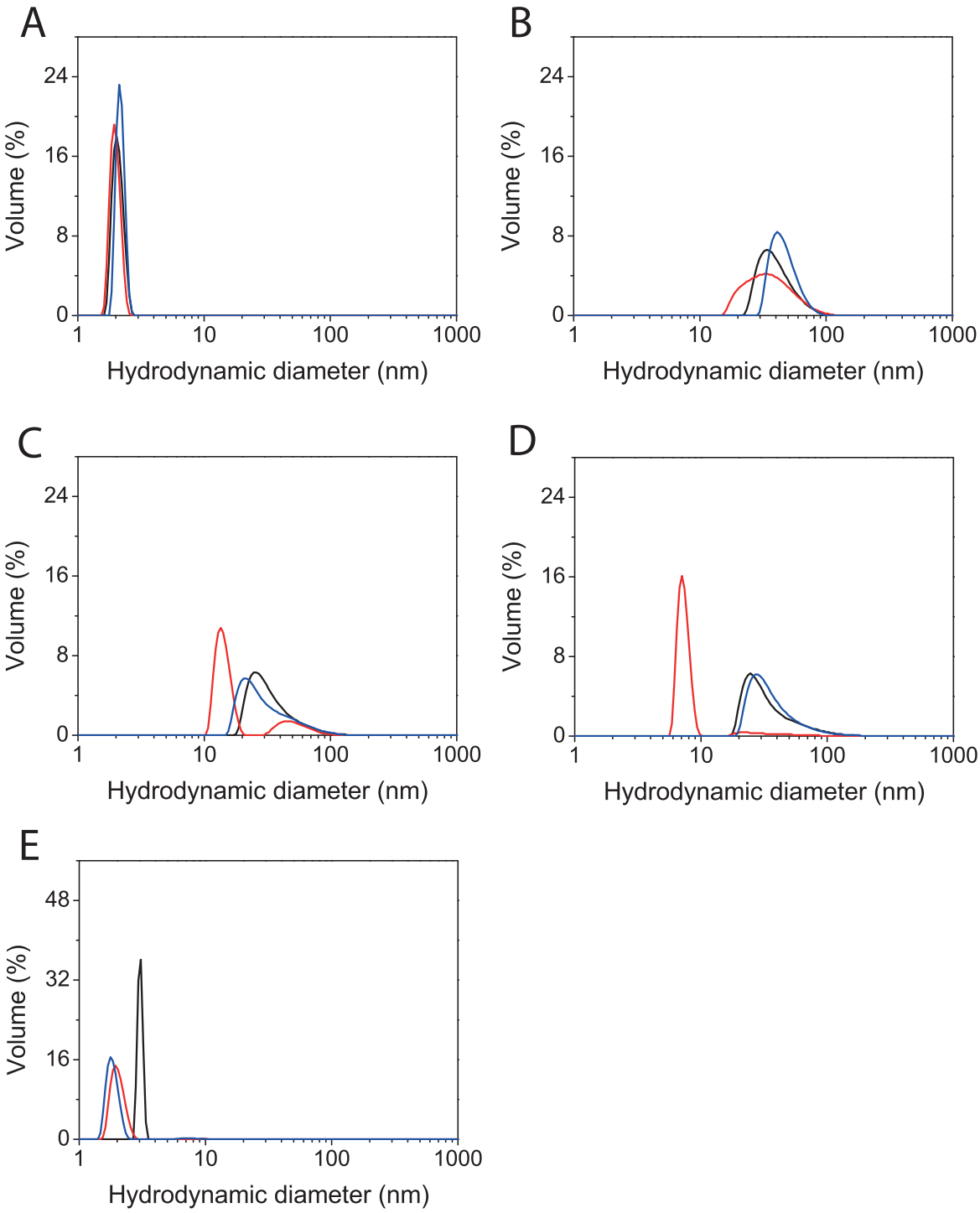

Figure 4.11 *Size distribution of soluble ovalbumin aggregate in 100 mM glucose over a heating period of 24 hours at 80 °C. A) 0 minutes heating, B) 30 minutes heating, C) 1 hour heating, D) 5 hours heating, E) 24 hours heating. Triplicate measurements represented by black, blue, and red lines.*

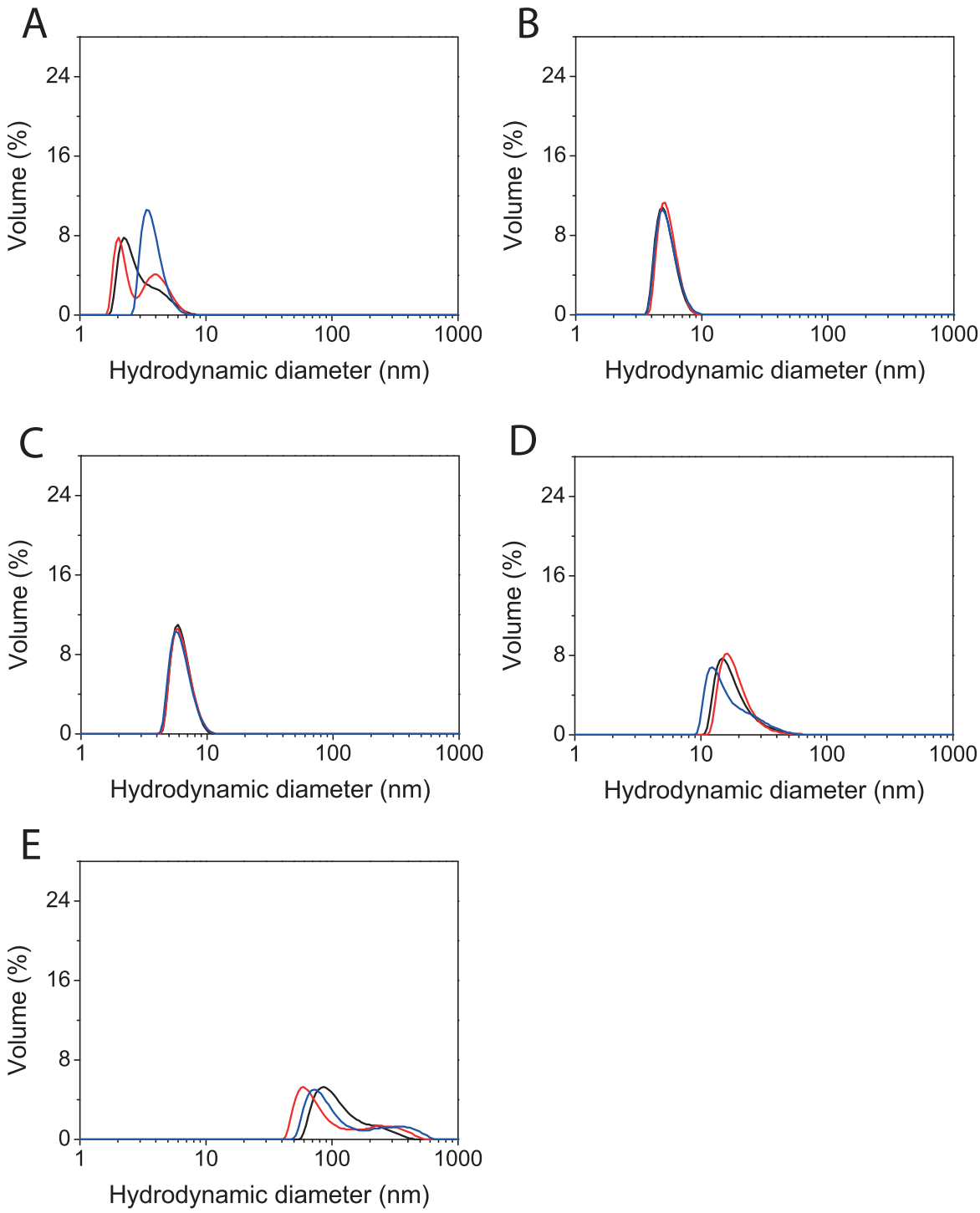

Figure 4.12 *Size distribution of soluble ovalbumin aggregate in 100 mM methylglyoxal over a heating period of 24 hours at 80 °C. A) 0 minutes heating, B) 30 minutes heating, C) 1 hour heating, D) 5 hours heating, E) 24 hours heating. Triplicate measurements represented by black, blue, and red lines.*

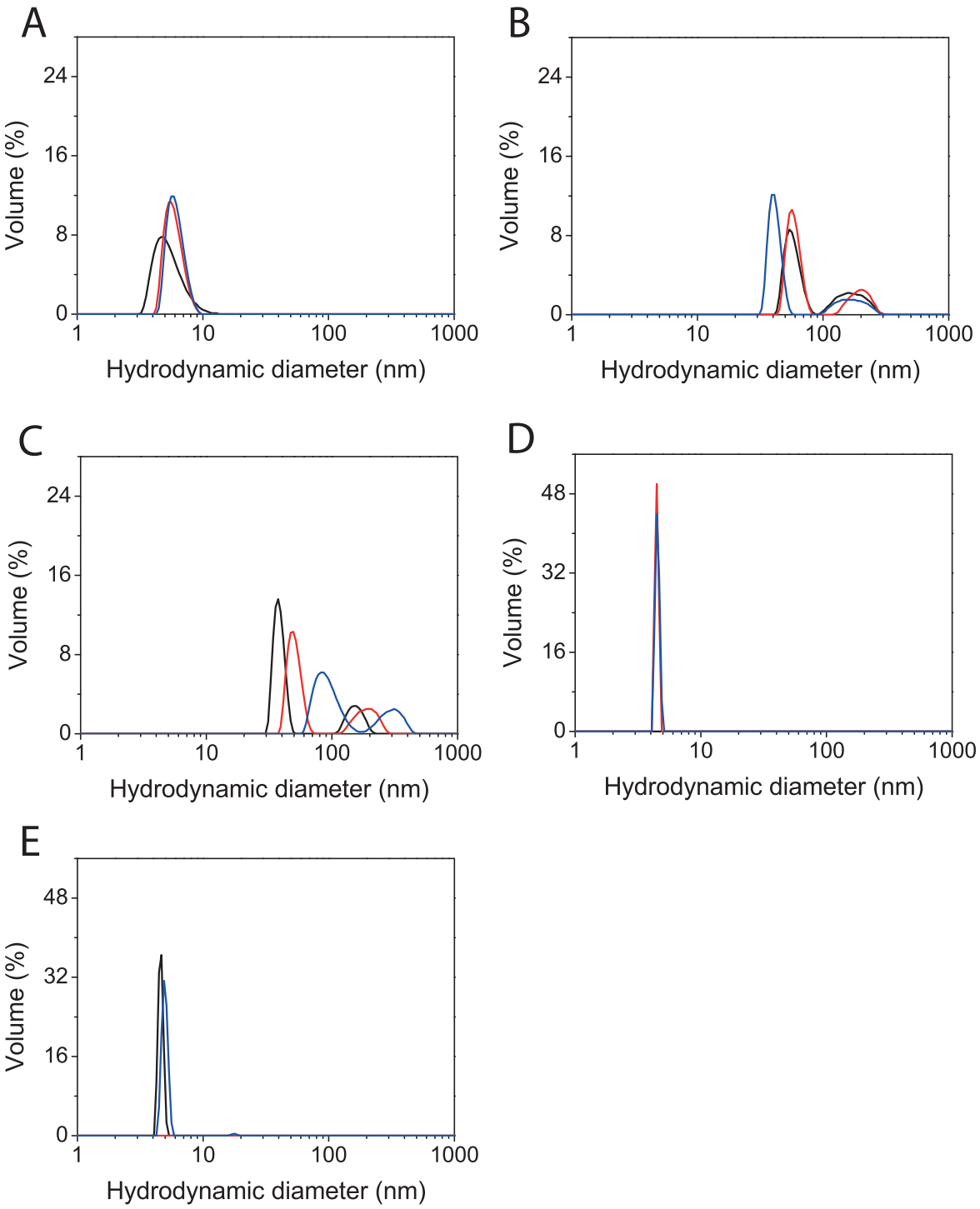

Figure 4.13 *Size distribution of soluble ovalbumin aggregate in 100 mM NaCl over a heating period of 24 hours at 80 °C. A) 0 minutes heating, B) 30 minutes heating, C) 1 hour heating, D) 5 hours heating, E) 24 hours heating. Triplicate measurements represented by black, blue, and red lines.*

The monomeric diameter of ovalbumin is about 4 - 5 nm (PDB entry: 1OVA). DLS attributes a smaller diameter to native ovalbumin of about 2 - 3 nm in Milli-*Q* water and in 100 mM glucose. In the presence of methylglyoxal there are two populations present, a 2 - 3 nm peak consistent with monomeric ovalbumin and a peak at 4 - 6 nm consistent with dimeric ovalbumin. In the presence of 100 mM NaCl there is a distinct peak at 4 - 6 nm consistent with dimeric ovalbumin species.

Heating of the solutions caused the onset of ovalbumin aggregation indicated by the size increase of soluble particles in solution. Within 30 minutes of heating the particle size increased by about two orders of magnitude for ovalbumin in the presence of water, glucose, and NaCl. However, ovalbumin in the presence of methylglyoxal remained a dimer. The picture is much the same after 1 hour of heating at 80 °C. After 5 and 24 hours of heating monomeric and dimeric ovalbumin species are reappearing in the water, glucose and NaCl samples. This is most likely explained by a growth of most aggregate to insolubility. Since the insoluble fraction was always removed by centrifugation, the remaining monomeric and dimeric ovalbumin molecules in solution are the main scattering particles in solution, despite being heavily reduced in number. Interestingly, there is no evidence of monomers or dimers in the methylglyoxal treated sample. This may indicate that monomeric species have been cross-linked to sizes beyond the dimer via methylglyoxal (Sections 2.1.4 and 3.2.5). Additionally, there is a further size increase of soluble ovalbumin in the presence of methylglyoxal to almost 1 μm. This is in contrast to all the other cases, where any aggregates greater than approximately 100 nm are precipitated out of solution.

The exact mechanism governing ovalbumin aggregation in the presence of methylglyoxal is complex. Methylglyoxal may react with the amino groups of lysine and guanidinium groups of arginine in a Maillard reaction (Aćimović et al. 2009; Degenhardt et al. 1998; Lo et al. 1994) (Section 2.1.4). Ovalbumin monomers carry 15 arginine and 20 lysine residues (Figure 4.14) that possibly react with methylglyoxal. Analysis of the molecular surface of the ovalbumin monomer crystal structure (Stein et al. 1991) reveals a rich decoration with lysine and arginine residues (Figure 4.14). Since lysine and arginine contribute to the protein net charge and IEP , the modification of these residues by methylglyoxal affects both net charge and IEP of the modified protein.

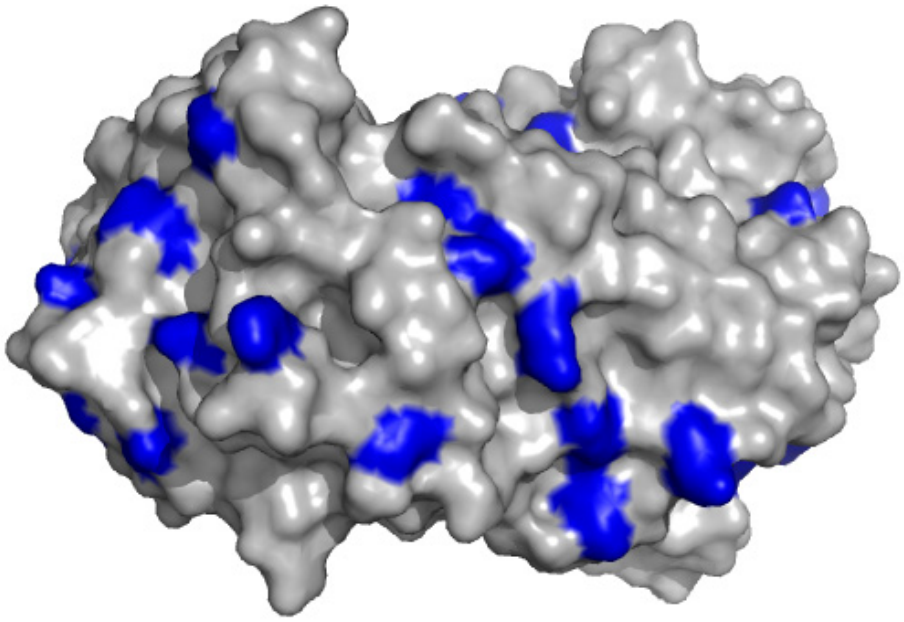

Figure 4.14 *Many of the 35 total lysine and arginine residues decorate the surface of ovalbumin (PDB entry: 1OVA). Arginine and lysine residues (blue).*

The 0.6 mg/mL ovalbumin solution treated with 100 mM methylglyoxal had a measured pH of 4. The low pH of the solution may have contributed to net charge changes of ovalbumin. The low pH 4 would produce a strong positive net charge of +20 (ovalbumin has a theoretical IEP 5.0 (Section 2.1.2), compared to a net charge of -10 at pH 7). However, the IEP of ovalbumin necessarily has to undergo changes during the reaction of the basic lysine and arginine with methylglyoxal to form neutral products. The ratio of modified lysine and arginine residues after heating is not known exactly. However, mass spectrometric analysis showed that 38% of detected arginine residues had reacted to form hydroimidazolone after 1 hour of heating at 100 °C (Section 3.3.1). A conservative estimation of 50 % reacted lysine and arginine residues after 24 hours of heating would entail a drop of the theoretical IEP to 4.1 (estimated by the EMBOSS software suite (Rice et al. 2000)) (Figure 4.15). This is close to the pH of the solution (pH 4) which would result in a low net charge of +2. The Coulombic repulsion between ovalbumin proteins would be negligible and therefore facilitate aggregation. However, if 100 % of lysine and arginine residues reacted the IEP would drop to 3.3 (Figure 4.15) which would entail a negative net charge (-15) at a pH 4 causing a stronger electrostatic repulsion between ovalbumin monomers even compared to unmodified ovalbumin at pH 7 (estimated charge using EMBOSS at pH 7 is -10).

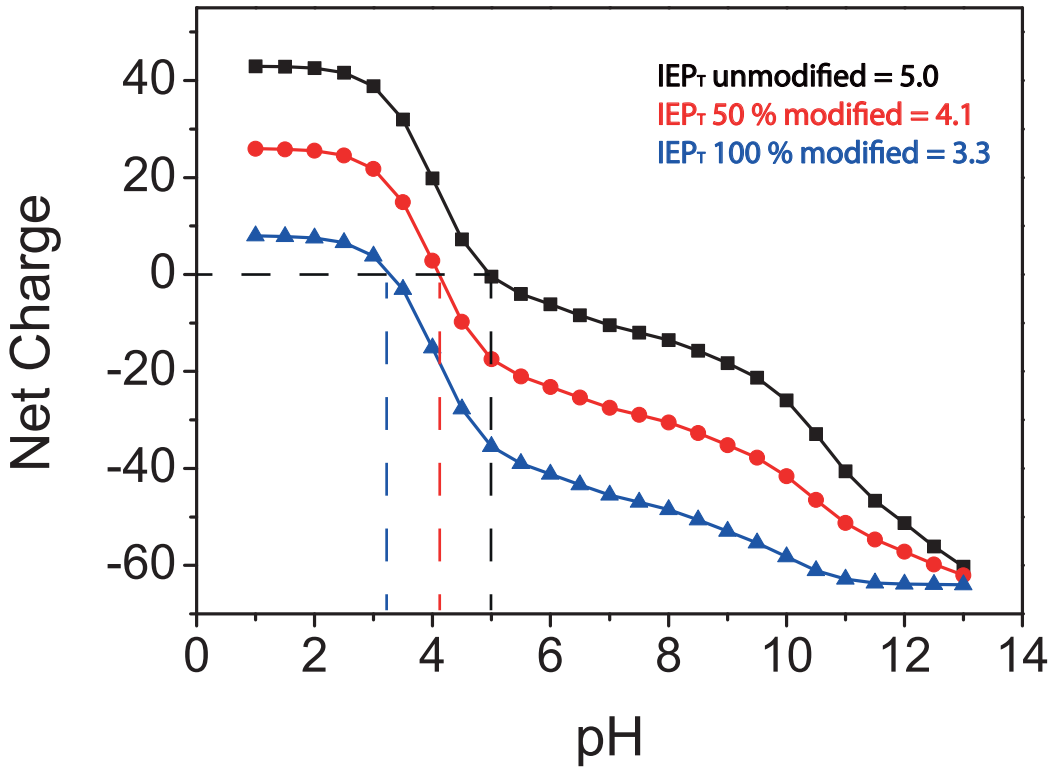

Figure 4.15 *Theoreical IEPs of ovalbumin when unmodified (black, IEP = 5.0); 50 % modified lysine and arginine residues (red, IEP = 4.1); 100 % modified lysine and arginine residues (blue, IEP = 3.3). All theoretical values were determined based on pK_a values of amino acid residues using* the *EMBOSS software suite (Rice et al. 2000).*

In conclusion, the soluble aggregates differ markedly from one another. By simple comparison of the size distribution curves the importance of added salt or Maillard reaction partner on aggregate size and kinetics becomes evident. In order to gain further insight into the finer mechanisms of ovalbumin aggregation small angle X-ray scattering studies were conducted.

4.4 Small Angle X-ray Scattering of Ovalbumin Aggregates

Ovalbumin solutions at a concentration of 0.6 mg/mL and 3.2 mg/mL in Milli-*Q* water and in the presence of 100 mM NaCl, 100 mM glucose, or 100 mM methylglyoxal were prepared. The SAXS experiments showed that the dilute concentration of 0.6 mg/mL did not cause interparticle interference effects. Moreover, the chosen concentration gave sufficient scattering signal for further analysis at the chosen sample to detector distances. The concentration of 3.2 mg/mL was chosen as it was the lowest concentration in the tested range where an interparticle interference is significant. Two typical scattering patterns that were recorded during the experiments are shown in Figure 4.16. The circular scattering is caused by ovalbumin in solution as well as by the buffer. It can be seen that aggregated ovalbumin scatters more strongly than native ovalbumin. The detector is made up of 10 individual panels. The beamstop that reaches from the bottom right to the centre of the scattering pattern prevents X-ray damage to the detector from the very intense direct beam.

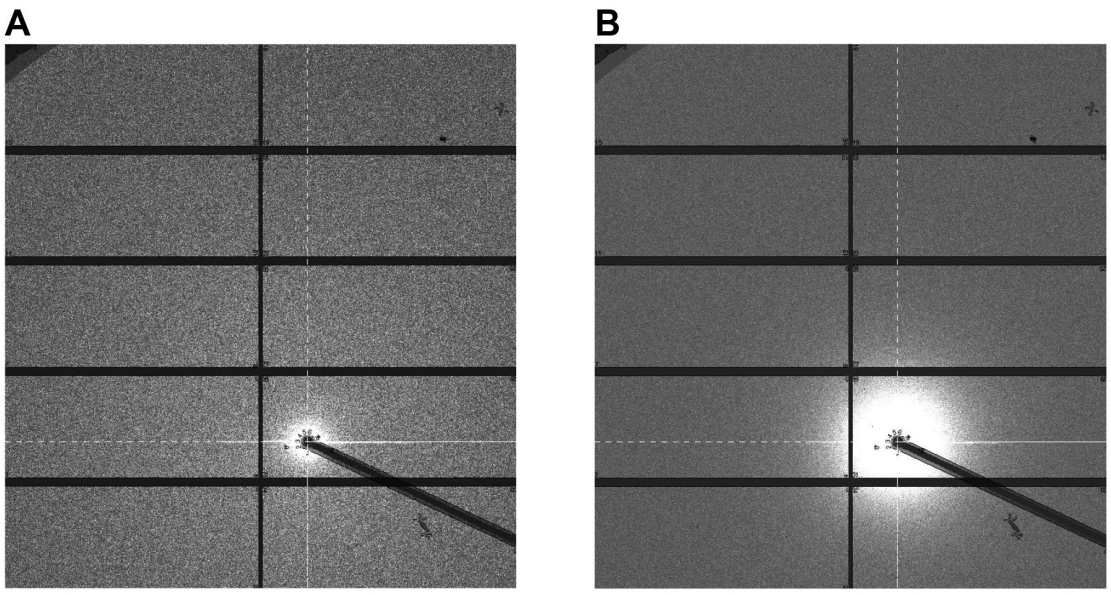

Figure 4.16 *Detector generated image of SAXS scattering pattern of ovalbumin in Milli-Q water (0.6 mg/mL at 7 m sample to detector distance). A) before heating, B) after 24 hours heating at 80 °C. The detector is made up of 10 individual panels. The beamstop that reaches from the bottom right to the centre of the scattering pattern prevents X-ray damage to the detector.*

4.4.1 Quaternary Structure of Native Ovalbumin in Solution

The initial oligomeric state of ovalbumin before aggregation was assessed prior to heat treatment. SAXS measurements of the native quaternary structure were undertaken in dilute systems (0.6 mg/mL protein concentration) to avoid particle-particle interactions. At the ovalbumin concentration of 0.6 mg/mL there was no evidence of particle-particle interaction (no structure factor) visible in the scattering patterns. In order to establish whether ovalbumin was monomeric or dimeric in solution at 0.6 mg/mL, the scattering profiles of ovalbumin in all four conditions (water, 100 mM glucose, 100 mM methylglyoxal, 100 mM NaCl) were measured before heating (Figure 4.17). The radii of gyration (Section 4.2.3.1) of all four protein solutions were between 25.5 ± 0.5 Å and 27.8 ± 1.3 Å (Table 4.3). These findings are consistent with previous literature (Weijers et al. 2005; Matsumoto & Inoue 1993), where R_g values of 26 Å and 27 Å were attributed to the monomeric ovalbumin. However, an R_g value of 28 ± 1 Å was also proposed to be consistent with dimeric ovalbumin in solution (Ianeselli et al. 2010), which is contradictory to the findings presented here and to the findings of Weijers et al. (2005) and Matsumoto & Inoue (1993).

As seen in Figure 4.17A the scattering of all four solutions before heating agree well with the theoretical scattering profile of the monomer (single chain A) of the crystal structure of the PDB entry 1OVA (Stein et al. 1991). In comparison, the theoretical scattering of the three possible ovalbumin dimers (Chains AB, AC, AD) all show marked differences in the scattering profiles (Figure 4.17B). The theoretical scattering was calculated using *CRYSOL* software (Svergun et al. 1995). *CRYSOL* analysis of chain A yielded an R_g value of 28.1 Å for the single chain A which is consistent with the obtained SAXS scattering profiles (25.5 ± 0.5 Å to 27.8 ± 1.3 Å). Additionally, the calculated (*Autoporod*) volumes and molecular weights of the experimental data agreed well with monomeric chain A of 1OVA. The molecular weight of chain A was determined to be 41.9 kDa compared to the experimentally determined average molecular weight of 35.5 kDa, calculated using *Autoporod*. The volumes were determined to be 59.4 nm^3 for the single chain A and 56.9 nm^3 for the experimentally determined volume, showing good agreement. All these findings strongly indicate the presence of a predominantly monomeric ovalbumin species at 0.6 mg/mL which is consistent with previous findings reporting monomeric ovalbumin between 0.1 mg/mL and 1 mg/mL (Matsumoto & Inoue 1993).

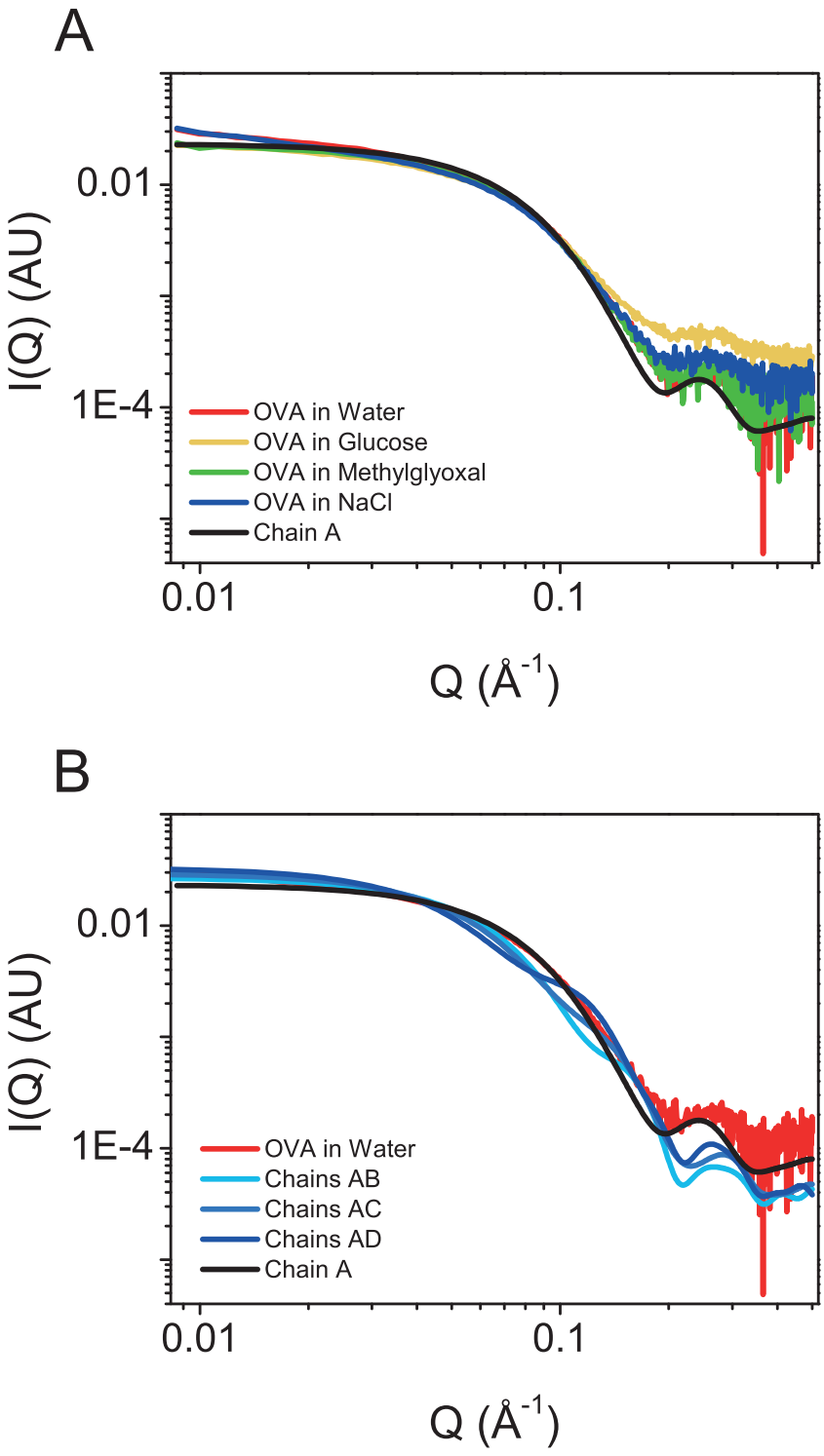

Figure 4.17: *SAXS scattering profiles of ovalbumin before heating, in the presence of water, glucose, methylglyoxal, and NaCl. A) 1.6 m camera to detector length, B) Theoretical scattering of monomeric and dimeric ovalbumin (combinations in shades of blue from light to dark: Chains AB, AC, AD, and monomer (black) compared with the measured scattering of ovalbumin in water (red).*

The experimentally determined scattering profiles of 0.6 mg/mL ovalbumin in Milli-*Q* water, methylglyoxal, and NaCl show high similarity across the entire *Q*-range (Figure 4.17A).

At high *Q* values, which correspond to small distances in real space (measured at 1.6 m sample to detector distance), there is no obvious sign of aggregation (Figure 4.17A). However, at lower *Q* values (measured at 7 m sample to detector distance) there is an intensity increase in the low *Q* region, indicative of early protein aggregation even without heating. The ovalbumin aggregation is most pronounced in the presence of Milli-*Q* water followed by NaCl, glucose and methylglyoxal.

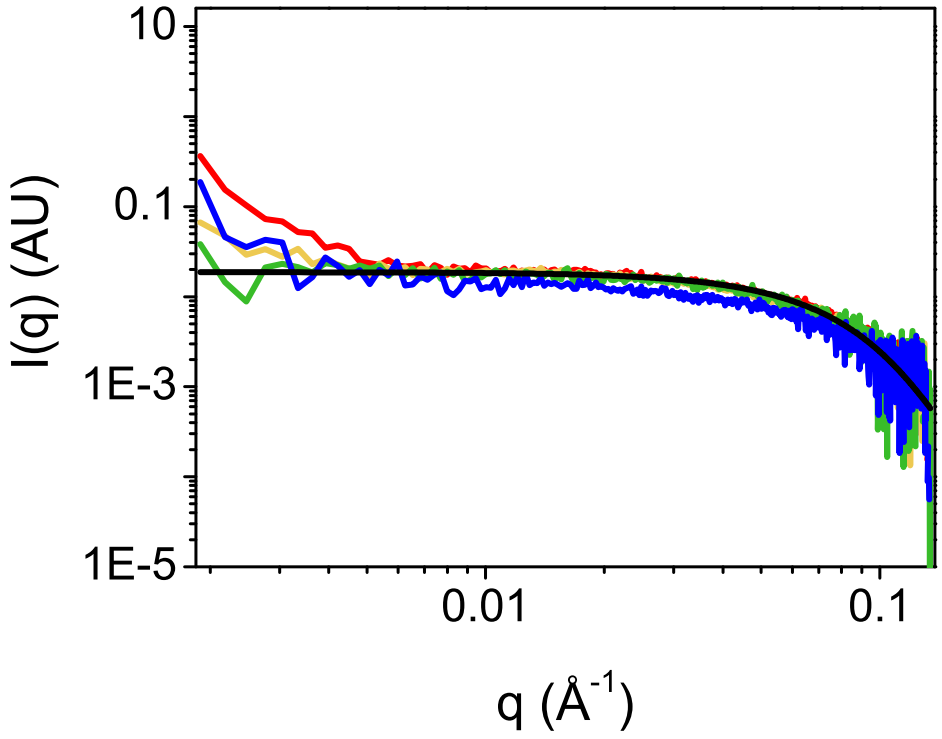

Figure 4.18 *7.0 m camera to detector length. Red line: ovalbumin in water, yellow line: ovalbumin in 100 mM glucose, green line: ovalbumin in 100 mM methylglyoxal, blue line: ovalbumin in 100 mM NaCl, black line: theoretical scattering of the ovalbumin crystal X-ray structure (PDB entry: 1OVA).*

4.5 Protein Concentration Effects on Ovalbumin in Solution

In addition to the buffer conditions, the protein concentration is one of the major factors that determine aggregate morphology. Ovalbumin has been shown to form fibrillar aggregates of varying contour lengths, ranging from 50 ± 14 nm to 190 ± 70 nm depending on the chosen protein concentration (Sagis et al. 2004). The longest fibrils were found near the protein concentration at which gel formation starts (c_g). Using SAXS, the analysis of a series of concentrated protein solutions allows the determination and characterisation of the structure factor (*S(Q)*) within the solution. *S(Q)* is a measurement of interparticle distances which in turn contains information about particle-particle interactions.

Therefore, a protein concentration dependent study on the effects of the respective buffer conditions was undertaken. The sample to detector distance was 3 m, corresponding to a *Q*-range of 0.005 $Å^{-1}$ - 0.3 $Å^{-1}$. Figure 4.19 illustrates marked differences of ovalbumin in the four different test solutions. Firstly, the low ovalbumin concentrations show similar scattering across all four buffer conditions. With increasing ovalbumin concentrations there is a distinct development of a scattering peak, especially of ovalbumin in water and in 100 mM glucose (Figure 4.19A and B). There is no obvious peak development in either methylglyoxal or NaCl buffer. Because the peak is only visible at high concentration and is also moving towards a higher *Q* value (corresponding to smaller distances in real space) with increasing protein concentration, it is very likely that the observed peak is a structure factor (*S(Q)*) related peak rather than a form factor (*P(Q)*) related peak (Ianeselli et al. 2010). Therefore the peak contains information about the predominant inter-protein distances of the proteins in solution, which naturally decreases as the volume fraction of protein in solution increases. Similar peak shifts have been observed previously by others (Ianeselli et al. 2010) in a concentration range of ovalbumin from 20 - 200 mg/mL. The presence of a peak indicates that the proteins in solution have a preferred interparticle distance rather than a broad random distribution. This is likely an effect of electrostatic repulsion (Coulomb repulsion) in the system, as native ovalbumin is negatively charged (net charge is -11 to -12) at pH 7 (Broersen et al. 2007; Ianeselli et al. 2010). The NaCl sample shows signs of aggregation at low *Q* values, whereas the scattering increase is less pronounced in the glucose and water samples. Interestingly, there is less aggregation in the methylglyoxal treated ovalbumin solution. The suppression of particle-particle repulsion by salt of ovalbumin has been observed previously (Ianeselli et al. 2010; Sugiyama et al.

2001) and is consistent with enhancing aggregation observed in DLS measurements. However, the lack of aggregation and lack of a $S(Q)$ in the methylglyoxal sample indicates a different mechanism to salt shielding (Section 4.5.1).

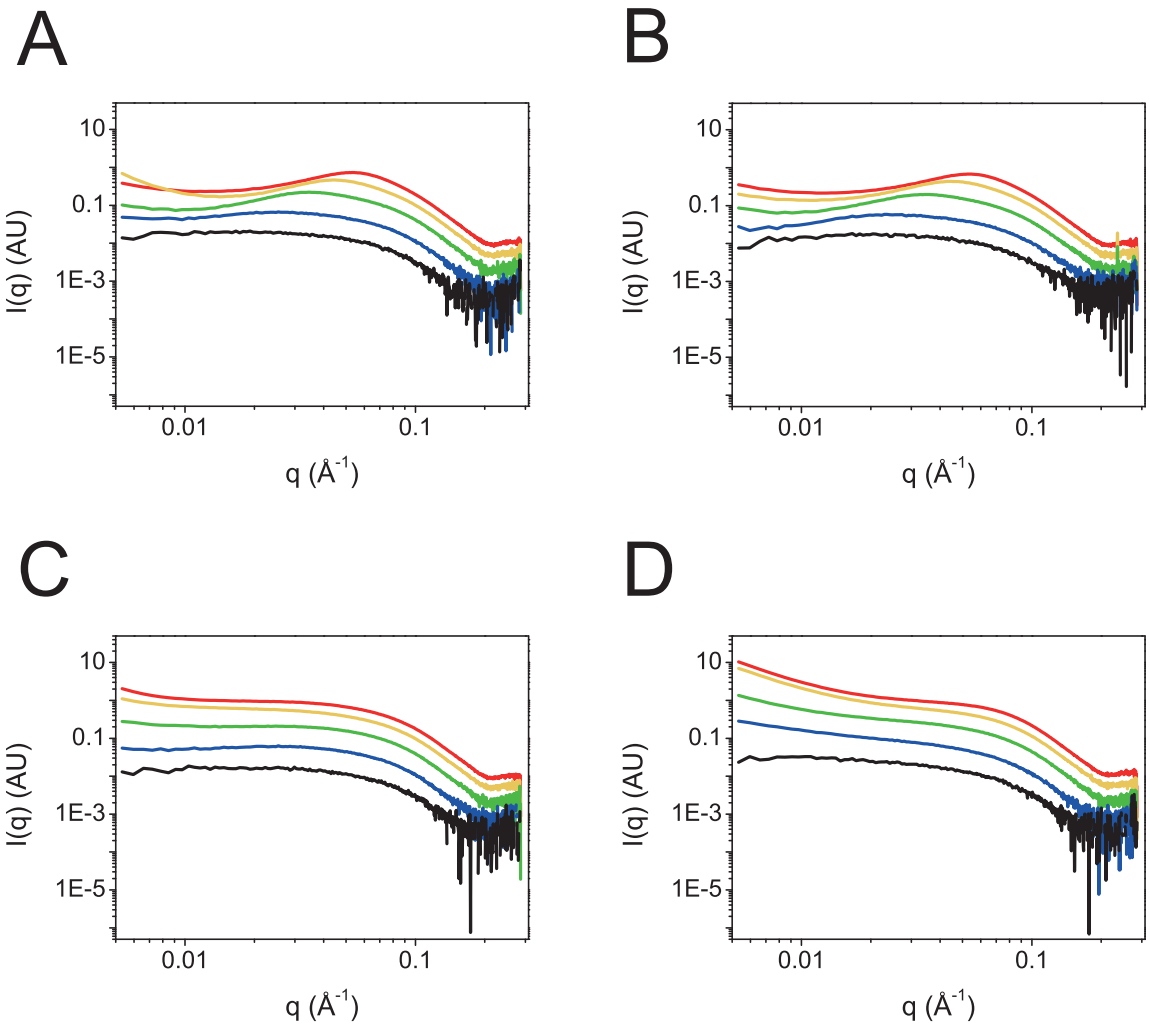

Figure 4.19 *Concentration range of ovalbumin in A) water, B) glucose, C) methylgyoxal, D) NaCl. From lowest concentration (black line) to highest concentration (red line). The concentrations are: black 0.8 mg/mL, blue 2.6 mg/mL, green 9.7 mg/mL, yellow 26.3 mg/mL, red 45.5 mg/mL.*

The SAXS data were fitted mathematically to determine both the form factor (to yield information about the particle shape) and structure factor (to gain insight into the interparticle interactions). Two ovalbumin concentrations were chosen for fitting, 0.8 mg/mL and 45.5 mg/mL. The low concentration allowed the fitting of a form factor (*P(Q)*) irrespective of a structure factor because protein-protein interactions are negligible (*S(Q)* = 1) at sufficiently low concentrations (Glatter & Kratky 1982). The high concentration allowed fitting of both form (*P(Q)*) and structure factor (*S(Q)*). All of the parameters for fitting are listed in Table 4.1 (ovalbumin at 0.8 mg/mL) and Table 4.2 (ovalbumin at 45.5 mg/mL). For fitting purpose the protein and solvent scattering length densities (SLDs) were fixed at calculated values, as was the background scattering. Water (the solvent) has a SLD of 9.43 x 10^{-6} $Å^{-2}$ (calculated using the SLD Calculator available at http://www.ncnr.nist.gov/resources/sldcalc.html), and an appropriate SLD was used for hydrated protein (10.5 x 10^{-6} $Å^{-2}$). For X-ray scattering, the SLD is proportional to the electron density and the classical electron radius (2.818 fm) (Koch et al. 2003). The SLD of water was held constant for all of the data fits, even for buffers that contained NaCl, glucose, or methylglyoxal because the buffers were made up of at least 98.2 % water. Therefore the contributions of other compounds were negligible for the overall SLD of the solution.

4.5.1 Determination of Ovalbumin Form Factor and Structure Factor

The shape of ovalbumin has previously been described as an ellipsoid with the dimensions 70 x 45 x 50 Å (PDB: 1OVA (Stein et al. 1991)). For data fitting, the uniform ellipsoid model was therefore chosen. The parameters for fitting the ellipsoid form factor ($P(Q)_{ell}$) to the 0.8 mg/mL ovalbumin solutions are listed in Table 4.1. The SAXS scattering data of the 0.8 mg/mL concentration were fitted without a structure factor because protein-protein interactions are negligible at this low concentration.

Table 4.1 *$P(Q)_{ell}$ fitting parameters for the 0.8 mg/mL ovalbumin solutions. Grey values are fixed values. Black values are variable fitted values. Typical error values for the radii were between ± 1.8 Å.*

	water	glucose	methylglyoxal	NaCl
Scale / 10^{-3}	1.84	1.78	1.76	1.95
r_a (rotation axis) / Å	44.2	44.3	44.5	65.6
r_b / Å	22.9	22.2	22.2	20.9
SLD ellipsoid / 10^{-6} Å^{-2}	10.51	10.49	10.48	10.54
SLD solvent / 10^{-6} Å^{-2}	9.43	9.43	9.43	9.43
Incoh. bkg /10^{-4} cm^{-1}	1.65	4.18	1.71	1.20
χ^2	116	112	107	152
$\sqrt{(\chi^2/n)}$	0.51	0.51	0.49	0.59

The ellipse radii r_a and r_b show that the fitted ellipsoids have diameters (d) of about 88-89 Å (d_a) and 42-46 Å (d_b) which is in good agreement with the ovalbumin dimensions previously reported (70 Å x 45 Å x 50 Å). Only ovalbumin in NaCl buffer deviates from the norm with a d_a of 131 Å but similar d_b. This could indicate that some ovalbumin molecules are forming dimers in the presence of NaCl (with an end-to-end dimerisation rather than side by side). This is consistent with dimeric ovalbumin species observed in DLS; however, Figure 4.17 indicates that ovalbumin is monomeric, albeit at a slightly lower protein concentration of 0.6 mg/mL. A graph of the low ovalbumin concentration fits (Figure 4.20) illustrates that the uniform ellipsoid as a representation of the ovalbumin molecule agrees well with the collected experimental data. The fitted curves generally overlay well with the experimental data (yellow lines of experimental data overlaid with dashed lines of fitted ellipsoid form factor).

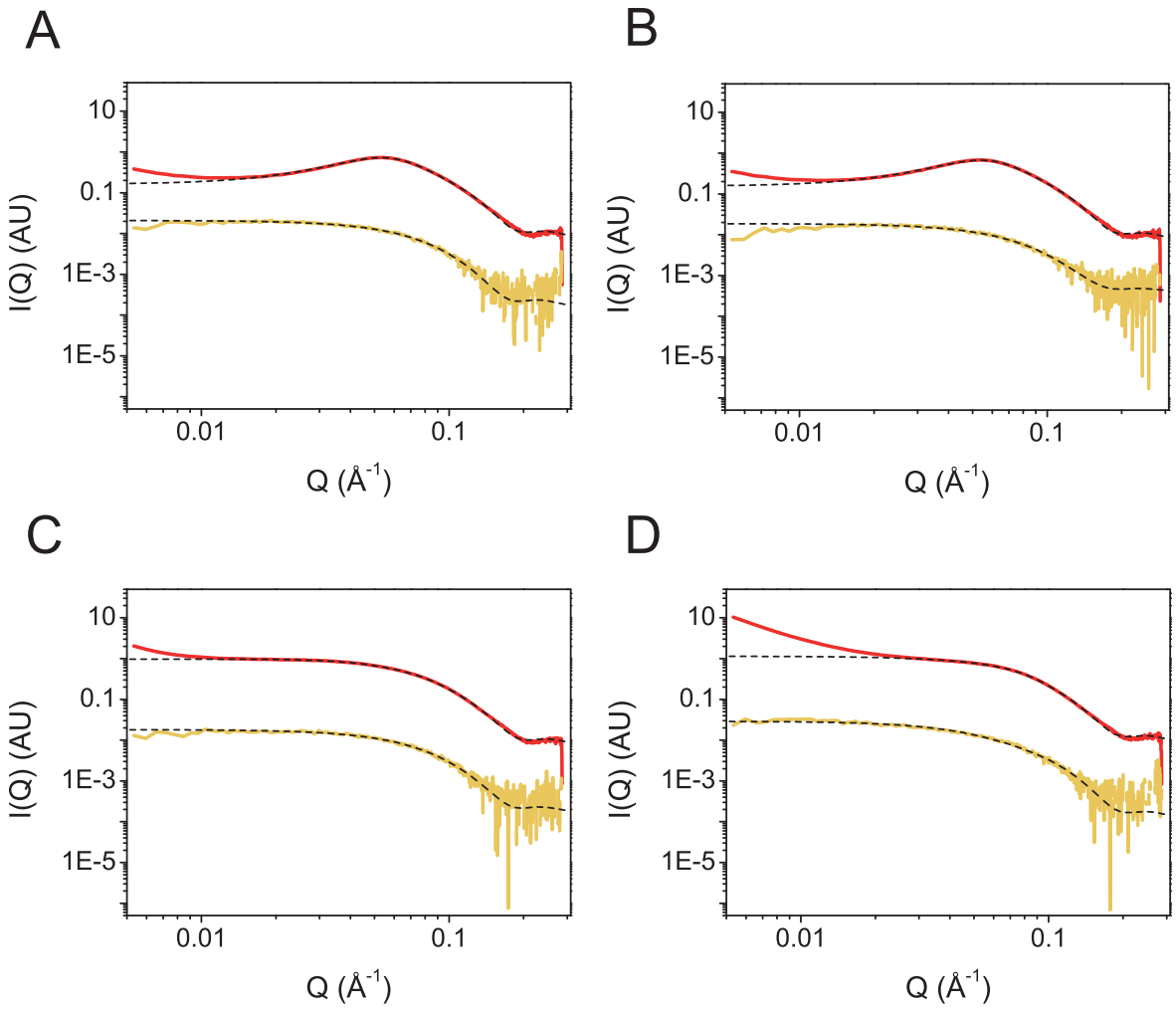

Figure 4.20 *Experimental SAXS data of ovalbumin overlaid with fitted ellipsoid model (dotted lines). A) water, B) glucose, C) methylgyoxal, D) NaCl. Yellow line 0.8 mg/mL, red line 45.5 mg/mL.*

For the high protein concentrations (45.5 mg/mL), $P(Q)_{ell}$ was fitted to the data in combination with a screened Coulomb structure factor $S(Q)_{SC}$ using the *NCNR SANS* analysis package (Kline 2006). The dimensions of ovalbumin at 45.5 mg/mL (Table 4.2) suggest that end-to-end dimers are formed in all four cases. The structure factor inclusion during fitting also suggests that the charge of the dimers is at about 10 for ovalbumin in water, glucose, and NaCl. This estimate is 2-fold lower than the expected 20 (the calculated net charge of the ovalbumin monomer at pH 7 is -10 (based on pK_a values of amino acid residues using the EMBOSS software suite (Rice et al. 2000)). The discrepancy between the two values cannot be explained by salt bridge formation upon dimerisation because of the principle of charge conservation.

Table 4.2 *Form factor of the ellipsoid ($P(Q)_{ell}$) in combination with a screened Coulomb structure factor ($S(Q)_{SC}$) fitting parameters for the 45.5 mg/mL ovalbumin solutions. Grey values are fixed values. Black values are fitted values. Typical error values for the radii were between ± 2.0 Å. The error for charge was ~ 0 in all cases apart from NaCl treated sample (error ± 7).*

	water	glucose	methylglyoxal	NaCl
Volume fraction	0.12	0.12	0.06	0.08
r_a (rotation axis) / Å	70.3	67.2	76.2	75.2
r_b / Å	21.5	21.5	21.0	21.2
SLD ellipsoid / 10^{-6} Å^{-2}	10.52	10.51	10.86	10.80
SLD solvent / 10^{-6} Å^{-2}	9.43	9.43	9.43	9.43
Charge	10.3	10.4	3.0	7.5
Monovalent salt / mM	0.14	0.50	6.74	252.77
Temperature / K	298	298	298	298
Dielectric constant	78	78	78	78
Incoh. bkg /10^{-3} cm^{-1}	7.70	7.60	7.56	9.01
χ^2	1862	1598	947	1080
$\sqrt{(\chi^2/n)}$	2.07	1.91	1.48	1.63

The lack of an obvious peak for both NaCl and methylglyoxal is indicative of reduction in the electrostatic repulsion of the proteins by these compounds. The shielding effect of NaCl was expected. Studies on ovalbumin that analysed the behaviour of ovalbumin at varying ionic strengths showed this shielding effect (Ianeselli et al. 2010). These studies showed that an increase of ionic strength lowers the electrostatic repulsion between ovalbumin molecules, leading to the onset of aggregation. The increased scattering of ovalbumin in NaCl at low *Q* distances is due to early aggregation of protein.

Compared to NaCl methylglyoxal does not carry any charges that could contribute to a Coulomb shielding effect. However, at 45.5 mg/mL protein concentration the pH of the ovalbumin solution in the presence of methylglyoxal was measured to be pH 5 (compared to pH 6.5 - 7.0 of ovalbumin in water, glucose, and NaCl) which is close to the IEP of ovalbumin (4.7). This could explain the absence of an interaction peak in the methylglyoxal treated samples at high concentrations because the proteins would not carry significant net charges (Figure 4.15).

The lack of a structure factor shown during SAXS studies in the presence of methylglyoxal (Figure 4.19) was observed before sample heating. From the mass spectrometric analysis (Section 3.3.1) it was observed that before heating only about 10 % of detected arginine

residues had reacted with methylglyoxal to form hydroimidazolone (Section 3.2.5). Ovalbumin with 10 % methylglyoxal modified lysine and arginine residues would have a theoretical IEP of 4.7 (estimated by the EMBOSS software suite (Rice et al. 2000)) (Figure 4.15) which is close to the measured pH 5 and would result in a low net charge of -5. The Coulombic repulsion between ovalbumin proteins would be low and therefore there would not be a characteristic Coulombic interaction peak. Chemically modified ovalbumin has previously been reported to form different aggregate structures. Succinylated and methylated ovalbumin variants with net charges of -1, -5, -12, and -26 at pH 7 have been reported to form different aggregate morphologies depending on the net charge (Weijers et al. 2008). Aggregate ordering was reported to increase with increasing protein net charge (Figure 4.21). Interestingly, the aggregates formed in the presence of methylglyoxal are also more ordered (Section 4.3 (DLS) and Section 4.7 (TEM)) and transparent (Figure 4.2), but in contrast to succinylation the order increased with decreasing net charge.

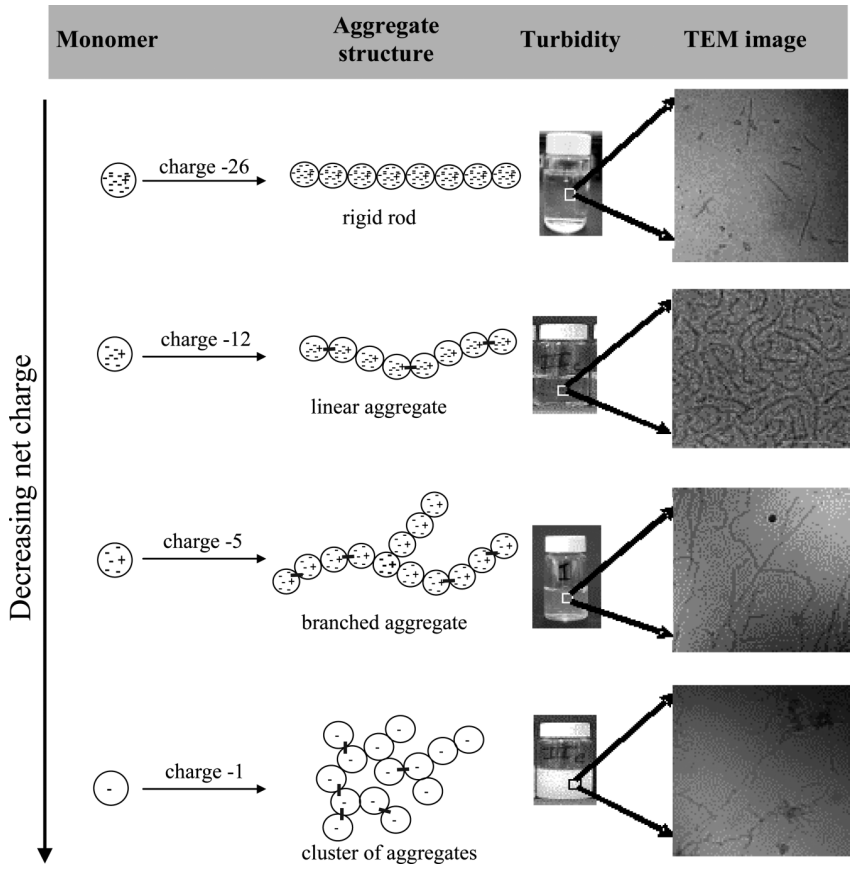

Figure 4.21 *Figure taken from (Weijers et al. 2008). Net charges of ovalbumin variants influence the aggregate morphologies.*

A further study was carried out, investigating in more detail the effects of methylglyoxal concentration on ovalbumin aggregation. A moderately concentrated ovalbumin solution of 3.2 mg/mL (i.e., high enough to show a clear structure factor) was studied in the presence of methylglyoxal at three methylglyoxal concentrations (0.025 mM, 2.5 mM, 100 mM), to investigate possible changes in structure factor. The measured pHs of the solutions were pH 4 at 100 mM methylglyoxal and pH 7 at 2.5 mM and 0.025 mM methylglyoxal. The methylglyoxal concentrations were chosen to form a range that covered equimolar ratio of methylglyoxal to available lysine/arginine residues (2.5 mM methylglyoxal). There are 35 lysine and arginine residues per ovalbumin monomer which is a concentration of 2.6 mM at an ovalbumin concentration of 3.2 mg/mL (molecular weight of ovalbumin is 43 kDa). Therefore 2.5 mM of methylglyoxal was chosen as an equimolar concentration. The 0.025 mM concentration was a 100-fold dilution and 100 mM was in excess of present lysine/arginine residues.

Figure 4.22 shows that with increasing methylglyoxal concentration, the structure factor peak flattens out (which can be seen in the Q region between 0.002 $Å^{-1}$ and 0.02 $Å^{-1}$) showing a clear relationship between methylglyoxal concentration and reduction in electrostatic repulsion. However, the observation is that with increasing methylglyoxal concentration the interaction peak flattens out. Theoretically, at constant pH 7, a higher concentration of methylglyoxal would result in a higher degree of lysine and arginine modification which in turn would lower the IEP of the protein and increase the negative charge on the protein. Therefore with increasing methylglyoxal concentration an increase of the structure factor related peak would be expected. Since the increasing concentration of methylglyoxal reduces the interaction peak, it is evident that lysine and arginine modification do not markedly contribute to the observed differences between 0.025 mM and 2.5 mM methylglyoxal. However, the reduction of the protein electrostatic repulsion (and consequent reduction of structure factor) at high methylglyoxal concentration may be attributed to both the low pH and the degree of methylglyoxal modification. In order to be neutral at pH 4, the ovalbumin monomers have to have lysine and arginine residues modified by methylglyoxal

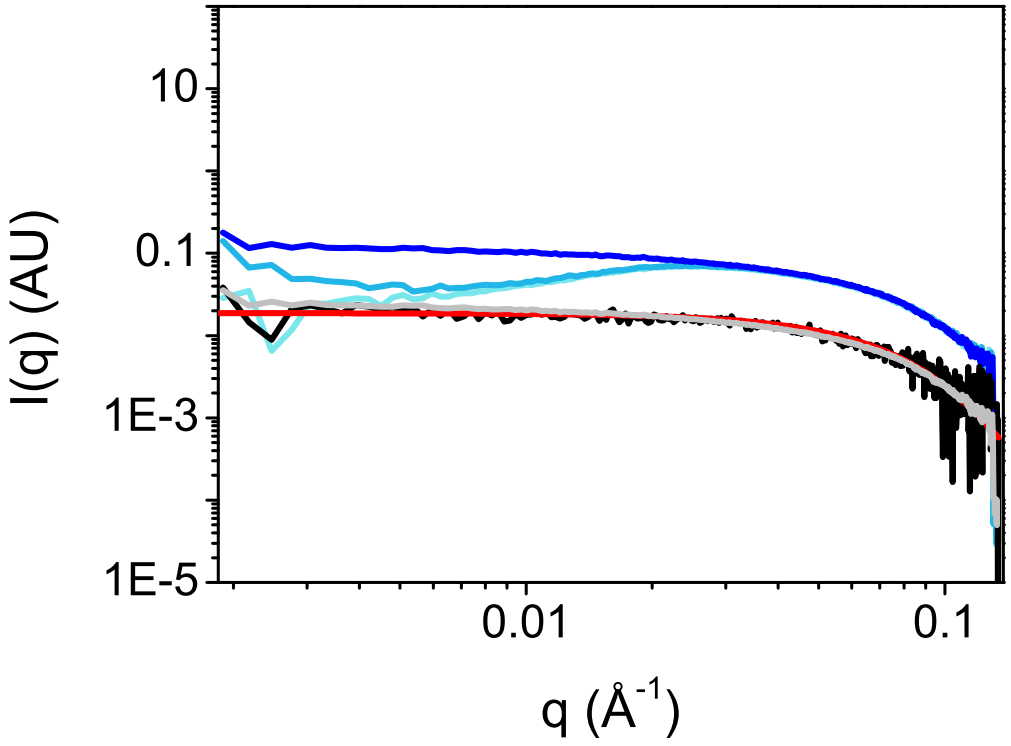

Figure 4.22 *Scattering plots of ovalbumin 0.8 mg/mL (black line) overlaid with the theoretical scattering of an ovalbumin monomer single chain A (red line). In comparison ovalbumin 3.2 mg/mL and 0.025 mM methylglyoxal (lightest blue), 2.5 mM methylglyoxal (middle blue), and 100 mM methylglyoxal (darkest blue). Grey line is the same as the darkest blue line but concentration normalised. Scattering plots were generated from Scatterbrain.*

Overall, it appears that the combination of pH drop and methylglyoxal reactivity at 100 mM methylglyoxal (but not at 2.5 mM or 0.025 mM) has a similar effect on protein orientation and dispersion as salt at ambient temperatures, albeit via two very different mechanisms. Furthermore, it is likely that the reaction between methylglyoxal and lysine/arginine contributes to a charge change as the solutions are heated and the reaction rate increased. The three 3.2 mg/mL ovalbumin solutions (100 mM, 2.5 mM, and 0.025 mM methylglyoxal) were heated at 80 °C for 24 hours in order to establish the differences in scattering behaviour (Figure 4.23). Heating leads to a substantially different aggregation behaviours between the three conditions which is likely due to available methylglyoxal which in turn would influences net charge and thereby the aggregation behaviour of proteins. This is established in a completely different SAXS scattering profile.

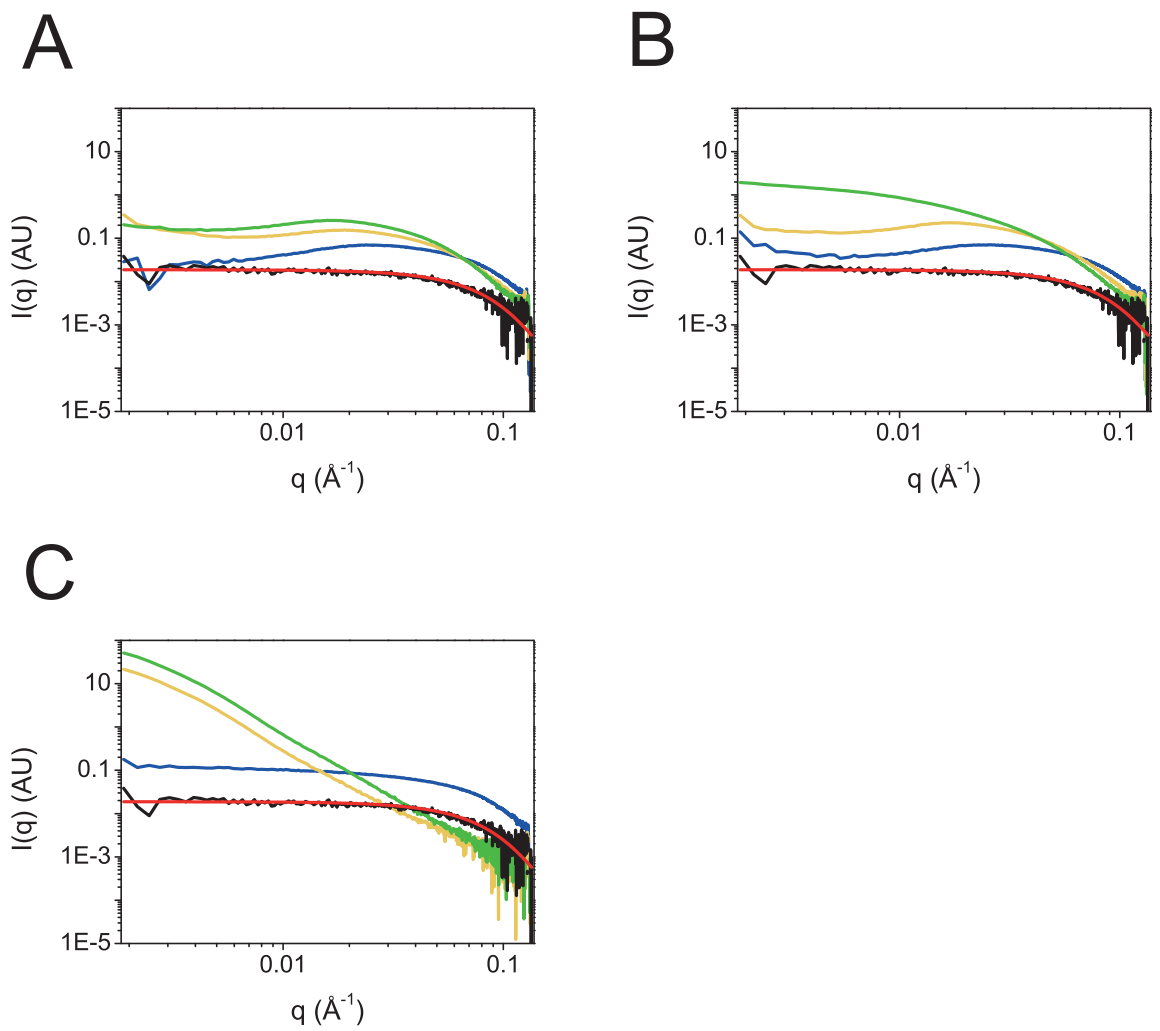

Figure 4.23: *Scattering of ovalbumin 0.8 mg/mL (black line) overlaid with the theoretical scattering of a ovalbumin monomer single chain A (red line). For comparison: ovalbumin at 3.2 mg/mL at 80 °C. A) 0.025 mM methylglyoxal, B) 2.5 mM methylglyoxal C) 100 mM methylglyoxal, blue line: 10 minutes heating, yellow line: 5 hours heating, green line: 24 hours heating. Scattering plots were generated from Scatterbrain.*

4.6 Heating Induced Changes of Ovalbumin Aggregates

Heating is known to cause protein denaturation followed by aggregation. For aggregation measurements, the sample to detector distance was held constant at 7 m, corresponding to a *Q*-range measured of approximately 0.002 $Å^{-1}$ - 0.2 $Å^{-1}$, in order to allow characterisation of large aggregates.

Sample heating was carried out at 80 °C over a 24 hour period. The scattering intensity graphs (Figure 4.24) shows an increase of scattering intensity in the low *Q* region. This general upturn is present in all four buffer systems and is indicative of growing aggregate size. The slope of the scattering profiles is steepest for the NaCl/ ovalbumin solution (Figure 4.24D) which is in good agreement with the DLS data.

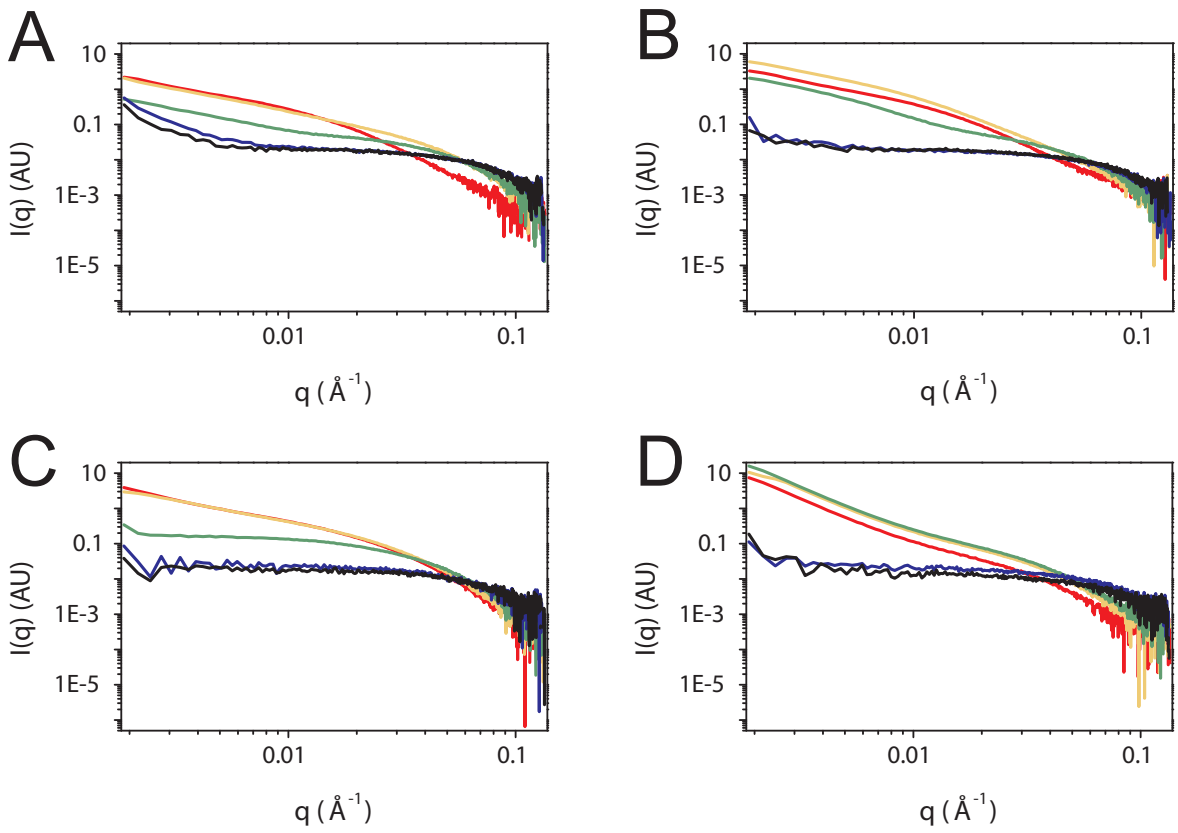

Figure 4.24 *Scattering plots of ovalbumin heated at 80 °C. Buffer conditions are A) water, B) 100 mM glucose, C) 100 mM methylglyoxal, D) 100 mM NaCl. Black line: before heating, blue line: 10 minutes heating, green line: 1 hour heating, yellow line: 5 hours heating, red line: 24 hours heating.*

There are distinct differences in the scattering profiles of all four samples, most notably in the rate of aggregation. Ovalbumin in the presence of NaCl seems to have reached the maximum measurable particle size after 1 hour. There is an obvious down shift of intensity at 24 hours heating time in the NaCl and in the glucose treated ovalbumin (Figure 4.24B and D). This is consistent with a net loss of the measured protein volume fraction in the X-ray pathway. The drop of intensity therefore indicates that some of the insoluble aggregate has precipitated and is no longer contributing to the total scattering of the sample. This

coincides with the observed trend seen in DLS experiments where large amounts of insoluble aggregates were present after 24 hours (Section 4.3). Additionally, the shape of the scattering intensity does not appear to change markedly in the presence of NaCl after 1 hour, while for water, glucose, and methylglyoxal there appear to be definite structure changes between 1 hour and 5 hours heating time.

4.6.1 Rate of Aggregate Growth

In an attempt to visualise the kinetics seen in Figure 4.24, two Q ranges were chosen to cover the two most dynamic scattering regions, one in the low Q region (Q = 0.003 - 0.025 Å^{-1}) and one in the high Q region (Q = 0.060 - 0.105 Å^{-1}) (Figure 4.25).

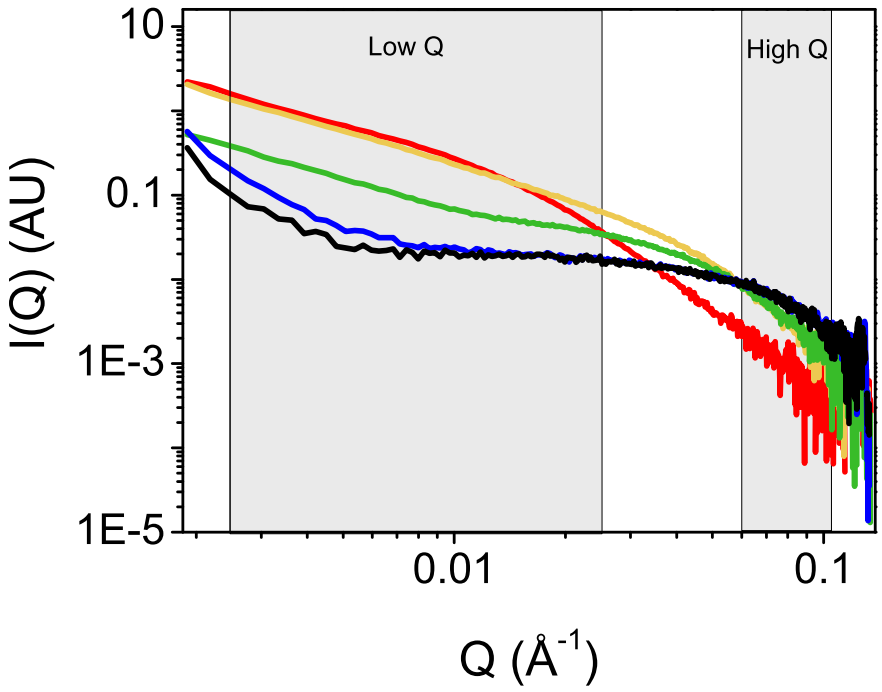

Figure 4.25 *Dynamic regions (grey areas) used for the kinetics analysis overlaid with scattering data from ovalbumin in the presence of Milli-Q water for 24 hours. Black line: before heating, blue line: 10 minutes heating, green line: 1 hour heating, yellow line: 5 hours heating, red line: 24 hours heating.*

The average scattering of the two Q ranges was calculated and plotted over time to monitor the decrease of small scattering particles compared to the increase of large scattering

particles (Figure 4.26). The increase of scattering in the low *Q* window can be related to the increase of aggregates over time while the decrease of scattering in the high *Q* window is indicative of ovalbumin monomer decrease. This fairly simple approach allows easy interpretation of some of the underlying aggregation kinetics. The approach of plotting average intensities in this manner can be justified with regard to the Porod scattering invariant. The scattering invariant law states that the total scattering of a system of fixed contrast and fixed total volume fraction of components is constant, regardless of how the components are arranged (Glatter & Kratky 1982). A caveat for this approach in this instance is that the total protein volume fraction of the studied system may be changing due to insoluble aggregate precipitation at long heating times. This effect is probably responsible for the decrease in the large particle scattering intensity at long time scales for the glucose and NaCl samples.

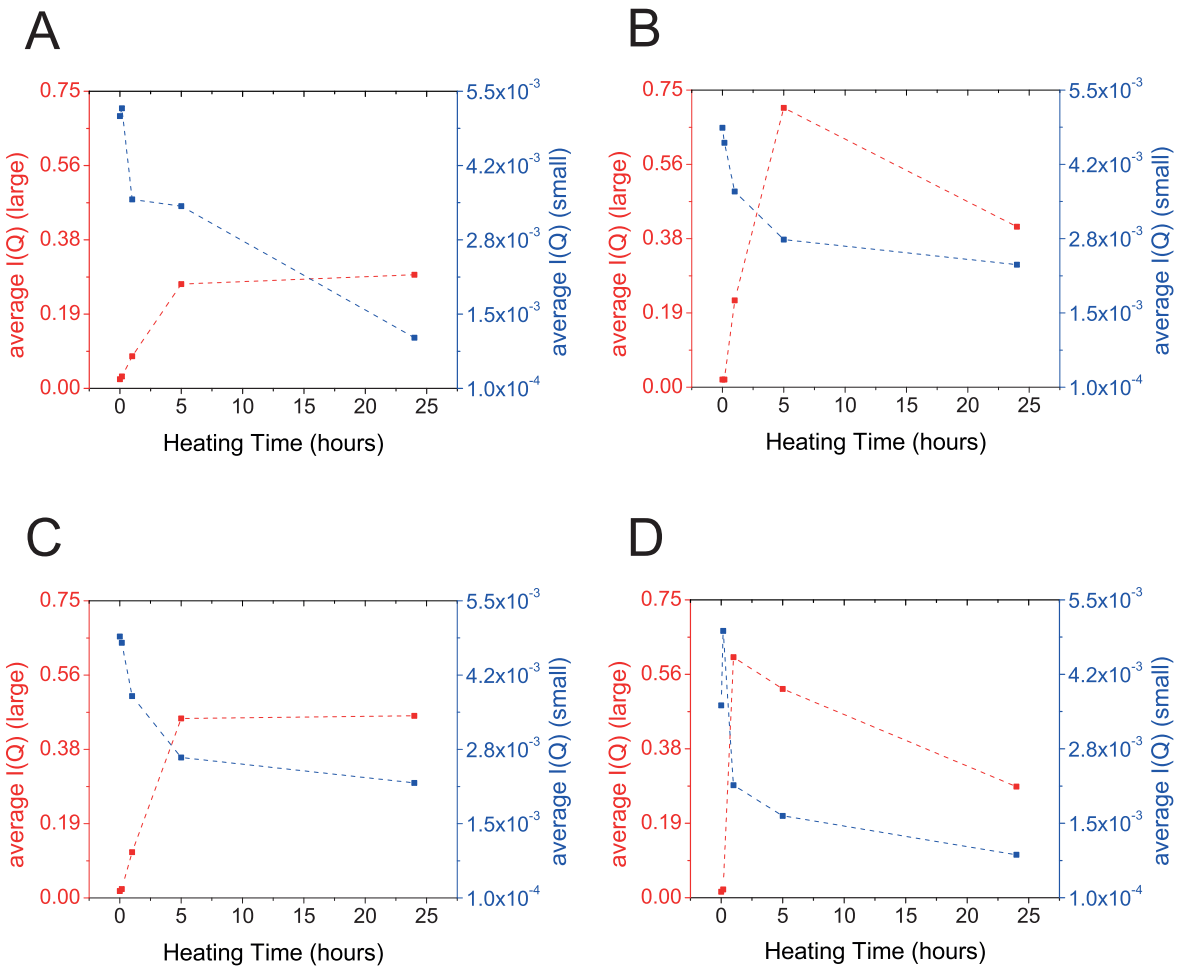

Figure 4.26 *Plots of dynamic I(Q) changes of ovalbumin heated at 80 °C. Buffer conditions are A) water, B) 100 mM glucose, C) 100 mM methylglyoxal, D) 100 mM NaCl.*

Red data set: low Q region (large aggregates), blue data set: high Q region representing monomers.

The plots of the dynamic ranges show that of the tested four buffer conditions ovalbumin in water undergoes the slowest aggregation (Figure 4.26A red data), followed by ovalbumin in methylglyoxal (Graph C), glucose (Graph B) and NaCl (Graph D). The decrease of monomeric ovalbumin scattering (blue data) follows the inverse pattern. All samples differ only marginally after the first 10 minutes of heating. The NaCl treated ovalbumin at 0 minutes displays a low starting intensity but the intensity after 10 minutes heating is very similar to the other three. After 1 hour the scattering intensity decreased in all four samples, where the drop is most pronounced in the NaCl treated samples. After 24 hours the scattering intensity decreased further indicating that most ovalbumin monomers are lost in NaCl, followed by water, glucose, and methylglyoxal. The average scattering intensity of the high Q region almost drops to zero for ovalbumin in NaCl (Figure 4.26D) indicating that only a very small number of monomers are present after 24 hours of heating.

4.6.2 Influence of Buffer Conditions on Aggregate Size

To determine particle size from SAXS measurements, the Guinier plot is often applied (Section 4.2.3.1). The Guinier approximation allows the measurement of the *radius of gyration* (R_g). In Figure 4.27 scattering data are presented in Guinier plots. For native ovalbumin the low Q values follow a linear trend over a wide range. This indicates the absence of aggregated protein (apart from the aggregate described in Figure 4.18) and that the Guinier fit can be used to determine R_g with confidence (Jacques & Trewhella 2010). With heat denaturation, the functions of all samples become more and more curved at low Q^2. The upturn in this area is associated with aggregation to form large structures (Jacques & Trewhella 2010).

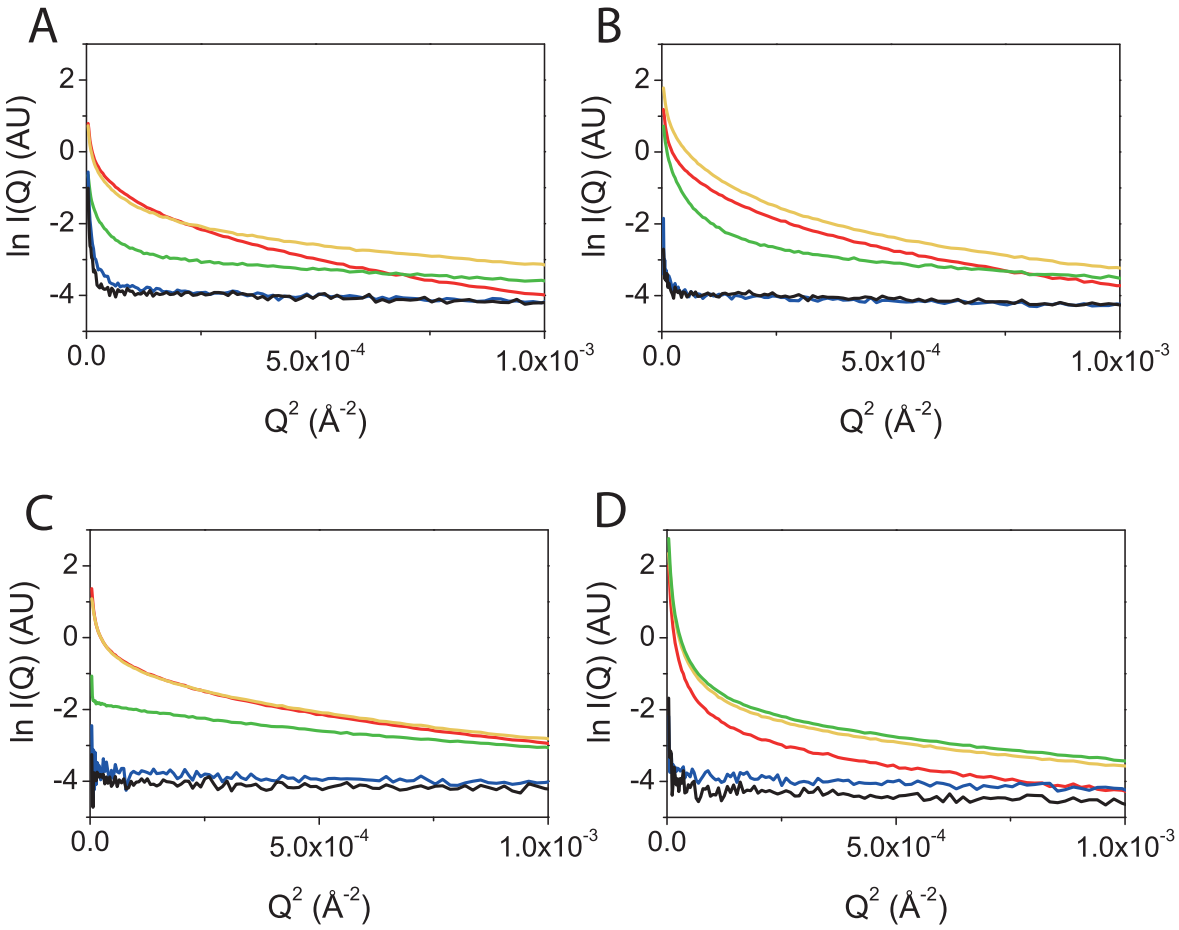

Figure 4.27: *Guinier plots of ovalbumin heated at 80 °C. A) Milli-Q water, B) 100 mM glucose, C) 100 mM methylglyoxal, D) 100 mM NaCl. Black line: before heating, blue line: 10 minutes heating, green line: 1 hour heating, yellow line: 5 hours heating, red line: 24 hours heating.*

Because of the non-linearity of the heated ovalbumin data, the Guinier approximation for determining R_g is potentially somewhat erroneous. Therefore, two different approaches were taken to determine R_g. The R_g values were determined using *Autoporod* software. *Autoporod* is part of the *ATSAS* software package but also integrated into *Scatterbrain* software developed at the Australian Synchrotron (Petoukhov et al. 2012; Petoukhov et al. 2007). *Autoporod* combines two computer softwares, i.e. *AutoRg* (determination of R_g) and *AutoGNOM* (determination of *P(r)*). *AutoRg* automatically runs Guinier analysis to establish R_g, which in turn is used to assign the maximum particle distance (D_{max}) for *P(r)* analysis by *AutoGNOM* (Petoukhov et al. 2012; Petoukhov et al. 2007). Within *AutoGNOM*, the most suitable D_{max} for *P(r)* analysis is determined by scanning the range 2

R_g to 4 R_g in 0.1 R_g steps (Petoukhov et al. 2007). Conversely, from the *P(r)* distribution analysis, the R_g can be calculated. Therefore, *Autoporod* returns two R_g values, i.e. one from Guinier analysis and one from the *P(r)* distribution. Figure 4.28 shows the progression of R_g as a function of heating time. Figure 4.28A shows the Guinier derived R_g and Figure 4.28B shows the *P(r)* derived R_g.

In addition to this fully automated Autoporod approach for *P(r)* analysis, the D_{max} was also adjusted manually. D_{max} values were scanned manually using *GNOM* until a good fit between experimental data and *P(r)* analysis data was achieved. The fitting criteria for manual scanning of D_{max} were the perceptual criteria embedded in *GNOM* software. These criteria include a χ^2 test, smoothness of the solution, and presence of systematic deviations between the restored and the experimental curve (Petoukhov et al. 2007; Semenyuk & Svergun 1991). The combined numerical value of the different quality criteria is then labelled as "good", "reasonable", "suspicious", and "bad". D_{max} adjustments were continued until a good or reasonable solution was achieved for each sample. Figure 4.28C shows the R_g values derived from *P(r)* analysis with manually adjusted D_{max}. Overall, the R_g values follow the same trend regardless of which approach was taken. Figure 4.28D shows the averaged plot of R_g with values listed in Table 4.3. The maximum R_g values are found for ovalbumin aggregates in the presence of NaCl followed by glucose, water and methylglyoxal. This is in good agreement with the results obtained in DLS experiments (Section 4.3). In contrast to the DLS experiments, some of the insoluble aggregate fraction was accessible via SAXS experiments, which explains the larger observed radii.

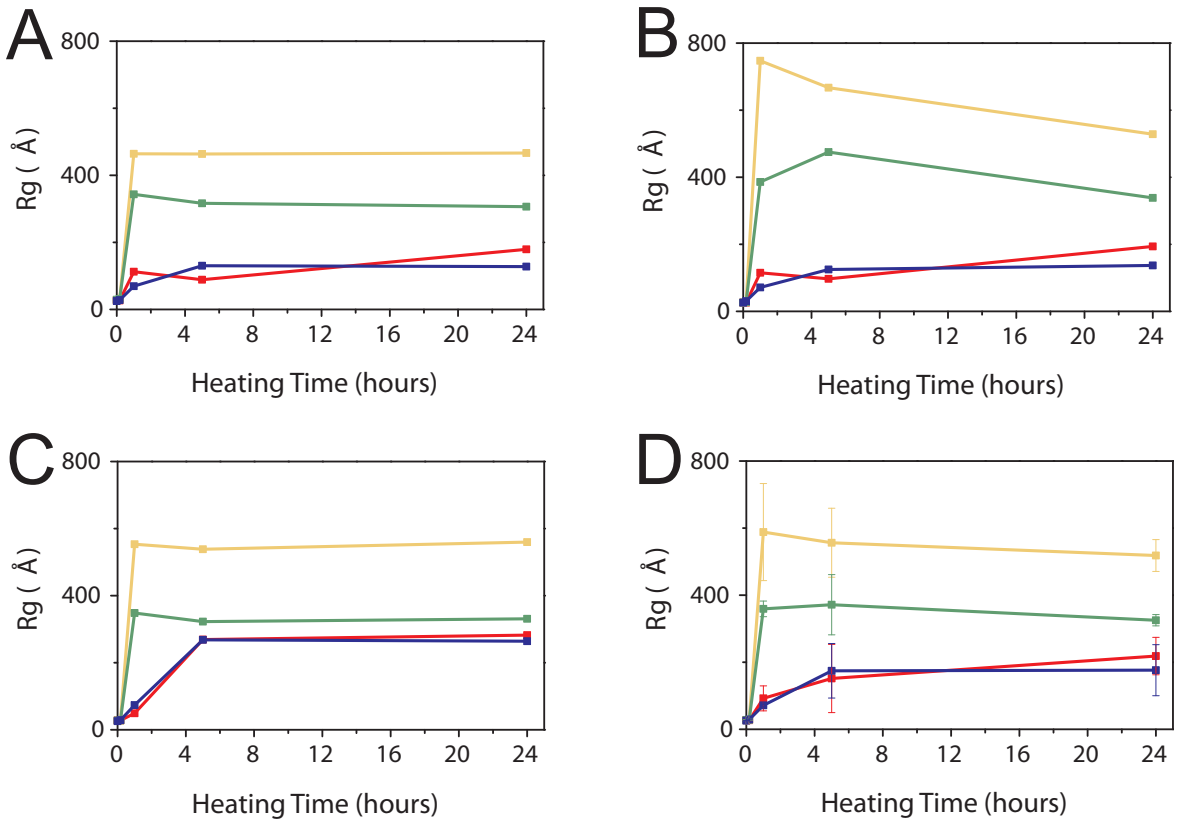

Figure 4.28: *A) Radius of gyration (R_g) determined by Guinier approximation in Autoporod, B) Radius of gyration (R_g) determined by GNOM through P(r) distribution approximation in Autoporod, C) Radius of gyration (R_g) determined by GNOM through P(r) distribution approximation with manual adjustment of D_{max}. D) average of A,B,C. R_g is shown over a heating period of 24 hours. Red line: water, blue line: methylglyoxal, green line: glucose, yellow line: NaCl.*

Table 4.3 *Radius of gyration (R_g) values for ovalbumin solutions at different heating times.*

Heating Time [h]	Milli-Q R_g of ovalbumin [Å]	NaCl R_g of ovalbumin [Å]	Glucose R_g of ovalbumin [Å]	Methylglyoxal R_g of ovalbumin [Å]
0	27.3 ± 0.9	26.1 ± 0.3	27.8 ± 1.3	25.5 ± 0.5
0.17	26.9 ± 0.9	27.8 ± 0.4	28.9 ± 2.3	29.1 ± 1.3
1	92 ± 37	590 ± 140	359 ± 23	71 ± 2.1
5	150 ± 100	560 ± 100	370 ± 90	175 ± 81
24	218 ± 56	520 ± 47	325 ± 17	176 ± 76

4.6.3 Aggregate Shape and Pair Distance Distribution Function

P(r) plots are utilised to determine the shape of the scattering particle. It is therefore possible to monitor conformational changes of proteins (Section 4.2.3.3). As can be seen in Figure 4.29, the peak for native ovalbumin (black line) is at about 29-30 Å which is in agreement with previous findings (Ianeselli et al. 2010). The slightly elongated tail towards longer distances indicates the ellipsoid shape of ovalbumin. Compared to ovalbumin in Milli-*Q* water and 100 mM glucose (Figure 4.29A, B), the *P(r)* function of ovalbumin in the presence of methylglyoxal and NaCl is more constrained (Figure 4.29C. D), representing a more compact shape of the ovalbumin molecule. However, after 10 minutes heating time, this difference disappears and the shapes of all four *P(r)* plots are very similar.

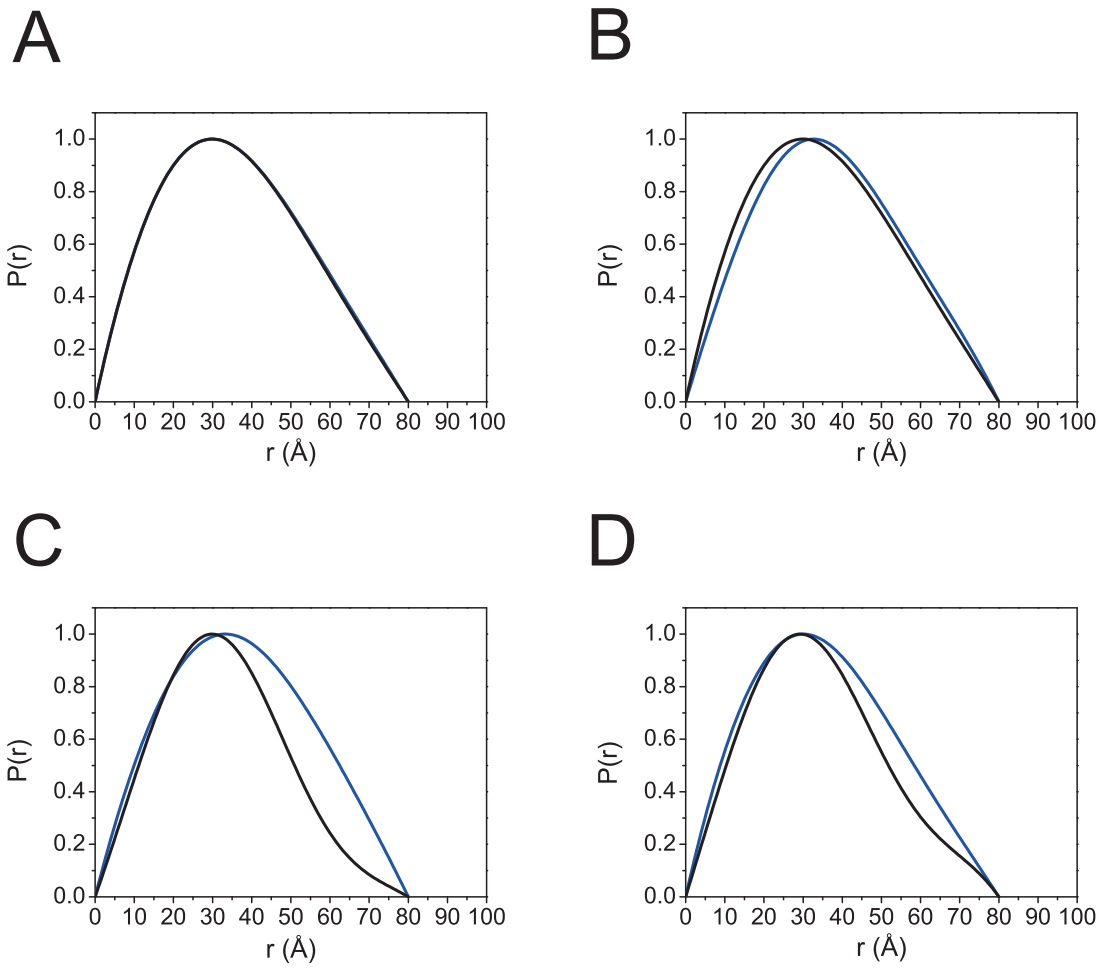

Figure 4.29 *P(r) plots of ovalbumin before heating (black line), and after 10 minutes heating at 80 °C. A) water, B) 100 mM glucose, C) 100 mM methylglyoxal, D) 100 mM NaCl.*

Further heating of the ovalbumin solutions results in aggregate formations that differ markedly in their pair distance distribution (Figure 4.30)

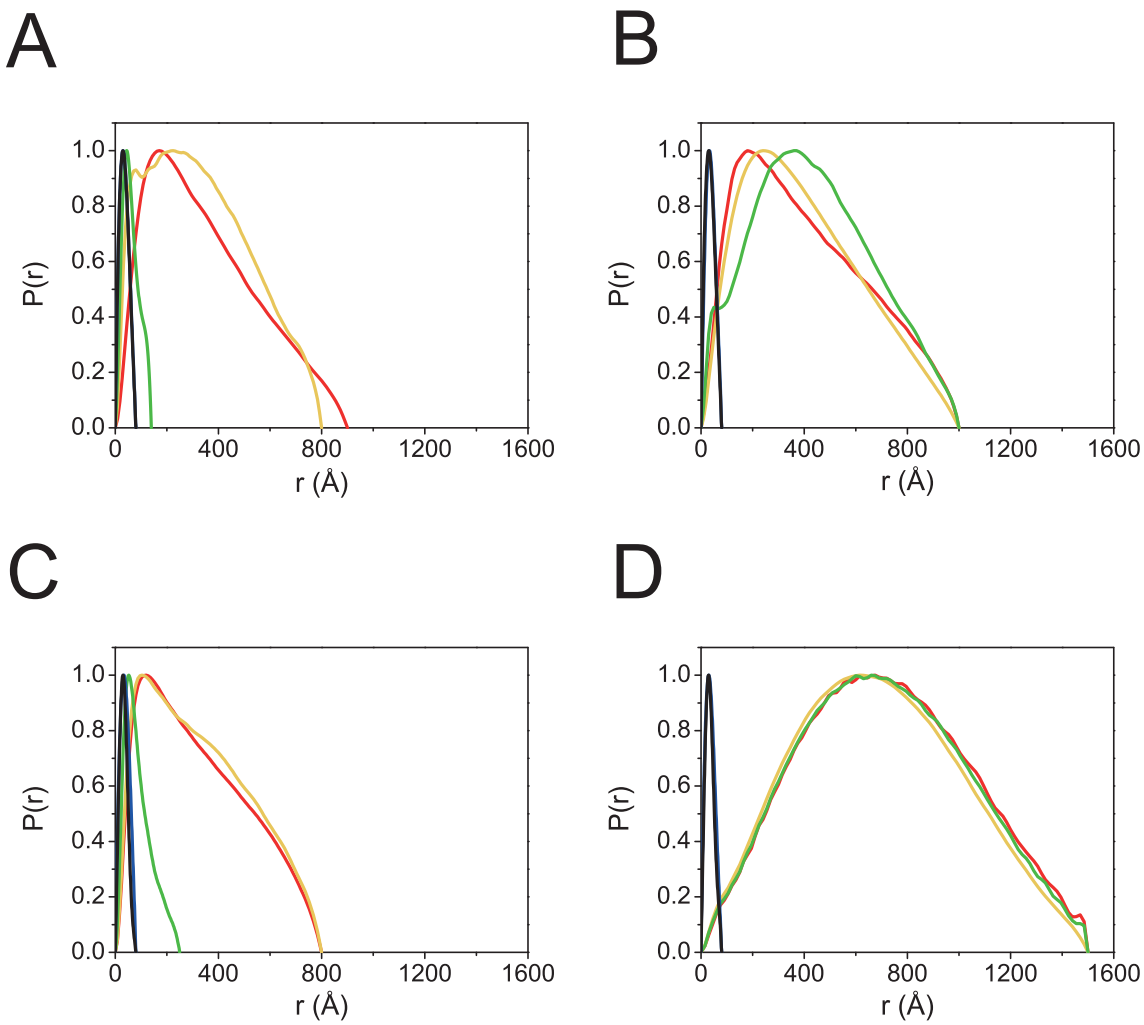

Figure 4.30 *P(r) plots of ovalbumin over 24 hours of heating. Buffer conditions are A) water, B) 100 mM glucose, C) 100 mM methylglyoxal, D) 100 mM NaCl. Black line: before heating, blue line: 10 minutes heating, green line: 1 hour heating, yellow line: 5 hours heating, red line: 24 hours heating. P(r) plots were generated using GNOM from the ATSAS software package.*

As aggregation continues over the 24 hour period the *P(r)* plots show a radical shift to larger pair distances (640 - 650 Å in the case of ovalbumin in 100 mM NaCl). The shape of the *P(r)* function of the aggregated ovalbumin in NaCl sample is representative of spherical aggregation particles. However, the remaining three conditions show that the *P(r)* function is not bell shaped, but rather representative of rod like or elongated particles (compare Figure 4.8, green line).

4.7 TEM Micrographs of Ovalbumin Aggregates

The analysis of SAXS data is often supported by microscopic techniques. Therefore TEM micrographs of the ovalbumin aggregates were obtained under the same experimental conditions as used in the DLS and SAXS measurements. The displayed micrographs are of samples from the soluble fraction (Figure 4.31 to Figure 4.34). Overall, there is no distinct growth pattern of discernible intermediates present in any of the samples. The 3D structure of the soluble aggregates is compacted onto a "2D" TEM grid. This stacking of aggregates on the grid may hinder accurate analysis of the underlying finer aggregate structures. The stacking was also observed in very dilute solutions of the soluble fraction. Where possible the finer underlying aggregate structures are pointed out (see arrows Figure 4.31 to Figure 4.34). These finer structures are about 10 nm in width. However, the accurate quantitative determination of the length distribution of these fine structures was not possible. Analysis by eye suggests a longer length for methylglyoxal and NaCl treated ovalbumin compared to water and glucose treated protein.

The large ovalbumin aggregates formed in the presence of water, glucose, and NaCl look very similar. In the NaCl treated ovalbumin solution there is generally less aggregate present and after 24 hours of heating aggregate is almost absent. This is consistent with the findings of DLS indicating that the centrifugation step eliminated large insoluble aggregates. It is furthermore consistent with the decrease of the volume fraction observed in SAXS experiments. Ovalbumin in the presence of methylglyoxal shows a distinct difference in the large aggregate morphology compared to the other three buffer conditions. There is a finer and more structured network rather than clumping. Moreover, at 10 minutes heating of ovalbumin in the presence of methylglyoxal, there are no large structures present. This is consistent with the DLS data which confirmed the absence of large soluble aggregates. However, the TEM micrographs show large structures after 30 minutes heating which were not seen in the DLS experiments.

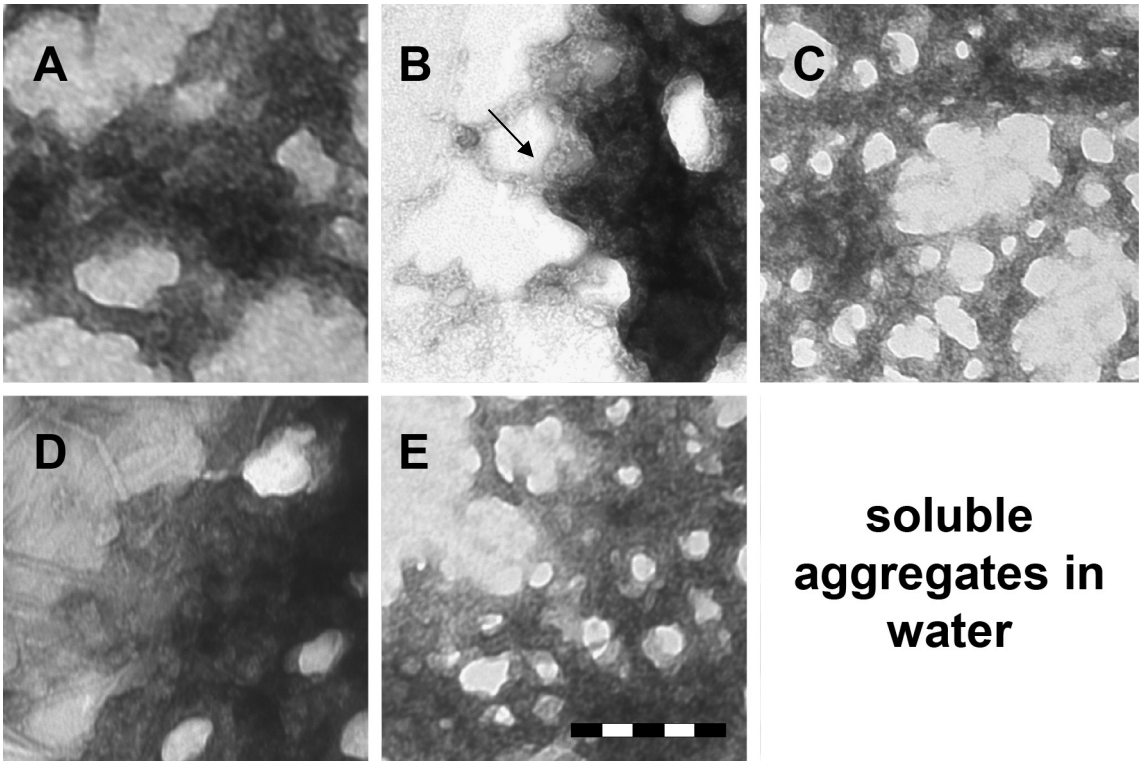

Figure 4.31 *Soluble aggregate formation of ovalbumin at 80 °C in water at five different heating times. A) 10 minutes, B) 30 minutes, C) 1 hour, D) 5 hours, E) 24 hours. The scale bar is 200 nm. The micrographs are representative of duplicate measurements.*

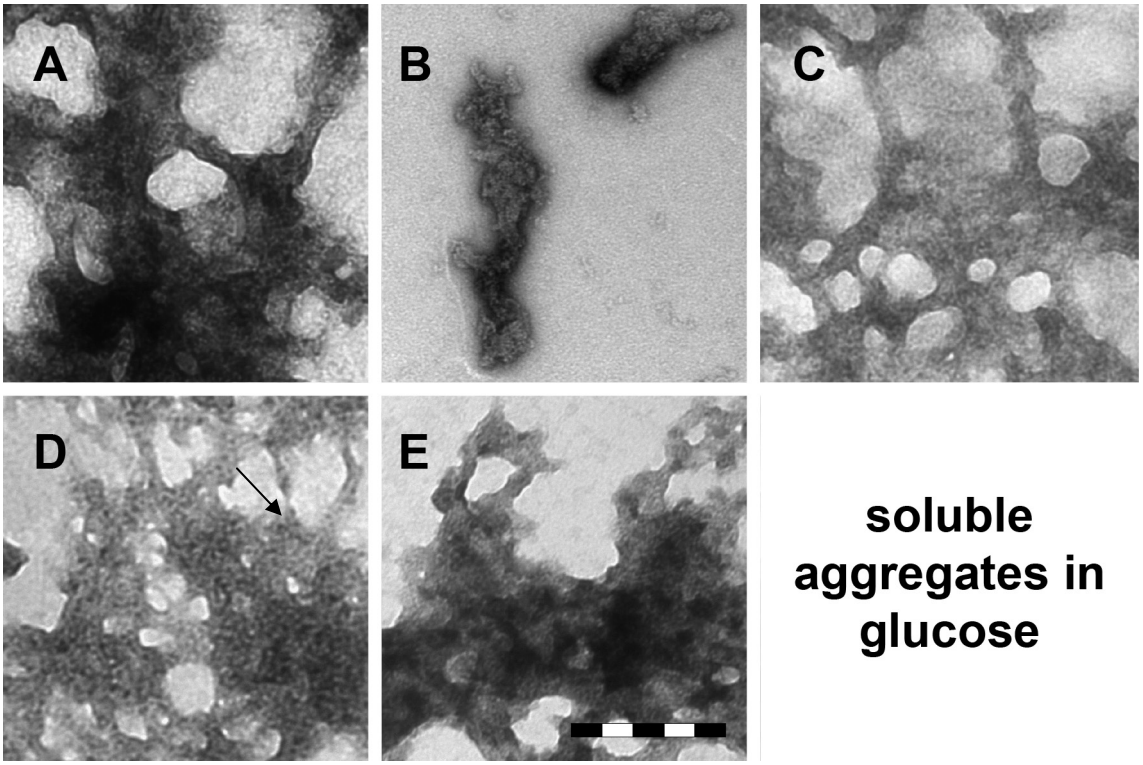

Figure 4.32 *Soluble aggregate formation of ovalbumin at 80 °C in 100 mM glucose at five different heating times. A) 10 minutes, B) 30 minutes, C) 1 hour, D) 5 hours, E) 24 hours. The scale bar is 200 nm. The micrographs are representative of duplicate measurements*

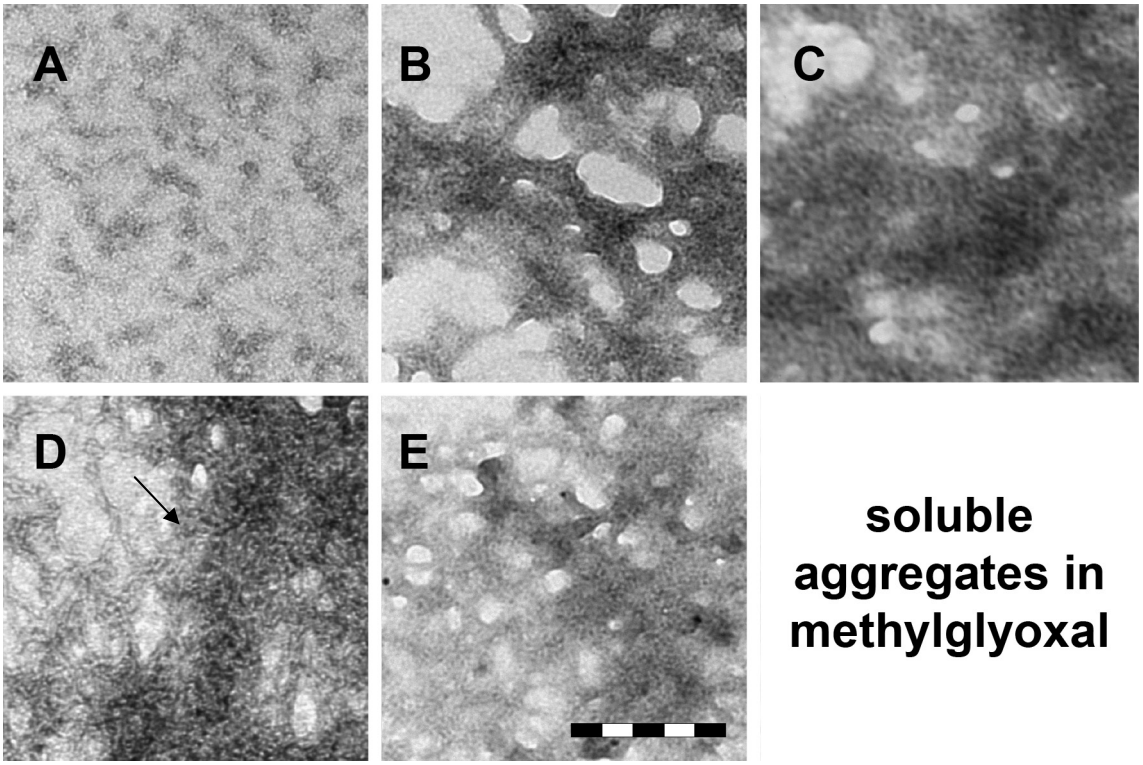

Figure 4.33 *Soluble aggregate formation of ovalbumin at 80 °C 100 mM methylglyoxal at five different heating times. A) 10 minutes, B) 30 minutes, C) 1 hour, D) 5 hours, E) 24 hours. The scale bar is 200 nm. The micrographs are representative of duplicate measurements*

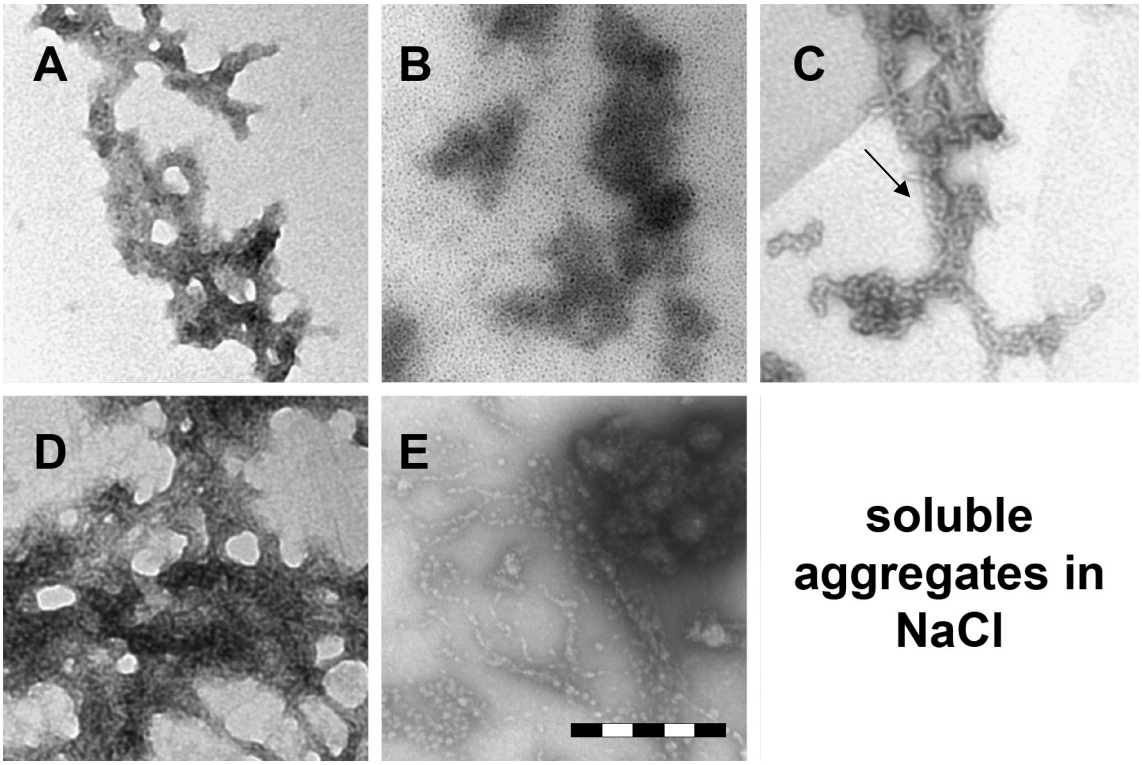

Figure 4.34 *Soluble aggregate formation of ovalbumin at 80 °C in 100 mM NaCl at five different heating times. A) 10 minutes, B) 30 minutes, C) 1 hour, D) 5 hours, E) 24 hours. The scale bar is 200 nm. The micrographs are representative of duplicate measurements*

The observation of distinct fine and overall structural features of the methylglyoxal treated ovalbumin sample prompted further model fitting to the SAXS data (Figure 4.35). A cylindrical form factor (Section 4.2.3.4) was chosen as the model and was fitted to the sample series. This was compared to an ellipsoid form factor fit to the methylglyoxal treated ovalbumin before heating.

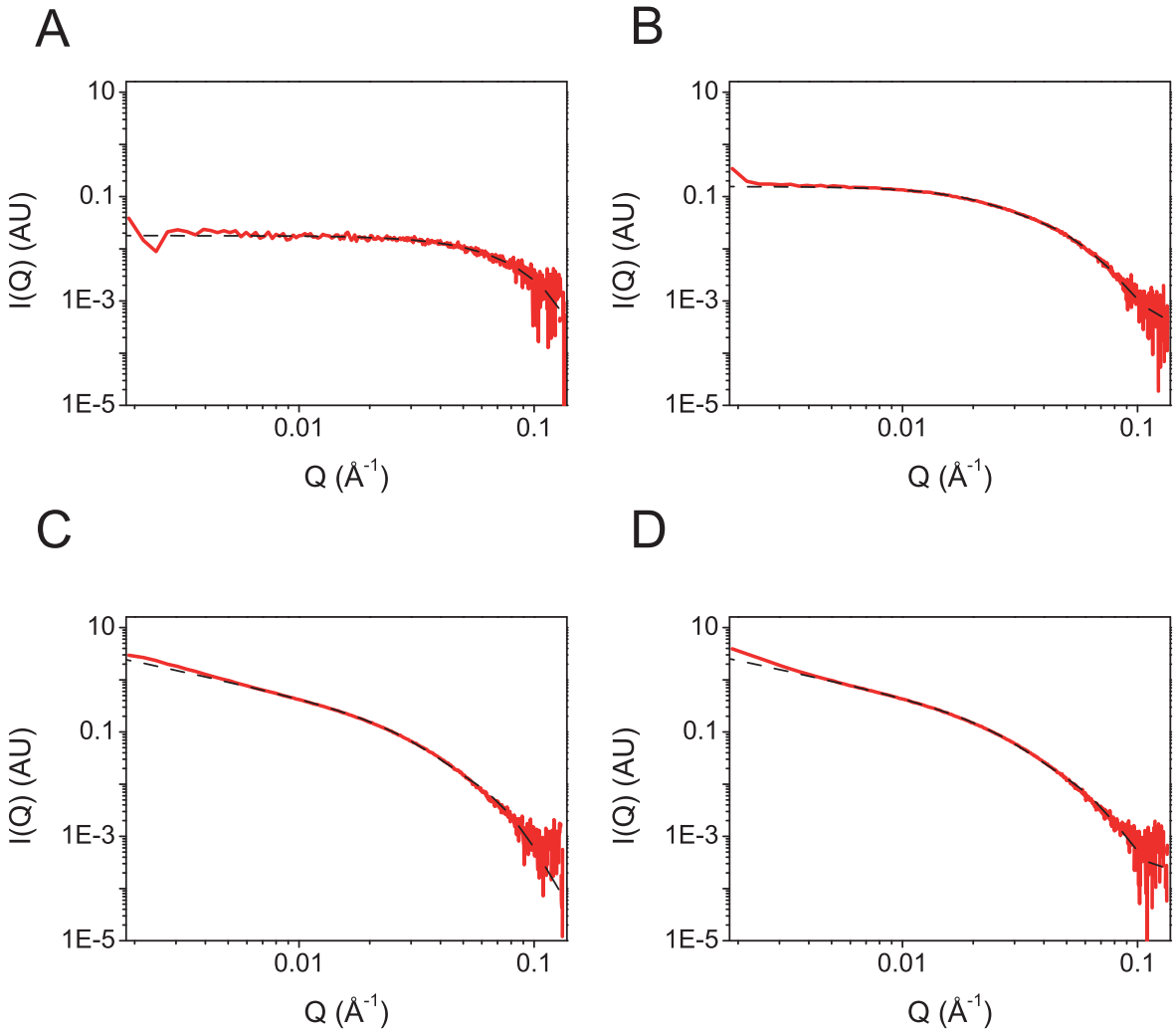

Figure 4.35 *Experimental SAXS data of ovalbumin heated for 24 hours at 80 °C at a protein concentration of 0.6 mg/mL. Data were fitted to $P(Q)_{ell}$ and $P(Q)_{Cyl}$ (dashed lines). A) before heating, B) 1 hour heating, C) 5 hours heating, D) 24 hours heating.*

The fitted models fit the data reasonably well, indicating that the ellipse and cylinder form factor models are appropriate fitting candidates. The derived structural information about the ovalbumin sizes are listed in Table 4.4. The two ovalbumin monomer radii are 22 Å and 45 Å which is good agreement with the ovalbumin monomer dimensions of 70 Å x 45

Å x 50 Å (PDB: 1OVA). The fitting data suggest that the radius within the first hour remains fairly constant. However, there is a 2 - 3 fold increase in length, indicative of end-to-end elongation. During further aggregation (5 hours and 24 hours) the cylinder radius increases to about 90 Å (9 nm) while the length increases to about 7700 - 8000 Å (770 - 880 nm). These large structures could represent the fine structure observed during TEM analysis, where the aggregate diameters (of fine strands) were determined to be about 10 nm (5 nm radius) (Figure 4.33).

Table 4.4 *Fitting parameters for the 0.6 mg/mL ovalbumin solutions at four time points. Grey values are fixed values. Black values are variable fitted values. Typical error values for the radii were between ± 1.5 Å. The error for cylinder length at 5 hours and 24 hours was ± 210 Å.*

	methylglyoxal 0 h	**methylglyoxal 1 h**	**methylglyoxal 5 h**	**methylglyoxal 24 h**
Scale / 10^{-3}	1.76	1.6	1.5	1.3
r_a (rotation axis) / Å	22.2	26.3	27.5	30.0
r_b / Å	44.5	46.1	86.6	95.9
Length / Å	89	224	8020	7680
SLD ellipsoid / 10^{-6} Å^{-2}	10.48	10.50	10.58	10.59
SLD solvent / 10^{-6} Å^{-2}	9.43	9.43	9.43	9.43
Incoh. bkg /10^{-4} cm^{-1}	1.71	0.3	0.0	0.1
χ^2	107	103	389	389
$\sqrt{(\chi^2/n)}$	0.49	0.5	0.9	0.9

4.8 Summary and Discussion

The analysis of polydisperse protein aggregation systems is extremely challenging. DLS and especially SAXS experiments clearly can contribute to understanding aggregation systems. Not only can SAXS provide high definition assessment of the oligomeric state prior to aggregation but also show the inter particle relation in solution. Moreover, it was shown that simple geometric models can be used to assess both the pre-aggregate native ovalbumin as well as the methylglyoxal treated aggregates. However, SAXS does rely on supplementary techniques. Other measurements such as dynamic light scattering, electron microscopy (SEM/TEM), and rheology are often necessary to conclusively determine the definite shape.

The protein aggregation experiments showed that NaCl treatment of ovalbumin led to the largest particle size resulting in an increased insolubility. Over the measured range ovalbumin in water behaved similarly to ovalbumin in glucose. Only at long heating times (between 5 hours and 24 hours) glucose treated ovalbumin became increasingly insoluble due to larger particle sizes. Methylglyoxal treated ovalbumin showed reduced protein-protein interactions due to pH changes and produced large soluble aggregates upon heating, unlike any of the other studied ovalbumin aggregates. This can be attributed to the reactivity of lysine and arginine groups with methylglyoxal, and can be contrasted with the markedly different behaviour when the protein-protein interactions were reduced by electrostatic screening through NaCl. The gained knowledge about ovalbumin aggregation may be relayed to the design of new food stuffs, for example where high soluble protein concentrations are desired (see Section 1.3.2).

4.9 References

Aćimović, J.M., Stanimirović, B.D. & Mandić, L.M., 2009. The role of the thiol group in protein modification with methylglyoxal. *Journal of the Serbian Chemical Society*, 74(8-9), pp.867–883.

Aymard, P., Nicolai, T., Durand, D. & Clark, A., 1999. Static and dynamic scattering of β-Lactoglobulin aggregates formed after heat-induced denaturation at pH 2. *Macromolecules*, 32(8), pp.2542–2552.

Berne, B.J. & Pecora, R., 1976. *Dynamic light scattering: with applications to chemistry, biology, and physics*, New York: Dover Publications.

Broersen, K., Weijers, M., de Groot, J., Hamer, R.J. & de Jongh, 2007. Effect of protein charge on the generation of aggregation-prone conformers. *Biomacromolecules*, 8(5), pp.1648–1656.

Cattoni, D.I., Kaufman, S.B. & Gonz´lez-Flecha, F.L., 2009. Kinetics and thermodynamics of the interaction of ANS with proteins. *Biophysical Journal*, 96(3), p.444a.

Chiti, F. & Dobson, C.M., 2006. Protein misfolding, functional amyloid, and human disease. *Annual Review of Biochemistry*, 75(1), pp.333–366.

Degenhardt, T.P., Thorpe, S.R. & Baynes, J.W., 1998. Chemical modification of proteins by methylglyoxal. *Cellular and Molecular Biology*, 44(7), pp.1139–1145.

Eijsink, V.G.H., Gåseidnes, S., Borchert, T.V. & van den Burg, B., 2005. Directed evolution of enzyme stability. *Biomolecular Engineering*, 22(1–3), pp.21–30.

Franke, D. & Svergun, D.I., 2009. DAMMIF, a program for rapid ab-initio shape determination in small-angle scattering. *Journal of Applied Crystallography*, 42(2), pp.342–346.

Gan, C.-Y., Cheng, L.-H. & Easa, A.M., 2008. Physicochemical properties and microstructures of soy protein isolate gels produced using combined cross-linking treatments of microbial transglutaminase and Maillard cross-linking. *Food Research International*, 41(6), pp.600–605.

Gerrard, J.A. et al., 2012. Aspects of physical and chemical alterations to proteins during food processing - some implications for nutrition. *The British Journal of Nutrition*, 108(S2), pp.S288–297.

Glatter, O. & Kratky, O., 1982. *Small angle X-ray scattering*, London: Academic Press.

Gregoire, S., Irwin, J. & Kwon, I., 2012. Techniques for monitoring protein misfolding and aggregation *in vitro* and in living cells. *Korean Journal of Chemical Engineering*, 29(6), pp.693–702.

Groenning, M., Norrman, M., Flink, J.M., van de Weert, M., Bukrinsky, J.T., Schluckebier, G. & Frokjaer, S., 2007. Binding mode of Thioflavin T in insulin amyloid fibrils. *Journal of Structural Biology*, 159(3), pp.483–497.

Guinier, A., 1955. *Small-angle scattering of X-rays*, New York: Wiley.

Al-Hakkak, J. & Al-Hakkak, F., 2010. Functional egg white–pectin conjugates prepared by controlled Maillard reaction. *Journal of Food Engineering*, 100(1), pp.152–159.

Howie, A.J., Brewer, D.B., Howell, D. & Jones, A.P., 2007. Physical basis of colors seen in Congo red-stained amyloid in polarized light. *Laboratory Investigation*, 88(3), pp.232–242.

Ianeselli, L. et al., 2010. Protein-protein interactions in ovalbumin solutions studied by small-angle scattering: effect of ionic strength and the chemical nature of cations. *The Journal of Physical Chemistry B*, 114(11), pp.3776–3783.

Jacques, D.A. & Trewhella, J., 2010. Small-angle scattering for structural biology-expanding the frontier while avoiding the pitfalls. *Protein Science*, 19(4), pp.642–657.

Jorbágy, A. & Király, K., 1966. Chemical characterization of fluorescein isothiocyanate-protein conjugates. *Biochimica et Biophysica Acta - General Subjects*, 124(1), pp.166–175.

Juárez, J., Taboada, P. & Mosquera, V., 2009. Existence of different structural intermediates on the fibrillation pathway of human serum albumin. *Biophysical Journal*, 96(6), pp.2353–2370.

Kaewmanee, T., Benjakul, S. & Visessanguan, W., 2011. Effect of NaCl on thermal aggregation of egg white proteins from duck egg. *Food Chemistry*, 125(2), pp.706–712.

Khurana, R., Gillespie, J.R., Talapatra, A., Minert, L.J., Ionescu-Zanetti, C., Millett, I. & Fink, A.L., 2001. Partially folded intermediates as critical precursors of light chain amyloid fibrils and amorphous aggregates. *Biochemistry*, 40(12), pp.3525–3535.

Kline, S.R., 2006. Reduction and analysis of SANS and USANS data using IGOR Pro. *Journal of Applied Crystallography*, 39(6), pp.895–900.

Koch, M.H.J., Vachette, P. & Svergun, D.I., 2003. Small-angle scattering: a view on the properties, structures and structural changes of biological macromolecules in solution. *Quarterly Reviews of Biophysics*, 36(02), pp.147–227.

Konarev, P.V., Volkov, V.V., Sokolova, A.V., Koch, M.H.J. & Svergun, D.I., 2003. PRIMUS: a Windows PC-based system for small-angle scattering data analysis. *Journal of Applied Crystallography*, 36(5), pp.1277–1282.

Kosters, H.A., Broersen, K., de Groot, J., Simons, J.-W.F.A., Wierenga, P. & de Jongh, H.H.J., 2003. Chemical processing as a tool to generate ovalbumin variants with changed stability. *Biotechnology and Bioengineering*, 84(1), pp.61–70.

Van der Linden, E. & Venema, P., 2007. Self-assembly and aggregation of proteins. *Current Opinion in Colloid & Interface Science*, 12(4–5), pp.158–165.

Lo, T.W., Westwood, M.E., McLellan, A.C., Selwood, T. & Thornalley, P.J., 1994. Binding and modification of proteins by methylglyoxal under physiological conditions. *Journal of Biological Chemistry*, 269(51), pp.32299–32305.

Mahler, H., Friess, W., Grauschopf, U. & Kiese, S., 2009. Protein aggregation: pathways, induction factors and analysis. *Journal of Pharmaceutical Sciences*, 98(9), pp.2909–2934.

Malvern Instruments, 2011. Dynamic Light Scattering: An Introduction in 30 Minutes. *Technical Note MRK656-01*.

Manning, M.C., Chou, D.K., Murphy, B.M., Payne, R.W. & Katayama, D.S., 2010. Stability of protein pharmaceuticals: an update. *Pharmaceutical Research*, 27(4), pp.544–575.

Matsumoto, T. & Inoue, H., 1993. Association state, overall structure, and surface roughness of native ovalbumin molecules in aqueous solutions at various ionic concentrations. *Journal of Colloid and Interface Science*, 160(1), pp.105–109.

Mertens, H.D.T. & Svergun, D.I., 2010. Structural characterization of proteins and complexes using small-angle X-ray solution scattering. *Journal of Structural Biology*, 172(1), pp.128–141.

Moraitakis, G. & Goodfellow, J.M., 2003. Simulations of human lysozyme: probing the conformations triggering amyloidosis. *Biophysical Journal*, 84(4), pp.2149–2158.

Nemoto, N., Koike, A., Osaki, K., Koseki, T. & Doi, E., 1993. Dynamic light scattering of aqueous solutions of linear aggregates induced by thermal denaturation of ovalbumin. *Biopolymers*, 33(4), pp.551–559.

Als-Nielsen, J. & McMorrow, D., 2011. *Elements of modern X-ray physics* 2nd ed., Chicester: Wiley.

Norman, A.I., Ivkov, R., Forbes, J.G. & Greer, S.C., 2005. The polymerization of actin: structural changes from small-angle neutron scattering. *The Journal of Chemical Physics*, 123(15), p.154904.

Oliveira, C.L.P., Behrens, M.A., Pedersen, J.S., Erlacher, K., Otzen, D. & Pedersen, J.S., 2009. A SAXS study of glucagon fibrillation. *Journal of Molecular Biology*, 387(1), pp.147–161.

Petoukhov, M.V. et al., 2012. New developments in the ATSAS program package for small-angle scattering data analysis. *Journal of Applied Crystallography*, 45(2), pp.342–350.

Petoukhov, M.V., Konarev, P.V., Kikhney, A.G. & Svergun, D.I., 2007. ATSAS 2.1 – towards automated and web□supported small□angle scattering data analysis. *Journal of Applied Crystallography*, 40(s1), pp.s223–s228.

Petoukhov, M.V. & Svergun, D.I., 2013. Applications of small-angle X-ray scattering to biomacromolecular solutions. *The International Journal of Biochemistry & Cell Biology*, 45(2), pp.429–437.

Putnam, C.D., Hammel, M., Hura, G.L. & Tainer, J.A., 2007. X-ray solution scattering (SAXS) combined with crystallography and computation: defining accurate macromolecular structures, conformations and assemblies in solution. *Quarterly Reviews of Biophysics*, 40(03), pp.191–285.

Rice, P., Longden, I. & Bleasby, A., 2000. EMBOSS: The European Molecular Biology Open Software Suite. *Trends in Genetics*, 16(6), pp.276–277.

Sagis, L.M.C., Veerman, C. & van der Linden, E., 2004. Mesoscopic properties of semiflexible amyloid fibrils. *Langmuir*, 20(3), pp.924–927.

Semenyuk, A.V. & Svergun, D.I., 1991. GNOM-a program package for small-angle scattering data processing. *Journal of Applied Crystallography*, 24(5), pp.537–540.

Stein, P.E., Leslie, A.G., Finch, J.T. & Carrell, R.W., 1991. Crystal structure of uncleaved ovalbumin at 1.95 A resolution. *Journal of Molecular Biology*, 221(3), pp.941–959.

Sugiyama, M., Nakamura, A., Hiramatsu, N., Annaka, M., Kuwajima, S. & Hara, K., 2001. Effect of salt and heating on a mesoscopic structure composed of ovalbumin globules in aqueous solution. *Biomacromolecules*, 2(4), pp.1071–1073.

Svane, A.S.P., Jahn, K., Deva, T., Malmendal, A., Otzen, D.E., Dittmer, J. & Nielsen, N.C., 2008. Early stages of amyloid fibril formation studied by liquid-state NMR: the peptide hormone glucagon. *Biophysical Journal*, 95(1), pp.366–377.

Svergun, D., Barberato, C. & Koch, M.H.J., 1995. CRYSOL – a program to evaluate X-ray solution scattering of biological macromolecules from atomic coordinates. *Journal of Applied Crystallography*, 28(6), pp.768–773.

Svergun, D. & Feigin, L.A., 1987. *Structure analysis by small angle X-ray and neutron scattering*, New York: Plenum Press.

Svergun, D. & Koch, M.H.., 2003. Small-angle scattering studies of biological macromolecules in solution. *Reports on Progress in Physics*, 66(10), pp.1735–1782.

Tang, C.-H., Wu, H., Chen, Z. & Yang, X.-Q., 2006. Formation and properties of glycinin-rich and β-conglycinin-rich soy protein isolate gels induced by microbial transglutaminase. *Food Research International*, 39(1), pp.87–97.

Tashiro, M., Kojima, M., Kihara, H., Kasai, K., Kamiyoshihara, T., Uéda, K. & Shimotakahara, S., 2008. Characterization of fibrillation process of α-synuclein at the initial stage. *Biochemical and Biophysical Research Communications*, 369(3), pp.910–914.

Vedadi, M. et al., 2006. Chemical screening methods to identify ligands that promote protein stability, protein crystallization, and structure determination. *Proceedings of the National Academy of Sciences of the United States of America*, 103(43), pp.15835–15840.

Wang, W., 1999. Instability, stabilization, and formulation of liquid protein pharmaceuticals. *International Journal of Pharmaceutics*, 185(2), pp.129–188.

Wang, W., Nema, S. & Teagarden, D., 2010. Protein aggregation-pathways and influencing factors. *International Journal of Pharmaceutics*, 390(2), pp.89–99.

Weijers, M., Broersen, K., Barneveld, P.A., Cohen Stuart, M.A., Hamer, R.J., De Jongh, H.H.J. & Visschers, R.W., 2008. Net charge affects morphology and visual properties of ovalbumin aggregates. *Biomacromolecules*, 9(11), pp.3165–3172.

Weijers, M., de Hoog, E.H.A., Cohen Stuart, M.A., Visschers, R.W. & Barneveld, P.A., 2005. Heat-induced formation of ordered structures of ovalbumin at low ionic strength studied by small angle X-ray scattering. *Colloids and Surfaces A: Physicochemical and Engineering Aspects*, 270-271, pp.301–308.

Weijers, M., Visschers, R.W. & Nicolai, T., 2002. Light scattering study of heat-induced aggregation and gelation of ovalbumin. *Macromolecules*, 35(12), pp.4753–4762.

Xu, J.Q., Shimoyamada, M. & Watanabe, K., 1998. Heat aggregation of dry-heated egg white and its inhibiting effect on heat coagulation of fresh egg white. *Journal of Agricultural and Food Chemistry*, 46(8), pp.3027–3032.

Chapter Five

5 Safety of Amyloid-like Aggregates for Food Applications

5.1 Introduction

Amyloid fibrils can be formed by denatured proteins, protein fragments or peptides. Denaturation can be induced by pH, heat, ultrasound, high pressure, partial proteolysis or combinations of these (Jones & Mezzenga 2012; Whittingham et al. 2002). The formed fibrils are generally insoluble under physiological conditions and display resistance to proteolysis by trypsin or Proteinase K (Conway et al. 2000; Nordstedt et al. 1994; Soto & Castaño 1996; Legname et al. 2004; Selvaggini et al. 1993). The amyloid fold is believed to be a generic protein conformation that can be assumed by many, if not all, peptides under the appropriate conditions (Chiti & Dobson 2006; Stefani & Dobson 2003). However, some peptide sequences have a particularly strong tendency to assume the amyloid fold (López de la Paz & Serrano 2004; Tenidis et al. 2000; von Bergen et al. 2000). Moreover, sequence mutations can drastically alter the likelihood of amyloid formation from a given peptide (Makin & Serpell 2005; Citron et al. 1992; Goate et al. 1991).

The amyloid fold consists of β-strands that are arranged perpendicular to the fibril axis. This so called cross-β confirmation can be studied by X-ray diffraction. The diffraction patterns usually have interference maxima at 4.8 Å (meridional reflections) and 10 - 11 Å (equatorial reflections) (Eanes & Glenner 1968; Serpell 2000; Sunde et al. 1997). These reflections represent the mean spacing between β-strands (4.8 Å meridional reflections) and β-sheets (10 - 11 Å equatorial reflections) as illustrated in Figure 5.1.

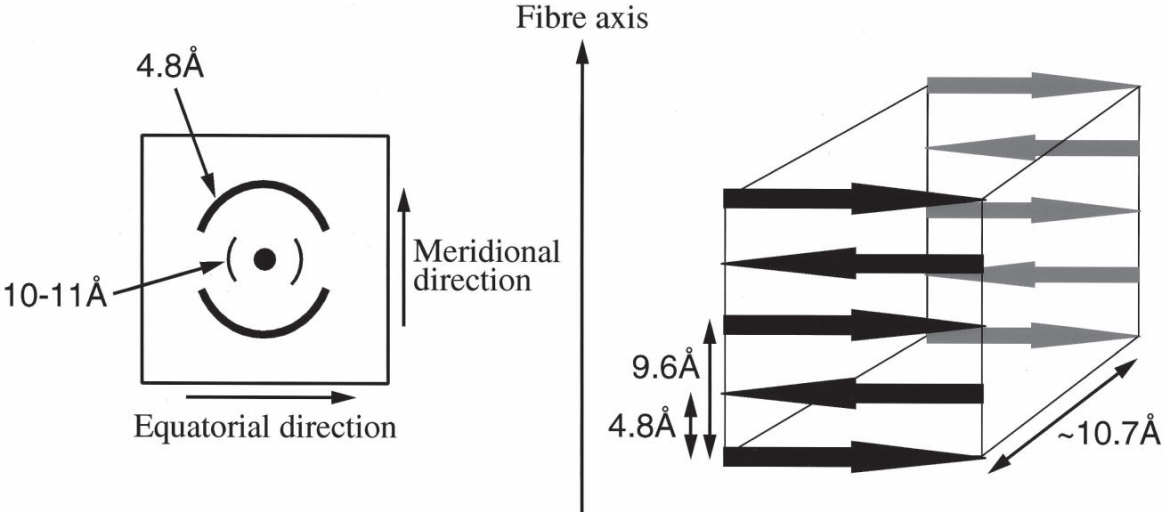

Figure 5.1 *Left) Detector showing the characteristic amyloid cross-β diffraction pattern, right) spacing of β-strands and β-sheets. Diagram taken from (Serpell 2000).*

Mature amyloid fibrils have a diameter of 6 - 12 nm and are made up of a varying number of protofilaments which themselves are made up of a number of intertwined β-sheets as illustrated in Figure 5.2 (Jiménez et al. 2002; Serpell et al. 2000). The extensive recurring β-sheet fold plays an important role in stabilising the fibril structure. In addition to X-ray diffraction, amyloid fibrils are routinely characterised using electron microscopy (EM) as well as atomic force microscopy (AFM). Amyloid specific fluorescent dyes such as Thioflavin-T (ThT) or Congo-Red (CR) further help in the characterisation of amyloid fibrils. ThT fluorescence increases upon binding of the dye to amyloid fibrils. The nature of the chemical interaction is not completely understood. It has been suggested that ThT binds parallel to the fibril axis in the grooves between adjacent β-sheets or adjacent protofilaments (Biancalana & Koide 2010; Groenning 2009; Groenning et al. 2007). Others suggest that ThT micelles bind to the fibril and are responsible for the increase in fluorescence (Khurana et al. 2005). CR binding to amyloid fibrils can be visualised under a polarised light microscope due to birefringence of the amyloid fold giving rise to "anomalous colors" (Howie et al. 2007; Nilsson 2004). In this work, TEM microscopy and ThT fluorescence were used to characterise fibrils.

Figure 5.2 *Protofilaments made up of four intertwined β-sheets. Diagram taken from (Sunde et al. 1997).*

5.1.1 *Disease Related Amyloid*

There are over 30 diseases, such as Alzheimer's disease, Creutzfeldt-Jakob disease, diabetes (type II), and Parkinson's disease, that are associated with amyloidosis (Chiti & Dobson 2006; Harrison et al. 2007). It has been suggested that amyloid related diseases share common amyloid aggregate structures and pathological pathways regardless of the source of protein (Glabe 2006; Kayed et al. 2003). A typical pathogenic pathway will be explained for the example of Alzheimer's disease (AD). In AD, the amyloid β-peptides (Aβ) are generated through proteolysis of the amyloid precursor protein (APP). Amyloidogenic Aβ are 40 - 42 amino acids long and are the building blocks of amyloid fibrils and plaques (Hardy & Selkoe 2002; Vassar 2005). The first step in amyloid formation is usually nucleation, followed by the association of amyloid forming peptides into soluble fibrillar oligomers. The soluble oligomers further aggregate to form insoluble amyloid plaques. Interestingly, AD pathogenesis has been linked to the soluble fibrillar oligomers, rather than mature fibrils (Tomic et al. 2009). The soluble fibrillar oligomers were found in high concentrations in AD brains. In contrast, plaques of insoluble fibrils were found in AD brains as well as normal control brains, and were therefore not directly linked to neurotoxicity. Soluble fibrillar oligomers are considered by many to be the most pathogenic aggregate species across the disease realm (Glabe & Kayed 2006; Glabe 2008; Haass & Selkoe 2007; Stroud et al. 2012). However, there is some indication that amyloid toxicity is caused by mature fibrils, rather than by fibrillar oligomers (Stefani 2010; Gharibyan et al. 2007; Xue et al. 2009). Xue et al. (2009) found a relationship between amyloid toxicity and fibril length, and/or rigidity of β_2-microglobulin (β_2m) *in vitro* (Xue et al. 2009). Bovine insulin has been reported to form either toxic rigid fibrils with parallel β-sheet conformation or non-toxic filaments with anti-parallel β-sheet character under reducing conditions (Zako et al. 2009).

It is commonly agreed that the toxicity of fibrillar aggregates is caused by membrane disruption (Tofoleanu & Buchete 2012; Glabe & Kayed 2006). This is often associated with Ca^{2+} release and oxidative damage (Stefani & Dobson 2003). Membrane disruption could be linked directly to the hydrophobicity and flexibility of the amyloid aggregate (Stefani 2010). Therefore, cell lines with differing membrane architectures may react differently to the same amyloid aggregate (Stefani 2010).

5.1.2 *Functional Amyloid*

Functional amyloid fibrils can be categorised into natural and synthetic fibrils. The amyloid fold is sometimes harnessed by nature for its functionality as a reinforcement material (e.g. in spider silk, bacterial attachment proteins, hydrophobins) (Chiti & Dobson 2006). The physicochemical properties of fibrils have been compared to steel and silk in terms of physical stress resistance (Smith et al. 2006). On the other hand, synthetic fibrils formed *in vitro* can be functionalised for specific new purposes, such as for new materials, nanowires, enzyme scaffolds, etc. (Graveland-Bikker & de Kruif 2006; Mankar et al. 2011; Pilkington et al. 2010; Reches & Gazit 2003). The origin of many synthetic fibrils are proteins that are not natively folded into the amyloid fold (bovine serum albumin (BSA), human serum albumin (HSA), insulin (INS), α-chymotrypsin, apomyoglobin, glucagon, calcitonin, crystallins, and hydrophobins, etc.) (Lassé et al. 2012). Functionalising amyloid fibrils *in vitro* relies on the amino acid diversity of proteins. It allows for a variety of surface chemistry to be carried out on fibrils. Successful examples of chemically modifying fibrils include cross-linking of enzymes (e.g., glucose oxidase, hydrolases) to fibrils (Raynes et al. 2011; Pilkington et al. 2010; Kim et al. 2012) and cross-linking of fibrils to other surfaces (e.g., cotton, glass beads, gold particles) (Scheibel et al. 2003; Reches & Gazit 2003). Additionally, new fibril based fabrics and cell tissue scaffolds have been explored (Gras 2007a; Gras 2007b; Mankar et al. 2011; Rao et al. 2012).

5.1.3 Amyloid-like Aggregates of Food Proteins

A study of recent food protein literature revealed that amyloid-like fibrils can be formed in several food proteins including whey protein isolate (WPI), kidney bean protein isolate (KPI), soy protein isolate (SPI), and ovalbumin (OVA) from egg white. In food technology, fibrils are desirable because of their robustness and their rheological behaviour in solutions (Loveday et al. 2011; Loveday et al. 2010; Kroes-Nijboer et al. 2012). Amyloid fibrils are good gelling agents/thickeners and can be used as foam stabilisers because of their high length to width ratio (Loveday et al. 2009). Fibrils could take on similar roles to carbohydrate polymers in emulsions. For example, fibrils formed by β-lg were able to induce depletion flocculation in a β-lg stabilised oil in water emulsion

(Blijdenstein et al. 2004). Interestingly, the depletion flocculation was dependent on β-lg fibril length. Moreover, OVA fibrils and WPI fibrils coated emulsion droplets in multi layer arrangements with high-methoxyl pectin (HMP) showed high emulsion stability (Rossier-Miranda et al. 2010; Sagis et al. 2008; Humblet-Hua et al. 2011). Amyloid-like structures from hydrophobins (type II) have been proposed as foam and aerated food stabilisers. The use of hydrophobins is currently being investigated by industry as a low fat ingredient for traditionally fat emulsion based foods such as cream, milk shakes, and ice cream (Aldred et al. 2008; Cox et al. 2009).

5.1.4 *Potential Toxicity of Non-Disease Related Amyloid Fibrils*

Surprisingly little research effort has been put into studying the biological safety of non-disease related amyloid-like fibrils and their applications. The inherent amyloid fibril toxicity found in disease related amyloids could pose potential problems if non-disease related amyloid aggregates display the same toxic behaviour towards cells as the disease related amyloids do. For example, the amyloid aggregates of the SH3 domain from bovine phosphatidyl-inositol-3'-kinase and the amino-terminal domain of the *E. coli* HypF protein showed toxicity towards NIH-3T3 cells (Bucciantini et al. 2002). In both cases, fibrillar oligomers rather than the mature amyloid fibrils were reported to be the toxic species.

The forming of amyloid-like structures from food proteins with the intent to use them in food formulations combined with the concern about amyloid fibril pathology *in vivo* were the driving factors for the present work. Four different food protein fibrils (WPI, KPI, SPI, and OVA) were synthesised and studied in detail. The well characterised insulin (INS) amyloid fibrils were used as a control in all experiments. Because one of the hallmarks of true amyloid fibrils is the resistance to proteases (Mishra et al. 2004; Nordstedt et al. 1994; Selvaggini et al. 1993; Watts et al. 2011), several *in vitro* digestibility assays using pepsin, pancreatin and Proteinase K, were carried out. Pepsin and pancreatin are both physiologically relevant proteases (protease-mixtures) and have served as *in vitro* model proteases to simulate the human stomach (pepsin) and small intestine (pancreatin) (Section 2.2). Therefore these studies provide a reasonable *in vitro* model to simulate and to monitor the passage and fate of food fibrils through the gastro-intestinal tract. Proteinase K is a broad-spectrum and highly active protease that has been used extensively to

characterise amyloid fibril protease resistance of disease related amyloid fibrils (Colby et al. 2010; Ebeling et al. 1974; Selvaggini et al. 1993). For toxicity studies, the cell viability was measured in the presence and absence of native protein, amyloid-like fibrils, sonicated (fragmented) fibrils, and pre-fibrillar intermediates to mimic possible states of the protein that may be found in food. Caco-2 cells and Hec-1a cell lines were used for cell viability studies. Caco-2 cells which are an excellent model for the intestinal barrier (Sambuy et al. 2005) as well as Hec-1a cells a further epithelial cell line were employed in the cell viability studies. Two different cell lines were chosen because their cellular membranes have altered compositions. Therefore the potential interaction of fibrils with the respective cell membranes could differ (Stefani 2010).

5.2 Food Fibril Characterisation

Fibril formation was carried out as described (Section 7.17) using literature methods (Loveday et al. 2010; Akkermans et al. 2007; Tang et al. 2010; Wang et al. 2011; Sagis et al. 2004; Tanaka et al. 2011; Nielsen et al. 2001). For characterisation purposes, the food fibrils were negatively stained with uranyl acetate and analysed by transmission electron microscopy (TEM) (Section 7.15). ImageJ software (http://rsb.info.nih.gov/ij/) was used for measuring fibril dimensions. All fibrils display high length to width ratios. WPI and INS form straight fibrils whereas KPI, SPI, and OVA form curly fibrils (Figure 5.3). The length of WPI fibrils reached several micrometers, while the diameter was consistently about 10 nm which is in good agreement with previously reported amyloid fibrils (Stromer & Serpell 2005). Fibrils formed by KPI, SPI, and OVA had similar morphologies and were about 8 nm in width and usually about 250 - 300 nm in length. INS formed long straight fibrils that were about 8 - 12 nm thick and usually 500 - 1000 nm long. Fibrils were formed at pH 1.6 - pH 2.0 and were stable for several weeks. The stability of fibrils at pH 7.5 was tested and confirmed by TEM over a period of 48 hours.

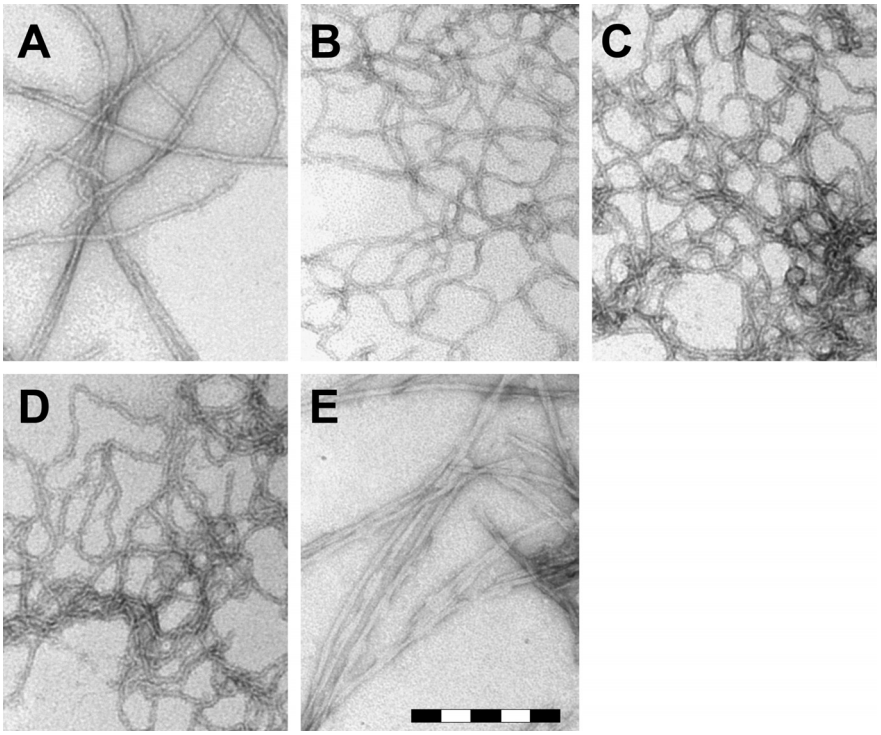

Figure 5.3: *TEM micrographs of A) WPI, B) KPI, C) SPI, D) OVA, E) INS at 89,000 x magnification. The scale bar is 200 nm. Images are representative of triplicate micrographs.*

In addition to fibril morphology, the ThT fluorescence was monitored over a period of 7 days. Figure 5.4 shows similar ThT fluorescence patterns for all of the five tested proteins. There is a sharp increase of ThT fluorescence during the initial heating phase of 22 hours. WPI and KPI show a gradual increase of fluorescence, whereas SPI, OVA, and INS show an almost instant increase within the first 3 hours of heating. After the heating period, the ThT fluorescence of all fibrils reached a intensity peak after 24 hours (with the exception of KPI fibrils. This ThT fluorescence decreased for ovalbumin over the following 7 days period. The fibril fluorescence indicates that a 7 day period was appropriate for fibril formation and that stable fluorescence levels were reached.

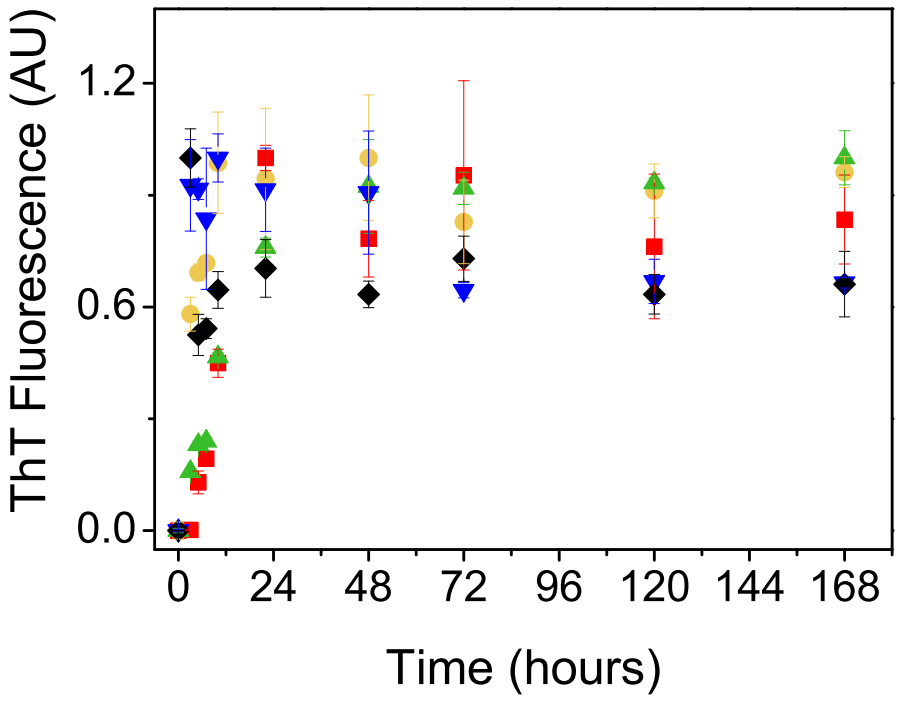

Figure 5.4: *Normalised ThT fluorescence during 7 day fibril formation. WPI (red), SPI (yellow), KPI (green), OVA (blue), INS (black). Error bars show one standard deviation of the mean from triplicate experiments.*

The proteins were analysed by SDS PAGE before heat and pH treatment and after heat and pH treatment. It was found that the fibril forming conditions were sufficient to hydrolyse the food protein (OVA, SPI, WPI) into peptides with a predominant molecular weight of less than 15 kDa (Figure 5.5).

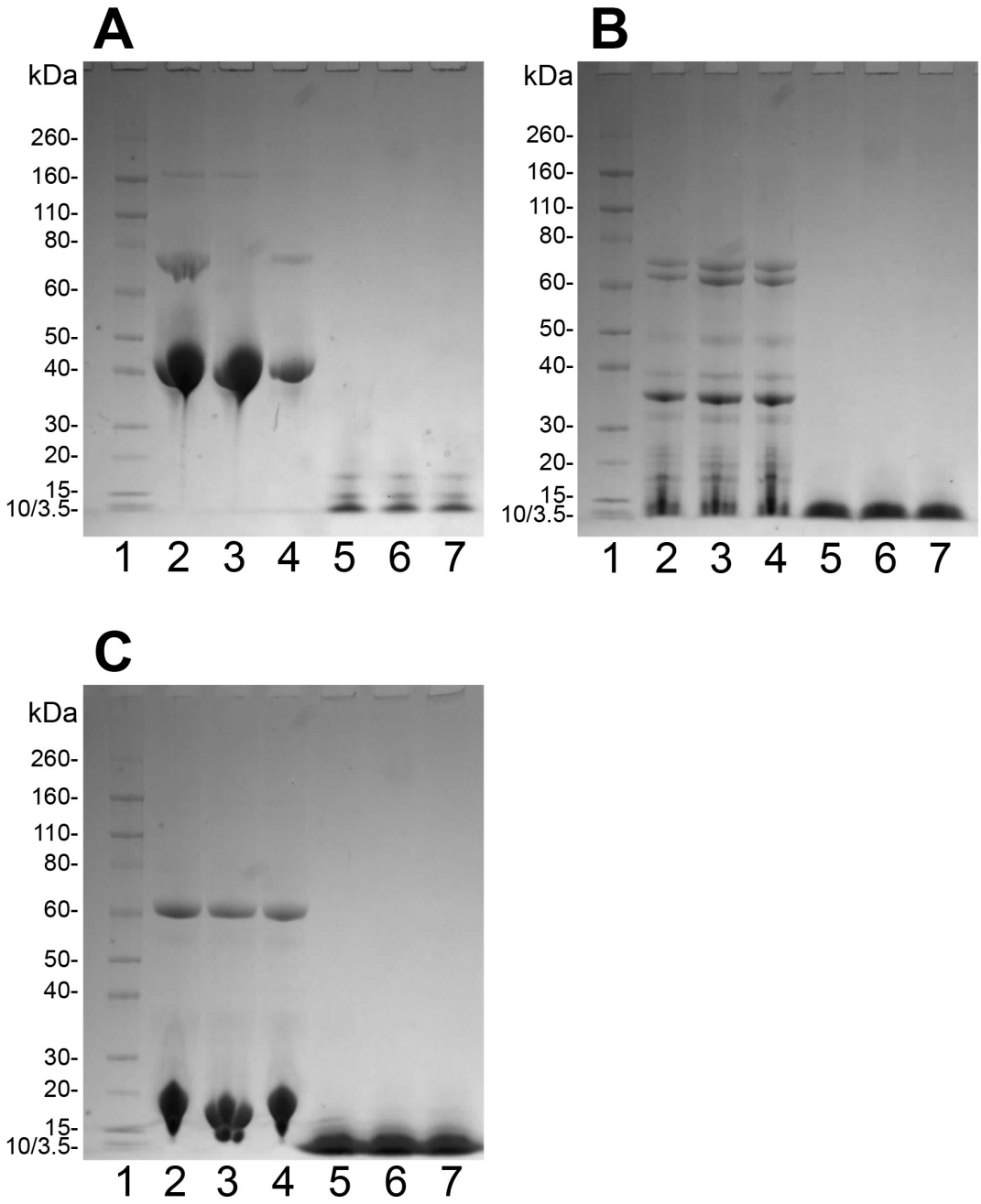

Figure 5.5 *SDS PAGE of A) OVA, B) SPI, C) WPI. Lane 1: Molecular weight marker, Lane 2: native protein before heating, Lane 3: native protein after 24 hours at 4 °C, Lane 4: same as 3 but at pH 2, Lane 5: same as 4 but heated 80 °C, 20 h, Lane 6: supernatant of 5, Lane 7: pellet of 5. Images are representative of triplicate measurements.*

The combination of acidic pH and elevated temperature has been shown to facilitate β-lg hydrolysis with subsequent fibrillation of the peptides (Figure 5.6) (Kroes-Nijboer et al. 2011). However, while hydrolysis might be sufficient, it is not clear if it is necessary for fibrillation of β-lg. There are two proposed mechanisms by which proteins can be

incorporated into fibrils (Jones & Mezzenga 2012). As Figure 5.6 illustrates, the protein can partially unfold and fibrillate or is hydrolysed prior to fibrillation. The proteins in this study were treated with harsh pH and temperature and consequently hydrolysed during the treatment, consistent with pathway 2 in Figure 5.6.

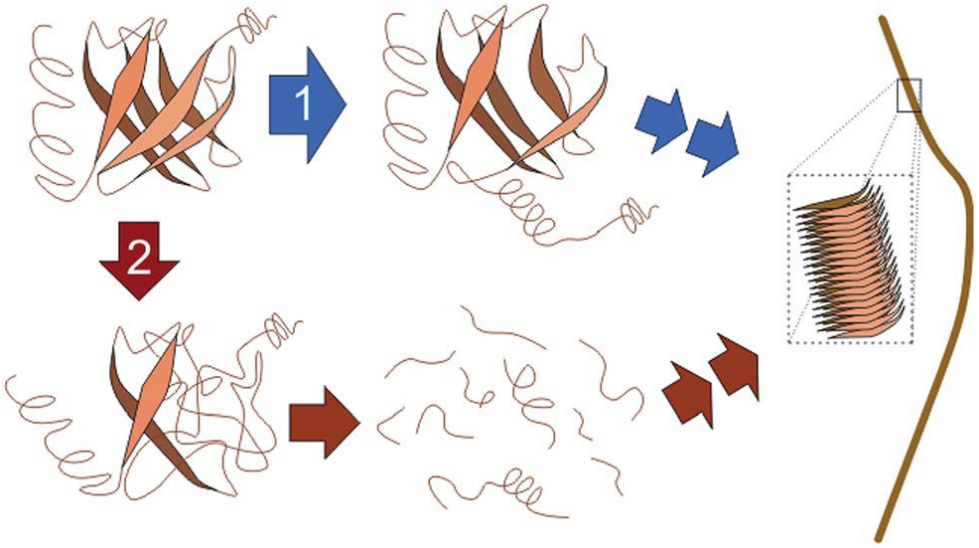

Figure 5.6 *Two common pathways of amyloid fibril formation. Diagram taken from (Jones & Mezzenga 2012).*

5.3 *Protease Resistance of Food Fibrils*

For the purpose of assessing the potential health risk of food fibrils, it is important to know whether or not the fibrils would withstand the digestion process. Therefore, the degree of fibril hydrolysis (by Proteinase K, pepsin, and pancreatin) was assessed by ThT fluorescence decrease and TEM analysis. Fibrils in the presence and absence of proteases were incubated at 37 °C for 3 hours to simulate passage through stomach and intestine. In humans the transit time has been reported to be 60 - 90 minutes in the stomach and 2 - 3 hours in the small intestine (Graff et al. 2000). The protease to protein ratio chosen for all enzymes and fibrils was 1:20 (w/w) in order to simulate physiological conditions more closely than the high enzyme to substrate ratio employed in Chapter 2 (Section 2.2). The pepsin activity of the pepsin product (Sigma No.: P7000) employed here is rated at 250 U/mg powder. At the chosen concentration (0.05 mg/mL) this corresponds to 12.5 U/mL. Measured levels of pepsin were found to be between 7-70 U/mL in undiluted stomach juice (without food) from healthy people (Ulleberg et al., 2011). These values necessarily

become diluted during food intake. In the standard assay the protease activity was 800 U/mL which is clearly higher than physiological. The chosen conditions differ from previous studies attesting high fibril digestibility in the presence of pepsin at an enzyme to substrate ratio (w/w) of 1:1.65 (Bateman, Ye, & Singh, 2010). ThT fluorescence during hydrolysis was monitored and compared to buffer controls (Figure 5.7). For data analysis, the fibril + buffer fluorescence at each time point was used to normalise the data.

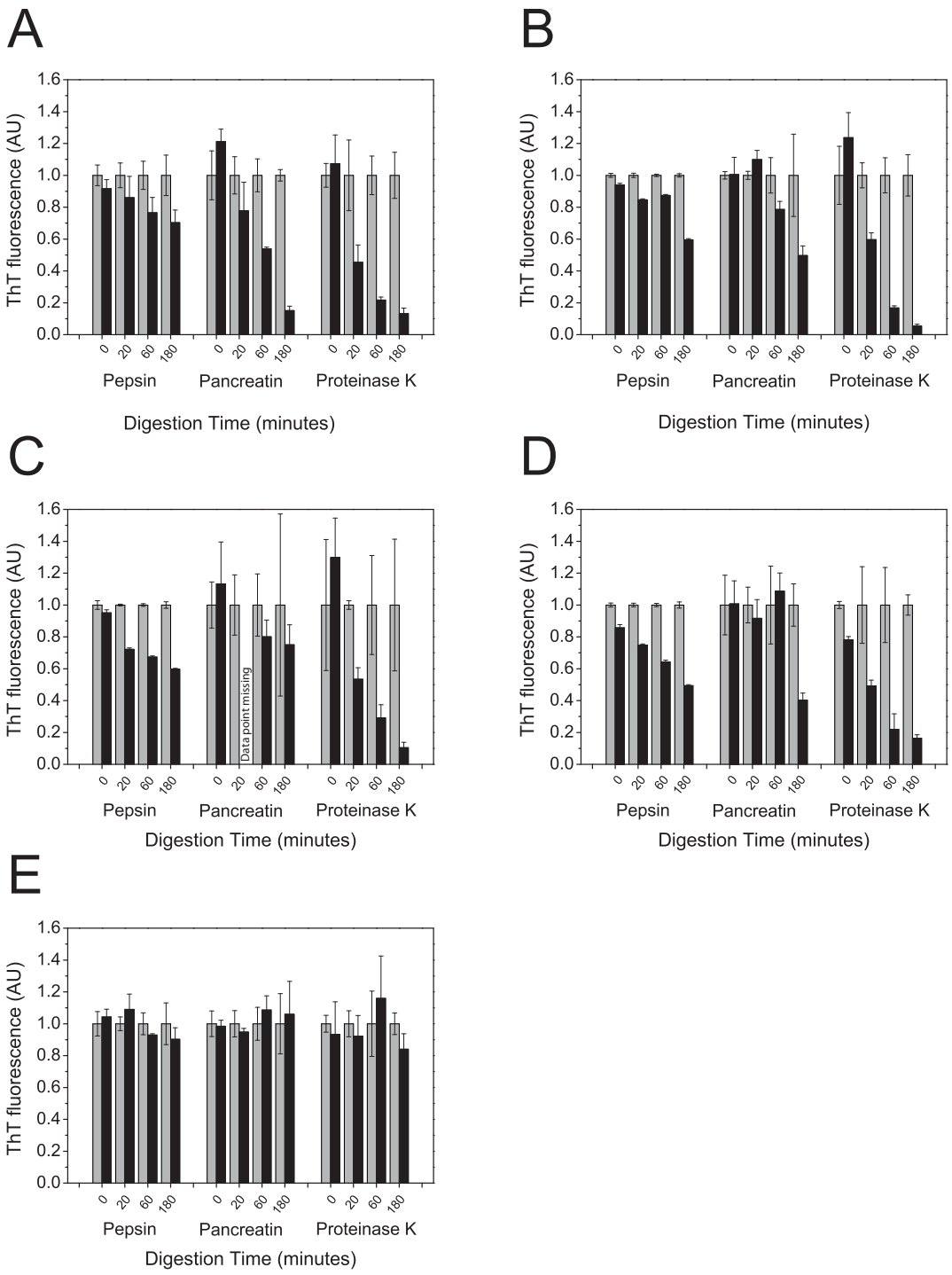

Figure 5.7: *Normalised ThT fluorescence of fibrils in the absence (grey) and presence (black) of proteases. The charts show changes in ThT fluorescence during proteolysis over three hours. Each panel is grouped into three data sets representing pepsin, pancreatin, and Proteinase K and the respective buffer controls. Measurements were taken at four time points (t = 0, 20, 60, and 180 min). Panel A) WPI-, B) KPI-, C) SPI-, D) OVA-, and E) INS-fibrils. Error bars show one standard deviation of the mean from triplicate experiments.*

The ThT fluorescence experiments show different levels of resistance to proteolytic breakdown by the different fibrils. Insulin fibrils that were used as a standard proved to be the most resistant fibrils over the 3 hour incubation period indicated by constant ThT fluorescence over the entire duration of the assay. This applies to all three proteases (pepsin, pancreatin, Proteinase K). In order to test whether the primary sequence of fibril forming proteins had an effect on proteolysis, an analysis of the potential cleavage sites for the employed proteases was carried out. The online service ExPASy PeptideCutter tool (http://web.expasy.org) (Gasteiger et al. 2005) was employed to estimate the potential protease cleavage sites of the fibril forming proteins. Since WPI, KPI, and SPI are protein mixtures, the major protein fractions (β-lactoglobulin, β-phaseolin, and glycinin G1 respectively) were chosen for analysis. Four different proteases (chymotrypsin, trypsin, pepsin, and Proteinase K) were used for the estimation of cleavage sites. Chymotrypsin and trypsin were chosen in place of pancreatin, which is an enzyme mixture containing chymotrypsin and trypsin. Table 5.1 lists the number and percentage of cleavage sites for each protein. From the percentage values, it is obvious that all five proteins expose similar numbers of cleavage sites. Glycinin has a slightly fewer cleavage sites compared to the remaining four proteins.

Table 5.1 *Number of cleavage sites for insulin, β-lactoglobulin, β-phaseolin, glycinin G1, and ovalbumin determined by PeptideCutter. The percentage values were calculated from the number of cleavages and the total residue number.*

Fibril	**INS**	**WPI**	**KPI**	**SPI**	**OVA**
Representative Protein	Insulin	β-lg	β-phaseolin	Glycinin G1	Ovalbumin
UniProt Identifier	INS_Bovin	LACB_BOVIN	PHSB_PHAVU	GLYG1_SOYBN	OVAL_CHICK
Total Residues	103	178	421	495	386
Number of Cleavages					
Chymotrypsin	27	43	96	85	80
Pepsin	39	57	129	119	97
Proteinase K	54	100	212	216	204
Trypsin	8	18	41	44	33
Percentage of Cleavages					
Chymotrypsin	26%	24%	23%	17%	21%
Pepsin	38%	32%	31%	24%	25%
Proteinase K	52%	56%	50%	44%	53%
Trypsin	8%	10%	10%	9%	9%

The four types of food protein fibrils display similar digestion patterns. The general pattern is a slightly higher resistance towards peptic digestion than towards pancreatic and Proteinase K digestion. After 3 hours of digestion by Proteinase K much of the fluorescence has dissipated indicating a complete hydrolysis of the food fibrils. However, there is still a remarkably high fluorescence after 3 hours of pepsin and pancreatin hydrolysis of the fibrils. This *in vitro* experiment therefore indicates that the fibrils could well remain intact as they pass through the gastrointestinal tract if taken up with food. However, previous findings attributed a high digestibility of fibrils formed from β-lactoglobulin under similar conditions (Bateman et al. 2010). The discrepancy between the findings may be partially explained by the higher and non-physiological enzyme to substrate ratios employed. Increasing the pepsin concentration to 10 mg/mL also resulted in the digestion of β-lactoglobulin fibrils (Li et al. 2012).

TEM micrographs of fibrils were obtained following the 3 hour hydrolysis in order to assess the change of morphology of the fibrils before and after treatment. As can be clearly seen in Figure 5.8, there are still considerable amounts of fibrils present after the 3 hour hydrolysis by pepsin, pancreatin and even by Proteinase K consistent with observations from TEM analysis.

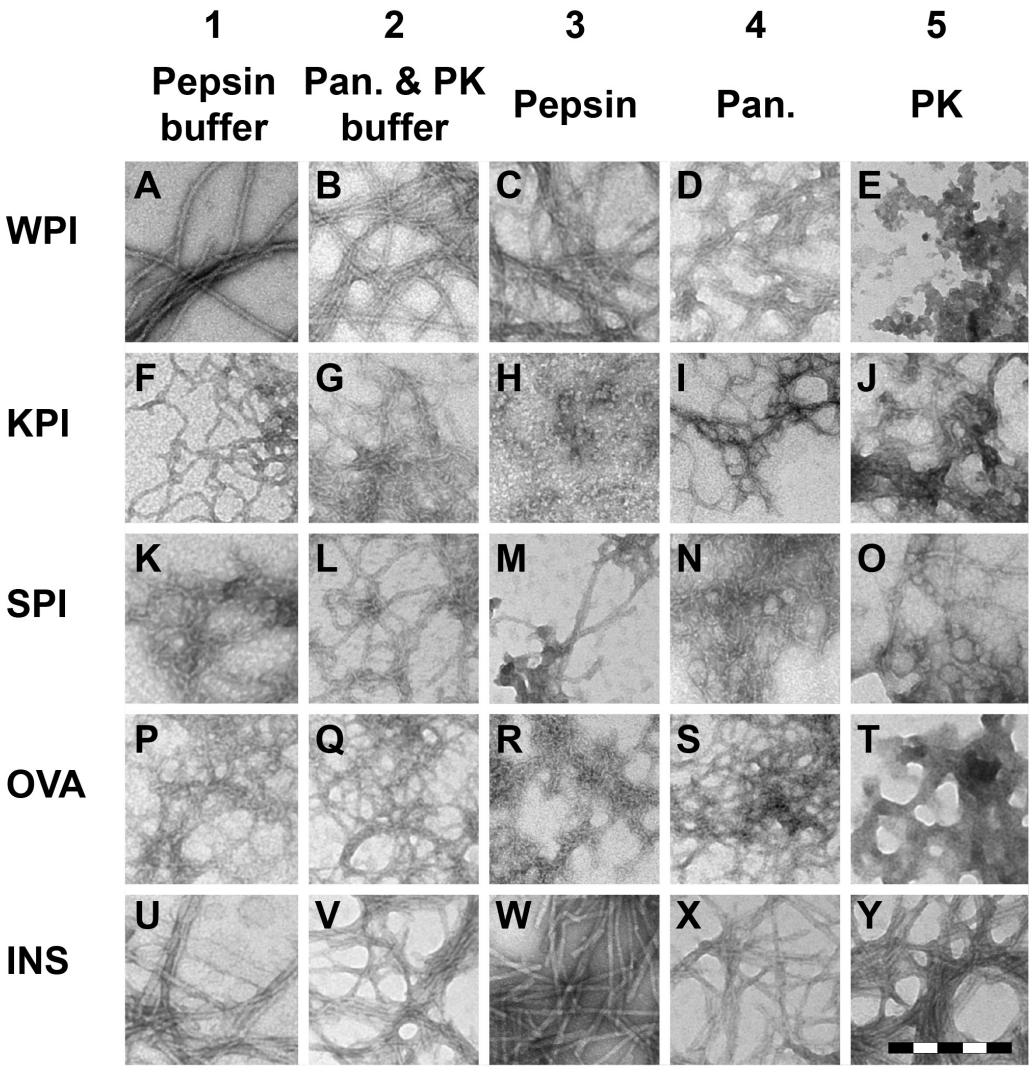

Figure 5.8: *TEM of fibrils after 3 hours of incubation in buffer (column 1, pepsin buffer; column 2, Pancreatin and Proteinase K buffer), and after 3 hours of proteolysis by pepsin (column 4), pancreatin (column 4) or Proteinase K (column 5). Panels are organised in rows depending on protein source. From top to bottom: WPI, KPI, SPI, OVA, INS.*

The presence of fibrils after hydrolysis on the TEM micrographs shows that the fibrils are fairly resistant towards proteolysis. Therefore, the two assays concluded that fibrils are partially digested, but remain in their fibrillar structure throughout the *in vitro* digestion. The partial resistance of the food fibrils to hydrolysis in the *in vitro* digestion system paired with known role of amyloid fibrils in disease suggested that an assessment of the potential effect of food fibrils on cell viability was important.

5.4 *Cell Viability in the Presence of Fibrils*

Two different cell lines were analysed in the presence and absence of the five types of fibrils (WPI, KPI, SPI, OVA, and INS) in order to assess the potential impact of fibrils on cell viability. Cell viability was assessed after 24 hours or 48 hours. Building on earlier studies exploring enzymatic digestion of mature fibrils (Section Figure 5.3) this section explores the effect of not only mature fibrils but also pre-fibrillar aggregates (heated for 22 hours but not stored for 7 days) and sonicated fibrils on cell viability. These conditions were tested as aggregate morphology may play an important role in cell toxicity (Stefani 2010; Xue et al. 2009). Native protein, pre-fibrillar aggregates, mature fibrils, and sonicated fibrils were tested for their potential to cause changes in cell viability of Caco-2 cells. For methodology of fibril formation see Section 7.17. These four different protein states were tested for all five types of fibrils (WPI, KPI, SPI, OVA, and INS). The 20 treatments of Caco-2 cells are listed in Table 5.2.

Table 5.2 *List of the 20 treatments of Caco-2 cells. Treatments 1 - 5, native protein, 6 - 10, Fibrils, 11 - 15, sonicated fibrils, 16 - 20, pre-fibrillar aggregates.*

Treatment	Protein State	Protein
1	Native protein	WPI
2		KPI
3		SPI
4		OVA
5		INS
6	Fibrils	WPI
7		KPI
8		SPI
9		OVA
10		INS
11	Sonicated fibrils	WPI
12		KPI
13		SPI
14		OVA
15		INS
16	Pre-fibrillar aggregates	WPI
17		KPI
18		SPI
19		OVA
20		INS

The Caco-2 cells were incubated for 24 hours in the presence of the above listed 20 different treatments. The water soluble tetrazolium (WST) cell proliferation assay was used to measure the cell viability after the treatment. The WST assay relies on the colour reaction of a reducible tetrazolium salt from a colourless oxidised form to the orange reduced form (Formazan) (Ishiyama et al. 1996). The colour change is a result of NADH production of the cells and therefore directly proportional to cell viability (Figure 5.9).

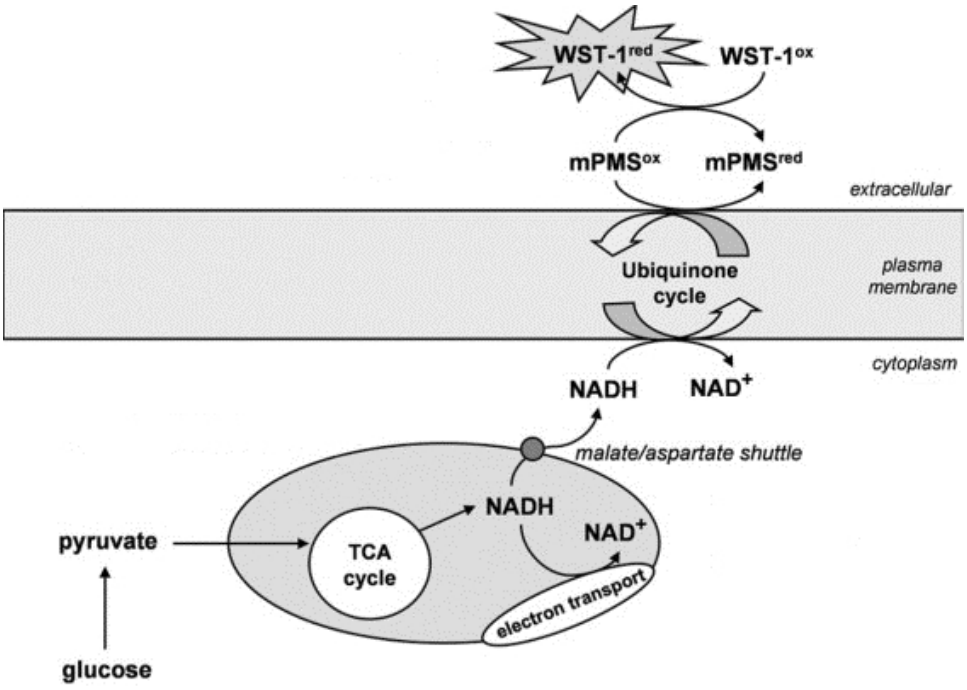

Figure 5.9 *Diagram of WST assay, modified from (Berridge et al. 2005).*

There was no marked decrease of cell viability caused by any of the 20 treatments after 24 hours (Figure 5.10). In fact, some treatments had a positive effect on cell viability. This could be an indication that the cells were capable of metabolising the protein, even when this protein is contained in fibrillar form. The controls of buffer and media only are very similar showing that the buffer conditions do not change the cell viability. 10 % DMSO is toxic to cells and was therefore used as a positive control. The no cell control also did not show any sign of viability, demonstrating that no contamination was present.

Interestingly, there is a recurring pattern dependent on the protein source rather than on the state of the protein. The order of preference of cells for protein of a specific origin starts with WPI as the least accessible protein source, followed by KPI, SPI, OVA, and finally

INS with the highest rate of viability (WPI < KPI < SPI < OVA < INS). Since all proteins were supplied at the same concentration (0.25 mg/mL final concentration), this might indicate preferences of this cell line towards specific protein origin. However, the fact that both native and fibrillar protein behave similarly is an intriguing result because the digestibility studies have shown that fibrils are somewhat resistant to proteolysis by pepsin, pancreatin, and Proteinase K (Figure 5.8), although Figure 5.7 suggests that fibrils are hydrolysed to a certain degree. The Caco-2 cell viability study shows that cells do not differentiate between native, fibrillar, sonicated fibrillar, or pre-fibrillar protein. This is a good indication that fibrils formed by food proteins are not toxic.

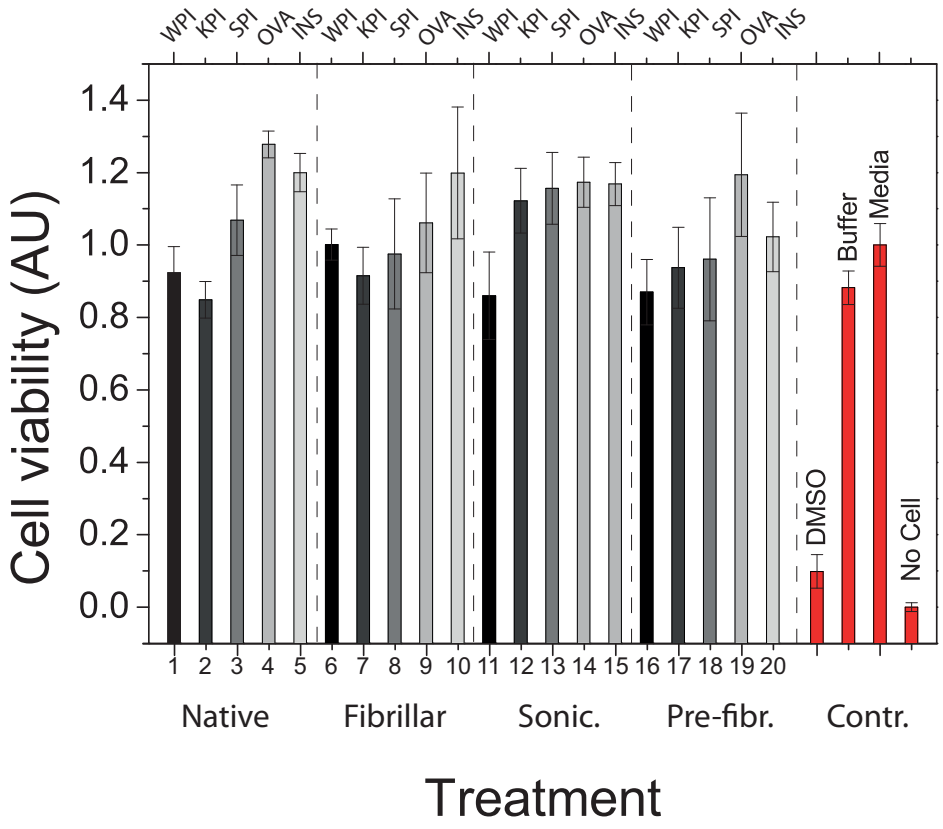

Figure 5.10: *WST cell proliferation assay of Caco-2 cells treated with WPI, KPI, SPI, OVA, and INS protein (0.25 mg/mL final protein concentration) after 24 hours incubation time. Black to light grey) WPI, KPI, SPI, OVA, and INS treatments, red) controls. Error bars show one standard deviation of the mean from four replicate experiments.*

In addition to the Caco-2 cell line, the Hec-1a epithelial cell line was also studied. Two concentrations of fibrillar protein were added to growing Hec-1a cells. The cells were incubated for 48 hours. Cell viability was evaluated using crystal violet assays, a method of similar accuracy as WST (Flick & Gifford 1984; Ishiyama et al. 1996). Again, no adverse effects of fibrils were observed over the studied time period (Figure 5.11). The cells grew equally well in the presence of the control (medium + buffer) compared to the treated cells.

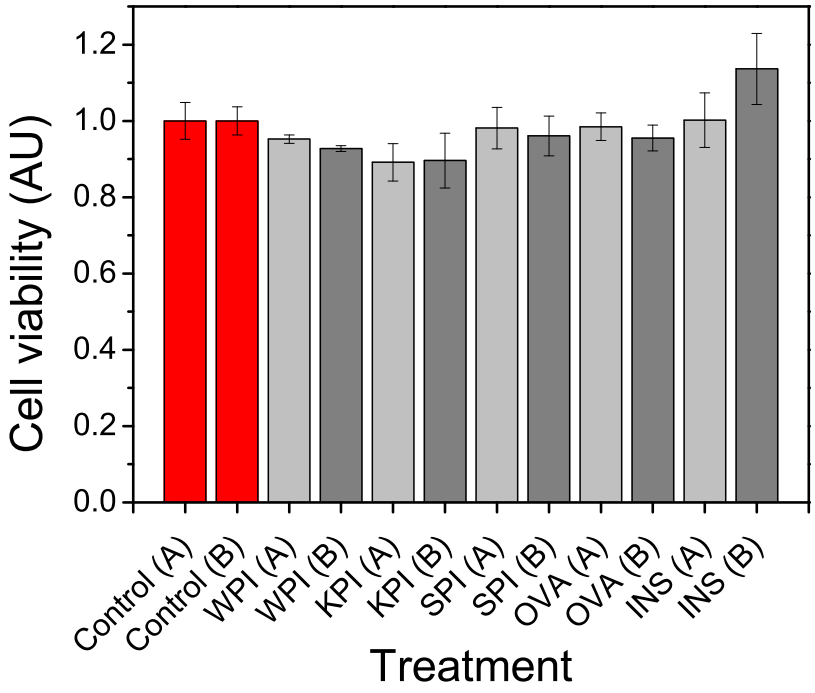

Figure 5.11 *Hec-1a cell viability after 48 hours of treatment with food fibrils WPI, KPI, SPI, OVA, and INS. Red) buffer controls, light grey) fibril concentration A = 0.2 mg/mL, dark grey) fibril concentration B = 0.1 mg/mL final concentration. Error bars show one standard deviation of the mean from four replicate experiments.*

A further study was undertaken to assess whether or not partially digested fibrils were toxic to cells. WPI fibrils were chosen as a representative model for a food fibril system. The assay conditions required careful optimisation because the enzymes used for fibril digestion needed to be inactivated before the digested sample was added to the cells. This had to be achieved without further disrupting the fibrillar structures. Therefore, the first approach was to use a Protease Inhibitor Cocktail (PIC) to inhibit the enzymes after the 3

hour digestion period. A series of treatments, which are listed in Table 5.3, was designed to enable an unambiguous distinction of effects of the different assay components.

Table 5.3 *Treatments and controls used for the assessment of fibril hydrolysis on cell viability. To stop enzymatic hydrolysis after 3 hours, Protease Inhibitor Cocktail (PIC) was added.*

Treatment	Fibrils	Enzyme	PIC	Time [min]	Addressed Question
1	-	-	-	180	Are untreated cells viable for 48 hours?
2	+	-	-	180	Are fibrils toxic?
3	-	+	-	180	Are enzymes toxic or active?
4	-	-	+	180	Is the PIC toxic to cells?
5	-	+	+	180	Are enzymes inhibited by PIC?
6	+	+	+	180	Are digested fibrils toxic?
7	+	+	+	0	Are digested fibrils toxic instantly?
8	-	-	-	180	Same as treatment 1.

The cells were pre-incubated in the absence of foetal bovine serum (FBS) to "starve" them overnight prior to the addition of treatments. This was done in order to assess if the protein is actually used as nutrient by the cells. The data were normalised against cell viability in the presence of buffer only (treatments 1 and 8) (Figure 5.12). In comparison to the previous experiments there is a marked increase of cell viability in the presence of fibrils (treatment 2). This indicates that the cells can utilise the fibrillar protein as a nutrient source, although the contribution of non-fibrillar peptide components could contribute to the observed effect. The yield of β-lactoglobulin fibrils formed under similar conditions has previously been assessed to be up to 50 % (Hettiarachchi et al. 2012) and up to 80 % (Li et al. 2012). The difficult complete separation of fibrillar species from non-fibrillar species is unlikely to be of relevance for food processes on an industrial scale. The reasons to use crude fibril solution was therefore based on both the high yield of fibrils as well as on sample preparation that would be relevant to food processing on an industrial scale. Treatment 3 shows that pancreatin is not active but that Proteinase K is still active. The PIC is toxic to cells as indicated in treatment 4. Therefore, the determination of decreased cell viability was not possible through assessment of treatments 5 - 7. However, there is a cumulative effect of toxicity of Proteinase K and PIC as indicated in treatment 5 compared to treatment 4.

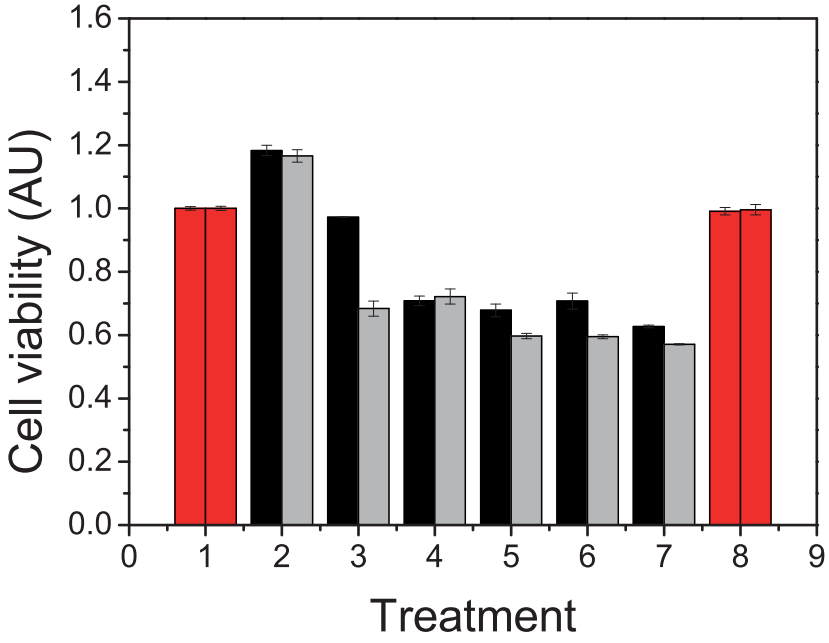

Figure 5.12 *Hec-1a cell viability after 48 h. Treatments 1 to 8 correspond to treatments 1 to 8 described in Table 5.3. Protein concentration A = 0.2 mg/mL. Black) pancreatin (pancreatin buffer for treatments without enzyme). Grey) Proteinase K (Proteinase K buffer for treatments without enzyme). Enzymatic proteolysis was stopped by addition of PIC. Error bars show one standard deviation of the mean from four replicate experiments.*

Table 5.4 *Treatments and controls used for the assessment of fibril hydrolysis on cell viability. Samples were heated to 95 °C for 15 minutes to stop enzymatic hydrolysis after 3 hours.*

Treatment	Fibrils	Enzyme	Heat	Time [min]	Addressed Question
1	-	-	-	180	Are untreated cells viable for 48 hours?
2	+	-	-	180	Are fibrils toxic?
3	-	+	-	180	Are enzymes toxic or active?
4	+	-	+	180	Is the heat inactivation affecting fibrils?
5	-	+	+	180	Are enzymes inhibited by heating?
6	+	+	+	180	Are digested fibrils toxic?
7	+	+	+	0	Are digested fibrils toxic instantly?
8	WPI	-	-	180	Native protein instead of fibrils.

As can be seen in Figure 5.13, the treatments 1 - 3 confirm again the results found for treatments 1 - 3 of the previous experiment (Figure 5.12). Treatment 4 shows that heat inactivated the enzymes and therefore is almost identical to treatment 2. Treatment 5 was expected to be at the same level as treatment 1. The only possibility of the decrease in cell viability would be an effect of the denatured enzymes on the cells. The denatured enzyme however does not seem to affect the cell viability if fibrils are present. Potentially, interactions between fibrils and aggregated denatured enzyme prevent the detrimental effect of denatured enzymes on cell viability. Treatments 6 and 7 show no difference between each other and the cell viability does not seem affected by digested fibrillar aggregates. Treatment 8 shows the effect of native WPI on cell viability, which is similar to the cell viability in the presence of fibrils (treatment 2).

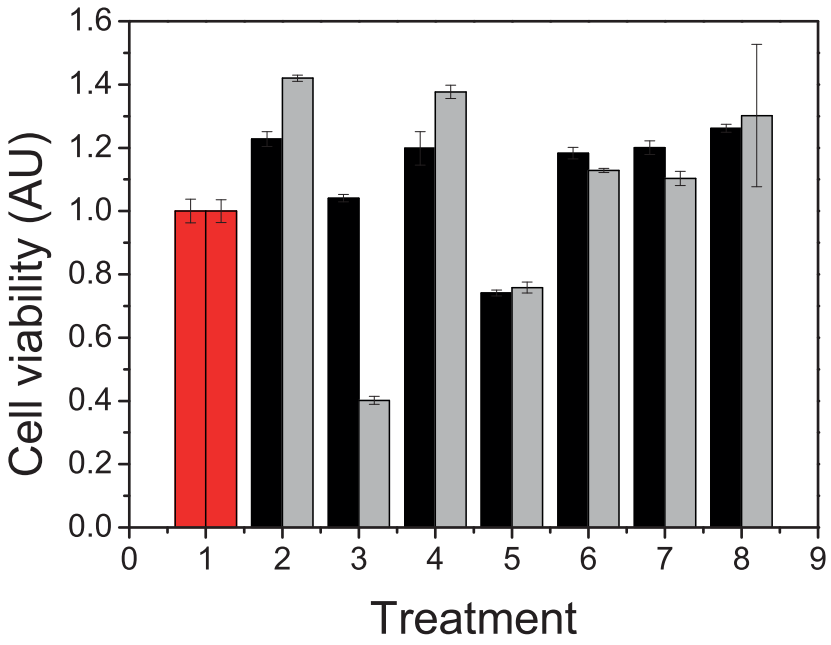

Figure 5.13 *Hec-1a cell viability after 48 h. Treatments 1 to 8 correspond to treatments 1 to 8 described in Table 5.4. Protein concentration A = 0.2 mg/mL. Black) pancreatin (pancreatin buffer for treatments without enzyme), grey) Proteinase K (Proteinase K buffer for treatments without enzyme). Enzymatic proteolysis was stopped by heating to 95 °C for 15 minutes. Error bars show one standard deviation of the mean from four replicate experiments.*

5.5 Summary and Discussion

The *in vitro* digestion studies indicate that amyloid fibrils formed by food proteins are somewhat resistant to proteolysis over a 3 hour time course. Therefore, there would be a chance for the fibrils to interact with gastro-intestinal cells during this time. The interaction of fibrils with the cell lines Caco-2 and Hec-1a was therefore studied to assess the impact of fibrils on cell viability. The results presented here alleviate some of the concerns about potential health risks of amyloid-like fibrils in food. In the case of the studied protein fibrils (and at the studied concentrations), there does not seem to be any detrimental effect of fibrils on cell viability. Instead, the *in vitro* studies suggest that the cells can perhaps utilise the fibrillar proteins as a source of nutrients, although the contribution of non-fibrillar peptide components requires further investigation. There was no indication that sonicated or pre-fibrillar aggregate species decreased cell viability.

5.6 References

Akkermans, C., Van der Goot, A.J., Venema, P., Gruppen, H., Vereijken, J.M., Van der Linden, E. & Boom, R.M., 2007. Micrometer-sized fibrillar protein aggregates from soy glycinin and soy protein isolate. *Journal of Agricultural and Food Chemistry*, 55(24), pp.9877–9882.

Aldred, D.L. et al., 2008. Aerated food products containing hydrophobin. *EP Patent 1621084*.

Bateman, L., Ye, A. & Singh, H., 2010. *In vitro* digestion of β-lactoglobulin fibrils formed by heat treatment at low pH. *Journal of Agricultural and Food Chemistry*, 58(17), pp.9800–9808.

Von Bergen, M., Friedhoff, P., Biernat, J., Heberle, J., Mandelkow, E.M. & Mandelkow, E., 2000. Assembly of tau protein into Alzheimer paired helical filaments depends on a local sequence motif ((306)VQIVYK(311)) forming β structure. *Proceedings of the National Academy of Sciences of the United States of America*, 97(10), pp.5129–5134.

Berridge, M.V., Herst, P.M. & Tan, A.S., 2005. Tetrazolium dyes as tools in cell biology: New insights into their cellular reduction. *Biotechnology Annual Review*, 11, pp.127–152.

Biancalana, M. & Koide, S., 2010. Molecular mechanism of Thioflavin-T binding to amyloid fibrils. *Biochimica et Biophysica Acta - Proteins and Proteomics*, 1804(7), pp.1405–1412.

Blijdenstein, T.B.J., Veerman, C. & van der Linden, E., 2004. Depletion-flocculation in oil-in-water emulsions using fibrillar protein assemblies. *Langmuir*, 20(12), pp.4881–4884.

Bucciantini, M. et al., 2002. Inherent toxicity of aggregates implies a common mechanism for protein misfolding diseases. *Nature*, 416(6880), pp.507–511.

Chiti, F. & Dobson, C.M., 2006. Protein misfolding, functional amyloid, and human disease. *Annual Review of Biochemistry*, 75(1), pp.333–366.

Citron, M. et al., 1992. Mutation of the β-amyloid precursor protein in familial Alzheimer's disease increases β-protein production. *Nature*, 360(6405), pp.672–674.

Colby, D.W. et al., 2010. Protease-sensitive synthetic prions. *PLoS Pathogens*, 6(1), p.e1000736.

Conway, K.A., Harper, J.D. & Lansbury, P.T., 2000. Fibrils formed *in vitro* from α-synuclein and two mutant forms linked to Parkinson's disease are typical amyloid. *Biochemistry*, 39(10), pp.2552–2563.

Cox, A.R., Aldred, D.L. & Russell, A.B., 2009. Exceptional stability of food foams using class II hydrophobin HFBII. *Food Hydrocolloids*, 23(2), pp.366–376.

Eanes, E.D. & Glenner, G.G., 1968. X-ray diffraction studies on amyloid filaments. *Journal of Histochemistry & Cytochemistry*, 16(11), pp.673–677.

Ebeling, W. et al., 1974. Proteinase K from *Tritirachium album limber*. *European Journal of Biochemistry*, 47(1), pp.91–97.

Flick, D.A. & Gifford, G.E., 1984. Comparison of *in vitro* cell cytotoxic assays for tumor necrosis factor. *Journal of Immunological Methods*, 68(1), pp.167–175.

Gasteiger, E., Hoogland, C., Gattiker, A., Duvaud, S., Wilkins, M.R., Appel, R.D. & Bairoch, A., 2005. Protein identification and analysis tools on the ExPASy server. In J. M. Walker, ed. *The Proteomics Protocols Handbook*. Portland: Humana Press, pp. 571–607.

Gharibyan, A.L., Zamotin, V., Yanamandra, K., Moskaleva, O.S., Margulis, B.A., Kostanyan, I.A. & Morozova-Roche, L.A., 2007. Lysozyme amyloid oligomers and fibrils induce cellular death via different apoptotic/necrotic pathways. *Journal of Molecular Biology*, 365(5), pp.1337–1349.

Glabe, C.G., 2006. Common mechanisms of amyloid oligomer pathogenesis in degenerative disease. *Neurobiology of Aging*, 27(4), pp.570–575.

Glabe, C.G., 2008. Structural classification of toxic amyloid oligomers. *Journal of Biological Chemistry*, 283(44), pp.29639–29643.

Glabe, C.G. & Kayed, R., 2006. Common structure and toxic function of amyloid oligomers implies a common mechanism of pathogenesis. *Neurology*, 66(1), pp.S74–S78.

Goate, A. et al., 1991. Segregation of a missense mutation in the amyloid precursor protein gene with familial Alzheimer's disease. *Nature*, 349(6311), pp.704–706.

Graff, Brinch & Madsen, 2000. Simplified scintigraphic methods for measuring gastrointestinal transit times. *Clinical Physiology*, 20(4), pp.262–266.

Gras, S.L., 2007a. Amyloid fibrils: from disease to design. New biomaterial applications for self-assembling cross-β fibrils. *Australian Journal of Chemistry*, 60(5), pp.333–342.

Gras, S.L., 2007b. Protein misfolding: a route to new nanomaterials. *Advanced Powder Technology*, 18(6), pp.699–705.

Graveland-Bikker, J.F. & de Kruif, C.G., 2006. Unique milk protein based nanotubes: food and nanotechnology meet. *Trends in Food Science & Technology*, 17(5), pp.196–203.

Groenning, M., 2009. Binding mode of Thioflavin T and other molecular probes in the context of amyloid fibrils - current status. *Journal of Chemical Biology*, 3(1), pp.1–18.

Groenning, M., Norrman, M., Flink, J.M., van de Weert, M., Bukrinsky, J.T., Schluckebier, G. & Frokjaer, S., 2007. Binding mode of Thioflavin T in insulin amyloid fibrils. *Journal of Structural Biology*, 159(3), pp.483–497.

Haass, C. & Selkoe, D.J., 2007. Soluble protein oligomers in neurodegeneration: lessons from the Alzheimer's amyloid β-peptide. *Nature Reviews Molecular Cell Biology*, 8(2), pp.101–112.

Hardy, J. & Selkoe, D.J., 2002. The amyloid hypothesis of Alzheimer's disease: progress and problems on the road to therapeutics. *Science*, 297(5580), pp.353–356.

Harrison, R.S., Sharpe, P.C., Singh, Y. & Fairlie, D.P., 2007. Amyloid peptides and proteins in review. In S. G. Amara et al., eds. *Reviews of Physiology, Biochemistry and Pharmacology*. Berlin: Springer Berlin Heidelberg, pp. 1–77.

Hettiarachchi, C.A., Melton, L.D., Gerrard, J.A. & Loveday, S.M., 2012. Formation of β-lactoglobulin nanofibrils by microwave heating gives a peptide composition different from conventional heating. *Biomacromolecules*, 13(9), pp.2868–2880.

Howie, A.J., Brewer, D.B., Howell, D. & Jones, A.P., 2007. Physical basis of colors seen in Congo red-stained amyloid in polarized light. *Laboratory Investigation*, 88(3), pp.232–242.

Humblet-Hua, K.N.P., Scheltens, G., van der Linden, E. & Sagis, L.M.C., 2011. Encapsulation systems based on ovalbumin fibrils and high methoxyl pectin. *Food Hydrocolloids*, 25(3), pp.307–314.

Ishiyama, M., Tominaga, H., Shiga, M. & Sasamoto, K., 1996. A combined assay of cell viability and *in vitro* cytotoxicity with a highly water-soluble tetrazolium salt, neutral red and crystal violet. *Biological & Pharmaceutical Bulletin*, 19(11), p.1518.

Jiménez, J.L., Nettleton, E.J., Bouchard, M., Robinson, C.V., Dobson, C.M. & Saibil, H.R., 2002. The protofilament structure of insulin amyloid fibrils. *Proceedings of the National Academy of Sciences of the United States of America*, 99(14), pp.9196–9201.

Jones, O.G. & Mezzenga, R., 2012. Inhibiting, promoting, and preserving stability of functional protein fibrils. *Soft Matter*, 8(4), pp.876–895.

Kayed, R., Head, E., Thompson, J.L., McIntire, T.M., Milton, S.C., Cotman, C.W. & Glabe, C.G., 2003. Common structure of soluble amyloid oligomers implies common mechanism of pathogenesis. *Science*, 300(5618), pp.486–489.

Khurana, R. et al., 2005. Mechanism of Thioflavin T binding to amyloid fibrils. *Journal of Structural Biology*, 151(3), pp.229–238.

Kim, S., Bae, S.Y., Lee, B.Y. & Kim, T.D., 2012. Coaggregation of amyloid fibrils for the preparation of stable and immobilized enzymes. *Analytical Biochemistry*, 421(2), pp.776–778.

Kroes-Nijboer, A., Venema, P., Bouman, J. & van der Linden, E., 2011. Influence of protein hydrolysis on the growth kinetics of β-lg fibrils. *Langmuir*, 27(10), pp.5753–5761.

Kroes-Nijboer, A., Venema, P. & Linden, E. van der, 2012. Fibrillar structures in food. *Food & Function*, 2012(3), pp.221–227.

Lassé, M., Gerrard, J.A. & Pearce, F.G., 2012. Aggregation and fibrillogenesis of proteins not associated with disease: a few case studies. In J. R. Harris, ed. *Protein Aggregation and Fibrillogenesis in Cerebral and Systemic Amyloid Disease*. Subcellular Biochemistry. Springer Netherlands, pp. 253–270.

Legname, G., Baskakov, I.V., Nguyen, H.-O.B., Riesner, D., Cohen, F.E., DeArmond, S.J. & Prusiner, S.B., 2004. Synthetic mammalian prions. *Science*, 305(5684), pp.673–676.

Li, C., Adamcik, J. & Mezzenga, R., 2012. Biodegradable nanocomposites of amyloid fibrils and graphene with shape-memory and enzyme-sensing properties. *Nature Nanotechnology*, 7(7), pp.421–427.

López de la Paz, M. & Serrano, L., 2004. Sequence determinants of amyloid fibril formation. *Proceedings of the National Academy of Sciences of the United States of America*, 101(1), pp.87–92.

Loveday, S.M., Rao, M.A., Creamer, L.K. & Singh, H., 2009. Factors affecting rheological characteristics of fibril gels: the case of β-lactoglobulin and α-lactalbumin. *Journal of Food Science*, 74(3), pp.47–55.

Loveday, S.M., Su, J., Rao, M.A., Anema, S.G. & Singh, H., 2011. Effect of calcium on the morphology and functionality of whey protein nanofibrils. *Biomacromolecules*, 12(10), pp.3780–3788.

Loveday, S.M., Wang, X.L., Rao, M.A., Anema, S.G., Creamer, L.K. & Singh, H., 2010. Tuning the properties of β-lactoglobulin nanofibrils with pH, NaCl and $CaCl_2$. *International Dairy Journal*, 20(9), pp.571–579.

Makin, O.S. & Serpell, L.C., 2005. Structures for amyloid fibrils. *Federation of European Biochemical Societies Journal*, 272(23), pp.5950–5961.

Mankar, S., Anoop, A., Sen, S. & Maji, S.K., 2011. Nanomaterials: amyloids reflect their brighter side. *Nano Reviews*, 2(6032), pp.1–12.

Mishra, R.S. et al., 2004. Protease-resistant human prion protein and ferritin are cotransported across Caco-2 epithelial cells: implications for species barrier in prion uptake from the intestine. *Journal of Neuroscience*, 24(50), pp.11280–11290.

Nielsen, L., Khurana, R., Coats, A. & Frokjaer, S., 2001. Effect of environmental factors on the kinetics of insulin fibril formation: elucidation of the molecular mechanism. *Biochemistry*, 40(20), pp.6036–6046.

Nilsson, M.R., 2004. Techniques to study amyloid fibril formation *in vitro*. *Methods*, 34(1), pp.151–160.

Nordstedt, C., Näslund, J., Tjernberg, L.O., Karlström, A.R., Thyberg, J. & Terenius, L., 1994. The Alzheimer Aβ peptide develops protease resistance in association with its polymerization into fibrils. *Journal of Biological Chemistry*, 269(49), pp.30773–30776.

Pilkington, S.M., Roberts, S.J., Meade, S.J. & Gerrard, J.A., 2010. Amyloid fibrils as a nanoscaffold for enzyme immobilization. *Biotechnology Progress*, 26(1), pp.93–100.

Rao, S.P., Meade, S.J., Healy, J.P., Sutton, K.H., Larsen, N.G., Staiger, M.P. & Gerrard, J.A., 2012. Amyloid fibrils as functionalizable components of nanocomposite materials. *Biotechnology Progress*, 28(1), pp.248–256.

Raynes, J.K., Pearce, F.G., Meade, S.J. & Gerrard, J.A., 2011. Immobilization of organophosphate hydrolase on an amyloid fibril nanoscaffold: towards bioremediation and chemical detoxification. *Biotechnology Progress*, 27(2), pp.360–367.

Reches, M. & Gazit, E., 2003. Casting metal nanowires within discrete self-assembled peptide nanotubes. *Science*, 300(5619), pp.625 –627.

Rossier-Miranda, F.J., Schroen, K. & Boom, R., 2010. Mechanical characterization and pH response of fibril-reinforced microcapsules prepared by layer-by-layer adsorption. *Langmuir*, 26(24), pp.19106–19113.

Sagis, L.M.C. et al., 2008. Polymer microcapsules with a fiber-reinforced nanocomposite shell. *Langmuir*, 24(5), pp.1608–1612.

Sagis, L.M.C., Veerman, C. & van der Linden, E., 2004. Mesoscopic properties of semiflexible amyloid fibrils. *Langmuir*, 20(3), pp.924–927.

Sambuy, Y., De Angelis, I., Ranaldi, G., Scarino, M.L., Stammati, A. & Zucco, F., 2005. The Caco-2 cell line as a model of the intestinal barrier: influence of cell and culture-related factors on Caco-2 cell functional characteristics. *Cell Biology and Toxicology*, 21(1), pp.1–26.

Scheibel, T., Parthasarathy, R., Sawicki, G., Lin, X.M., Jaeger, H. & Lindquist, S.L., 2003. Conducting nanowires built by controlled self-assembly of amyloid fibers and selective metal deposition. *Proceedings of the National Academy of Sciences of the United States of America*, 100(8), p.4527.

Selvaggini, C. et al., 1993. Molecular characteristics of a protease-resistant, amyloidogenic and neurotoxic peptide homologous to residues 106-126 of the prion protein. *Biochemical and Biophysical Research Communications*, 194(3), pp.1380–1386.

Serpell, L.C., 2000. Alzheimer's amyloid fibrils: structure and assembly. *BBA - Molecular Basis of Disease*, 1502(1), pp.16–30.

Serpell, L.C., Sunde, M., Benson, M.D. & Tennent, G.A., 2000. The protofilament substructure of amyloid fibrils1. *Journal of Molecular Biology*, 300(5), pp.1033–1039.

Smith, J.F., Knowles, T.P.J., Dobson, C.M., MacPhee, C.E. & Welland, M.E., 2006. Characterization of the nanoscale properties of individual amyloid fibrils. *Proceedings of the National Academy of Sciences of the United States of America*, 103(43), pp.15806–15811.

Soto, C. & Castaño, E.M., 1996. The conformation of Alzheimer's β peptide determines the rate of amyloid formation and its resistance to proteolysis. *Biochemical Journal*, 314(Pt 2), pp.701–707.

Stefani, M., 2010. Biochemical and biophysical features of both oligomer/fibril and cell membrane in amyloid cytotoxicity. *FEBS Journal*, 277(22), pp.4602–4613.

Stefani, M. & Dobson, C.M., 2003. Protein aggregation and aggregate toxicity: new insights into protein folding, misfolding diseases and biological evolution. *Journal of Molecular Medicine*, 81(11), pp.678–699.

Stromer, T. & Serpell, L.C., 2005. Structure and morphology of the Alzheimer's amyloid fibril. *Microscopy Research and Technique*, 67(3-4), pp.210–217.

Stroud, J.C., Liu, C., Teng, P.K. & Eisenberg, D., 2012. Toxic fibrillar oligomers of amyloid-β have cross-β structure. *Proceedings of the National Academy of Sciences of the United States of America*, 109(20), pp.7717–7722.

Sunde, M., Serpell, L.C., Bartlam, M., Fraser, P.E., Pepys, M.B. & Blake, C.C., 1997. Common core structure of amyloid fibrils by synchrotron X-ray diffraction. *Journal of Molecular Biology*, 273(3), pp.729–739.

Tanaka, N. et al., 2011. The mechanism of fibril formation of a non-inhibitory serpin ovalbumin revealed by the identification of amyloidogenic core regions. *Journal of Biological Chemistry*, 286(7), pp.5884 –5894.

Tang, C.-H., Zhang, Y.-H., Wen, Q.-B. & Huang, Q., 2010. Formation of amyloid fibrils from kidney bean 7S globulin (phaseolin) at pH 2.0. *Journal of Agricultural and Food Chemistry*, 58(13), pp.8061–8068.

Tenidis, K. et al., 2000. Identification of a penta- and hexapeptide of islet amyloid polypeptide (IAPP) with amyloidogenic and cytotoxic properties. *Journal of Molecular Biology*, 295(4), pp.1055–1071.

Tofoleanu, F. & Buchete, N.-V., 2012. Alzheimer Aβ peptide interactions with lipid membranes: fibrils, oligomers and polymorphic amyloid channels. *Prion*, 6(4), pp.339–345.

Tomic, J.L., Pensalfini, A., Head, E. & Glabe, C.G., 2009. Soluble fibrillar oligomer levels are elevated in Alzheimer's disease brain and correlate with cognitive dysfunction. *Neurobiology of Disease*, 35(3), pp.352–358.

Ulleberg, E.K., Comi, I., Holm, H., Herud, E.B., Jacobsen, M. & Vegarud, G.E., 2011. Human gastrointestinal juices intended for use in *in vitro* digestion models. *Food Digestion*, 2(1-3), pp.52–61.

Vassar, R., 2005. β-Secretase, APP and Aβ in Alzheimer's disease. *Alzheimer's Disease*, pp.79–103.

Wang, J.-M., Yang, X.-Q., Yin, S.-W., Yuan, D.-B., Xia, N. & Qi, J.-R., 2011. Growth kinetics of amyloid-like fibrils derived from individual subunits of soy β-conglycinin. *Journal of Agricultural and Food Chemistry*, 59(20), pp.11270–11277.

Watts, J.C. et al., 2011. Protease-resistant prions selectively decrease shadoo protein. *PLoS Pathogens*, 7(11), p.e1002382.

Whittingham, J.L., Scott, D.J., Chance, K., Wilson, A., Finch, J., Brange, J. & Guy Dodson, G., 2002. Insulin at pH 2: structural analysis of the conditions promoting insulin fibre formation. *Journal of Molecular Biology*, 318(2), pp.479–490.

Xue, W.-F., Hellewell, A.L., Gosal, W.S., Homans, S.W., Hewitt, E.W. & Radford, S.E., 2009. Fibril fragmentation enhances amyloid cytotoxicity. *Journal of Biological Chemistry*, 284(49), pp.34272–34282.

Zako, T., Sakono, M., Hashimoto, N., Ihara, M. & Maeda, M., 2009. Bovine insulin filaments induced by reducing disulfide bonds show a different morphology, secondary structure, and cell toxicity from intact insulin amyloid fibrils. *Biophysical Journal*, 96(8), pp.3331–3340.

Chapter Six

6 Summary and Conclusions

6.1 Introduction

The objective of this work, as outlined in the introduction, was to investigate whether structural changes to food protein during processing may influence the nutritional value of the protein. As food proteins are an essential part of the daily diet they form an integral part of our lives. Understanding the complex mechanisms that govern the physicochemical determinants of protein aggregation, and the relationship of the aggregated state to nutritional value, may contribute to an improvement in protein quality, textural properties and functionality in food.

Egg white (EW) was used as a model system and the processing conditions were carefully chosen to simulate a wide range of actual food systems. Structural characterisations of EW aggregates were carried out by electron microscopy, dynamic light scattering, and small angle X-ray scattering. The relationship of aggregate structure and nutritional impact was probed by *in vitro* analysis of EW digestibility as well as by mass spectrometric analysis of nutritionally relevant amino acid modifications that occurred during protein processing. Furthermore, the safety of amyloid-like fibrils derived from four different food proteins was assessed by *in vitro* digestibility tests and cell toxicity assays. As new food components such as amyloid fibrils are suggested as new structural food ingredients it is important to carefully assess the safety of such protein derived structures.

6.2 Characterisation of Nutritional Value of Proteins

A wide range of EW treatment conditions was screened (Chapter Two) for structural differences in the EW and how they translated to resistance of EW to proteolysis. The *in vitro* digestion assay confirmed that heating of EW increased its *in vitro* digestibility which was consistent with previous findings. Interestingly, the pre-treatment of raw and boiled EW with 200 mM NaCl or pre-adjustment of pH to pH 2, 5, 7, 9, 12 did not markedly

influence the protein *in vitro* digestibility even though structural differences were discovered to be present amongst samples. Such a wide range of conditions had not previously been assessed and contributes to the understanding of the structure-function relationship of food systems. The results suggest that protein preparations of different pH may be equally well digested by the body as long as the digestion conditions are kept constant. This insight may prove to be important when optimising the texture of existing foods, without compromising nutritional quality. Interestingly, under all test conditions, the EW aggregates displayed higher resistance to the *in vitro* pepsin digestion compared to the *in vitro* pancreatin digestion. Previous studies on protein/oil mixtures have reported increased protein resistance to *in vitro* gastric digestion compared to *in vitro* pancreatic digestion. The proposed mechanism for decreased gastric digestion was the inaccessibility of hydrophobic residues to pepsin cleavage (Chen et al. 2006), which may also explain the difference observed here.

The impact of Maillard reaction partners on EW digestibility was assessed. The results confirmed the previously reported decreased digestibility of Maillard reacted protein compared to pure protein (Friedman 2003). Highly resistant cross-linked EW protein species of high molecular weight were observed in the presence of glutaraldehyde and methylglyoxal even at room temperature and short heating times (10 minutes at 80 °C) respectively. Long heating times (24 hours at 80 °C) of EW in the presence of glucose, fructose, and lactose decreased digestibility to a similar degree as methylglyoxal treated EW after 5 hours of heating at 80 °C. These findings suggest that food processing at lower temperatures and shorter heating times are beneficial to retain protein digestibility. A decrease of protein digestibility is likely to occur in foods that are susceptible to the Maillard reaction such as fried, roasted, and baked foods.

Chapter Three addressed the determination of the degree of chemical modification of amino acids of processed EW. For the first time, a holistic approach was used, based on mass spectrometric analysis, to assess the severity of a wide range of amino acid modifications before and after EW processing. The results showed a time and temperature dependent increase of detectable amino acid modifications. The monitoring of dehydration and deamidation proved to be the most reliable method to monitor the progression of hydrothermally induced damage of EW because these modifications were detected abundantly. Furthermore the progression of methylglyoxal modification of arginine

residues was assessed. After 1 hour of EW heating at 100 °C, 38 % of detectable arginine residues had been modified to hydroimidazolone. This finding is consistent with the observed decrease of digestibility after short incubation times of methylglyoxal and EW (Chapter Two). The high proportion of modified arginine residues combined with the decreased protein digestibility implies that important peptide recognition sites for proteolytic enzymes such as trypsin were rendered unrecognisable by the modification.

The combination of *in vitro* digestibility and mass spectrometric analysis of marker modifications may prove a powerful tool to provide quick and thorough insight into the effects of protein processing on the nutritional value of a given food.

6.3 Characterisation of Aggregate Structure

Building on the macroscopic observations made (Chapter Two) attention was focussed on developing methods to probe aggregation dynamics at the molecular level. This was achieved by analysing the aggregation of EW by DLS, TEM, and SAXS (Chapter Four). Purified ovalbumin was used as a model protein to circumvent the complex analysis required for a heterogeneous mixture of proteins. It was found that ovalbumin at 0.6 mg/mL is monomeric in Milli-Q water, 100 mM glucose, 100 mM methylglyoxal. In the presence of 100 mM NaCl ovalbumin was observed as monomer and dimer using DLS and SAXS. It is likely that the dimerisation point of ovalbumin in NaCl is close to 1 mg/mL. This is consistent with findings suggesting that ovalbumin is monomeric between 0.1 mg/mL and 1 mg/mL (Matsumoto & Inoue 1993). At 45.5 mg/mL, ovalbumin was found to exist as a dimeric species.

An attempt was made to observe the conversion of monomeric ovalbumin into larger structures upon heat treatment in order to generate a model of ovalbumin aggregation. However, neither DLS nor SAXS was able to capture the early stages of aggregation. Instead, a detailed analysis of aggregate growth over time was undertaken. The results clearly showed that the presence of NaCl contributed to electrostatic shielding of Coulombic repulsion of ovalbumin in solution. This in turn enabled fast aggregation kinetics compared to ovalbumin in water and glucose solutions. For the most part, the aggregation of ovalbumin in the presence of glucose and water were very similar to each

other and no shielding effect was observed. Even at long heating times, the presence of the Maillard reaction partner glucose did not contribute to marked changes in aggregate structure compared to that of pure ovalbumin in water.

The most interesting observations of ovalbumin aggregation were made for samples treated with methylglyoxal. Methylglyoxal treated ovalbumin aggregated in a markedly different manner as shown by all three techniques, DLS, TEM, and SAXS. An in depth analysis showed two contributing factors that were responsible for the observed differences. Firstly, the addition of methylglyoxal to the ovalbumin solution (at 45.5 mg/mL) lowered the pH of the solution to pH 5, which is near the IEP of ovalbumin (4.7). This resulted in the absence of electrostatic repulsion between ovalbumin monomers. This was observed by SAXS studies and fitting structure factor models to the scattering data. Secondly, a methylglyoxal specific effect (at 100 mM methylglyoxal and 3.2 mg/mL ovalbumin concentration) suggested that the charge and IEP of ovalbumin had decreased due to reaction with lysine and arginine residues. Since both effects (pH and methylglyoxal reactivity) were closely interlinked it was not possible to selectively attribute the observed structural difference to a single mechanism but a combination of pH effect and IEP lowering properties of methylglyoxal by reacting with lysine and arginine residues. The results indicate that Maillard chemistry may impact on the aggregation properties of food proteins (such as ovalbumin) thereby changing the texture as well as the nutritional qualities, flavour and aroma.

The structural analysis of late stage aggregates using SAXS was only possible for the non-random aggregates that were characteristic in the methylglyoxal treated samples but not for ovalbumin aggregated in water, glucose, or NaCl. The heated methylglyoxal treated samples displayed scattering behaviour that corresponded to cylindrical structures that were also observed during TEM analysis. It was shown that the cylindrical models overlaid well with the scattering data and the cylinder radius (9 nm) corresponded reasonably well to the TEM measured cylinder diameter (5 nm).

The determination of aggregation at the molecular level proved to be challenging, predominantly because the aggregation system studied was a disordered system. However, SAXS scattering proved to be a powerful tool for assessing aggregation kinetics and could

even contribute to shape determination of aggregates if the aggregates were ordered. It could not provide high resolution information about random aggregates.

6.4 Safety of Food Fibrils

Amyloid fibrils are associated with neurodegenerative diseases such as Alzheimer's disease, Creutzfeldt-Jakob disease, and Parkinson's disease. More recently, non-disease-related amyloid fibrils were shown to have desirable functional properties that make them attractive for new materials, tissue engineering, and enzyme scaffolds. Additionally, food proteins have been studied as new ingredients to include in food formulations based on their structural properties and low calorie count compared to carbohydrates and lipids. Chapter Five discussed the potential issue of including protein aggregates that resemble disease related protein aggregates into food systems with the concern of potential toxicity of these food derived fibrils.

To the author's knowledge this work presents, for the first time, an analysis of the interaction of food fibrils with human cell lines. Food fibrils displayed some resistance to *in vitro* hydrolysis using pepsin, pancreatin, and Proteinase K. Therefore it was concluded that the fibrils may indeed have time to interact with cells of the gastrointestinal tract.

Toxicity studies were carried out on *in vitro* cell cultures including the Caco-2 cell line which has been reported to be a good model of the intestinal barrier (Sambuy et al. 2005). Further experiments were conducted using Hec-1a cells which are an endometrial cancer cell line. Overall, fibrils did not display toxicity towards cells in any of the chosen test conditions (including mature fibrils, pre-fibrillar aggregates, and sonicated mature fibrils). Moreover it was shown that cells proliferated equally well in the presence of fibrils when compared to native protein at the same concentration. Fibrils were also metabolised by cells that had been deprived of protein prior to fibril treatment. The presented work therefore suggests that food fibrils may be safe food ingredients.

6.5 Summary and Future Work

In summary, this work has successfully characterised EW digestibility and amino acid modifications over a wide range of processing conditions. The use of SAXS to unravel complex aggregation kinetics and structural rearrangements proved to be challenging but showed potential in characterising ordered aggregates. Food fibrils were characterised in terms of cytotoxicity and this study alleviates some concerns about their potential toxicity towards human intestinal cells.

Future work should correlate mass spectrometrically determined marker amino acid modifications (e.g., deamidation, hydroimidazolone formation) to *in vivo* bioavailability. If good agreement can be shown between animal models and the *in vitro* analysis, *in vivo* models may be able to be used less frequently thereby saving animal lives, cost, and time.

Due to limited access to the high demand SAXS beamline of the Australian Synchrotron further experiments in buffered solution could not be carried out. Future aggregation studies of ovalbumin should include working in buffered systems (which was deliberately avoided in the presented work to analyse buffer unbiased protein aggregation) of methylglyoxal to gain insight independent of pH fluctuations. This should be carried out in combination with an ovalbumin sample series which should be pH buffered to shed light on the exact mechanisms involved, with appropriate buffer only controls. Furthermore, SAXS and DLS analysis would benefit from an improved experimental set-up for conducting analysis of protein aggregation. This would include a heated and stirred solution, constantly circulated through the capillary/cuvette whilst acquiring scattering data. By doing so, a seamless set of scattering data could be collected that would allow a detailed analysis of intermediate structures in real time.

The preliminary work on fibril toxicity should be correlated to *in vivo* animal studies using fibrillar and non-fibrillar protein feed. Toxicity should be tested for each food fibril that is proposed as a new food ingredient because fibrils differ in terms of surface chemistry and morphology (Bucciantini et al. 2004; Chiti & Dobson 2006), which could influence the interaction with cell membranes and thereby cytotoxicity (Stefani & Dobson 2003).

6.6 References

Bucciantini, M., Calloni, G., Chiti, F., Formigli, L., Nosi, D., Dobson, C.M. & Stefani, M., 2004. Prefibrillar amyloid protein aggregates share common features of cytotoxicity. *Journal of Biological Chemistry*, 279(30), pp.31374–31382.

Chen, L., Remondetto, G.E. & Subirade, M., 2006. Food protein-based materials as nutraceutical delivery systems. *Trends in Food Science and Technology*, 17(5), pp.272–283.

Chiti, F. & Dobson, C.M., 2006. Protein misfolding, functional amyloid, and human disease. *Annual Review of Biochemistry*, 75(1), pp.333–366.

Friedman, M., 2003. Nutritional consequences of food processing. *Forum of Nutrition*, 56(1), pp.350–352.

Matsumoto, T. & Inoue, H., 1993. Association state, overall structure, and surface roughness of native ovalbumin molecules in aqueous solutions at various ionic concentrations. *Journal of Colloid and Interface Science*, 160(1), pp.105–109.

Sambuy, Y., De Angelis, I., Ranaldi, G., Scarino, M.L., Stammati, A. & Zucco, F., 2005. The Caco-2 cell line as a model of the intestinal barrier: influence of cell and culture-related factors on Caco-2 cell functional characteristics. *Cell Biology and Toxicology*, 21(1), pp.1–26.

Stefani, M. & Dobson, C.M., 2003. Protein aggregation and aggregate toxicity: new insights into protein folding, misfolding diseases and biological evolution. *Journal of Molecular Medicine*, 81(11), pp.678–699.

Chapter Seven

7 Experimental

7.1 General Materials and Methods

Unless otherwise stated, chemicals were purchased from Sigma-Aldrich, Invitrogen, or Roche. Eggs were bought from local farms around Christchurch, New Zealand. Soy beans and kidney beans were bought in local shops in Christchurch, New Zealand. Spray-dried egg white was generously provided by Zeagold, New Zealand. Whey protein isolate 895 (WPI) was generously supplied by Fonterra, New Zealand.

pH measurements were carried out on an UltraBasic UB10 pH meter (Denver Instrument Co.) fitted with a high-performance glass body pH/Tris electrode. For centrifugation of small volumes (< 2 mL), an Eppendorf 5810R with a fixed F-45-30-11 rotor was used. Larger volumes were centrifuged using a Thermo Scientific Sorvall RC6 plus centrifuge equipped with either a FiberLite® F21-8x50y, F14-6x250y, or F10-6x500y rotor.

7.2 Protein Extraction and Purification

Ovalbumin (OVA) was purified from day-fresh chicken egg white. Soy protein isolate (SPI) and kidney bean protein isolate (KPI) were prepared from freshly ground soy bean and kidney bean flour.

7.2.1 *Ovalbumin Purification*

Ovalbumin (OVA) was purified from day-fresh hen egg white using anion exchange chromatography (de Groot & de Jongh 2003). 100 mL of fresh hen egg white was diluted in 200 mL OVA extraction buffer (Table 7.1) and stirred over night at 4 °C. The solution was then centrifuged at 10,000 rpm for 20 minutes. The supernatant was then added to 250 g of DEAE (2-(Diethylamino)ethyl) Sephacel (pre-equilibrated with OVA DEAE buffer (Table 7.1)). This suspension was stirred overnight to allow binding of OVA to the resin.

The resin was collected and washed with 3 L of distilled water. Subsequently, 200 mL fractions of NaCl at different concentrations (20 mM, 40 mM, 60 mM, 80 mM, 100 mM, 200 mM, 1000 mM) were used to elute ovalbumin. The fractions were collected and tested for OVA purity using SDS PAGE. Usually the 100 mM fraction contained pure protein that did not require further purification. This fraction was sterile filtered and subsequently dialysed against distilled water. The remaining fractions were discarded.

Table 7.1 *Composition of OVA extraction and DEAE buffer.*

Solution	Contents and Instructions
OVA extraction buffer	50 mM Tris HCl 10 mM β-mercaptoethanol adjust pH to pH 7.5
OVA DEAE buffer	50 mM Tris HCl adjust pH to pH 7.5

7.2.2 *Soy Bean Protein Isolate (SPI)*

The extraction method of soy protein from soy beans was modified from (Akkermans et al. 2007). 25 g of finely ground soy bean flour was dissolved in 200 mL of SPI extraction buffer (Table 7.2) and stirred for 45 minutes at room temperature. The suspension was centrifuged for 30 minutes at 13,000 - 18,000 rpm. The supernatant was filtered several times through muslin cloth, No.4 Whatman paper, and 0.2 µm syringe filters. The filtrate was then dialysed in 300 volumes of distilled water. The dialysed SPI was adjusted to pH 1.6 with concentrated HCl and centrifuged at 13,000 - 18,000 rpm for 15 minutes. The supernatant was sterile filtered through 0.2 µm filters and stored at 4 °C until further use.

Table 7.2 *Composition of SPI extraction buffer.*

Solution	Contents and Instructions
SPI extraction buffer	30 mM Tris 10 mM β-mercaptoethanol adjust to pH 8.0 with NaOH

7.2.3 *Kidney Bean Protein Isolate (KPI)*

The protein extraction from kidney beans was modified from (Tang et al. 2010). 25 g of finely ground kidney bean flour was dissolved in 200 mL of KPI extraction buffer (Table 7.3). The solution was quickly adjusted to pH 3.5 with concentrated HCl and stirred at room temperature for 15 minutes. The solution was filtered and centrifuged at 13,000-18,000 rpm for 30 minutes. The supernatant was diluted with 5 volumes 4 °C cold water to precipitate the protein. The precipitate was centrifuged and resuspended in 50 mL resuspension buffer (Table 7.3). This washing procedure was repeated three times. The washed KPI was dialysed in 300 volumes of distilled water. The dialysed KPI was adjusted to pH 1.6 with concentrated HCl and centrifuged at 13,000-18,000 rpm for 15 minutes. The supernatant was sterile filtered through 0.2 μm filters and stored at 4 °C until further use.

Table 7.3 *Composition of KPI extraction solutions.*

Solution	Contents and Instructions
KPI extraction buffer	0.5 M NaCl 25 mM HCl
Resuspension buffer	0.5 M NaCl

7.3 Buffer Exchange and Dialysis

Buffer exchange or desalting of protein solutions was carried out using either a 5 mL HiTrap™ Desalting column or 12,000 MWCO dialysis tubing stored in 0.1 % sodium azide. 3 column volumes of buffer were used to equilibrate the column. After loading the sample, the desired buffer was used to elute the sample. For dialysis, the tubing was washed in distilled water before the sample was loaded into the tubing. Dialysis was then carried out in 100 - 300 volumes of distilled water at 4 °C.

7.4 Protein Concentration Determination

Three different methods to determine protein concentration were trialled: Bradford, Biuret and UV A_{280} assays. The Biuret method showed consistent and reliable results across the measured protein range. The protein content of all protein solutions was therefore quantified using the Biuret method. BSA was used as a standard at the appropriate concentration range. Unknown proteins were diluted to the appropriate concentration.

7.4.1 Bradford Protein Assay

The Bradford assay is based on the colour reaction between protein and Coomassie Brilliant Blue G-250 (Bradford 1976). The dye changes from brown to blue in the presence of protein. Assays were performed in triplicate in 96 well plates. The wells were preloaded with 10 µL protein solution at the appropriate concentration. 200 µL of Bio-Rad protein assay reagent (Table 7.4) was added to the protein solution and mixed thoroughly on a plate shaker. Plates containing the mixed samples were incubated at room temperature for 5 min before reading the absorbance at 595 nm on a Labtech FLUOstar OPTIMA plate reader. Samples were blanked against the respective protein buffer. A standard curve was generated using BSA in a concentration range from 0 to 0.2 mg/mL.

Table 7.4 *Bio-Rad protein assay reagent.*

Solution	Contents and Instructions
Bio-Rad protein assay reagent	dilute Bio-Rad protein reagent 1:5 in Milli-Q water filter through 0.2 µm syringe filter

7.4.2 Biuret Protein Assay

The Biuret protein assay relies on complex formation between peptide bonds and copper to develop a measurable colour change (Krohn 2002). Assays were performed in triplicate in 96-well plates. The wells were preloaded with 50 µL protein solution. 200 µL of Biuret reagent (Table 7.5) was added to the protein solution and mixed thoroughly on a plate

shaker. Plates containing the mixed samples were incubated at room temperature for 20 min before reading the absorbance at 540 nm on a Spectramax M-series multimode plate reader. Samples were blanked against the respective protein buffer. A standard curve was generated using BSA in a concentration range from 0 to 2.0 mg/mL.

Table 7.5 *Biuret reagent components.*

Solution	Contents and Instructions
Biuret reagent	In 400 mL Milli-Q water: 4 g NaOH 4.5 g Sodium Tartrate 1.5 g $CuSO_4$ * $5H_2O$ 2.5 g Potassium Iodide Make to 500 mL

7.4.3 NanoDrop UV (A_{280})

Protein concentrations were measured using a Thermo Scientific NanoDrop™ ND-1000 Spectrophotometer (Thermo Fischer Scientific). For pure protein, the absorbance coefficient was determined by using the online software Protein Calculator v3.3 (www.scripps.edu). The calculating operations are based on the number of aromatic tryptophan and tyrosine residues but also depend on the presence of disulfide bonds which absorb light at 280 nm (Gill & von Hippel 1989). For protein mixtures an absorbance coefficient of 1.0 M^{-1} cm^{-1} was used. After calibration of the machine with water and blanking with respective buffer, the absorbance of 2 µL of protein solution was measured. Measurements were undertaken at 280 nm in triplicate. Through application of Beer's law the concentration of protein was calculated automatically by the NanoDrop software.

7.5 Polyacrylamide Gel Electrophoresis (PAGE)

PAGE was run to confirm the purity of proteins, the degree of Maillard cross-linking and fibrillation of proteins. In PAGE, proteins are accelerated by an electric field. Due to differences in IEP and resulting net charge at a given pH, proteins are separated by charge. In addition, the polyacrylamide functions as a molecular sieve, separating the proteins

based on size, shape. In PAGE, polyacrylamide gels are generally made up of two different gels, a stacking gel and a separation gel. The stacking gel allows focusing the protein sample into a fine band. As the proteins continue into the separation gel, the finer polymerisation of acrylamide allows for finer separation (Laemmli 1970).

7.5.1 Native Polyacrylamide Gel Electrophoresis (Native PAGE)

In native PAGE, proteins are not deliberately denatured. Proteins are separated based on molecular weight, intrinsic charge, and the overall shape of the polypeptide chain. Native PAGE can indicate quaternary structure (e.g. monomer and multimer distinction) and protein-protein interaction.

For native PAGE, 5 µL Novex® Sharp protein standard (Invitrogen) was used as a protein ladder. NuPAGE Novex® 4 - 12% Bis-Tris gels or 4 - 20 % Tris-glycine gels were run according to the manufacturer's recommendations in a NuPAGE® gel electrophoresis box at 4 °C. Protein samples were mixed with 2 x Tris-glycine native sample buffer. Tris-glycine gels were run at a constant voltage of 125 V in 1 x Tris-glycine native running buffer (Table 7.6). The gels were stained with Coomassie staining solution. Gels were destained for at least one hour. To facilitate staining and destaining, gels were briefly heated in a microwave for 30 seconds to approximately 50 °C. Alternatively, the staining of gels was undertaken using Simple blue stain (Table 7.6) using a three step protocol (http://www.labtimes.org). After electrophoresis, gels were placed in distilled water and microwaved for 30 seconds. Water was discarded and the gel covered in Simply blue stain before microwaving for 30 seconds. The gel was then gently shaken for 15 minutes at room temperature. Gel photographs were taken using a Genius^2 BioImaging System (Syngene).

7.5.2 Sodium Dodecyl Sulfate PAGE (SDS-PAGE)

SDS-PAGE is the most commonly used denaturing electrophoresis. The amphiphilic SDS binds non-covalently to protein (1.4 g of SDS / 1 g of protein). The negatively charged sulfate group contributes to the linearisation of the polypeptide chain by electrostatic

repulsion. Additionally, the negative charge allows for fast electrophoretic separation of SDS coupled proteins in an electric field. Reducing agents such as DTT or β-mercaptoethanol can be included in sample preparation to reduce disulfide bonds. Samples are normally heated at 70 - 90 °C for 2-5 min before being loaded onto the gel. The high temperature allows the protein to unfold and accelerates disulfide bond reduction. For SDS PAGE, 5 μL Novex® Sharp protein standard (Invitrogen) was used as a protein ladder. SDS-PAGE was run to confirm the purity of proteins but also the degree of Maillard cross-linking and fibrillation of proteins. NuPAGE Novex® 4 - 12% Bis-Tris gels or 4 - 20 % Tris-glycine gels were run according to the manufacturer's recommendations in a NuPAGE® gel electrophoresis box at room temperature. Protein samples were mixed with reducing agent and either 4 x lithium salt of dodecyl sulfate (LDS) sample buffer (Invitrogen) or 2 x Tris-glycine SDS sample buffer depending on the nature of the gel. For Bis-Tris gels, electrophoresis was run at a constant voltage of 170 V in 1 x MOPS running buffer at room temperature. Tris-glycine gels were run at a constant voltage of 125 V in 1 x Tris-glycine SDS running buffer. The gels were stained with Coomassie staining solution. Gels were destained for at least one hour. To facilitate staining and destaining, gels were briefly heated in a microwave oven for 30 seconds to approximately 50 °C. Alternatively, the staining of gels was undertaken using Simply blue stain using a three step protocol. After electrophoresis, gels were placed in distilled water and microwaved for 30 seconds. Water was discarded and the gel covered in Simple blue (Table 7.6) stain before microwaving for 30 seconds. The gel was then gently shaken for 15 minutes at room temperature. Gel photographs were taken using a Genius^2 BioImaging System (Syngene).

Table 7.6 *PAGE buffer compositions.*

Solution	Contents and Instructions
MOPS running buffer (1x)	50 mM MOPS 50 mM Tris base 0.1 % SDS 1 mM EDTA [pH 7.7]
Tris-glycine SDS running buffer (1x)	25 mM Tris base 192 mM glycine 0.1 % SDS [pH 8.3]
Tris-glycine native running buffer (1x)	25 mM Tris base 192 mM glycine [pH 8.3]
Coomassie staining solution (1x)	2.5 g/L Coomassie R-250 10 % (v/v) acetic acid 45 % (v/v) methanol 45 % distilled water
Destaining solution (1x)	30 % methanol 10 % acetic acid 60 % distilled water
Tris-glycine SDS sample buffer (2x)	126 mM Tris HCl 20 % glycerol 4 % SDS 0.005 % bromophenol blue [pH 6.8]
Tris-glycine native sample buffer (2x)	126 mM Tris HCl 20 % glycerol 0.005 % bromophenol blue [pH 6.8]
LDS sample buffer (4x)	564 mM Tris base 424 mM Tris HCl 40 % glycerol 8 % LDS 2.04 mM EDTA 0.88 mM Coomassie Blue G-250 0.7 mM phenol red [pH 8.5]
Reducing agent (10x)	1 M DTT 10 mM sodium acetate (pH 5.2) sterile filtered stored at -20 °C
Simple blue stain (1x)	60-80 mg/L Coomassie G-250 dissolved in 35 mM HCl

7.6 Egg White Treatment

10 egg whites of day-fresh chicken eggs were pooled and homogenised using a household kitchen blender for 10 seconds. For the preliminary assessment of whether pH and salt concentration affects digestibility, the egg white was adjusted to five different pH values (2, 5, 7, 9, and 12) with 1 M HCl or 1 M NaOH and two salt conditions at each pH (0 mM and 200 mM NaCl). The different egg white samples were then subjected to various temperature treatments (room temperature, 60 °C, 80 °C, 100 °C) for 10 minutes prior to subjection to the digestibility assay.

7.6.1 Maillard Reaction

Egg white samples were treated with different potential Maillard reaction partners at different concentrations from 0 - 200 mM. The studied Maillard partners were fructose, glucose, lactose, methylglyoxal and glutaraldehyde.

7.7 *In Vitro* Digestion

In vitro digestion was carried out based on methods developed in previous studies and the U.S. Pharmacopeia with slight modifications (Fu et al. 2002; Kim et al. 2008; United States Pharmacopeia 2009). Firstly, protein samples were homogenised using a glass tissue homogeniser to simulate mastication. The homogenised sample was subjected to amylase (Sigma No.: A3176) digestion to mimic polysaccharide breakdown in the mouth for 5 minutes at 37 °C. The pH was then adjusted to 1.5 with 1 M HCl. Following acidification, porcine pepsin (Sigma No.: P7000, 250U/mg) was added and the sample was incubated for 30 minutes at 37 °C. Samples were then neutralised with 1 M $NaHCO_3$ to stop any further pepsin digestion. Subsequently, the pH of the sample was adjusted to 7.5 with 167 mM KH_2PO_4 and pancreatin (Sigma No.: P1750) was added. The sequential standard enzyme assay (amylase, pepsin, pancreatin) results in addative volume changes. The respective volumes at each enzymatic addition gave active concentrations of 0.3 mg/mL amylase, 3.1 mg/mL pepsin, and 2.5 mg/mL pancreatin. These values correspond to final enzyme to protein ratios (w/w) of 0.04 for amylase, 0.4 for pepsin, and 0.5 for pancreatin. For

amyloid fibril digestion, the protein to substrate ratio was 0.05 for all employed proteases and fibrils. Samples were digested for up to 8 hours at 37 °C. For the OPA assay, pepsin digested samples were neutralised to stop further proteolysis and pancreatin digested samples were acidified. The samples were centrifuged for two minutes at 14,000 rpm, and subsequently frozen and stored at -20 °C until analysed. Three replicates were used in all digestion experiments.

7.8 *o*-Phthaldialdehyde (OPA) Assay

The OPA colorimetric assay was used to determine the degree of hydrolysis (DH) after *in vitro* proteolysis. The assay was performed in a cuvette (spectrophotometer) or in a 96-well plate (plate reader) at 340 nm. The protein containing sample solution was mixed with OPA reagent (Table 7.7) in a 1:10 (v/v) (protein solution:OPA reagent) ratio. Samples were mixed thoroughly and incubated for exactly 2 minutes. The DH was calculated from the blanked absorbance readings following established protocols (Adler-Nissen 1976; Nielsen et al. 2001b). Absorbance readings were compared to a 1.3 mM serine standard to calculate the α-NH_2 equivalents (aa_{eq}) that were generated during hydrolysis. All samples and standards were blanked against OPA solution and water. Equation 7.1 describes the calculation of (aa_{eq}) for any sample (Nielsen et al. 2001b). Abs is the blanked absorbance value, c_{ser} the serine concentration in mM, V is the sample volume in L, d is the dilution factor (required if the sample was diluted for the OPA assay), m is the mass of the food sample (egg white) in g, and $\%_{protein}$ is the percentage of protein in the sample (~10 % for egg white).

Equation 7.1

$$aa_{eq} = \frac{\left(\left(\frac{Abs_{sample}}{Abs_{standard}}\right) * c_{ser}\right) * V * d * 100}{(m * \%_{protein})}$$

From (aa_{eq}), the number of hydrolysis equivalents (h) can be approximated through the relationship shown in Equation 7.2 (Adler-Nissen 1979; Nielsen et al. 2001b).

Equation 7.2

$$h = \frac{(aa_{eq} - \beta)}{\alpha}$$

The values of α and β are slightly variable (α ~ 0.796-1.093 and β ~ 0.342-0.457) for proteinacous foods such as soy, casein, and gelatine (Adler-Nissen 1979). A valid estimation for any other protein can be undertaken with α at 1.00 and β at 0.40 (Adler-Nissen 1979). The degree of hydrolysis (DH) can then be calculated from Equation 7.3 (Nielsen et al. 2001b).

Equation 7.3

$$DH = \frac{h}{h_{tot}} * 100\%$$

Where h are the hydrolysis equivalents formed during proteolysis in mmol/g protein and h_{tot} is the hydrolysis equivalents at complete hydrolysis to amino acids in mmol/g protein. If not known from amino acid analysis, h_{tot} is set to be 8 mmol/g assuming an average weight of 125 g/mol of amino acids within proteins (Nielsen et al. 2001b).

Table 7.7 *OPA assay reagents and serine standard.*

Solution	Contents and Instructions
OPA assay reagent	100 mM sodium borate 0.1 % SDS 0.3 mM 2 % ethanol 5.7 mM DTT
Serine standard	1.3 mM serine stored at -20 °C

7.9 Mass Spectrometry

Sample preparation:

Three egg whites of day-fresh hen eggs were pooled, homogenized, and then sub-samples analysed before and after boiling for 10 minutes or 60 minutes (in the presence and absence of glucose or methylglyoxal). Samples were enzymatically digested as described (Speicher et al. 2000) with some modifications. Briefly, 10 mg of each sample (boiled and raw) was reduced with 50 µL 50 mM TCEP (tris(2-carboxyethyl)phosphine) and alkylated using 50 µL 360 mM acrylamide prior to tryptic digest for 20 hours. Peptides were simultaneously extracted and cleaned from the digestion mixture using Empore^{TM} discs (Meng et al. 2008) and resuspended using 0.2% acetic acid in 2% acetonitrile, before being analysed using mass spectrometry.

LC-MS/MS:

Isolated peptides were analysed using an Ultimate nanoscale HPLC (LC Packings, Amsterdam, The Netherlands) equipped with Famos autosampler and Switchos column switching module. The loading pump was an LC-10AT isocratic pump (Shimadzu) at a flow rate of 8 µL/min. Samples were loaded on the trap column (5 mm, 300 µm ID) and separated on a 190 mm, 75 µm ID analytical column (both in-house packed with Microsorb C18 300 Å, 5 µM media, Varian) coupled to a QSTAR Pulsar *i* mass spectrometer (AB Sciex, Foster City, CA, USA) using a Proxeon stainless steel nanospray capillary at 2200 V. The gradient was 2-55% B (acetonitrile/0.2% formic acid) over 60 min at a flow rate of 150 nL/min. MS data were acquired from m/z 400 - 1200 and MS/MS from 100 - 1600 m/z accumulating four cycles over 1.5 s duration each.

Data evaluation:

For protein identification, data were searched against the NCBInr database using Mascot v2.2.06 (Matrix Science, London, UK). Enzyme specificity was set to semi-trypsin. Error tolerance was set to 100 ppm for LC-MS and 0.4 Da for MS/MS. Data were compiled and analysed using ProteinScape 2.1 (Bruker) with acceptance thresholds for protein and peptide scores set at 40 and 20, respectively. Protein and peptide lists were compiled using the Protein-Extractor functionality in ProteinScape including automatic assessment of true

and false positive identification of peptide matches according to the peptide settings detailed above.

For evaluation and interpretation of peptide modification, parallel searches for varying target amino acid modifications, particularly oxidative modifications (Dyer et al. 2010), were conducted.

The proteomic data generated were transformed into a manageable data set by (a) setting an appropriate peptide MS/MS score threshold of 45 and (b) omitting redundant peptides; choosing only the highest scoring peptides for each modification found. The MS/MS score threshold is a measurement of likely accuracy for the predicted peptide sequence, calculated through comparison of observed fragment ions with theoretical fragmentation, with a higher threshold lowering the probability of detecting a false positive of the same mass in the chosen protein databank. Analysis of the data showed very consistent results for oxidative and other amino acid modifications between MS/MS score thresholds of 45-55. A MS/MS score of 45 was chosen to ensure high confidence in correct peptide determination, while enabling broad peptide coverage.

To compare amino acid modifications between samples, a recently developed damage scoring system was utilised to enable robust protein damage comparison (Dyer et al. 2010). A weighted score rather than a total score for amino acid modification was used to account for differences during sample preparation and MS runs (e.g. number of peptides analysed). The weighted modification score (s_w) was defined by Equation 7.4:

Equation 7.4

$$s_w = \frac{aa_{mod}}{aa_{tot}} \times f_{mod}$$

s_w weighted modification score

aa_{mod} number of a specific amino acid residues carrying a specific modification (within the peptides meeting the identification threshold requirements)

aa_{tot} total number of a specific amino acid residue (within total observed peptides meeting the threshold identification requirements)

f_{mod} modification factor that gives a damage ranking for specific modifications based on the relative level of modification from the native state (e.g. $f_{mod} = 1$ for single oxidation, $f_{mod} = 2$ for double oxidation, $f_{mod} = 3$ for triple oxidation)

The weighted modification score for amino acid residue damage was divided into two sub-categories, namely oxidative damage (accounting for single, double, triple oxidation) and other damage (deamidation, carbamylation, etc.).

7.10 Differential Scanning Fluorometry (DSF)

For the determination of the protein melting point, DSF was used as the preferred option because of its high throughput compared to DSC. DSF is commonly used to assess protein stability (Ericsson et al. 2006). The dye employed in this technique fluoresces when exposed to hydrophobic protein regions during protein denaturation. 16 µL of protein sample (1 mg/mL) was mixed with 80 µL of buffer and 4 µL of 250 x SYPRO® Orange dye. Blanks were carried out with 24 µL, of buffer and 1 µL of dye. All samples and blanks were loaded into 96-well thin-wall PCR plates (BioRad) in triplicate. The plate was sealed with Bio-Rad® Microseal® 'B' Film. The sealed plate was then loaded into a BioRad IQ5 Multicolor Real-Time PCR Detection System with iCycler (BioRad). Samples were heated from 20 °C to 95 °C in increments of 0.2 °C, with a 10 second dwell time at each temperature. Fluorescence changes were monitored simultaneously with a charge-coupled device camera. The wavelengths for excitation and emission were 490 nm and 575 nm, respectively. Melting temperatures were determined as the maximum point of inflection using -*d*RFU/*d*t.

7.11 Circular Dichroism (CD)

UV circular dichroism (CD) was used to analyse the secondary structure of proteins. In CD, circularly polarised light interacts with chiral secondary structure of proteins. The α-helical proteins have absorption minima at 222 nm and 208 nm and a positive maximum at 193 nm. Predominantly β-sheeted proteins have a negative maximum at 218 nm and a positive maximum at 195 nm (Greenfield 2006). CD assays were carried out using samples with a concentration of 0.1 to 0.5 mg/mL. A quartz cuvette with 1 mm path length was used. CD spectra were recorded from 190 nm to 250 nm in 0.5 nm increments, using a Jasco J-815 circular dichroism spectrophotometer. The reported protein spectra were blanked against buffer spectra.

7.12 Differential Scanning Calorimetry (DSC)

Differential scanning calorimetry measures the absorbed or excreted energy of a closed system. In protein stability studies, DSC was used to measure the necessary energy to denature a protein from its native to an unfolded form. The protein denaturation is typically endothermic, therefore requires an energy input. This increase in required energy input into the system is measurable. The shape of the heat flow curve and its position enables analysis of the melting midpoint as well as change in enthalpy (ΔH). Due to the endothermic character of protein denaturation ΔH is negative (Chiu & Prenner 2011).

Both protein solution (1 mg/mL) and the respective protein buffer were degassed under vacuum for 30 minutes. A Nano DSC (TA Instruments) was used to analyse protein stability. The DSC cells were conditioned twice with buffer in both sample and reference capillary to ensure that both capillaries were behaving uniformly. Subsequently, protein solution was loaded into the sample capillary and buffer into the reference capillary. At a constant pressure of 3 bar a temperature scan from 20 - 90 °C was performed with a scanning rate of 1 °C/ min. After run completion, the buffer reference heat flow curve was subtracted from the protein sample heat flow curve. NanoAnalyse software (TA Instruments) was used to determine the melting midpoint.

7.13 Dynamic Light Scattering (DLS)

Dynamic light scattering was used to analyse the size distribution profile and hydrodynamic radius of particles in solution. DLS relies on the measurement of the light scattering interference caused by particles in solution. The interference fluctuates over time, because particles move due to Brownian motion. The interference therefore depends on the size of the particles because large particles move slowly whereas small particles move quickly through solution. To avoid dust and aggregate contamination, samples were prepared carefully. All samples were centrifuged for 5 minutes at 13,200 rpm and the supernatant containing soluble protein was transferred into a clean disposable low volume cuvette. Dynamic light scattering experiments were performed on a Malvern Zetasizer Nano at a fixed backscattering angle of 173 °. For analysis, Malvern Zetasizer Software 6.32 was utilised. Protein was chosen as the scattering material and water as the dispersant.

Each measurement was carried out in triplicate and the results were averaged and checked for data quality using Malvern Zetasizer Software 6.32.

7.14 Small Angle X-ray Scattering (SAXS)

Samples were prepared by resuspending freeze dried ovalbumin in Milli-Q water followed by sterile filtering (0.2 μm). The protein stock and buffers were then mixed in a 1:1 ratio (v/v) to give final protein concentrations of 0.6 mg/mL and 3.2 mg/mL. The final buffer concentration (glucose, methylglyoxal, NaCl) was 100 mM. The samples were heated at 80 °C for a period of 24 hours. Aliquots were taken at different time intervals and placed on ice until further analysis. For analysis, samples and buffers were degassed for 15 minutes and then centrifuged for 4 minutes at 900 rpm.

Scattering experiments were performed at the Australian Synchrotron, Melbourne. The employed photon energy of the X-rays was 12 keV (λ = 1.03 Å). Two sample to detector distances were chosen to measure both the finer molecular details (1.6 m distance) and larger aggregated protein structures (7 m) using a Pilatus 1M detector. A longer distance allows the measurement of larger structures because large particles scatter stronger than small particles. The measurable *Q*-range at 1.6 m was from 0.617 $Å^{-1}$ to 0.086 $Å^{-1}$ and at 7 m from 0.1344 $Å^{-1}$ to 0.0019 $Å^{-1}$. Samples were loaded into a quartz capillary. The sample flowed through the capillary at a speed of 2 μL/s in order to prevent damage to the samples through X-ray radiation. Samples were exposed to a series of 2 s X-ray exposures (10 exposures = 20 s total exposure time). Potential sample damage was monitored by comparing the first and the last exposures of each exposure series. The deposition of damaged protein on the quartz capillary, also known as capillary fouling, was monitored by buffer control runs between every sample. The capillary was also washed regularly with guanidine solution, detergent solution, and water. High concentration and highly aggregated samples were run at the end of each experiment series. The generated data were calibrated to absolute intensity *I(Q)* using silver behenate as a standard and water as a secondary standard.

For data analysis, the multiple 2 s scattering patterns of samples and buffers were analysed for consistency and subsequently averaged. The averaged buffer scattering was subtracted

from the sample scattering. Averaging and subtracting was carried out in ScatterBrainAnalysis v1.0.3 software, developed at the Australian Synchrotron. The averaged and background corrected scattering profiles were analysed using ScatterBrainAnalysis v1.0.3 software and the ATSAS software package, developed at EMBL, Hamburg. Many thanks go to Nigel Kirby and Nathan Cowieson from the Australian Synchrotron for their support and to Duncan McGillivray (University of Auckland) for his expert advice in data analysis.

7.15 *Transmission Electron Microscopy (TEM)*

Formvar-coated copper grids (200 mesh) (ProSciTech) were coated with protein samples and negatively stained with a 1 % uranyl acetate solution (Whittingham et al. 2002). In brief, 5 μL of protein solution was dispensed onto Parafilm. TEM grids were placed onto the protein drop for 1 minute and subsequently placed on three 5 μL drops of Milli-Q water for 20 seconds each. This was followed by placing the grids onto a 5 μL drop of uranyl acetate for 1 minute. TEM micrographs (14,000 x and 89,000 x magnification) were obtained on a Morgagni 268D TEM (FEI Company, Oregon, USA) operating at 80 kV, fitted with a 40 μm objective aperture. Samples were viewed in triplicate. Many thanks go to Jackie Healy (University of Canterbury) for her efforts to obtain TEM micrographs.

7.16 Scanning Electron Microscopy (SEM)

Electron micrographs were obtained by Neil Andrews (University of Canterbury) using a Leica S440 electron microscope (Wetzlar, Germany). Samples were freeze fractured to observe the internal microstructure. Both solid and liquid samples were immersed in liquid nitrogen and subsequently freeze-dried overnight (Yasir et al. 2007). Following freeze-drying, the samples were mounted on an aluminum stub and coated in gold using a Polaron sputter coater at 1.2 kV and 20 mA for two minutes. The samples were then analysed by SEM at 10 kV and 50 pA, and at 20 mm working distance.

7.17 Amyloid Fibril Formation

7.17.1 Fibril Formation of WPI

A 10 mg/mL solution of WPI in Milli-Q water was adjusted to pH 1.6 using concentrated HCl. The solution was stirred at 4 °C over night and then incubated at 80 °C for 22 hours (Loveday et al. 2010). After heat incubation, the samples were cooled down on an ice bath for 10 minutes and finally stored at room temperature for 7 days to allow for fibril formation. Thioflavin T (ThT) fluorescence and TEM were used to monitor fibrillation.

7.17.2 Fibril Formation of SPI and KPI

The freshly made and undiluted SPI/ KPI solutions were adjusted to pH 1.6 using concentrated HCl. The solutions were then incubated at 80 °C for 22 hours (Akkermans et al. 2007; Tang et al. 2010; Wang et al. 2011). After heat incubation, the samples were cooled down on an ice bath for 10 minutes and finally stored at room temperature for 7 days to allow for fibril formation. ThT fluorescence and TEM were used to monitor fibrillation.

7.17.3 Fibril Formation of OVA

A 10 mg/mL solution of lyophilised ovalbumin in 15 mM β-mercaptoethanol was prepared to reduce the sample at 37 °C for two hours in a shaking incubator. The reduced sample was diluted eightfold into 100 mM NaCl, pH 1.6. The solutions were subsequently sterile filtered. The solutions were then incubated at 80 °C for 22 hours (Sagis et al. 2004; Tanaka et al. 2011). After heat incubation, the samples were cooled down on an ice bath for 10 minutes and finally stored at room temperature for 7 days to allow for fibril formation. ThT fluorescence and TEM were used to monitor fibrillation.

7.17.4 Fibril Formation of Insulin

5.8 mg/mL of insulin (Sigma) were dissolved in 100 mM NaCl, 25 mM HCl (pH 1.6) and sterile filtered (Nielsen et al. 2001a). The solution was incubated at 60 °C for 22 hours. After heat incubation, the samples were cooled down on an ice bath for 10 minutes and finally stored at room temperature for 7 days to allow for fibril formation. ThT fluorescence and TEM were used to monitor fibrillation.

7.17.5 Pre-fibrillar Aggregates and Fibril Sonication

For cytotoxicity studies mature fibrils were compared with pre-fibrillar aggregates and sonicated fibrils. For the formation of pre-fibrillar aggregates the fibril formation protocols were followed. However, proteins were not incubated at room temperature for 7 days but instead used straight after the 10 minute cooling step. The sonication of mature fibrils was carried out in Eppendorf tubes that were placed in a sonicating water bath for 15 minutes.

7.18 Thioflavin T (ThT) Fluorescence

ThT dye is an amyloid protein specific dye. The increase of ThT fluorescence was used to monitor fibrillation of proteins (LeVine 1999). 20 µL sample was first loaded into a black 96-well Greiner Plate with flat, transparent bottom. 180 µL ThT solution Table 7.8 was added to each sample and the plate was stirred on a plate shaker for 20 seconds. After 6 minutes of incubation at room temperature, the samples were analysed on a Labtech FLUOstar OPTIMA plate reader. Samples were excited at 450 nm and the emitted light at 485 nm was measured. Sample buffer was used as blank and experiments were undertaken in triplicate.

Table 7.8 *ThT assay component.*

Solution	Contents and Instructions
ThT buffer	50 mM Tris base (0.606 g / 100 mL) 100 mM NaCl (0.584 g/ 100 mL) Adjust to pH 7.5 Filter through 0.2 µm
ThT dye	2.5 mM ThT in ThT buffer Filter through 0.2 µm
ThT solution	176 µL ThT buffer 4 µL ThT dye

7.19 Proteolysis of Fibrils

Fibrils were diluted to 1.0 mg/mL using 25 mM HCl (pH 1.6). For pancreatin and Proteinase K (PK) hydrolysis the pH of the fibril solutions was adjusted to 7.5. For pepsin it was kept at pH 1.6. Enzymes were added in an enzyme:fibril ratio of 1:20 (w/w). The total volume was adjusted with distilled water to yield a final protein concentration of 0.9 mg/mL. The fibril samples were incubated with the enzymes for 3 hours, taking 135 µL aliquots at various time intervals (0, 20, 60, 180 minutes). PK and pancreatin hydrolysis were terminated by adjustment to pH 1 - 2 with 1 M HCl, pepsin digestion through adjustment to pH 7 with 1 M $NaHCO_3$. Hydrolysis progression of protein fibrils was monitored via TEM and decrease of ThT fluorescence.

Table 7.9 *Fibril proteolysis buffers and enzyme stocks.*

Solution	Contents and Instructions
Pepsin buffer	10 mM HCl 100 mM NaCl 5 mM $CaCl_2$ Sterile filter [pH 3-4]
PP buffer	50 mM Tris base 100 mM NaCl 5 mM $CaCl_2$ Sterile filter [pH 7.5]
Pepsin (20 mg/mL)	40 mg/mL pepsin in pepsin buffer Dilute 1:1 with 100 % glycerol Aliquot into 200 µL Freeze and store at -20 °C
Pancreatin (20 mg/mL)	40 mg/mL pancreatin in PP buffer Dilute 1:1 with 100 % glycerol Aliquot into 200 µL Freeze and store at -20 °C
Proteinase K (20 mg/mL)	40 mg/mL Proteinase K in PP buffer Dilute 1:1 with 100 % glycerol Aliquot into 200 µL Freeze and store at -20 °C

7.20 Cell Subculturing

7.20.1 Caco-2 Cell Line

Caco-2 cells (passage 31) were cultured according to recommended culture practices with slight modifications (Natoli et al. 2012). Cells were grown in working medium I (Table 7.10) before being washed with PBS and harvested in trypLE Express, centrifuged at 240 g and taken up in 10 mL working medium I. Viable cell density was determined using an Invitrogen Countess® automated cell counter. The Caco-2 cells were diluted to 2 x 10^5 cells/mL in $M199^+$ and used to seed 96-well plates (100 µL/well) for 24 hours at 37 °C. The work with Caco-2 cell culture was kindly supported by Dulantha Ulluwishewa (AgResearch, Grasslands, New Zealand).

7.20.2 Hec-1a Cell Line

Hec-1a cells (Kamat et al. 2007) (passage 10) were cultured in working medium II (Table 7.10). Cells were washed with PBS and harvested in trypsin EDTA (1x) for 10-15 minutes. The cells were diluted 1:1 in PBS and centrifuged at 1,500 rpm for 5 minutes. The supernatant was replaced and the pellet taken up in 10 mL of Working medium II. Viable cell density was determined using a hemocytometer. The Hec-1 cells were diluted to 4 x 10^8 cells/mL in working media II and used to seed 24-well plates (500 µL/well) for 48 hours at 37 °C. The work with Hec-1a culture was kindly supported by Kenny Chitcholtan (Otago University, New Zealand).

Table 7.10 *Working media used to culture Caco-2 and Hec-1 cells.*

Solution	Contents and Instructions
Working medium I	M199 medium (Sigma) Non-Essential amino acids (1x) Penicillin (100 U/mL) Streptomycin (100 mg/mL) Fetal bovine serum (FBS) (10 %)
Working medium II	Minimum Essential Medium (GIBCO®) GlutaMax (1x) Penicillin (100 U/mL) Streptomycin (100 mg/mL) Fetal bovine serum (FBS) (5 %)

7.21 Cytotoxicity Assays

7.21.1 Caco-2 Cell Line

Tha Caco-2 cell line is a widely used model for the human intestinal barrier, especially for toxicity studies (Natoli et al. 2012; Sambuy et al. 2005). Medium was removed from the seeded Caco-2 cells prior to treatment. Each treatment consisted of 50 µL sample protein at 1 mg/mL in PBS mixed with 150 µL of Working medium I (Table 7.10). Cells were incubated at 37 °C for 24 hours or 48 hours. At least 8 replicates for each condition were measured. The four used controls were 1) no cells, 2) cells + medium, 3) cells + medium + buffer, 4) cells + medium + DMSO.

7.21.1.1 Water Soluble Tetrazolium (WST) Assay

After cell treatment, medium was removed and Working medium I mixed with 10 % Cell Proliferation Reagent WST-1 (Roche) was added to the treated cells. The WST-1 reagent is a soluble tetrazolium salt first described by Ishiyama et al. 1993 (Ishiyama et al. 1993).The cells were incubated for 2 h at 37 °C before reading absorbance at 450 nm and 650 nm on a Spectramax plate reader. The background absorbance at 650 nm was subtracted from the 450 nm absorbance value.

7.21.2 Hec-1a Cell Line

Medium was removed from the seeded Hec-1a cells prior to treatment. Each treatment consisted of 50 µL of sample protein at 1 mg/mL in PBS mixed with 450 µL of Working medium II respectively. Cells were incubated at 37 °C for 48 hours. At least 8 replicates for each condition were measured. The used control was cells + medium + buffer.

7.21.2.1 Crystal Violet Assay

The medium of the treated cells was discarded and 300 µL of crystal violet (Flick & Gifford 1984) stain was added to each of the 24 wells. After staining for 15 minutes the

excess stain was thoroughly washed off with distilled water until completely removed. The plates were dried before resolubilising the stained cells in 1 mL of 2 % SDS solution per well. After solubilising the dye containing cells, the absorbences of the solutions were measured at 570 nm on a Labtech FLUOstar OPTIMA plate reader.

Table 7.11 *Crystal violet assay reagents.*

Solution	**Contents and Instructions**
Crystal violet dye	0.2 g crystal violet powder 2 mL ethanol 98 mL Milli-Q water
2 % SDS solution	1 g SDS ad. 50 mL with Milli-Q water

7.22 References

Adler-Nissen, J., 1979. Determination of the degree of hydrolysis of food protein hydrolysates by trinitrobenzenesulfonic acid. *Journal of Agricultural and Food Chemistry*, 27(6), pp.1256–1262.

Adler-Nissen, J., 1976. Enzymic hydrolysis of proteins for increased solubility. *Journal of Agricultural and Food Chemistry*, 24(6), pp.1090–1093.

Akkermans, C., Van der Goot, A.J., Venema, P., Gruppen, H., Vereijken, J.M., Van der Linden, E. & Boom, R.M., 2007. Micrometer-sized fibrillar protein aggregates from soy glycinin and soy protein isolate. *Journal of Agricultural and Food Chemistry*, 55(24), pp.9877–9882.

Bradford, M.M., 1976. A rapid and sensitive method for the quantitation of microgram quantities of protein utilizing the principle of protein-dye binding. *Analytical Biochemistry*, 72(1–2), pp.248–254.

Chiu, M.H. & Prenner, E.J., 2011. Differential scanning calorimetry: An invaluable tool for a detailed thermodynamic characterization of macromolecules and their interactions. *Journal of Pharmacy and Bioallied Sciences*, 3(1), pp.39–59.

Dyer, J.M., Plowman, J.E., Krsinic, G.L., Deb-Choudhury, S., Koehn, H., Millington, K.R. & Clerens, S., 2010. Proteomic evaluation and location of UVB-induced photo-oxidation in wool. *Journal of Photochemistry and Photobiology B: Biology*, 98(2), pp.118–127.

Ericsson, U.B., Hallberg, B.M., Detitta, G.T., Dekker, N. & Nordlund, P., 2006. Thermofluor-based high-throughput stability optimization of proteins for structural studies. *Analytical Biochemistry*, 357(2), pp.289–298.

Flick, D.A. & Gifford, G.E., 1984. Comparison of *in vitro* cell cytotoxic assays for tumor necrosis factor. *Journal of Immunological Methods*, 68(1), pp.167–175.

Fu, T.J., Abbott, U.R. & Hatzos, C., 2002. Digestibility of food allergens and nonallergenic proteins in simulated gastric fluid and simulated intestinal fluid - a comparative study. *Journal of Agricultural and Food Chemistry*, 50(24), pp.7154–7160.

Gill, S.C. & von Hippel, P.H., 1989. Calculation of protein extinction coefficients from amino acid sequence data. *Analytical Biochemistry*, 182(2), pp.319–326.

Greenfield, N.J., 2006. Using circular dichroism spectra to estimate protein secondary structure. *Nature Protocols*, 1(6), pp.2876–2890.

De Groot, J. & de Jongh, H.H.J., 2003. The presence of heat-stable conformers of ovalbumin affects properties of thermally formed aggregates. *Protein Engineering*, 16(12), pp.1035–1040.

Ishiyama, M., Shiga, M., Sasamoto, K. & Mizoguchi, M., 1993. A new sulfonated tetrazolium salt that produces a highly water-soluble formazan dye. *Chemical and Pharmaceutical Bulletin*, 41(6), pp.1118–1122.

Kamat, A.A. et al., 2007. Clinical and biological significance of vascular endothelial growth factor in endometrial cancer. *Clinical Cancer Research*, 13(24), pp.7487–7495.

Kim, E., Petrie, J., Motoi, L., Morgenstern, M., Sutton, K., Mishra, S. & Simmons, L., 2008. Effect of structural and physicochemical characteristics of the protein matrix in pasta on *in vitro* starch digestibility. *Food Biophysics*, 3(2), pp.229–234.

Krohn, R.I., 2002. The colorimetric detection and quantitation of total protein. In J. S. Bonifacino, ed. *Current Protocols in Cell Biology*. Hoboken: Wiley, pp. H1–H28.

Laemmli, U.K., 1970. Cleavage of structural proteins during the assembly of the head of bacteriophage T4. *Nature*, 227(5259), pp.680–685.

LeVine, H., 1999. Quantification of β-sheet amyloid fibril structures with Thioflavin T. *Methods in Enzymology*, 309(1), pp.274–284.

Loveday, S.M., Wang, X.L., Rao, M.A., Anema, S.G., Creamer, L.K. & Singh, H., 2010. Tuning the properties of β-lactoglobulin nanofibrils with pH, NaCl and $CaCl_2$. *International Dairy Journal*, 20(9), pp.571–579.

Meng, W., Zhang, H., Guo, T., Pandey, C., Zhu, Y., Kon, O.L. & Sze, S.K., 2008. One-step procedure for peptide extraction from in-gel digestion sample for mass spectrometric analysis. *Analytical Chemistry*, 80(24), pp.9797–9805.

Natoli, M., Leoni, B.D., D'Agnano, I., Zucco, F. & Felsani, A., 2012. Good Caco-2 cell culture practices. *Toxicology in Vitro*, 26(8), pp.1243–1246.

Nielsen, L., Khurana, R., Coats, A. & Frokjaer, S., 2001a. Effect of environmental factors on the kinetics of insulin fibril formation: elucidation of the molecular mechanism. *Biochemistry*, 40(20), pp.6036–6046.

Nielsen, P.M., Petersen, D. & Dambmann, C., 2001b. Improved method for determining food protein degree of hydrolysis. *Journal of Food Science*, 66(5), pp.642–646.

Sagis, L.M.C., Veerman, C. & van der Linden, E., 2004. Mesoscopic properties of semiflexible amyloid fibrils. *Langmuir*, 20(3), pp.924–927.

Sambuy, Y., Angelis, I.D., Ranaldi, G., Scarino, M.L., Stammati, A. & Zucco, F., 2005. The Caco-2 cell line as a model of the intestinal barrier: influence of cell and culture-related factors on Caco-2 cell functional characteristics. *Cell Biology and Toxicology*, 21(1), pp.1–26.

Speicher, K., Kolbas, O., Harper, S. & Speicher, D., 2000. Systematic analysis of peptide recoveries from in-gel digestions for protein identifications in proteome studies. *Journal of Biomolecular Techniques*, 11(2), pp.74–86.

Tanaka, N. et al., 2011. The mechanism of fibril formation of a non-inhibitory serpin ovalbumin revealed by the identification of amyloidogenic core regions. *Journal of Biological Chemistry*, 286(7), pp.5884 –5894.

Tang, C.-H., Zhang, Y.-H., Wen, Q.-B. & Huang, Q., 2010. Formation of amyloid fibrils from kidney bean 7S globulin (phaseolin) at pH 2.0. *Journal of Agricultural and Food Chemistry*, 58(13), pp.8061–8068.

United States Pharmacopeia, 2009. *The United States Pharmacopeia and National Formulary (NSF 32-NF27)* 32nd ed., Rockville: United States Pharmacopeial Convention.

Wang, J.-M., Yang, X.-Q., Yin, S.-W., Yuan, D.-B., Xia, N. & Qi, J.-R., 2011. Growth kinetics of amyloid-like fibrils derived from individual subunits of soy β-conglycinin. *Journal of Agricultural and Food Chemistry*, 59(20), pp.11270–11277.

Whittingham, J.L., Scott, D.J., Chance, K., Wilson, A., Finch, J., Brange, J. & Guy Dodson, G., 2002. Insulin at pH 2: structural analysis of the conditions promoting insulin fibre formation. *Journal of Molecular Biology*, 318(2), pp.479–490.

Yasir, S.B.M., Sutton, K.H., Newberry, M.P., Andrews, N.R. & Gerrard, J.A., 2007. The impact of transglutaminase on soy proteins and tofu texture. *Food Chemistry*, 104(4), pp.1491–1501.